Investigating roles for the deubiquitylating enzymes in the PtdIns3-K/PKB pathway in cancer

Joseph Jeromy Tholsifiso Sacco

Thesis submitted in accordance with the requirements of the University of Liverpool for the degree of Doctor of Philosophy

December 2012

Investigating roles for the deubiquitylating enzymes in the PtdIns3-K/PKB pathway in cancer

Joseph Jeromy Tholsifiso Sacco

Phosphatidylinositol 3-kinase (PtdIns3-K) signalling is a crucial survival pathway in multiple malignancies, and an exciting target for drug development. The pathway is subject to multiple regulatory mechanisms including ubiquitylation, a reversible process that can influence protein stability, localisation and activity. A family of approximately 80 deubiquitylating enzymes (DUBs) are responsible for the cleavage of ubiquitin and ubiquitin chains from protein substrates. The DUBs are attractive drug targets and have increasingly been implicated in cellular processes germane to malignancy, including the PtdIns3-K pathway. The aim of this study was to systematically identify DUBs involved in regulating the pathway, with a particular view to identifying potential novel drug targets.

The project employed a DUB siRNA library to perform a series of RNAi screens using two complementary approaches. In the first approach, the effects of DUB depletion on the protein level of nine PtdIns3-K pathway components (p110α, p110β, p110γ, p85α, p170, PDK1, PTEN, Akt, and mTOR) were assayed by immunoblotting. DUBs whose depletion either increased or decreased the protein level of these components were subject to further validation. Of particular interest were five DUBs (PRPF8, TNFAIP3, USP32, USP34 and OTUD1) whose depletion decreased the level of PDK1. In addition, depletion of three closely related members of the Josephin family of DUBs (ATXN3, ATXN3L and JOSD1) resulted in an increase in the protein level of the tumour suppressor PTEN. In view of the potential clinical utility of upregulating PTEN, the latter DUBs were prioritised for further investigation. Initial investigation indicates that all three DUBs alter PTEN level at a transcriptional rather than post-transcriptional or post-translational level. Initial work suggests the effects of ATXN3 may be independent of its known function in modulation of histone acetylation status.

The second approach utilised a U2OS cell line stably transfected with EGFP tagged FOXO3, in which PtdIns3-K dependent FOXO3 translocation could be assessed by live-cell imaging. This enabled the design of a functional screen in which the effects of DUB depletion on downstream PtdIns3-K signalling were assessed. Among the DUBs identified in this screen was USP45, depletion of which enhanced nuclear translocation of FOXO3-EGFP in response to PtdIns3-K inhibition. Several DUBs regulating FOXO3-EGFP abundance were also identified by this assay, including USP1 and USPL1 whose depletion respectively decreased and increased FOXO3-EGFP levels. This screen additionally identified three DUBs (USP8, OTUD4 and DUB4) whose depletion was synthetically lethal with PI-103 treatment.

In summary, several novel DUB modulators of the PtdIns3-K pathway were identified that, subject to further mechanistic and functional studies, may increase the options available for targeting this vital pathway in malignancy.

Table of Contents

List of figures

List of Tables

Abbreviations

AMPK	AMP activated protein kinase
Atg8	Autophagy related 8
Atg12	Autophagy related 12
ATXN3	Ataxin 3
ATXN3L	Ataxin 3-like
BAD	BCL2-associated agonist of cell death
BAP1	BRCA1- associated protein 1
BCA	Bicinchoninic acid
BCL6	B-cell lymphoma 6
BD	Binding domain
BSA	Bovine serum albumin
βTRCP	β-transducin repeat containing E3 ubiquitin protein ligase
cDNA	Complementary DNA
CHIP	C-terminus of Hsc70-interacting protein,
COP1	constitutive photomorphogenic protein 1
COSMIC	Catalogue of somatic mutations in cancer
CS	CHORD-SGT1 domain
CYLD	Cylindromatosis protein
DAXX	Death associated protein 6
DEPC	Diethylpyrocarbonate
DMEM	Dulbecco's Modified Eagle Medium
DMSO	Dimethyl sulphoxide
DNA	Deoxyribonucleic acid
DTT	Dithiothreitol
DUB	Deubiquitylating enzyme
DUSP	Domain present in ubiquitin-specific proteases
ECAAC	European Collection of Cell Cultures
EDTA	Ethylenediaminetetraacetic acid
EGF	Epidermal growth factor
EGFP	Enhanced green fluorescent protein
EGFR	Epidermal growth factor receptor
ERAD	Endoplasmic reticulum associated protein degradation

ErbB2	v-erb-b2 erythroblastic leukemia viral oncogene homolog 2
ErbB3	v-erb-b2 erythroblastic leukemia viral oncogene homolog 3
esiRNA	Endoribonuclease prepared siRNA
FANCD2	Fanconi anaemia, complementation group D2
FBS	Foetal Bovine Serum
FOXO	Forkhead box O
GPCR	G-protein coupled receptor
Grb2	Growth factor receptor bound protein 2
GSK3	Glycogen synthase kinase 3
HBSS	Hank's buffered saline solution
H and N	Head and neck
HDAC	Histone deacetylase
HECT	Homologous to E6-AP C-Terminus
HEPES	4-(2-hydroxyethyl)-1-piperazineethanesulfonic acid
IC50	Half maximal inhibitory concentration
IGF	Insulin like growth factor
IKK	I-kappa-B kinase
IKKγ	I-kappa-B kinase subunit gamma
IRS-1	Insulin receptor substrate-1
ISG15	Interferon-induced 15kDa protein
iSH2	inter-src homology 2
Jab1	Jun activation domain-binding protein 1
JNK	c-Jun N-terminal kinase
JOSD1	Josephin domain containing 1
JTT	Jones-Taylor-Thornton
LCK	Lymphocyte specific protein tyrosine kinase
MATH	Meprin and TRAF homology domain
MDM2	Mouse double minute 2, human homolog of
MPN	Mpr1p and Pad1p N-terminus,
mRNA	messenger RNA
mTOR	Mammalian target of rapamycin
mTORC2	mTOR complex 2
MVB	Multivesicular body

NCBI	National centre for biotechnology information
NEDD8	neural precursor cell expressed, developmentally down-regulated 8
NEDD4.1	neural precursor cell expressed, developmentally downregulated 4.1
NEMO	NFκB essential modulator
NFκB	Nuclear factor of kappa light chain polypeptide gene enhancer in B-cells
NMR	Nuclear magnetic resonance spectroscopy
NPL4	Nuclear protein localisation 4
NSCLC	Non-small cell lung cancer
NZF	Nuclear protein localisation 4 zinc finger
OTU	Ovarian tumour proteases
PARP	Poly ADP ribose polymerase
PBS	Phosphate buffered saline
PCNA	Proliferating cell nuclear antigen
PCR	Polymerase chain reaction
PDK1	Phosphoinositide dependent kinase 1
PH	Pleckstrin homology
PHLPP1	PH domain and leucine rich repeat protein phosphatase 1
PKB	Protein kinase B
PML	Promyelocytic leukaemia protein
PtdIns3-K	Phosphatidylinositol3-Kinase
PRAS40	Proline rich Akt substrate 40kDa
PRPF8	Pre-mRNA processing factor 8
PRU	Pleckstrin homology receptor for ubiquitin
PSMD14	26S proteasome non-ATPase regulatory subunit 14
PTEN	Phosphatase and tensin homologue
PTENP1	PTEN pseudogene 1
PX	Phox homology
QPCR	Quantitative RT-PCR
RAP80	Receptor associated protein 80
REST	RE1 silencing transcription factor

RING	Really interesting new gene
RIP1	Receptor interacting protein
RNA	Ribonucleic acid
RNAi	RNA interference
RPN13	Regulatory particle, non-ATPase-like 13
RT	Reverse transcription
SAHA	Suberoylanilide hydoxamic acid
Scg3	Secretogranin III
SDS-PAGE	SDS polyacrylamide gel electrophoresis
SH2	src homology 2,
SH3	src homology 3
siRNA	short interfering RNA
Skp2	S-phase kinase-associated protein 2
STAMBPL1	STAM binding protein-like 1
SUMO	Small ubiquitin like modifier
TAB	TAK1 binding protein
TAK1	TGFβ-activated kinase 1
TBC	Domain in Tre-2, Bub2 and Cdc16
TBS	Tris buffered saline
TEMED	Tetramethylethylenediamine
TGFβ	Transforming growth factor beta
Tm	Melting temperature
TNFα	Tumour necrosis factor α
TNFAIP3	Tumour necrosis factor alpha-induced protein 3
TRAF2	TNF associated factor 2
TRAF6	TNF receptor associated receptor 6
TRAIL	TNF related apoptosis-inducing ligand
TSC1/2	Tuberous sclerosis 1/2
TTC3	Tetratricopeptide repeat domain 3
UBC	Ubiquitin-conjugating
UBD	Ubiquitin binding domains
UBE2D3	Ubiquitin-conjugating enzyme E2D 3
UBL	Ubiquitin-like

UCH	Ubiquitin C-terminal hydrolase
UCL1	Ubiquitin carboxyl-terminal esterase L1
UCHL3	Ubiquitin carboxyl-terminal esterase L3
UIM	Ubiquitin interacting motif
UM	Uveal melanoma
USP	Ubiquitin specific proteases
VEGFR	Vascular endothelial growth factor receptor
VHL	von Hippel-Lindau
VPS	Vacuolar protein sorting-associated protein
WWP2	WW domain containing E3 ubiquitin protein ligase 2
XIAP	x-linked inhibitor of apoptosis
ZnF	Zinc finger
ZnF-MYND	(Myeloid, nervy and DEAF1)-type zinc fingers
ZRANB1	Zinc finger, RAN-binding domain containing 1

Acknowledgements

I would firstly like to thank my supervisors, Mike Clague and Judy Coulson, who enabled this PhD to happen. From helping me design a project to suit both my interests as a clinician and nascent scientist, to putting up with my interminable delays during the write up, they have helped shape my understanding of science and inspired me. In this vein, I would also like to thank Sylvie Urbé and Ian Prior, for their interest, advice and help during my project.

Several people contributed directly to the work of this thesis. Firstly, Monica Faronato, who taught me many of the methods employed in this project, and who prepared lysates from the cell panel that I used to assess FOXO expression (fig 3.26). Han Liu for helping me to produce a library of lysates in which each of the DUBs had been separately depleted (chapter 3), and for his breadth of knowledge relating to biochemistry, which he was always willing to impart. Thank you also to JiaLih Wong, who helped in some of my initial deconvolution experiments and who generated a library of esiRNA which I used in validating some of the candidates from my immunoblotting screen. Special thanks to Tinnie Yau who worked on some of the experiments in chapter 6 under my supervision. Thanks also to Yvonne Tang who helped me with my immunoblot screens for DUB regulators of PtdIns3-K catalytic subunits in chapter 3, and Claire Heride who helped me with setting up the microscopy screen. A general thank you to all of the fifth floor folk past and present, and including but not limited to, Ewan, Craig, Viktor, Becca, Sara, Amos, Anna, Monika, Dean, Veronica, Maria, Seb, Anna, Sarah, Vruti, Jen, Jenna. It has been a privilege working with you!

I would especially like to thank Clatterbridge Cancer Research, and all the patients and members of the public who contribute to CCR, for funding me. I trust your faith in me will be warranted! Thank you also to many of my colleagues at the Clatterbridge Cancer Centre, and in particular Susan O'Reilly, for their support.

And so to my family. My father, Rob and mother, Lie for instilling in me an endless curiosity and interest in the natural world, for their dedication to making the world a better place and for their faith in my abilities. My brothers for providing sibling rivalry, and for being my best friends. My daughter, Michelle, for being such a wonderful, rounded individual, and for enriching my life. Finally my wife Ruth, for so many reasons, not least of which was her (almost) infinite patience over the last few days of thesis writing which turned into weeks and then months.

Chapter 1

Introduction

1.1 Beyond kinases: Identifying novel druggable targets in the PtdIns3-K pathway

The last few decades have seen a dramatic expansion in our understanding of the mechanisms by which cancer cells undergo malignant transformation, escape apoptosis, evade the immune system, and subsequently metastasise [1, 2]. An understanding of these molecular mechanisms has in turn driven the establishment of a new field of rational cancer drug development to provide targeted therapies. Much of the early work on targeted therapy in cancer medicine has concentrated on the phosphorylation system, and more specifically, the kinases; a crucial family of enzymes involved in diverse signalling pathways, which are commonly aberrantly activated in cancer. However, while inhibition of kinases has proven a very successful strategy [3, 4], these represent only a small percentage of the druggable genome [5]. A large proportion of cancers are also primarily resistant to existent targeted therapies or develop secondary resistance after a relatively short period of response [6, 7] and there is thus a clear need for the identification of new targets for drug development.

The ubiquitin system has clear parallels with phosphorylation, involving the reversible post-translational modification of proteins leading to diverse functional consequences [8]. Many of the components of the ubiquitylation machinery are amenable to small molecule inhibition, and are thus potential drug targets. These include the deubiquitylating enzymes (DUBs, deubiquitylases), a family of approximately 80 enzymes, which catalyse the removal of ubiquitin from protein substrates. The deubiquitylases have been shown to be involved in a wide range of pathways germane to malignancy [9], and are an area of intense research in our laboratory and elsewhere.

In this PhD project, I set out to systematically investigate the role of DUBs in the phosphatidylinositol 3-kinase (PtdIns3-K) pathway, a crucial survival pathway, which is dysregulated in a large proportion of malignancies. Previous work has shown that several components of this pathway are ubiquitylated, and five DUBs, namely USP1, USP4, USP7, USP46 and UCHL1 have been implicated in its regulation. However, the full extent of DUB involvement in this pathway is unknown, and through the use of a series of siRNA screens I therefore aimed to identify further DUBs, and thus potential drug targets, involved in regulating the PtdIns3-K pathway.

1.2 Ubiquitin and ubiquitylation

Ubiquitin was originally described almost 40 years ago [10], although its function was initially unknown. However, in work which would later be recognised in the award of the 2004 Nobel Prize; Ciechanover, Hershko, and Rose elucidated the role of ubiquitin in the proteolytic degradation of proteins [11-13]. Subsequently, ubiquitylation has been shown to be the most versatile of post-translational modifications, with the ability to form several alternative chain structures, and to alter a protein's function and localisation, as well as its stability [8].

1.2.1 The structure of ubiquitin

Four genes encode ubiquitin in humans; UBB, UBC, UBA52 and RB27A, which in all cases require processing of the precursor polypeptide to release free ubiquitin. UBB and UBC both encode multiple ubiquitin repeats that are cleaved to release free ubiquitin [14], while UBA52 and RB27A consist of a single ubiquitin molecule fused to the N-terminus of the L40 and S27a ribosomal proteins respectively [15]. Ubiquitin is a small globular protein made up of 76 amino acids with a molecular weight of approximately 8.5 KDa. The crystal structure of free, unconjugated ubiquitin has been determined [16, 17], and is represented in fig 1.1i.

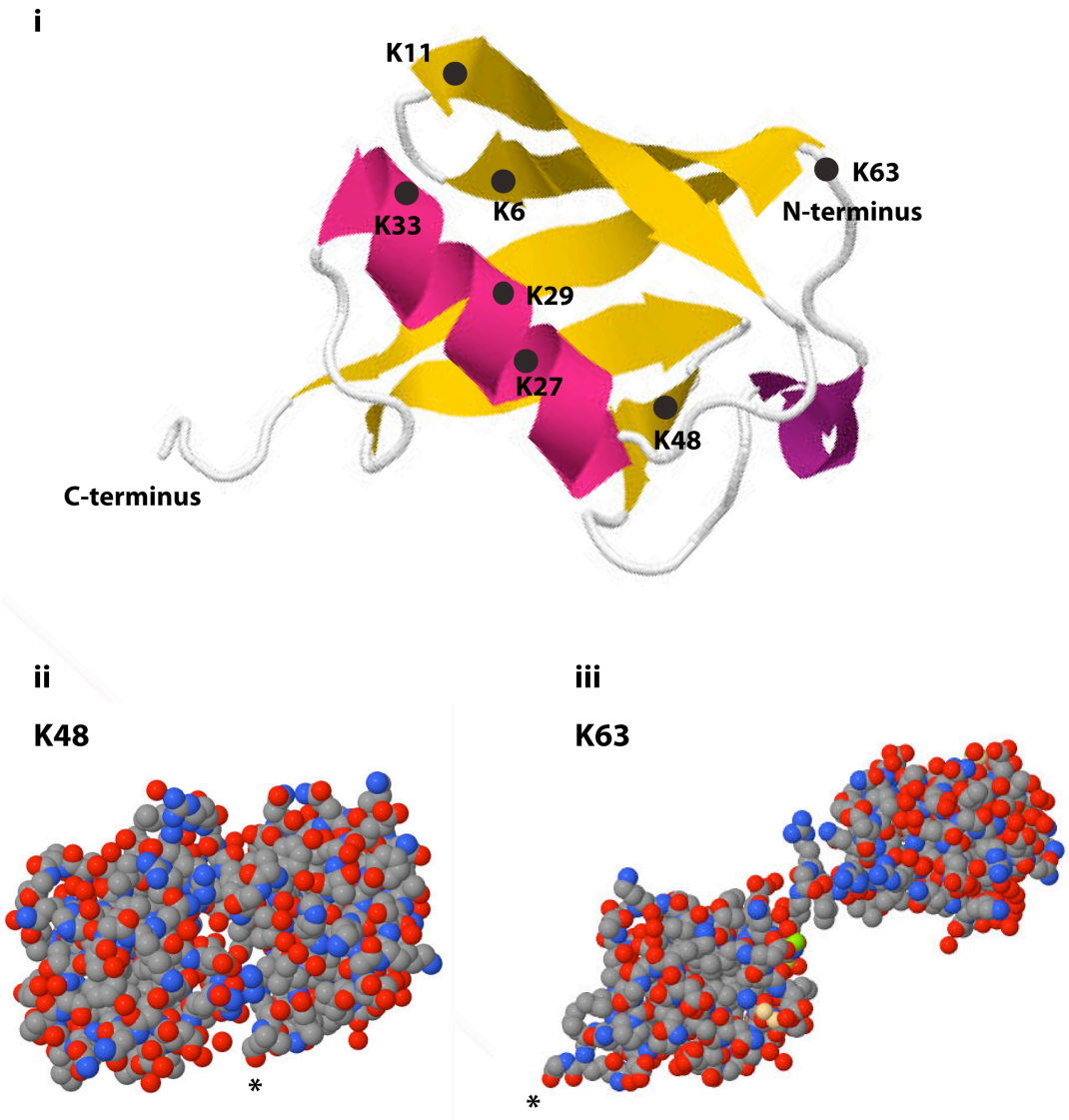

Fig 1.1. Ubiquitin lends itself to the formation of diverse chain structures. i. Representation of the crystal structure of ubiquitin, highlighting its secondary structure and approximate position of lysine residues (shown by the filled circles and designated K6 etc.). β-sheet is shown in yellow, with alpha-helical regions in purple and magenta. **ii, iii.** Space-fill models of K48 and K63 linked diubiquitin. The position of the C-terminus of the proximal ubiquitin moiety (which would normally be attached to substrate by an isopeptide bond) is indicated by the asterisk. Structures of ubiquitin (1UBI [17]), K48 and K63 linked diubiquitin (3AUL [18] and 2JF5 [19] respectively) were obtained from the Research Collaboratory for Structural Bioinformatics Protein Data Bank (http://www.rcsb.org/pdb/home/home.do), and visualised using Jmol version 12.2.15.

Ubiquitin is linked to protein substrates through an isopeptide bond formed between the ubiquitin C-terminal glycine residue and a lysine side-chain in the substrate. The modification of a substrate by the addition of a single ubiquitin moiety is termed monoubiquitylation (also known as monoubiquitination), and monoubiquitylation of multiple lysine residues is termed multi-monoubiquitylation.

Ubiquitin itself contains seven lysine residues (K6, K11, K27, K29, K33, K48 and K63), to which further ubiquitin moieties may be conjugated, thus forming polyubiquitin chains on substrates. These are each identified by the lysine residue involved in the linkage. The N-terminus may also be employed for chain propagation, leading to the formation of linear chains. In addition to these eight homotypic chains, further chain diversity may occur through the formation of heterotypic chains which contain different linkages within the same chain, and which may be branched [20, 21].

The structures of five ubiquitin chain linkages have been characterised to date, using a combination of techniques including crystallography and nuclear magnetic resonance spectroscopy (NMR) [22]. The structures of the two most studied linkages, K48 and K63, are shown in figure 1.1ii and iii respectively. These two linkages exhibit very different conformations. K48 chains adopt a compact, constrained conformation in which the two ubiquitin moieties form an intermolecular surface (fig 1.1ii) [18, 23], whereas K63 chains adopt an open, flexible structure in which the only point of contact between the two moieties is the isopeptide bond between the two (fig 1.1iii) [19, 24]. Linear polyubiquitin chains adopt a very similar structure to K63 linkages [19], while K6 [25] and K11 [26] linkages result in closed structures more akin to K48- linked chains.

The first linkages to be described were K48, which were shown to be involved in recognition of substrates by the proteasome [27]. This was followed 6 years later by the identification of K63 polyubiquitin chains, which were shown to result in a non-degradatory signal involved in DNA repair [28]. The majority of work in the ubiquitin field has focused on these chain

linkages, and it is only relatively recently that the diversity of the different chain linkages has become apparent. However, several studies employing mass spectroscopy have now identified all eight linkages in both yeast and mammalian cells [29-31]. Xu *et al.* used mass spectroscopy to determine the abundance of the different chain structures in *S. cerevisiae* and found that K48 chain linkages were the most abundant (29%) as expected [29]. However, the next most abundant were K11 chains comprising 28% of chains, followed by K63 (16%), K6 (11%), K27 (9%), K33 (4%) and K29 (3%). This study also showed that all non-K63 linkages can target substrates for proteasomal degradation [29].

1.2.2 Ubiquitin binding domains

The combination of monoubiquitylation, and homotypic or heterotypic polyubiquitin chains, generates an incredible diversity of substrate modifications. Recognition of the different conformations of ubiquitin moieties is essential in order for these to function as different signals. This occurs through ubiquitin binding domains (UBDs), which are modular elements that bind non-covalently to ubiquitin [32]. The first of these to be described was a ubiquitin interacting motif (UIM) which was involved in the recognition of polyubiquitylated substrate by the yeast proteasomal subunit S5a [33]. Since then more than 20 different UBDs have been described, which fall into five main families (table 1.1).

Two hydrophobic patches on the surface of ubiquitin, around residues Phe4 and Ile44, appear to be essential for the recognition of polyubiquitin chains [34]. Ile44 in particular is involved in binding by the majority of UBDs [32]. Different conformations of ubiquitin chain alter the relative orientation of functional surfaces, and thus hydrophobic patches [19], and influence the ability of different UBDs to bind. The specificity of interaction between UBD-containing proteins and their ubiquitylated binding partners additionally relies on multiple other factors, which are reviewed in [32, 35].

UBD family and example	Representative Proteins	Function	Ref
α-Helix			
UIM	S5a, Vps27, STAM, epsins and RAP80	Proteasomal degradation, endocytosis, MVB biogenesis and DNA repair	[33, 36-38]
Zinc Finger (ZnF)			
NZF	NPL4, Vps36, TAB2 and TAB3	ERAD, MVB biogenesis and kinase regulation	[39-41]
PH Domain			
PRU	RPN13	Proteasome function	[42, 43]
Ubc-like			
UBC	UBE2D3	Ubiquitin transfer	[44]
Others			
Jab1/MPN	PRPF8	RNA splicing	[45]

Table 1.1. Ubiquitin binding domain (UBD) families. A single example is shown for each family. Jab1/MPN- Jun activation domain-binding protein 1/ Mpr1p and Pad1p N-terminus, MVB- multivesicular body, NPL4- nuclear protein localisation 4, NZF- nuclear protein localisation 4 ZnF, PH- pleckstrin homology, Prp8- pre-mRNA processing factor 8 homolog, PRU- pleckstrin homology receptor for ubiquitin, RAP80- receptor associated protein 80, RPN13- regulatory particle, non-ATPase-like 13, TAB- TAK1 binding protein, UBC- ubiquitin-conjugating, UBE2D3- ubiquitin-conjugating enzyme E2D 3, UIM- ubiquitin interacting motif, VPS-vacuolar protein sorting-associated protein. (adapted from [32]).

1.2.3 Cellular functions of ubiquitin

Ubiquitylation of protein substrates plays a vital role in a wide variety of cellular processes. Principal among these are those pertaining to protein degradation by the proteasome, endolysosome, or autophagosome. In each of these processes, ubiquitylation acts as key degradatory signal (reviewed in [46]). Targeting proteins for proteasomal degradation usually occurs through the addition of a chain of at least four ubiquitin molecules [47]. While initially thought to only involve K48 linkages, recent work has indicated that all chain linkages, with the exception of K63, may be involved [29].

Endocytosis provides a mechanism for internalisation of membrane proteins, which are either recycled back to the plasma membrane or degraded by the lysosome. Ubiquitylation of substrates plays a vital role in sorting of endocytosed proteins [48], with K63 polyubiquitylation in particular determining degradation by the lysosome [49-51]. The third degradatory pathway, autophagy, involves both the non-selective degradation of bulk

cytosol, and the selective removal of organelles, protein aggregates or intracellular pathogens [52]. Both polyubiquitylation and monoubiquitylation have been implicated in the tagging of substrates for subsequent autophagy [53, 54], and autophagy is also dependent on two ubiquitin-like (UBL) molecules Atg8 (autophagy related 8, LC3 in mammalian cells) and Atg12 (autophagy related 12).

Ubiquitylation of protein substrates is by no means exclusively a degradatory signal, and both monoubiquitylation and K63 polyubiquitylation may alter the functional status of substrates. Examples include the monoubiquitylation of FANCD2 (Fanconi anaemia, complementation group D2) and PCNA (proliferating cell nuclear antigen), both of which are involved in DNA repair pathways [55, 56], and NFκB (nuclear factor of kappa light chain polypeptide gene enhancer in B-cells) signalling where several components are K63 polyubiquitylated (discussed in section 1.4.3). Additionally, monoubiquitylation may alter the compartmentalisation of substrate; an example of this being monoubiquitylation of PTEN, which promotes nuclear localisation [57].

1.2.4 Targeting the ubiquitin proteasome system (UPS)

The involvement of ubiquitylation in multiple cellular processes with relevance to cancer has led to interest in the possibility of targeting the ubiquitylation machinery as a therapeutic strategy [58]. While research in this area is generally at a very early stage, the development of the proteasome inhibitor, bortezomib, has provided an early proof of concept. Bortezomib is clinically active in multiple myeloma [59] and mantle cell lymphoma [60]. Although bortezomib has failed thus far to demonstrate single agent efficacy in other tumour types, preclinical work indicates that its use in combination therapy may extend its clinical activity [61, 62]. In addition, several newer proteasome inhibitors, which may prove to have different clinical activity, are in development [63]. Other components of the ubiquitylation machinery are also under investigation in this context, including the E3 ubiquitin ligases [64] and the deubiquitylating enzymes (section 1.4.7). Interestingly, an inhibitor of the E3 ligase MDM2 (RG7112) has recently demonstrated activity in an

exploratory clinical study of 20 patients with liposarcoma [65]. MDM2 (mouse double minute 2, human homolog of) is a p53 E3 ligase, and its inhibition in this trial led to p53 stabilisation and a reduction in Ki67 expression in tumours. A partial response was observed in one patient and stable disease in 14 others [65]. A trial investigating RG7112 in combination with doxorubicin in this patient population is currently underway.

1.2.5 The ubiquitin conjugating machinery

The isopeptide bond between a ubiquitin moiety and a substrate lysine side chain is formed through the sequential action of a sequence of three enzymes, namely an E1 ubiquitin activating enzyme, an E2 ubiquitin conjugating enzyme and an E3 ubiquitin protein ligase ([66] and represented in fig 1.2). The human genome encodes two E1 enzymes, around 40 E2 conjugating complexes and over 600 E3 ubiquitin ligases [67-70].

The process commences with the ATP and Mg^{2+}-dependent, E1-mediated activation of ubiquitin's C-terminal glycine. Firstly, the E1 sequentially binds ATP and ubiquitin leading to the formation of an adenylate intermediate. This is then attacked by the catalytic cysteine residue, forming a thioester bond between the ubiquitin C-terminus and the E1 [71, 72]. The adenylation reaction is repeated with a second ubiquitin molecule, however the latter does not form a thioester bond. The covalently bound (activated) ubiquitin is then transferred to the cysteine residue on the E2, where it again forms a thioester bond [66].

The E2 enzyme dissociates from the E1 before binding to the cognate E3 enzyme, in turn leading to the E3 mediated conjugation of the ubiquitin's C-terminal glycine to a lysine side chain on the substrate. There are two main types of E3 enzyme and these have different mechanisms of actions. The HECT (homologous to E6-AP C-Terminus) ligases form a thioester linkage to ubiquitin before transferring the ubiquitin to its acceptor lysine side chain [73], while RING (really interesting new gene) ligases [74] are catalytically inert and act as a scaffold to bring the E2 and substrate into proximity, after which

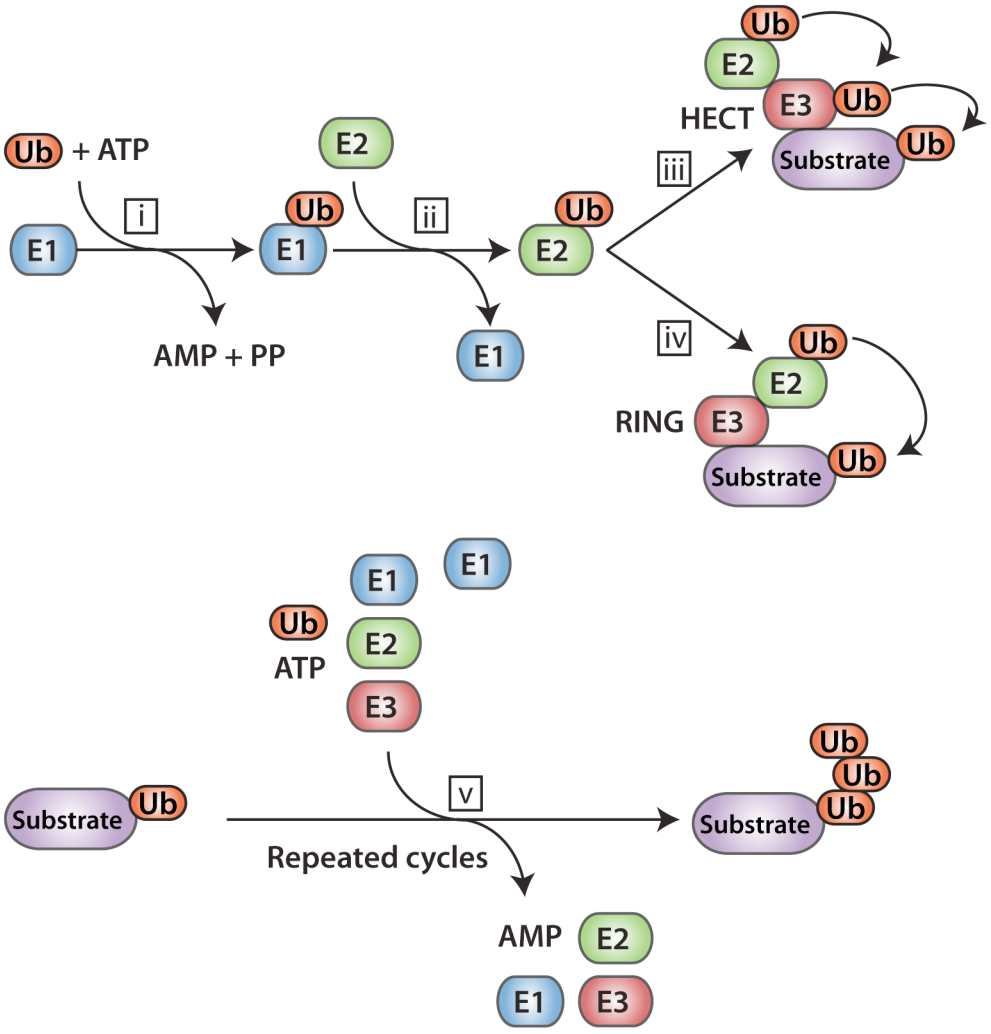

Fig 1.2 Ubiquitylation of substrates involves the sequential action of 3 enzymes. i. Ubiquitin is activated by an E1 activating enzyme in the presence of ATP and Mg^{2+}, and forms a thioester bond to the catalytic cysteine. **ii.** Activated ubiquitin is transferred to an E2 conjugating enzyme. **iii,iv**. Ubiquitin is transferred to an acceptor lysine on the protein substrate. In the case of HECT (homologous to E6-AP C-Terminus) E3 ligases (**iii**), the ubiquitin moiety is first transferred onto the E3 ligase which catalyses ubiquitylation of substrate. RING (really interesting new gene) ligases (**iv**) are catalytically inactive and act as a scaffold, bringing together the E2 into proximity with the substrate, thus allowing E2 dependent catalysis of ubiquitin conjugation. **v**. Repeated cycles of ubiquitylation are required for the construction of polyubiquitin chains.

the ubiquitin is transferred directly from the E2 to the substrate [75, 76]. In certain cases, the RING also activates the E2 [73]. Both families of E3 ligases provide substrate specificity, hence their much greater diversity in comparison to E1s or E2s [68, 70].

1.2.6 Ubiquitin like molecules

In addition to ubiquitin, almost twenty other molecules encoded by the genome adopt a similar structure and are conjugated to substrates in a manner analogous to ubiquitylation. These ubiquitin like (UBL) molecules include small ubiquitin like modifier (SUMO), neural precursor cell expressed, developmentally down-regulated 8 (NEDD8), interferon-induced 15kDa protein (ISG15), and autophagy related genes 8 and 12 (Atg8 and Atg12). Similarly to ubiquitin, UBLs are involved in a wide range of cellular functions. However individual UBLs may have very specialised roles. For example, Atg8 and Atg12 are both specifically involved in the formation of the autophagosome [77, 78]. While not directly the subject of this work, UBLs interact extensively with ubiquitylation and share some of the same machinery. For example, neddylation of the cullin RING E3 ligase is essential for its activity [79]. In addition several enzymes with the ability to cleave both ubiquitin and UBLs exist; these are discussed in section 1.3 below.

1.3 Deubiquitylation and the deubiquitylases

Protein ubiquitylation is reversible, thus enabling ubiquitin dependent signalling to be terminated. Deubiquitylating enzymes (DUBs, deubiquitylases) cleave the isopeptide bond between ubiquitin and substrate, and/or between ubiquitin moieties in a polyubiquitin chain [80]. The human genome encodes approximately 90 deubiquitylases, of which around 80 are catalytically active. The DUBs can be divided into five families on the basis of their catalytic domains; namely ubiquitin specific proteases (USPs), ubiquitin C-terminal hydrolases (UCHs), ovarian tumour proteases (OTUs, also known as otubains), Josephins, and JAB1/MPN/MOV34 (JAMMs).

1.3.1 The DUB families

The USP family is the largest, containing at least 56 members (fig 1.3). The subfamily of USP17-like genes is represented here by USP17 and DUB3. It consists of multiple, closely related members (several of which are annotated to be pseudogenes or catalytically inactive) that arose due to ancestral duplication and of which several exist within a tandemly repeated block on

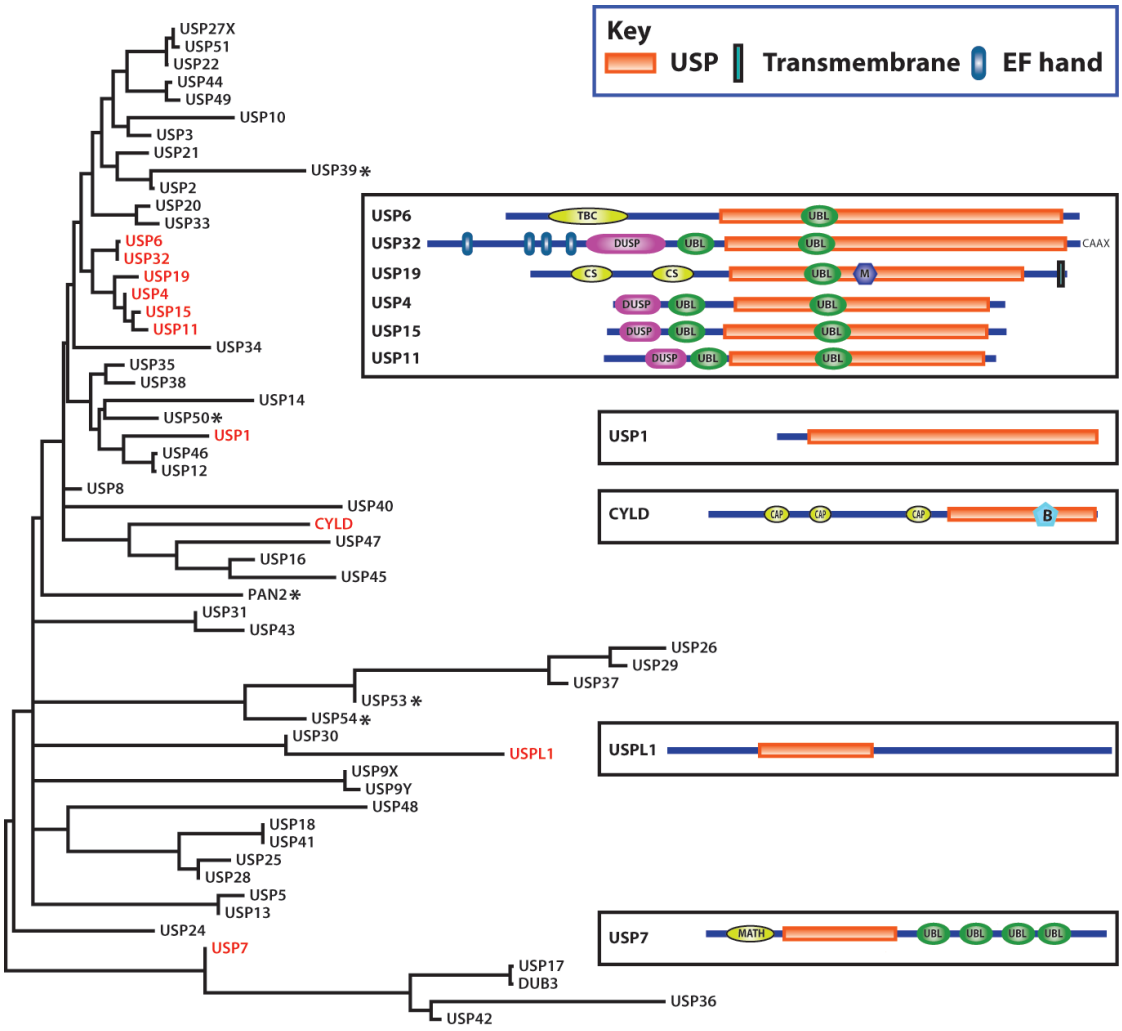

Fig 1.3 The USP family of Deubiquitylases. A molecular phylogenetic analysis was conducted in MEGA5 (www.megasoftware.net [81]). The evolutionary history was inferred by using the Maximum Likelihood method based on the JTT matrix-based model [82]. The tree with the highest likelihood is shown. The tree is drawn to scale, with branch lengths measured in the number of substitutions per site. The analysis was performed using the full-length primary NCBI RefSeq (www.ncbi.nlm.nih.gov/RefSeq) amino acid sequences. All positions containing gaps and missing data were eliminated. There were a total of 46 positions in the final dataset. Domain architecture was adapted from [80]. DUBs that are predicted to be catalytically inactive are indicated by an asterisk [80]. (DUSP: domain present in ubiquitin-specific proteases, UBL: Ubiquitin-like, B: B-box, TBC: domain in Tre-2, Bub2 and Cdc16, M: ZnF-MYND [(myeloid, nervy and DEAF1)-type zinc fingers], CS: CHORD-SGT1 domain, MATH: meprin and TRAF homology domain, CAP: CAP-Gly domain).

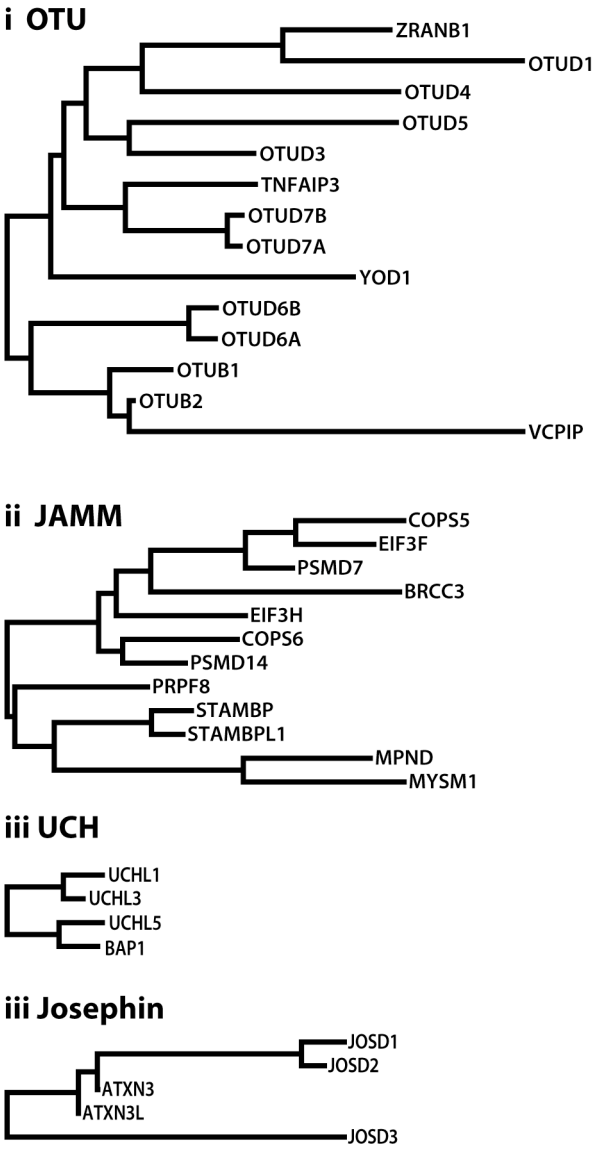

Fig 1.4 The OTU, JAMM, UCH and Josephin families of deubiquitylases. Molecular phylogenetic analyses were conducted for each DUB family as described in figure 1.3. The analyses were performed using the full-length primary NCBI RefSeq (www.ncbi.nlm.nih.gov/RefSeq) amino acid sequences. The trees were drawn to scale, with branch lengths measured in the number of substitutions per site

chromosome 4 [83]. Fig 1.3 illustrates both the existence of clusters of closely related USPs, and the overall diversity of the family. The domain architecture of several examples is shown, illustrating the wide variety of domains that are likely to be involved in protein-protein interactions, including ubiquitin-like domains (UBLs) and UBDs [80, 84]. Phylogenetic trees for the other four families are shown in fig 1.4.

1.3.2 DUB catalytic activity

Four of the five DUB families (USPs, UCHs, OTUs and Josephins) are cysteine proteases, while the last family (JAMMs) are metalloproteases. The cysteine proteases usually depend on a catalytic triad consisting of a histidine, a cysteine and an aspartate or asparagine residue. The histidine residue serves to reduce the pKa of the catalytic cysteine residue, thus enabling a nucleophilic attack on the isopeptide bond [80]. The aspartate or asparagine residue aligns and polarises the histidine residue. However, the latter residue is not always essential for DUB activity, as exemplified by the Otubain family member, TNFAIP3 (tumour necrosis factor alpha-induced protein 3, also known as A20) [85]. The nucleophilic attack results in the release of the substrate, and the formation of an acyl-intermediate involving a covalent bond formed between the cysteine residue and the conjugated (distal) ubiquitin. The intermediate is stabilised by a so-called oxyanion hole provided by surrounding residues. Finally the intermediate is hydrolysed by a water molecule, which leads to release of free ubiquitin [80, 86].

The mechanism of action of the metalloprotease DUBs (JAMMs) has been elucidated in a study in which the catalytic domain of STAMBPL1 (STAM binding protein-like 1, also known as AMSH-LP) was crystallised alone or in combination with K63 linked diubiquitin [87]. The catalytic domain contains a JAMM/MPN+ motif, which co-ordinates two zinc ions. The catalytic zinc ion activates a water molecule that attacks the isopeptide bond, leading to the formation of a charged intermediate, which is in turn collapsed to release the amino group of the proximal ubiquitin [80, 87].

1.3.3 DUB specificity and regulation

New DUB substrates are continually being identified, and the degree to which DUBs exhibit substrate specificity remains uncertain. Some DUBs clearly exhibit broad substrate specificity. Examples include the three DUBs that associate with the 19S proteasome (PSMD14, USP14 and UCHL5), and which deubiquitylate a wide range of proteins delivered to the proteasome [88]. On the other hand only a small number of substrates have been identified for some DUBs. An example is USP20 whose substrates include

type II deiodinase, the β_2 adrenergic receptor, VHL (von Hippel-Lindau), TRAF6 (TNF receptor associated receptor 6) and TAX [89-93]. This may however partly reflect the immaturity of the field, and indeed several DUBs (such as the Josephins ATXN3L, JOSD1 and JOSD2) have no known substrates to date.

DUB specificity is likely generated through multiple mechanisms [80]. Firstly, a subset of DUBs show linkage-specificity. For example, USP14 is selective for K48 chains [94], while another member of the USP family, CYLD (cylindromatosis gene), preferentially hydrolyses K63 and linear chains [95]. Most USP family members are however relatively promiscuous, and will cleave multiple chain types [19]. While the mechanisms for linkage specificity remain relatively unknown, a recent paper has deciphered a mechanistic reason for the Otubain ZRANB1's (zinc finger, RAN-binding domain containing 1) specificity for K29 and K33 ubiquitin chains. This involves an unpredicted ankyrin repeat domain which serves as a ubiquitin-binding fold that orientates ubiquitin chains such that K29 or K33 linkages are preferentially cleaved [96].

DUBs may also discriminate between cleavage from the free end of a ubiquitin chain, cleavage in the middle of the chain, or removal of the entire chain from substrate. For example, USP14 is only DUB able to cleave the distal ubiquitin from chains [94], while DUBs such as CYLD and TNFAIP3 cleave between ubiquitin moieties in the chain [95, 97]. USP14 has a Fingers subdomain, which prevents binding to internal linkages [94], this is absent in CYLD for example. PSMD14 on the other hand is an example of a DUB which cleaves the bond between substrate and the proximal ubiquitin [88].

UCH enzymes have a prominent loop that covers the active site and prevents the binding of large folded ubiquitin conjugates [80, 98]. This finding is supported by the inability of UCL1 (ubiquitin carboxyl-terminal esterase L1) and UCHL3 (ubiquitin carboxyl-terminal esterase L3) to cleave tetraubiquitin *in vitro* [19]. It has been suggested that UCH enzymes may therefore be ideally suited to the removal of monoubiquitin from non-structured protein

regions [80]. However, details relating to the removal of monoubiquitin from substrate remain scarce [80].

Two DUBs (USP5 and USP13) have been shown to contain a specific ZnF-UBD domain, which recognises the C-terminal diglycine motif in unanchored ubiquitin chains [99]. These DUBs act to recycle ubiquitin by cleaving unanchored ubiquitin chains, regardless of chain linkage, and thereby replenish the cellular free ubiquitin pool [80, 100, 101].

DUBs also generally exhibit specificity for ubiquitin, and do not cleave linkages between ubiquitin-like molecules. All DUB catalytic domains have a ubiquitin binding site that forms multiple interactions with the distal ubiquitin, principally, but not exclusively with the Ile44 patch [80, 84]. Additionally, the C-terminus of the distal ubiquitin, which extends from the binding site towards the catalytic triad and is held in place for catalysis, is distinct from that of ubiquitin-like molecules such as NEDD8, which prevents cleavage of the latter [80]. Exceptions do occur however, and include USP21, ataxin 3 (ATXN3), UCHL1 and UCHL3, which are reported to have dual activity against both ubiquitin and NEDD8 [102-105], and USP18, which has activity against linear ISG15 chains [106].

Several other factors are likely to be involved in determining substrate specificity. Many DUBs contain domains that are involved in protein-protein interactions and which may enable substrate recognition (reviewed in [80]). In addition, in a recent study in which the localisation of 66 green fluorescent protein tagged DUBs was systematically assessed, several DUBs were found to be localised to distinct organelles or structures [107], which may serve to colocalise DUB and substrate. In certain cases, DUB specificity may also require binding to substrate to induce conformational changes that unblock the active site [98]. DUBs are also subject to multiple post-translational modifications, including phosphorylation, which is likely to regulate their activity and localisation [80].

1.4 DUBs and cancer

Since the discovery of the first deubiquitylases approximately two decades ago [108, 109], it has become clear that this family of enzymes is involved in virtually all cellular processes [110]. These encompass many processes germane to cancer; including signalling pathways, cell cycle regulation, DNA damage repair, and regulation of tumour suppressors (reviewed in [9, 111]). Several DUBs have also been shown to have direct tumour suppressor or oncogenic roles (examples of which are discussed in sections 1.4.1 and 1.4.2.). The role of DUBs in cancer is also supported by a recent study which used *in situ* hybridisation to investigate DUB expression in cancer [112]. In this study, 33 DUBs were found to be expressed in one or more tissue samples and of these, 22 were differentially expressed in cancer samples [112].

1.4.1 DUBs with tumour suppressor function

The identification of mutations in the CYLD gene as the cause for cylindromatosis, a rare familial disease characterised by the formation of multiple skin adnexal tumours (cylindromas), led to the first description of a DUB with tumour suppressor functions [113, 114]. Subsequently CYLD deletion was also shown in sporadic cylindromas and other skin adnexal tumours [115, 116], and more recently CYLD has also been shown to have tumour suppressor functions in both basal and squamous cell carcinomas of the skin (reviewed in [117]). In basal cell carcinomas the CYLD gene is not mutated, however it is profoundly downregulated at both the mRNA and protein level due to recruitment of the transcriptional repressor Snail to the CYLD promoter [118]. Snail is an effector of Hedgehog signalling, which is constitutively activated in basal cell carcinoma [119-121]. The role of CYLD in squamous cell carcinomas is less clear, however an inactivating mutation has been shown to increase the malignant potential of squamous carcinomas in a xenograft model [122]. CYLD has also been associated with the pathogenesis of several other malignancies [123]. In a mouse model, CYLD deficiency led to increased susceptibility to induced colonic inflammation and colonic tumours [124].

Several CYLD substrates have been described, including TNF associated factor 2 (TRAF2) and TRAF6, I-kappa-B kinase subunit gamma (IKKγ), TGFβ-activated kinase 1(TAK1) and lymphocyte specific protein tyrosine kinase (LCK) [125-130]. The best-studied role for CYLD is the negative regulation of the NFκB signalling pathway (discussed in section 1.4.3), however CYLD also negatively regulates JNK (c-Jun N-terminal kinase) signalling [128] which is likely to also contribute to CYLD's tumour suppressor function [131]. CYLD is also involved in T-cell development [129] and function [130], which may further contribute to its role in cancer predisposition.

TNFAIP3, a member of the OTU family of DUBs and a negative regulator of NFκB signalling ([132] and section 1.4.3), is also a tumour suppressor. Loss of TNFAIP3 expression through genetic deletion, mutation or silencing by promoter methylation, has been shown in a wide range of lymphoid malignancies [133-136]. Recently, loss of TNFAIP3 expression has also been reported in colorectal cancer where it is associated with poor prognosis [137].

A third tumour suppressor, BAP1 (BRCA1- associated protein 1), was first identified through a yeast two-hybrid screen for BRCA1 RING finger interactors [138]. The same study showed that BAP1 enhanced BRCA1 mediated inhibition of breast cancer cell growth, and additionally showed rearrangements and deletions of BAP1 in lung carcinoma cell lines [138]. BAP1 was subsequently shown to be lost in a large proportion of metastasising uveal melanomas (UMs) [139]. While UM is a rare tumour type, BAP1 additionally appears to have tumour suppressor functions in other tumour types. In one study in mesothelioma, 42% of 53 tumours exhibited BAP1 genomic loss, mutation or both [140], while in a second study, biallelic BAP1 loss was reported in 16 out of 23 (60%) mesotheliomas [141]. Inactivating mutations in BAP1 have also been shown in 14% of 176 renal cell carcinomas [142]. Low BAP1 expression has also been shown to correlate with poor prognosis in non-small cell carcinomas of the lung [143]. These studies have been supported by several recent reports showing that

germline BAP1 mutations predispose to lung adenocarcinomas and mesotheliomas as well as cutaneous and ocular melanomas [144-148].
The tumour suppressor function of BAP1 has been shown to require both its deubiquitylating activity and nuclear localisation in a lung cancer cell line and in a nude mouse xenograft model [149]. BAP1 is known to reverse the monoubiquitylation of histone H2A [150], and its knockdown leads to the accumulation of monoubiquitylated H2A. In a recent study, HDAC inhibition appeared to reprogramme rapidly growing UM cancer cells into a low-grade more differentiated state. No established cell line with a BAP1 mutation was available, however HDAC inhibition in BAP1 mutant primary cell lines reversed the morphologic consequences of BAP1 loss. BAP1 had also previously been shown to form a complex with HCF-1, which is involved in regulation of gene transcription [151], indicating that its tumour suppressor function may be multifaceted.

1.4.2 DUBs as oncogenes

Several DUBs show increased activity in cancer through either mutation or upregulated expression. Translocations of USP6 (also known as TRE17) are found at high frequencies in aneurysmal bone cysts [152, 153], which are benign bone tumours, although malignant transformation has been reported [154]. Five translocation partners have been identified, and in each case lead to the placement of the USP6 coding sequence downstream of a strong promoter, leading to its aberrantly increased expression [152, 155]. The mechanism by which USP6 leads to development of aneurysmal bone cysts remains uncertain. However, USP6 has been shown to upregulate NFκB signalling, leading in turn to an induction in the expression of matrix metalloproteinases [156].

USP4 was originally characterised as an oncogene on the basis of its ability to transform NIH 3T3 cells [157], and it has subsequently been shown to be overexpressed in several different cancer subtypes [158, 159]. Several functions have been attributed to USP4, including downregulation of p53 [159] and induction of TGFβ (transforming growth factor β) signalling [160],

which may help explain its oncogenic characteristics. However, USP4 is also known to deubiquitylate TRAF2 and TRAF6 and to downregulate NFκB signalling [161], indicating that it may have different effects on tumourigenesis in different contexts.

The role of Ubiquitin C-terminal hydrolase-L1 (UCHL1) in cancer remains poorly understood, and both oncogenic and tumour suppressor functions have been described. Overexpression of UCHL1 has been reported in several tumour types including non-small cell lung cancer [162, 163], colorectal cancer [164], pancreatic cancer [165], osteosarcoma [166] and oesophageal squamous carcinoma [167]. In addition, overexpression has also been associated with tumour progression, size and invasiveness [164, 165]. However, other reports have indicated the UCHL1 promoter may be hypermethylated leading to its silencing in tumours including breast cancer [168] nasopharyngeal carcinoma [169, 170], oesophageal squamous carcinoma [171] and hepatocellular carcinoma [172].

The divergent findings of these sets of studies are similarly reflected in *in vitro* studies investigating UCHL1 substrates and mechanism of action. UCHL1 has been shown to reduce the rate of β-catenin degradation, leading to increased proliferation and migration in a colorectal cancer cell line [173]. On the other hand, ectopic expression of UCHL1 in two breast cancer cell lines, in which UCHL1 had been shown to be silenced by promoter methylation, inhibited colony formation and proliferation, and led to apoptosis [168].

Other DUBs which have oncogenic characteristics include USP28 which stabilises Myc [174] and USP2 which stabilises MDM2 [175], Cyclin A1 [176] and Aurora A [177]. USP2 additionally stabilises fatty acid synthase and is overexpressed in prostate cancer [178]. Its functional inactivation leads to apoptosis in prostate cancer cell lines [178, 179].

1.4.3 DUBs and signalling pathways

The deubiquitylases have been implicated in the regulation of most, if not all, signalling pathways relevant to cancer. Prime among these is the NFκB pathway, which is regulated at multiple levels by DUBs [180]. The NFκB pathway is a crucial regulator of immunity that is frequently dysregulated in cancer [181]. NFκB is normally sequestered in a complex with IκB. Upstream receptor stimulation leads to activation of the IκB kinase (IKK) complex, which phosphorylates IκB leading to its dissociation from NFκB. IκB then undergoes K48 polyubiquitylation and is degraded by the proteasome, leaving NFκB free to translocate to the nucleus where it regulates transcription of target genes [182]. Several proteins that promote NFκB signal transduction (including NFκB essential modulator [NEMO], TRAF2 and TRAF6) undergo activating K63 polyubiquitylation. CYLD, which as discussed 1.4.1 is a tumour suppressor, disassembles these K63 chains thus inactivating the proteins and downregulating the pathway [126, 127]. CYLD is transcriptionally upregulated by NFκB and acts as a negative feedback loop [183].

TNFAIP3 is a second negative regulator of the NFκB pathway. It possesses both DUB and E3 ligase activity and regulates its substrates (TRAF6 and RIP1 [receptor interacting protein 1]) through a ubiquitin editing function in which K63 chains are removed and replaced with K48 linkages thus promoting degradation of substrate [184, 185]. Other DUBs which have been implicated in NFκB signalling including the Otubain OTU7B, and USP21 which both negatively regulate the pathway [186, 187], and USP2 which upregulates TNFα (tumour necrosis factor α) induced NFκB signalling.

Deubiquitylases have been implicated in several other signalling pathways including TGFβ [188-191] and Wnt [192-196] signalling. The involvement of DUBs in the regulation of the PtdIns3-K pathway will be discussed in section 1.5.3.

1.4.4 DUBs and the regulation of tumour suppressor stability and function

Loss of tumour suppressor function is a common event in oncogenesis. While classically described as occurring due to genomic mutations, it has become clear that several other mechanisms may be involved. These include post-translational modifications, such as ubiquitylation, which may regulate the stability and function of tumour suppressors [197, 198]. Such ubiquitylation may be reversible, and several deubiquitylases have been shown to play essential roles in the regulation of tumour suppressors, including p53, PTEN and the FOXO (Forkhead box O) family of transcription factors [175, 199-205].

Several E3 ligases that regulate p53 ubiquitylation and thus stability have been identified [206]. These include MDM2 which is the best characterised and which is itself transcriptionally regulated by p53 [207]. A number of DUBs that deubiquitylate and stabilise p53 have also been described [199-201, 204], including USP7 which additionally deubiquitylates and stabilises MDM2 [208]. USP7 loss has been shown in certain contexts to lead to MDM2 degradation and thus p53 stabilisation [208-210]. Interestingly, p53 stabilisation has also been shown in cells treated with a USP7 inhibitor [211]. This inhibitor also induced p53-dependent apoptosis, thus supporting USP7 inhibition as a therapeutic strategy [211]. A second DUB, USP2, has also been shown to stabilise MDM2 and thus promote p53 degradation [175], and may similarly represent a drug target in cancer.

Regulation of PTEN (phosphatase and tensin homolog) and FOXO monoubiquitylation by USP7 will be discussed in section 1.5.4.

1.4.5 Targeting DUBs as a therapeutic strategy in cancer

The clinical activity of the proteasome inhibitor, bortezomib, in the management of multiple myeloma and mantle cell lymphoma (section 1.2.4) ignited interest in the ubiquitin proteasome system as a source of potential cancer drug targets. The deubiquitylases are particularly promising in this regard, and several large pharmaceutical companies, including Genentech

and Servier, have active DUB inhibitor programmes. Research in this area is at a relatively early stage, and to date there are no inhibitors in clinical trials.

While historically cysteine proteases have proven less amenable to small molecule inhibition, recently early compounds with partial specificity against certain DUBs have been developed. Among these is a USP7 inhibitor which has been shown to stabilise and activate p53, and to induce apoptosis in a p53 dependent manner [211]. A second USP7 inhibitor has also recently been described which induces apoptosis in bortezomib resistant cell lines [62].

Hybrigenics have also synthesised selective USP8 inhibitors [212], following their observation that USP8 silencing led to cell cycle arrest and apoptosis in several cell lines ([213] and section 5.4). Recently, two partially selective reversible inhibitors of USP1 were identified in a high throughput screen of several small molecule libraries containing a total of 9525 molecules. Both molecules acted synergistically with cisplatin in reducing proliferation of a cisplatin resistant non-small cell cancer cell line [214].

Additional DUB inhibitors have also been described, including a third USP7 inhibitor [215], several UCHL3 inhibitors [216], a partially selective DUB inhibitor with activity against USP9X, USP5, USP14 and UCHL5 [217], and a USP14 inhibitor [218]. Novel platforms for DUB drug discovery have recently been described and are likely to facilitate the development of further inhibitors [215, 219].

1.5 The Phosphatidylinositol 3-Kinase (PtdIns3-K)/Akt pathway

The PtdIns3-K/Akt cascade is a crucial signal transduction pathway, which links growth factor and cytokine receptors with a cascade of downstream effectors, and is involved in the regulation of several key cellular processes including survival, growth and proliferation [220]. The pathway is vital in many, if not most, malignancies. Several components of the pathway act as oncogenes (e.g. Akt), and the pathway is negatively regulated by tumour suppressors such as PTEN. Aberrations at all levels of the pathway are found in malignancies, and the pathway provides several possible targets for cancer drug development [221]. Inhibitors of a downstream effector of the pathway, mTOR (mammalian target of rapamycin), are already in the clinic [222, 223], while several inhibitors of p110α and Akt are in clinical development [224].

1.5.1 The PtdIns3-K family

In the late 1980's, work in Lewis Cantley's laboratory led to the discovery of an enzyme which catalysed the phosphorylation of phosphatidylinositol (4,5) bisphosphate at position D-3 of the inositol ring [225, 226]. Since then several other enzymes with this activity (phosphoinositide 3-kinases) have been described, and these have been shown to play a vital role in many cellular processes including cell growth, proliferation and survival as well as vesicular transport (reviewed in [227]).

The PtdIns3-Ks are divided into three classes on the basis of structure and substrate specificity (fig 1.5, [227]). Class I enzymes are heterodimeric and are made up of a regulatory and catalytic subunit. There are four catalytic isoforms, designated p110α (also known as PIK3CA), p110β (PIK3CB), p110δ (PIK3CD) and p110γ (PIK3CG). The first three make up the class IA family and bind to p85 regulatory subunits (of which there are five isoforms), while p110γ is the sole catalytic member of class IB, and interacts with p101 (PIK3R5) or p84/p87 (PIK3R6) regulatory subunits. Class I PtdIns3-Ks are activated by receptor tyrosine kinases (RTKs) and G-protein coupled

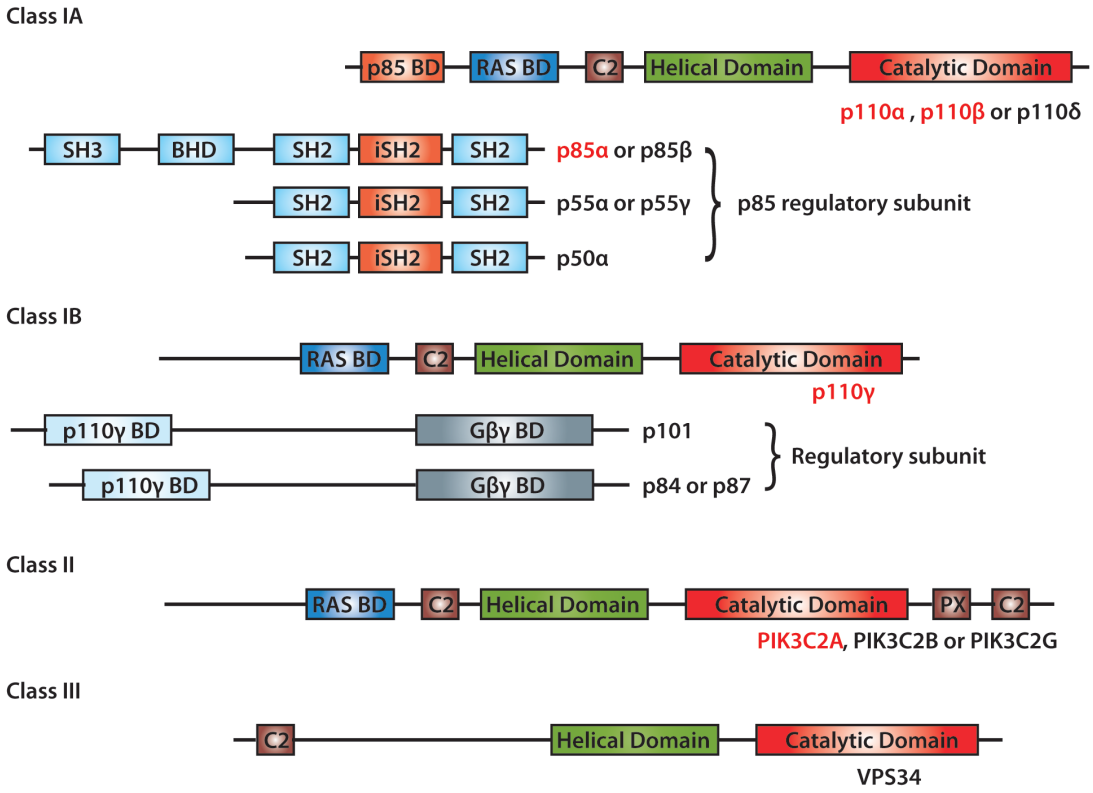

Fig 1.5. Phosphatidylinositol 3-kinase classes. PtdIns3-K isoforms, that were specifically investigated in my PhD project are highlighted in red**.** BD- binding domain, C2- putative membrane binding domain, SH2- src homology 2, SH3- src homology 3, iSH2- inter-src homology 2, PX- phox homology. (Adapted from Liu P et al [228])

receptors (GPCRs), and phosphorylate PtdIns(4,5)P_2 to produce PtdIns(3,4,5)P_3.

There are three mammalian class II PtdIns3-Ks; p170 (PIK3C2A), PIK3C2B and PIK3C2G. Class II PtdIns3-Ks do not have regulatory subunits, and their activation by upstream signalling is unclear. However there is evidence to suggest activation by both tyrosine kinase and GPCR ligands [229, 230]. Class II PtdIns3-Ks are able to phosphorylate both PtdIns and PtdIns4P *in vitro* [231, 232], However current evidence suggests that, *in vivo*, class II generates PtdIns3P only [233, 234].

VPS34 (vacuolar protein sorting 34, also known as PIK3C3) is the only class III PtdIns3-K, and is the sole representative of the PtdIns3-K family in fungi

and plants. Conserved in all eukaryotes, Vps34 is the ancestral PtdIns3-K. Vps34 catalyses the generation of PtdIns3P only [235, 236], and functions in multiprotein complexes, which regulate vesicular traffic including autophagy [237], endocytosis [238] and phagocytosis [239]. Signalling by class I PtdIns3-K leads to the activation of protein kinase B (PKB also known as Akt) and a host of downstream effectors comprising the PtdIns3-K/PKB pathway, which I will describe from now on as the PtdIns3-K pathway for simplicity. Class IA PtdIns3-Ks are particularly associated with malignancy, and unless otherwise stated the following is limited to their description.

1.5.2 The PtdIns3-K pathway is a phosphorylation cascade

A wide variety of growth factors and cytokines can activate the PtdIns3-K pathway, including members of the human epidermal growth factor receptor family (such as EGFR and ErbB2), the insulin like growth factor (IGF) receptor and angiogenesis receptors such as vascular endothelial growth factor receptor (VEGFR). Signalling through the PtdIns3-K pathway is initiated by the binding of ligands to their cognate receptors, leading to phosphorylation of specific tyrosine residues (fig 1.6). These pTyr residues are recognised by Src Homology 2 (SH2) domain containing proteins, including the p85 subunits of class IA PtdIns3-K. Binding of p85 to pTyr leads to a change in p85 conformation, which relieves p85-dependent inhibition of p110 catalytic activity. Binding of p85 to pTyr also serves to localise p110 to the membrane thus bringing it into contact with its substrate. p85 recruitment may also occur through adapter proteins such as insulin receptor substrate-1 (IRS-1) [240] or growth factor receptor bound protein 2 (Grb2) [241]. In addition class IA PtdIns3-K can also be activated through Ras [242], and recent evidence suggests that activation may also occur directly through G-protein coupled receptors (GPCRs) [243, 244].

Once activated, p110 catalyses the phosphorylation of position 3 of the inositol ring of PtdIns(4,5)P_2, which is located on the inner leaflet of the plasma membrane (fig 1.4). PtdIns(3,4,5)P_3 is the key second messenger in the PtdIns3-K pathway and its generation by PtdIns3-K is finely balanced by the tumour suppressor, PTEN [245]. PTEN was first identified in 1997 by two

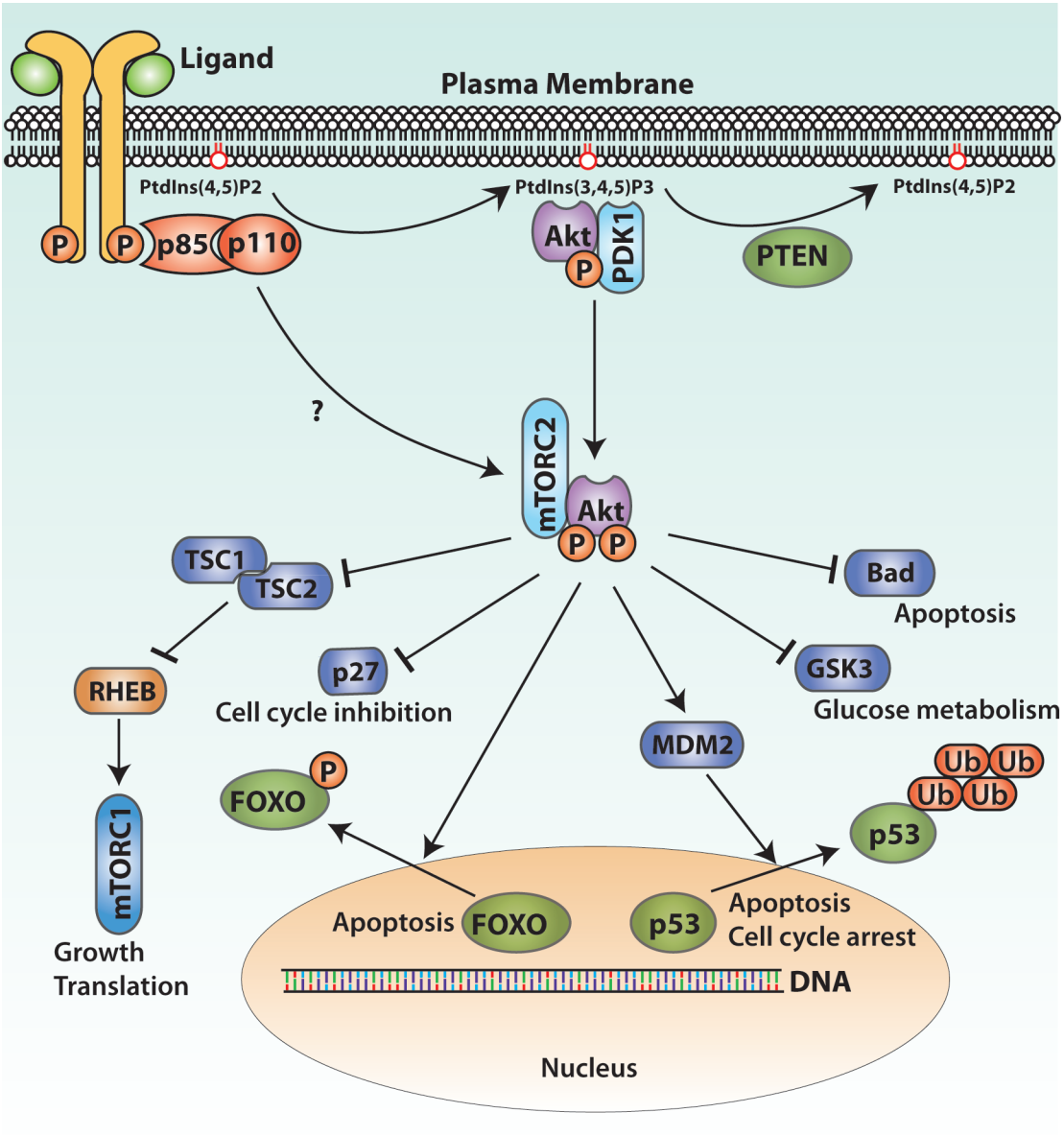

Fig 1.6. Schematic representation of the PtdIns3-K pathway. Heterodimeric class I PtdIns3-K is made up of p85 and p110 subunits and is activated by p85 binding to receptor pTyr residues. PtdIns3-K may also be activated by Ras or G-protein coupled receptors (not shown). Following its activation p110 catalyses the phosphorylation of PtdIns(4,5)P_2, and generates the second messenger PtdIns(3,4,5)P_3, which serves to recruit and localise PDK1 and Akt to the membrane. PDK1 catalyses the phosphorylation of Akt T308, a second phosphorylation (S473) is catalysed by mTOR complex 2 (mTORC2). Activation of mTORC2 is dependent on activation of PtdIns3-K but the mechanism remains unclear. Akt phosphorylates a host of downstream effectors, examples of which are shown, along with examples of their functions. Phosphorylation of FOXO leads to its nuclear exclusion and thus prevents its function as a transcription factor. MDM2 dependent K48 ubiquitylation of p53 leads to its degradation. The pathway is negatively regulated by PTEN, which dephosphorylates PtdIns(3,4,5)P_3 to PtdIns(4,5)P_2.

research groups who independently found PTEN to be disrupted in multiple sporadic tumours as well as in cancer predisposition syndromes [246, 247].

This finding was supported by the generation of PTEN knockout mice, which demonstrated increased susceptibility to multiple malignancies [248-250]. Interestingly, PTEN may function as a haploinsufficient tumour suppressor [251, 252], and subtle changes in PTEN protein expression can alter cancer susceptibility [253]. While PTEN has multiple functions which contribute to its role as a tumour suppressor (reviewed in [254]), its major role appears to be the dephosphorylation of PtdIns(3,4,5)P_3 [245], and loss of PTEN leads to deregulated PtdIns3-K signalling which in turn increases cell survival [255, 256].

PtdIns(3,4,5)P_3 engages downstream effectors in an elegant fashion, acting as a scaffold for the recruitment and phosphorylation of Akt by phosphoinositide dependent kinase 1 (PDK1). Both proteins contain Pleckstrin Homology (PH) domains [257] which preferentially bind to PtdIns(3,4,5)P_3 [258, 259]. PDK1 phosphorylates the activation loop of a large group of kinases which belong to the AGC family (named after three founder members; protein kinase **A**, protein kinase **G**, protein kinase **C**) and which include Akt [260, 261]. Binding of Akt to PtdIns(3,4,5)P_3 serves two functions, it colocalises Akt with its kinase, PDK1, and it induces a conformational change in Akt which enables its phosphorylation [262]. Notably, although PDK1 activity requires phosphorylation of its activation loop, this is an autophosphorylation and PDK1 is constitutively active [263].

Full activation of Akt requires phosphorylation at two sites, T308 within the activation loop, and S473 within the hydrophobic motif. The identity of the kinase responsible for the second phosphorylation event at S473 remained unknown until 2005, when this was shown to be due to the activity of the mTOR (mammalian target of rapamycin) in complex with rictor and GβL [264]. mTOR is a large protein kinase which exists in two distinct complexes, one containing raptor (mTORC1) [265-267] and the second containing rictor (mTORC2) [267]. Phosphorylation of Akt S473 by mTORC2 appears to be

dependent on activation of the PtdIns3-K pathway [268, 269] but the mechanism by which this is regulated remains unclear.

Akt was originally discovered as the oncogene responsible for the transforming activity of the mouse retrovirus, AKT8 [270]. Subsequently three human homologues, each of which is encoded by a different gene, have been described; namely Akt1 [271-273], Akt2 [271, 274] and Akt3 [275]. Each isoform is made up of a PH, kinase and regulatory domain, and they all share extensive sequence homology, particularly in the catalytic domain [275]. Akt1 and Akt2 are widely expressed, while Akt3 is predominantly expressed in brain, testis, lung, heart, kidney, fat and mammary tissue [273-275], and as discussed in section 1.5.3, all three isoforms have been implicated in cancer.

Akt is a master kinase, with over 120 substrates reported thus far (data retrieved from www.phosphosite.org/homeAction.do [276]). Phosphorylation of these effectors serves overall to promote cell survival, growth and proliferation. While Akt dependent phosphorylation directly activates some substrates (for example the anti-apoptotic protein XIAP [277]), it also leads to inactivation of others (for example the pro-apoptotic protein, BAD [278]). A selection of effectors are discussed below.

mTORC1 is a large multi-protein complex and key Akt effector, that promotes translation and growth, and inhibits autophagy [279]. Its activation by Akt is complex, and likely occurs through several mechanisms. The first of these involves Akt dependent phosphorylation of TSC2 (tuberous sclerosis 2), which leads to its dissociation from TSC1 [280, 281]. The TSC1/TSC2 complex is a GTPase activating protein (GAP) for the small G protein Rheb [282]. Inhibition of TSC2 thus leads to activation of Rheb, which in turn activates mTORC1 [283]. Secondly, recent evidence suggests Akt may activate mTORC1 through phosphorylation of PRAS40 (proline rich Akt substrate 40kDa) [284, 285]. Additionally, Akt dependent regulation of cellular ATP level and AMPK (AMP activated protein kinase) may indirectly lead to mTORC1 activation [286]

MDM2 (mouse double minute 2, human homologue of) is a further Akt substrate. Its phosphorylation by Akt leads in turn to an increase in polyubiquitylation and degradation of tumour suppressor, p53 [287, 288]. Akt promotes proliferation through its phosphorylation of several components of the cell cycling machinery, including p27, p21 and cyclin D1. Akt mediated phosphorylation of p27 leads to its nuclear exclusion, thus antagonising cell cycle arrest through derepression of cyclin E/CDK2 [289-291]. Glycogen synthase kinase 3 (GSK3) is serine/threonine kinase with functions in a wide range of intracellular processes, including cellular metabolism, proliferation, and survival [292]. Its phosphorylation by Akt leads to inactivation, and in turn promotes cell cycling and survival.

The FOXO proteins (FOXO1, FOXO3, FOXO4 and FOXO6) are members of the Forkhead superfamily of transcription factors, and tumour suppressors [293]. The latter has been established in mouse models, in which conditional knockout of FOXO1, FOXO3 and FOXO4 resulted in the spontaneous development of tumours [294]. Interestingly, knockout of any two of the above did not result in an increase in tumours supporting extensive redundancy between the FOXO proteins [294]. FOXO proteins promote apoptosis and cell cycle arrest, this occurs through transcription of genes such as p21 [295], p27 [296], Fas ligand [297] and B-cell lymphoma 6 (BCL6) [298]. The FOXO proteins are regulated in part by the PtdIns3-K pathway; Akt dependent phosphorylation leads to their nuclear exclusion and binding to the chaperone 14.3.3, thus preventing their transcriptional activity [297, 299-303].

1.5.3 The PtdIns3-K pathway in cancer and therapeutics

As discussed in section 1.5.2 above, the PtdIns3-K pathway contains both oncogenes and tumour suppressors. These are frequently mutated in a wide variety of different tumour groups, leading to constitutive activity of the pathway (table 1.2). In addition, upregulation of the PtdIns3-K pathway may also occur as a consequence of increased upstream signalling, or through epigenetic and post-translational mechanisms (table 1.2) Regulation of PTEN

Mechanism	Examples of tumour groups	ref
Oncogene mutation		
p110α	Breast, colon, endometrial, glioblastoma, ovarian	[304, 305] *
p85α	Glioblastoma, ovarian, colon, endometrial	[306, 307]
p85β	Endometrial	[307]
Akt1	Breast, colorectal, squamous lung	[308-310]
Akt2	Colorectal	[311]
Akt3	Melanoma	[312]
PDK1	Colorectal	[311]
mTOR	Renal	[313]
Oncogene amplification		
p110α	H and N, squamous lung, cervical, gastric, oesophageal	[314-320]
p110β	Breast, ovarian	[321, 322]
Akt1	Gastric	[271]
Akt2	H and N, pancreatic, ovarian, breast	[314, 323-325]
PDK1	Breast	[326]
Upstream activation		
EGFR mutation	NSCLC, glioblastoma	[327-329]
Her2 amplification	Breast, gastric	[330-332]
PTEN loss		
LOF mutation/ deletion	Endometrial, glioblastoma, melanoma, prostate, breast, bladder, ovarian, lung	[246] *
Epigenetic silencing	Breast, colorectal	[333, 334]
Post-translational	Bladder, lung	[335, 336]
Mechanism unreported[$]	Breast	[337-340]

Table 1.2. PtdIns3-K pathway upregulation in cancer. Examples of the mechanisms by which the pathway is activated, and tumour groups in which this occurs, are given. *COSMIC- catalogue of somatic mutations in cancer (www.cancer.sanger.ac.uk/cancergenome/projects/cosmic/). [$]These studies reported non-genomic loss of PTEN, but did not identify the relevant mechanism(s). NSCLC- non-small cell lung cancer, H and N- head and neck cancer. (adapted from [221, 341]).

in particular, occurs at multiple levels, and loss of its function may occur through several mechanisms (reviewed in [197, 254]).

The upregulation of the PtdIns3-K pathway in virtually all tumour types has led to extensive interest in the potential for drugs targeting the pathway, and most global pharmaceutical companies have a range of inhibitors against the PtdIns3-K pathway in their development pipelines. These include pan-class I inhibitors, class I isoform specific inhibitors, Akt inhibitors, mTOR inhibitors and dual PtdIns3-K/mTOR inhibitors [341]. The greatest success thus far has been obtained with the mTOR inhibitors, two of which have now been licenced for clinical use (temsirolimus and everolimus) following successful phase III trials in kidney cancer, pancreatic neuroendocrine tumours and breast cancer [342-344]. Additionally, an inhibitor of p110δ is in late phase trials in chronic lymphocytic leukaemia [345]. The remainder of the inhibitors remain in early phase trials, and the full potential of this class of drugs remains to be seen.

In view of the relatively high rates of non-genomic PTEN silencing in cancer, its reactivation through pharmaceutical means would be of potential clinical value [197]. While research in this field remains at a very early stage, inhibitors of x-linked inhibitor of apoptosis (XIAP), one of the E3 ligases that promotes PTEN degradation, are in early development [346], and PTEN transcription may be increased by histone deacetylase (HDAC) inhibition [347-349].

1.5.4. Regulation of the PtdIns3-K pathway by ubiquitylation

The PtdIns3-K pathway is extensively regulated by ubiquitylation, which regulates not only the stability of components, but also their localisation and activation status (fig 1.7). Key among these is Akt, which undergoes both K48 and K63 polyubiquitylation. The former is catalysed by the E3 ligase TTC3 (tetratricopeptide repeat domain 3) [350]. Notably, TTC3 preferentially ubiquitylates phosphorylated Akt [350], suggesting its degradation may be coupled to its activation, thus serving as an inbuilt mechanism to switch off signalling after initial activation. K63 polyubiquitylation on the other hand enhances Akt membrane localisation, and activation through its

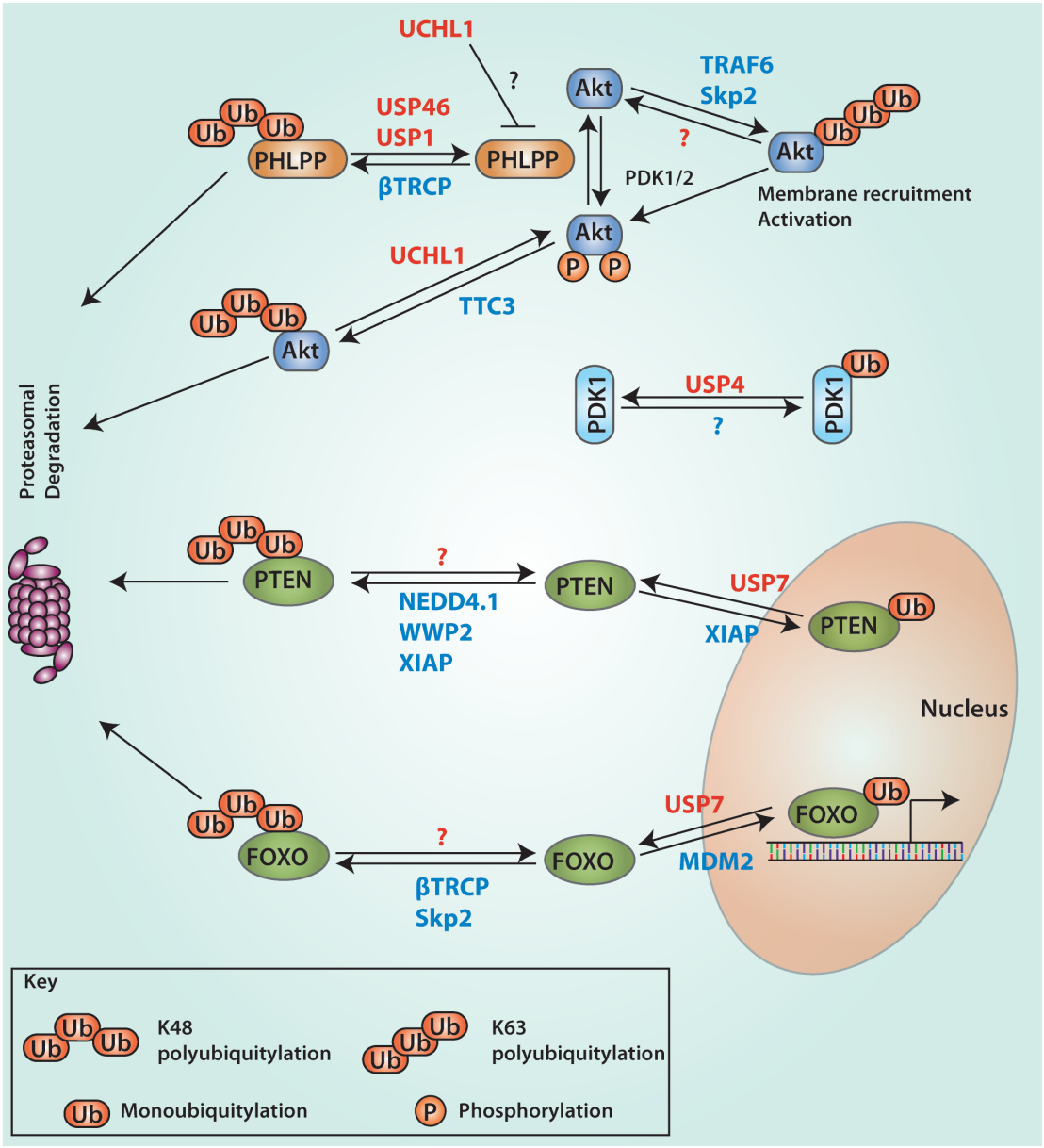

Fig 1.7. Ubiquitin dependent regulation of PtdIns3-K components. Deubiquitylases are identified in red text, while E3 ligases are shown in blue. (βTRCP: β-transducin repeat containing E3 ubiquitin protein ligase, TRAF6: TNF receptor associated receptor 6, Skp2: s-phase kinase-associated protein 2, TTC3: tetratricopeptide repeat domain 3, NEDD4.1: neural precursor cell expressed, developmentally downregulated 4.1, WWP2: WW domain containing E3 ubiquitin protein ligase 2, XIAP: x-linked inhibitor of apoptosis, MDM2: mouse double minute 2, human homologue of, CHIP: C-terminus of Hsc70-interacting protein, COP1: constitutive photomorphogenic protein 1).

phosphorylation [351]. Both TRAF6 (TNF receptor associated receptor 6) and Skp2 (s-phase kinase-associated protein 2) have been shown to catalyse Akt K63 polyubiquitylation [351, 352], however the latter study also

showed that different receptors appear to engage different E3 ligases, with IGFR utilising TRAF6, and HER family receptors utilising Skp2 [352].

The deubiquitylase, UCHL1, has been implicated in the removal of K48 chains from Akt, leading to its rescue from proteasomal degradation [353]. This study specifically investigated Akt in relation to stress-induced vascular injury, and the findings have not yet been confirmed in an alternative model. However, UCHL1 has also been shown to have a separate effect on Akt, leading to its increased phosphorylation [354]. This was mediated through a reduction in the protein level of the Akt phosphatase, PHLPP1 (PH domain and leucine rich repeat protein phosphatase 1), although the mechanism by which this occurs is unknown [354]. On the other hand, the stability of PHLPP1 is known to be regulated by ubiquitylation, with the E3 ligase βTRCP (beta-transducin repeat containing E3 ubiquitin protein ligase) promoting its degradation [355]. In a negative feedback loop, Akt activation leads to stabilisation of PHLPP1, which in turn leads to the dephosphorylation, and thus inactivation, of Akt [355]. Two deubiquitylases have been shown to reverse the polyubiquitylation of PHLPP1, namely USP46 and USP1 [356, 357].

Recently, PDK1 has been shown to be monoubiquitylated, although the functional relevance of this was not determined [358]. In a screen of 70 DUBs, only overexpression of USP4 reversed monoubiquitylation of PDK1. However depletion of USP4 did not alter Ub-PDK1 levels, suggesting the presence of other DUBs which are able to deubiquitylate PDK1 [358].

PTEN may be either polyubiquitylated (K48) or monoubiquitylated, with the former leading to its proteasomal degradation, and the latter to nuclear localisation. The E3 ligases NEDD4.1 (neural precursor cell expressed, developmentally downregulated 4.1), XIAP (x-linked inhibitor of apoptosis) and WWP2 (WW domain containing E3 ubiquitin protein ligase 2) have all been shown to polyubiquitylate PTEN [335, 359, 360]. Notably, polyubiquitylation of PTEN is known to inhibit its phosphatase activity, in addition to promoting its degradation [361]. PTEN polyubiquitylation also has

an inverse relationship with its phosphorylation at the c-terminus. This phosphorylation prevents subsequent ubiquitylation, and stabilises PTEN, while on the other hand both mono and polyubiquitylation inhibit PTEN phosphorylation [361-364]. Monoubiquitylation of PTEN promotes its nuclear localisation and is essential for its full tumour suppressor function [57, 203]. Studies in promyelocytic leukaemia cells have shown that monoubiquitylation of PTEN may be reversed by USP7, which in turn is regulated by a PML/DAXX (promyelocytic leukaemia protein/death associated protein 6) network [203].

The FOXO proteins may also be either polyubiquitylated or monoubiquitylated. K48 polyubiquitylation is mediated by several different E3 ligases, namely MDM2, Skp2, CHIP (C-terminus of Hsc70-interacting protein) and COP1 [365-368]. The recruitment of different E3 ligases may partly depend on phosphorylation status, with MDM2 dependent ubiquitylation requiring phosphorylation by ERK [365], while Skp2 dependent ubiquitylation requires prior phosphorylation of S256 by Akt [366]. Alternatively, this may represent cell type specificity with CHIP and COP1 catalysing FOXO polyubiquitylation in smooth muscle and hepatocellular carcinoma cells respectively [367, 368].

MDM2 has also been shown to monoubiquitylate FOXO4 following oxidative stress leading to nuclear localisation and increased transcriptional activity, but not altered stability [369]. USP7 reverses this monoubiquitylation of FOXO4 leading to its nuclear exclusion, and allowing its acetylation, which is inhibitory [205]. The study also showed that FOXO3 is similarly regulated [205].

The above discussion illustrates the importance of reversible ubiquitylation in the regulation of the PtdIns3-K pathway. However, there are clearly gaps in our knowledge (fig 1.6), and very likely to be other, as yet undiscovered, components including deubiquitylases.

1.6 Aims and Objectives

In this research project, I set out to investigate the role of the deubiquitylating enzymes in the regulation of the PtdIns3-K pathway in an unbiased manner, with the intention of ultimately identifying potential drug targets. For this purpose I utilised a series of siRNA screens and two main strategies. In the first I assessed the effects of DUB knockdown on the protein level of multiple components of the PtdIns3-K pathway, while in the second I used a translocation assay to assess the effects of DUB depletion on the downstream activation of the PtdIns3-K pathway. Candidate DUBs identified in the screens were subject to validation by deconvolution of the siRNA pool. Investigation into the mechanisms by which these DUBs regulate the PtdIns3-K pathway was pursued for selected candidates.

Specifically, I aimed to:

- Identify DUBs involved in regulating the PtdIns3-K pathway using siRNA screening
- Elucidate the role of these DUBs in the pathway
- Identify potential cancer drug targets

Chapter 2

Materials and methods

2.1 Cell Biology

2.1.1 Reagents

Cell culture reagents, plasticware and chemicals were obtained from Gibco (Invitrogen, UK), Corning Inc (NY, USA) and Sigma-Aldrich (Poole, UK) respectively, unless otherwise stated. Recombinant human epidermal growth factor (EGF) was obtained from Peprotech (London, UK). Vorinostat was obtained from Selleck Chemicals (Houston, USA). Unless otherwise stated, all inhibitor stock solutions were made up in dimethyl sulphoxide (DMSO) (Sigma-Aldrich), aliquoted and stored at -20^{o}C, then thawed on the day of the experiment and added to the cells in warm media at the required concentration. The maximum final DMSO concentration used was 0.2% v/v.

The DUB siRNA screens and deconvolution of hits were performed using a library of siRNA oligonucleotides that had previously been designed in collaboration with Qiagen (Crawley, UK). The library is made up of 4 siRNA oligonucleotides directed towards each of 92 DUB genes. Both pools and individual oligonucleotides were arrayed on 96 well plates for ease of use in screening and follow up experiments. The DUB library includes all known transcribed DUBs (including those predicted to be catalytically inactive), with the exception of OTUD3 and some members of the USP17 family. The latter constitute part of a tandemly repeated sequence, with multiple copies including pseudogenes and catalytically inactive DUBs [370]. Three members of the family (USP17, DUB3 and DUB4) are included in the library. A summary of the DUBs targeted and the sequences of each oligonucleotide, is provided in appendix A. The library has now been used extensively in the host laboratory for similar projects including screens for regulators of E-cadherin (JiaLih Wong, PhD thesis in preparation) and TGFβ signalling (Monika Chojnowska-Monga, PhD thesis [371]).

Where necessary, siRNA oligonucleotides were repurchased from Qiagen to replenish the library (appendix A). Additional siRNA oligonucleotides that were employed in this work are summarised in Table 2.1. A subset of targets (UCHL3, USP20, USPL1, YOD1, USP2, ATXN3, JOSD1, OTUD4, STAMBPL1 and USP7) were also depleted using endoribonuclease prepared siRNA (esiRNA), this was generated in the host laboratory by a colleague (JiaLih Wong) using the technique described by R. Kittler et al [372]. esiRNA primer sequences were obtained from the RIDDLE database (bioinformatics.age.mpg.de/ bioinformatics/RiDDLE.html), with the exception of USP2, YOD1 and ATXN3. These DUBs were either not included in the RIDDLE database (ATXN3), the primers were predicted to produce a low proportion of efficient siRNA (USP2), or PCR was unsuccessful using the RIDDLE database primers (YOD1). Primers for these were designed in-house (JiaLih Wong) and are listed in table 2.2.

2.1.2 Cell culture

A549 (human lung adenocarcinoma) and U2OS (human osteosarcoma) cells were obtained from the European Collection of Cell Cultures (ECAAC), while FKHRL1-U2OS cells were obtained from Thermo Scientific (Bioimage products, Lafayette, USA). The latter cell line consists of U2OS cells that stably express FKHRL1 (FOXO3) fused to the N-terminus of enhanced green fluorescent protein (EGFP). Expression of FOXO3-EGFP is controlled by a CMV promoter, and expression was maintained by continuous culture in Geneticin (G418) containing media. A wider panel of lung cancer cell lines was sourced and cultured as described previously [373].

A549 and U2OS cells were maintained in high glucose (4.5g/l) Dulbecco's Modified Eagle Medium (DMEM) containing 2% GlutaMAX (#31966-21) supplemented with 10% heat-inactivated Foetal Bovine Serum (FBS), 0.1mM MEM non-essential amino acids, 100units/ml Penicillin and 100units/ml Streptomycin. FKHRL1-U2OS cells were maintained in high glucose DMEM (#31966-21) supplemented with 10% heat-inactivated FBS, 100units/ml

Protein Target	siRNA Designation	Sense sequence	Catalogue number	Company
AllStars negative control	Non-targeting (siC)	Not provided	1027280	Qiagen
Akt1	AKT1_10	CACGCTTGGTCCCGAGGCCAA	SI02757244	Qiagen
Akt2	AKT2_5	AACAACTTCTCCGTAGCAGAA	SI00299166	Qiagen
Akt3	AKT3_12	ACCAGAGGTGTTAGAAGATAA	SI02757762	Qiagen
PTEN	PTEN_6	AAGGCGTATACAGGAACAATA	SI00301504	Qiagen
PDK1	PDPK1_5	AAGGGCATCATTCACAGGGAC	SI00301140	Qiagen
PDK1	PDPK1_8	AAGCGGTTAGGCTGTGAGGAA	SI00605780	Qiagen
ATXN3L	ATXN3L_D1	CAACACTGGTTTACTATTATT	D-024927-01	Dharmacon
ATXN3L	ATXN3L_D2	CAACAAGCATATTCTGTATTT	D-024927-02	Dharmacon
ATXN3L	ATXN3L_D3	GGAAACACATCGCAAGATCTT	D-024927-03	Dharmacon
ATXN3L	ATXN3L_D4	CCGCAGTCTATTGAGTTATT	D-024927-04	Dharmacon

Table 2.1. siRNA sequences.

Target Gene	Primers	Length of esiRNA
USP2	*FW.GCTAATACGACTCACTATAGGGAGAG***CCAATGATGTGGTGAGCCCAT** *RV.GCTAATACGACTCACTATAGGGAGAC***GCAGCGACAGCATGTTGGCT**	**449 bp**
YOD1	*FW.GCTAATACGACTCACTATAGGGAGAG***GGATCTCAGCAATGGGGATAC** *RV.GCTAATACGACTCACTATAGGGAGAC***GGAGGTGTATCTGGATCAGG**	**405 bp**
ATXN3	*FW.GCTAATACGACTCACTATAGGGAGAG***GGGCATTTTTCTTGGATCTTT** *RV.GCTAATACGACTCACTATAGGGAGAC***CAGAGTTTAGGAACGCACCA**	**552 bp**

Table 2.2 esiRNA primers. FW: forward primers, RV: reverse primers. Bases in italics designate T7 promoter sequences, while the sequence in bold designates the start of the esiRNA sequence

penicillin, 100units/ml streptomycin and 0.5mg/ml Geneticin. All cells were cultured in a humidified incubator at 37°C and 5% CO_2. Cells were maintained in exponential growth phase by growing to confluency in 100mm dishes and splitting every 48 hours. Cells were washed with sterile warm phosphate buffered saline (PBS) and detached from the plate using 0.05% trypsin-EDTA. A549 and U2OS cells were split at a ratio of 1:4 to 1:5, while FKHRL1-U2OS cells were split at a ratio of 1:3 to 1:4.

2.1.3 siRNA and esiRNA transfections

Unless otherwise stated (see sections 2.1.3.1-2 below), siRNA transfections were performed in 6-well plates. Cells were seeded the day before transfection (table 2.3) in full DMEM and allowed to attach overnight.

Immediately prior to transfection, the media was replaced with 800µL of DMEM containing no additives, after two washes with the same. Transfections were performed using either Oligofectamine or Lipofectamine RNAiMAX transfection reagent (both from Invitrogen) as per the manufacturers instructions. A final siRNA concentration of 20nM (Oligofectamine) or 10nM (RNAiMAX) was employed, while esiRNA transfections were performed in RNAiMAX using a final concentration of 150ng/ml.

For Oligofectamine transfections two solutions were prepared, the first of which (solution A) was made up of 20pmol of siRNA diluted in 182µl OptiMEM I (#51985-026) while the second (solution B) consisted of 3.3µl of Oligofectamine reagent made up to 18µl in OptiMEM. Following a 5-minute incubation, the two solutions were combined and incubated for a further 20 minutes before being added drop-wise to the cells. Two solutions were similarly prepared for RNAiMAX transfections, the first containing 12pmol siRNA or 180pg esiRNA and the second containing 2µL of RNAiMAX reagent, and both of which were made up to 200µL in OptiMEM. The two solutions were combined and incubated for 10 to 20 minutes before being added to the cells. For both methods of transfection, FBS was added to a final concentration of 10%, four hours after transfection, and the following day the media was replaced with fresh full media.

Cell type	48 hour transfection (cells per well)	72 hour transfection (cells per well)
A549 cells	1 x 10^5	6 x 10^4
FKHRL1-U2OS	1.2 x 10^5	-

Table 2.3 Cell seeding densities for siRNA transfections (6-well plate)

2.1.3.1 DUB siRNA library screen for immunoblotting

Transfection of cells for the immunoblotting screen (chapter 3) is described here. A549 cells were seeded in 150mm dishes at a density of 9 x 10^7 cells per dish, and allowed to attach overnight. Transfections were performed using Oligofectamine in a similar manner to that described above. Prior to transfection, 9.5ml of no addition DMEM was added to each dish after washing. Solution A contained 50µl of siRNA oligonucleotide pool (10µM) made up to 2730µl with OptiMEM, while solution B contained 49.5µl of Oligofectamine made up to 270µl in OptiMEM. Incubations were performed as described above, and the final concentration of siRNA oligonucleotide was 40nM.

2.1.3.2 Reverse transfection (96 well plates)

Transfections for the translocation screen (chapter 4) and synthetic lethality experiments (chapter 5) were performed using a reverse transfection method and RNAiMAX transfection reagent according to the manufacturer's protocol. RNAiMAX was diluted 1 in 20 prior to transfection. A reaction mix of 3µl of diluted RNAiMAX and 2µl of siRNA oligonucleotide (at a concentration of 1.2µM) made up to 20µl with OptiMEM, was dispensed in each well. An incubation of 10-20 minutes followed, during which time cells were harvested and resuspended in antibiotic free DMEM at a concentration of 3 x 10^4 cells/ml. 100µl of cells were then added to each well thus obtaining a final siRNA concentration of 20nM, and 3000 cells per well. The rim of wells around the edges of each plate were not used for transfections and instead filled with PBS to improve humidification and minimise edge effects. The

plates were then incubated overnight, and the following day the media in each well was replaced with 200µl of fresh, full media.

2.1.4 Cycloheximide chase

Cycloheximide (Sigma-Aldrich) was used to inhibit mRNA translation and thus synthesis of new protein, in order to assess the degradation half-life of PTEN, and other proteins (section 6.7). A549 cells were seeded in six well plates and transfected with ATXN3_5, USP20_2, non-targeting siRNA, or mock-transfected using RNAiMAX transfection reagent as described in section 2.1.3. The cells were incubated for a total of 72 hours after transfection. Prior to lysis, 100µg/ml of cycloheximide was added for the indicated durations (0, 1, 2, 4, 8, 20 hrs) in full media. Lysis was performed using NP40 buffer as described in section 2.1.8.1. Lysates were immunoblotted for the indicated proteins as described in sections 2.2.4-6.

2.1.5 Akt depletion and EGF stimulation

This experiment was performed to enable identification of the different bands detected by the Akt antibody (section 3.7). A549 cells were seeded in six well plates and transfected with siRNA against Akt1, Akt2, or Akt3, non-targeting siRNA, or mock-transfected using Oligofectamine as described in section 2.1.3. 48 hours after transfection half of the wells were serum starved for 4 hours, then 20ng/ml of EGF added for 15 min. All wells were then lysed using the hot lysis method (section 2.1.7.3), and lysates immunoblotted for Akt and actin (sections 2.2.4-6).

2.1.6 Actinomycin D chase

Actinomycin D (Sigma-Aldrich) was employed to inhibit transcription, and thus to enable assessment of the rate of transcript degradation (section 6.6). This was performed in either non-transfected A549 cells (seeded in 6-well plates at a density of 2 x10^5 cells per well the day before the experiment) or following a 48-hour transfection in A549 cells. Transfections were performed as described in section 2.1.3. On the day of the experiment, the cells were treated with actinomycin D to a final concentration of 5µg/ml for the indicated

times prior cell lysis and total RNA extraction, after which quantitative RT-PCR (QPCR) was performed as described in sections 2.3.4-6.

2.1.7 HDAC inhibition

The non-selective histone deacetylase (HDAC) inhibitor, vorinostat (also known as suberoylanilide hydoxamic acid [SAHA]), was used to investigate a potential mechanism for ATXN3 dependent regulation of PTEN/PTENP1 transcription (section 6.7). Cells were seeded at a density of 3 x 10^5 cells per well, allowed to attach, then the following day vorinostat added to the concentrations indicated, and the cells incubated for 16 hours. Alternatively, A549 cells were transfected with siRNA in 6-well plates as described in section 2.1.3 and incubated for 32 hours, after which 2μM vorinostat was added in full medium and the cells incubated for a further 16 hours. Cell lysis, RNA extraction and QPCR were performed as described as described in sections 2.3.4-6.

2.1.8 Cell lysis

2.1.8.1 NP40 lysis

The cells were placed on ice, the medium aspirated and the cells washed twice with ice cold PBS. NP40 lysis buffer (0.5% NP40, 25mM Tris (pH 7.5), 100mM NaCl, 50mM NaF) containing phosphatase and protease inhibitors (Complete protease inhibitor cocktail tablets and phosSTOP phosphatase inhibitor cocktail tablets respectively, both from Roche, Basel, Switzerland) was added and the cells were lysed for 15min with rocking. The lysate was cleared by centrifugation at 16,000g for 10 min at 4°C in a bench top centrifuge. Protein assays and sample preparation were performed as described in section 2.2.3.

2.1.8.2 Cell fractionation

The lysis method employed in the large scale library screen was adapted from that of Dignam et al [374], and involved the sequential use of a 0.5% NP40 buffer to extract predominantly cytosolic proteins, followed by a high salt buffer (Dignam's buffer C) to extract nuclear proteins and finally boiling in

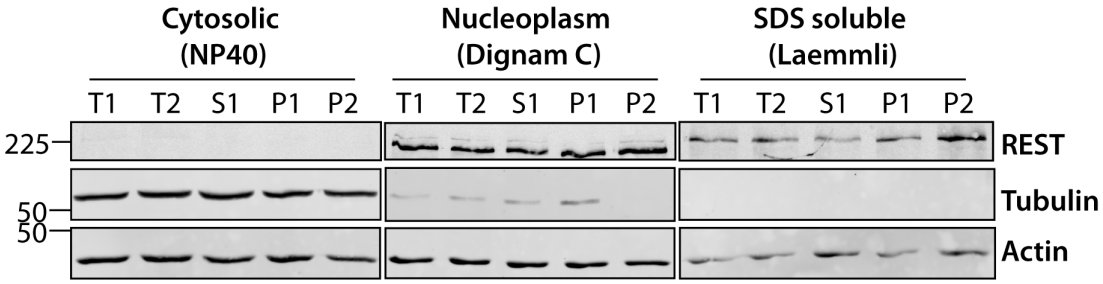

Figure 2.1. Optimisation of lysis protocol. A549 cells were grown in 15cm dishes and lysed when confluent. The cells were either trypsinised first, pelleted then NP40 added (T1 and T2), scraped off the plate into NP40 (S), or lysed directly on the plate with NP40 (P1 and P2), with nuclei scraped off subsequently. In the P2 method, after the NP40 fraction was aspirated, the nuclei were washed once with NP40 before being scraped off the plate. In T1 the cells were removed in 1.5mls of PBS, while in T2 5mls of PBS was used. In all cases following NP40 lysis, nuclei were pelleted and subsequent lysis was performed in Dignam's buffer C and Laemmli buffer. Reasonable fractionation was obtained in all cases, though as less tubulin was carried forward into the Dignam C fraction with P2, this method was subsequently used for the screen.

Laemmli buffer to extract remaining protein from the non-solubilised pellet. Several variations were tested as shown in fig 2.1. A reasonable fractionation of proteins was obtained, as exemplified by the cytosolic protein, tubulin, the predominantly nuclear transcription factor REST (RE1 silencing transcription factor), and actin, which is found in both compartments (fig 2.1). In brief, NP40 lysis was performed as outlined above, nuclei were scraped off into PBS and spun down in a micro-centrifuge. The insoluble fraction was then resuspended in Dignam C buffer (20mM HEPES pH 7.9, 25% glycerol, 420mM NaCl, 1.5mM $MgCl_2$, 0.2mM EDTA) containing phosphatase and protease inhibitors, and incubated at 8^{o}C on a vortex shaker for 40 minutes. Samples were then centrifuged at 16,000g for 10 min at 4°C in a bench top centrifuge (Eppendorf) and the supernatant recovered as the nuclear fraction. The pellet was resuspended in Laemmli buffer (50mM Tris pH 6.8, 2% SDS, 10% glycerol) and incubated at 110°C for 10 mins with frequent vortexing. The samples were again centrifuged at 16,000g for 10 min at 4°C, and the supernatant recovered as the Laemmli fraction. NP40, Dignam C and Laemmli lysates were processed as described in section 2.2.3.

2.1.8.3 Hot lysis

Cells grown in 6-well plates or 3cm dishes were rinsed twice in warm (37^{o}C) PBS before lysis. The PBS was aspirated from the cells which were then transferred immediately onto a dry heat block at 110^{o}C, and preheated 100-150µl Laemmli buffer added. Working quickly to avoid evaporation, the plate was immediately scraped with a rubber policeman and the viscous lysate aspirated and placed in a preheated screw cap tube. The lysate was then incubated for a further 10 minutes at 110°C with frequent vortexing. After cooling the lysate was cleared by centrifugation and processed as described in section 2.2.3.

2.2 Protein biochemistry

2.2.1 Reagents

ProtoGel 30% Acrylamide/Bisacrylamide solution (37.5:1 w/v ratio, #EC-890), ProtoGel resolving (♯EC-892) and stacking (#EC-893) buffers, were all obtained from National Diagnostics (Atlanta, USA). Tween-20 and Tetramethylethylenediamine (TEMED, #303853V) were obtained from VWR (Lutterworth, UK). Ammonium persulphate (APS) and Ponceau S were obtained from Sigma-Aldrich (Poole, UK). Perfect protein (#69079-3) and Rainbow markers (#RPN800E) were obtained from Merck Biosciences (Darmstadt, Germany) and GE healthcare (Amersham, UK) respectively. The latter was diluted 1 in 5 in sample loading buffer prior to use. BioTrace NT nitrocellulose membrane (0.2µm pore size) was obtained from VWR (Lutterworth, UK). Bovine serum albumin (BSA, #40-00-410) and Marvel skimmed milk powder were obtained from First Link (Wolverhampton, UK) and Premier Brands (St Albans, UK) respectively.

2.2.2 Antibodies

Lists of primary and secondary antibodies, including the conditions used for immunoblotting, are provided in tables 2.4 and 2.5 respectively. Secondary antibodies were used in the same blocking buffer as the primary. During the course of the project, two of the 680nm channel secondary antibodies were

Target Protein	Species	Source (Catalogue No.)	Blocking Buffer	Dilution (time)
p110α	Rabbit	Cell Signaling (4249)	BSA	1:1000 (O/N)
p110β	Rabbit	Cell Signaling (3011)	BSA	1:1000 (O/N)
p110γ	Rabbit	Cell Signaling (5405)	Marvel	1:1000 (O/N)
p170	Mouse	BD Biosciences (611046)	BSA	1:250 (O/N)
p85α	Mouse	BD Biosciences (610045)	Marvel	1:2500 (O/N)
PTEN	Mouse	Santa Cruz (sc-7974)	*Marvel/BSA	1:250 (O/N)
PDK1	Rabbit	Cell Signaling (3062)	BSA	1:1000 (O/N)
PDK1	Rabbit	Cell Signaling (5662)	BSA	1:1000 (O/N)
PDK1	Rabbit	BD Biosciences (611071)	BSA	1:1000 (O/N)
PDK1	Sheep	Dundee (s682)	Marvel	1:1000 (O/N)
pPDK1	Rabbit	Cell Signalling (3061)	BSA	1:1000 (O/N)
Akt	Rabbit	Cell Signaling (9272)	BSA	1:1000 (O/N)
pAkt (S473)	Rabbit	Cell Signaling (4060)	BSA	1:1000 (O/N)
pAkt (T308)	Rabbit	Cell Signaling (9275)	BSA	1:1000 (O/N)
FOXO1	Rabbit	Bethyl (A300-397A)	Marvel (PBST)	1: 3000 (1hr or O/N)
FOXO3	Rabbit	Bethyl (A300-297A)	BSA	1: 5000 (O/N)
FOXO4	Goat	Santa Cruz (sc-5221)	BSA	1: 200 (O/N)
mTOR	Mouse	Cell Signaling (4517)	Marvel	1: 1000 (O/N)
GFP	Sheep	Ian Prior, University of Liverpool	Marvel	1: 1000 (1hr or O/N)
YOD1	Rabbit	Gift from C. Schlieker	Marvel	1: 1000 (O/N)
USP7	Rabbit	Abcam (ab4080)	Marvel	1: 2000 (O/N)
USP8	Rabbit	Sigma (HA004869)	Marvel	1:1000 (O/N)
USP15	Rabbit	Bethyl (A300-923A)	Marvel	1: 1000 (O/N)
USP20	Rabbit	Bethyl (A301-189A)	BSA	1:1000 (O/N)
USP20	Rabbit	Aviva (ARP59314)	Marvel (PBST)	1:750 (O/N)
USP33	Mouse	Sigma (WH0023032M1)	Marvel	1: 1000 (1hr)
USP47	Rabbit	Bethyl (A301-048A)	Marvel	1:2000 (O/N)
ATXN3	Mouse	BioLegend (650401)	BSA	1:1000 (O/N)
PSMD14	Rabbit	Zymed (38-0200)	Marvel	1: 250 (O/N)
Actin	Mouse	Abcam (Ab6276)	Marvel	1:10000 (1hr)
Actin	Rabbit	Sigma (A2066)	Marvel	1:2000 (O/N)

Table 2.4. Primary antibodies employed in this study (continued overleaf).

Target Protein	Species	Source (Catalogue No.)	Blocking Buffer	Dilution (time)
α-Tubulin	Rabbit	Sigma (T5168)	Marvel	1:10000 (O/N)
PARP p85	Mouse	Cell Signaling (9546)	Marvel	1: 2000 (O/N)
REST	Rabbit	Millipore (07-579)	3% Marvel TBS (no tween)	1: 2000 (O/N)

Table 2.4 Primary antibodies employed in this study. Unless otherwise indicated incubations were performed in 5% Bovine Serum Albumin TBS 0.1% tween (BSA) or 5% Marvel TBS 0.1% tween (Marvel). *PTEN blots were blocked in Marvel, and antibody incubations performed in BSA. PBST: phosphate buffered saline 0.1% tween. O/N: overnight incubations at 8^{o}C, 1hr: 1hour incubation at room temperature.

Catalogue Number	Antibody	Dilution
926-32213	IRDye 800CW Donkey anti-Rabbit	1:15000
926-32212	IRDye 800CW Donkey anti-Mouse	1:15000
926-32214	IRDye 800CW Donkey anti-Goat	1:15000
926-32223	IRDye 680 Donkey anti-Rabbit	1:15000
926-32222	IRDye 680 Donkey anti-Mouse	1:15000
926-32224	IRDye 680 Donkey anti-Goat	1:15000
926-68023	IRDye 680LT Donkey anti-Rabbit	1:20000
926-68020	IRDye 680LT Donkey anti-Mouse	1:20000

Table 2.5 Secondary antibodies employed in this study. All secondary antibodies were obtained from LiCor Biosciences (Nebraska, USA).

replaced with a newer version (designated LT), which were used at a more dilute final concentration (table 2.5).

2.2.3 Protein assay and sample preparation

All protein assays were performed using a bicinchoninic acid (BCA) protein assay kit (#23225, Pierce, UK) according to the manufacturer's instructions, using a bovine serum albumin (BSA) standard. Absorbance was read using a MultiSkan Spectrum plate reader (Thermo Scientific, Massachusetts, USA).

Following the protein assay, samples for immunoblotting were adjusted to equal concentrations and loading buffer added. 5X loading buffer containing

15% SDS (w/v), 312.5mM Tris-HCl pH 6.8, 50% glycerol (w/v), and 16% βmercaptoethanol, was added to either NP40 or Dignam C lysates. A second loading buffer was added to Laemmli lysates. This was prepared at a 10X concentration and contained 1M dithiothreitol (DTT) and 1% bromophenol blue. Samples were then boiled for 10 minutes at 98^{o}C prior to storage at -20^{o}C.

2.2.4 SDS polyacrylamide gel electrophoresis (SDS-PAGE)

SDS-PAGE was performed using either Mini Gels poured using a BioRad Mini-Protean® 3 system (California, USA) as per the manufacturer's instructions, or larger gels for the immunoblotting screens, which were prepared using a FlowGen Flow200 system obtained from Scientific Laboratory Supplies (SLS, Nottingham, UK). The percentage concentration of acrylamide used was determined by the target protein molecular weight. Each gel was made up of a resolving (table 2.6), and a stacking (table 2.7) component. Quantities given here are for a single 1.5mm mini gel, quantities for larger gels were scaled up as required. Alternatively precast NuPAGE Bis-Tris 4-12% gradient gels (#NP0316BOX, Invitrogen) were used.

Equal amounts of each sample were loaded, along with molecular weight markers (5µl each of Perfect Protein and diluted Rainbow Marker). For the immunoblotting screen (chapter 3), gels with 36 wells were made. Each gel was loaded with twenty-three sample lysates flanked by mock and non-targeting siRNA controls. Perfect Protein and Rainbow Markers were run alongside the samples. Four gels were required to run all 92 samples. MiniGels were run at 200V for approximately 40-60 minutes, while FlowGen gels were run for 30 min at 90V followed by 90 min at 140V. Both types of gels were run in electrophoresis buffer containing 50mM TrisHCl, 01% SDS and 38mM glycine. NuPAGE gels were run according to manufacturers instructions in NuPAGE MOPS buffer containing NuPAGE antioxidant at 200V for an hour in an CCell SureLock Mini-Cell system (Invitrogen).

	Percentage Acrylamide		
Constituent	**8%**	**10%**	**12%**
ProtoGel (ml)	5.3	6.7	8
Resolving Buffer (ml)	5.2	5.2	5.2
Water (ml)	9.2	7.9	6.6
10% APS (µl)	150	150	150
TEMED (µl)	15	15	15

Table 2.6. Resolving Gel Constituents.

ProtoGel (ml)	1.3
Stacking Buffer (ml)	2.5
Water (ml)	6.1
10% APS (µl)	50
TEMED (µl)	10

Table 2.7. 4% stacking gel

2.2.5 Immunoblotting protocol

Following SDS-PAGE, protein was transferred onto nitrocellulose using a Genie blotter apparatus (Idea Scientific, Minneapolis, USA) with a fixed voltage of 25V over 1hour 15min. A 25mM tris-glycine, 20% Methanol transfer buffer was employed. Transfer and estimation of loading was assessed by Ponceau-S staining. Blots were then blocked using either 5% marvel or 5% BSA in TBS (20mM Tris base, 137 mM NaCl, pH 7.6) 0.1% Tween-20 for an hour. Primary antibody was added in the same blocking buffer and the blots were incubated on a rocker for either an hour at room temperature or overnight at 4^{o}C. Concentrations and conditions for each antibody are described in section 2.2.2. Blots were washed three times for 5 minutes each in TBS 0.1%T before addition of appropriate secondary antibody (table 2.5), which was again diluted in the same blocking buffer. After a one-hour incubation, the blots were washed twice in TBST 0.1%T and once in TBS, each time for 5 minutes

2.2.6 Signal detection and quantification

An Odyssey infrared scanner (LiCor, Nebraska, USA) was employed to detect secondary antibodies. Two-channel detection (800nm and 700nm) allowed the simultaneous assay of two secondary antibodies coupled to alternative fluorophores. Quantification was performed using Odyssey software. A box was drawn around each band of interest, and the integrated intensity of the signal within the box calculated (counts/mm^2). The signal was normalised to background, which was determined as the median value of pixels immediately above and below each band.

2.3 Molecular biology

2.3.1 Reagents

Reagents for reverse transcription and quantitative reverse transcription polymerase chain reaction (QPCR) were acquired from Promega (Madison, USA) and BioRad (California, USA) unless otherwise stated. All primers were purchased from Eurofins MWG Operon (Ebersberg, Germany).

2.3.2 Agarose gel electrophoresis

Agarose gels (between 1.2% and 2% agarose) were prepared by adding electrophoresis grade agarose to 0.5X TBE buffer (45mM Tris-borate, 1mM EDTA). The mixture was heated in a microwave until all the agarose had dissolved. Ethidium bromide was then added to a final concentration of 0.5µg/ml, the gel poured and allowed to set at room temperature. DNA or RNA samples were made up in 6X sample buffer (30% (v/v) glycerol, 0.25% (w/v) bromophenol blue, 0.25 % (w/v) xylene cyanol FF), loaded onto the gel and resolved in a horizontal electrophoresis tank containing 0.5X TBE buffer run at 100V for approximately an hour. DNA or RNA bands were visualised using an GeneFlash UV transilluminator (Syngene, Cambridge,UK).

2.3.3 Primer design and validation

Unless otherwise stated, primers were designed in-house, aiming for the following: a 20mer with approximately 50% GC content, a melting temperature (Tm) of approximately 60^{o}C, a GC clamp of 1-2 nucleotides at

the 3' end and an amplicon of 80-250 spanning an exon boundary. The primer Tm's and the likelihood of primer dimers or secondary structure formation were checked using NetPrimer (www.premierbiosoft.com/netprimer /index.html).

Initial assessment of Primer pairs was performed using an endpoint PCR. 2µl of cDNA (which was prepared as described in section 2.3.5), 1.5µl each of forward and reverse primer (both at 100µM concentration) and 15µl of Hotstar Taq Mastermix (Qiagen) were made up to 30µl in nuclease-free sterile distilled water. PCR was performed in a ThermoHybaid Px2 thermocycler (Thermo Scientific) using an activating step (95^{o}C for 5 minutes) followed by 40 cycles at the following temperatures: 94^{o}C for 30s, 60^{o}C for 30s, 72^{o}C for 30s. The PCR product was assessed by electrophoresis on a 2% agarose gel as described in section 2.3.2. Primer pairs were judged satisfactory if there was a single PCR product at the expected molecular weight, and there were minimal primer dimers visible. Primer pairs were also validated by QPCR (section 2.3.6), where melt curves were assessed for the presence of primer dimers or secondary products. A list of QPCR primers is given in table 2.8.

2.3.4 RNA extraction

Cell lysis and extraction of RNA was performed using an RNeasy Mini kit and QIAshredder columns (Qiagen) as per the manufacturer's instructions. An in-column DNAse treatment step was included for samples in which QPCR for PTEN or PTENP1 was to be performed. Each primer pair amplifies across a single exon and the primers therefore also detect genomic PTEN and PTENP1 respectively. The DNAse step was therefore included to remove all genomic contamination from the RNA. The RNA concentration and purity of each sample was assayed using a ND-1000 NanoDrop spectrophotometer (Thermo Scientific, Massachusetts, USA). The ratio of absorbance at 260nm to that at 280nm was assessed, and a ratio of between 1.8 and 2.0 was considered satisfactory. RNA integrity was also assessed by electrophoresis

Target	Primers (Tm in ^{o}C)	Amplicon (bp)
Actin	ACTBF: CACCTTCTACAATGAGCTGCGTGTG (64.6) ACTBR: ATAGCACAGCCTGGATAGCAACGTAC (64.8)	158
PDK1	PDPK1for: AAGCAGGCTGGCGGAAACC (61.0) PDPK1rev: AGAACTTTGTTGACAGGATCC (57.3)	142
PTEN[¶]	PTEN_FW: GTTTACCGGCAGCATCAAAT (55.3) PTEN_RV: CCCCCACTTTAGTGCACAGT (59.4)	197
PTENP1[¶]	PTENP1_FW: TCAGAACATGGCATACACCAA (55.9) PTENP1_RV: TGATGACGTCCGATTTTTCA (53.2)	152
TNFAIP3	TNFAIP3FOR: TGCCCAGGAATGCTACAGATAC (60.3) TNFAIP3REV: TGGACGGGGATTTCTATCACC (59.8)	227
PRPF8	PRPF8FOR: TATGACCACCAGCCGTTGAG (59.4) PRPF8REV: CCATATTGAGTGCCTTGGACG (59.8)	186
OTUD1	OTUD1For: CCGACCATCTCGACCACTTC (61.4) OTUD1Rev: GTGTCCGTTACTGAGCCAACTG (62.1)	229
ATXN3*	RT_ATXN3_F1: GTATGCAAGGTAGTTCCAGAAAC (58.9) RT_ATXN3_R1: TGTTGCTGCTTTTGCTGCTGT (57.9)	126
ATXN3L	ATXN3L_FW: GAACTAAGCCGCCAAGAAACC (59.8) ATXN3L-RV: GCTTCTGTTCCTGCTGATGC (59.4)	186
JOSD1	JOSD1_FW: AAGATGCCCGAGTGGATTGG (59.4) JOSD1_RV: TCCTCCAACTCTGATGAGCCTC (62.1)	126
USP20	USP20_FW: ACCTTTGCCCTCACCTTGAC (59.4) USP20_RV: TGAATGGTGCTGTGGTCAGC (59.4)	174
SCG3	SCG3for: GATCCAGATGGTCTTCATCAAC (58.4) SCG3rev: CTGATTCTCAGTCCAGCTTGTG (60.3)	266

Table 2.8. QPCR primers used in this screen. All primers are oriented in 5' to 3' direction. [¶]Primers designed by Poliseno *et al*. [375]. *ATXN3 primers were used at half the standard concentration, to reduce primer dimer formation.

on a 1.2% agarose gel. This was prepared as described in section 2.3, with added precautions to avoid RNAse contamination. These included cleaning the equipment with RNaseZAP (Sigma-Aldrich) and the use of diethylpyrocarbonate (DEPC) treated water to prepare buffers. RNA samples were made up in 6X sample buffer, heated to 80^{o}C for 2 minutes, loaded onto the gel and resolved as described in section 2.3. Degraded RNA was suggested by the presence of a low molecular weight smear, while RNA of good quality was indicated by the presence of two clear bands representing 28S and 18S ribosomal RNA at a ratio of approximately 2:1.

2.3.5 Reverse transcription

For each sample, a reaction mix containing 1µg RNA and 0.5µg of oligo dT primer made up to 11 µl with nuclease free distilled water was incubated at 70^{o}C for 5 minutes, following which tubes were immediately chilled on ice. To each reaction mix, the following was added: 4µl of 5x reverse transcription buffer (MBI Fermentas, NY, USA), 2µl PCR nucleotide mix (containing dATP, dCTP, DGTP and dTTP each at 10mM in water, Promega), 0.5µl RNasin and 1.5µl of Nuclease free ddH_2O. The reaction mix was incubated at 37^{o}C for 5 minutes, then held at 37^{o}C while 1µl of M-MuLV reverse transcriptase (MBI Fermentas, NY, USA) was added. This was followed by incubation at 42°C for 1 hr for synthesis of complementary DNA (cDNA), and then denaturation at 70°C for 10 min. Samples (cDNA) were immediately removed to ice for 5 minutes, then diluted to 100µl with nuclease free distilled water and stored at -20^{o}C. An RT- control was included in each reverse transcription experiment. This was generated as described above, however the reverse transcription enzyme was not added to the reaction mix.

2.3.6 Quantitative RT Polymerase Chain Reaction (QPCR)

This was performed using an IQ5 real time PCR detection system and SYBR green supermix (BioRad). A total reaction volume of 15µl was made up for each sample, consisting of 1µl of cDNA (prepared as described in section 2.3.3), 0.25µl each of forward and reverse primers (at 20µM) and 7.5µl of iQ SYBR green supermix (2X), made up with nuclease free distilled water. In the case of ATXN3, primers were used at half the above concentration to minimise primer dimer formation. Samples were arrayed on a 96 well PCR plate (Biorad #), and sealed with a plastic cover (Biorad #). Each QPCR experiment included blank (no template) and RT- (section 2.3.5) controls. An initial enzyme activation/denaturation incubation at 95°C for 3 min was performed followed by 40 cycles using a 2-step PCR protocol (denature/anneal/read) for 30 seconds at each temperature. Melt curves were read at 1°C intervals from approximately 55 to 95°C to check for amplification of a single product. Data were analysed using BioRad software, and a cycle threshold (Ct) set in exponential amplification phase. Ct values

were determined for each sample and compared to the reference gene (actin) using the $2^{-\Delta\Delta Ct}$ method [376].

2.4 Live cell imaging and analysis

2.4.1 Reagents

Cells were cultured in standard plastic 96 well plates (Corning, #3595). During imaging, cells were maintained in Hanks buffered saline solution (HBSS). 10X HBSS (#14065-049) was obtained from Gibco, diluted to 1X HBSS with sterile, autoclaved water and supplemented with 10mM HEPES, 2mM glutamine and 1mM pyruvate. DRAQ5 and DRAQ7 were obtained from Biostatus (Shepshed, UK). Wortmannin, LY294002, PI-103 and TGX-221 were obtained from Calbiochem (Merck, Darmstadt, Germany). GDC-0941 was obtained from Axon Medchem (Groningen, The Netherlands) while MK-2206 was obtained from Selleck Chemicals (Houston, USA). HBX90,397 and HBX90,659 were a gift from Hybrigenics (Paris, France). Ratjadone A was obtained from Alexis Biochemicals (Enzo, Exeter, UK).

2.4.2 Translocation screen

2.4.2.1 Assay Development

The translocation screen (chapter 4) employed FKHRL1-U2OS cells (Thermo-Fisher), which stably express FOXO3-EGFP. In these cells, FOXO3-EGFP subcellular localisation reflects PtdIns3-K activity. In the presence of PtdIns3-K signalling FOXO3-EGFP is predominantly cytoplasmic, while PtdIns3-K inhibition leads to its nuclear translocation. An initial experiment to assess the effects of different PtdIns3-K inhibitors was carried out. FKHRL1 cells were seeded in a 96 well plate at a density of 5,000 cells per well, in 200µl full media containing geneticin, and allowed to attach overnight.

The following day the cells were washed and the media replaced with phenol red free media containing 2.5µM DRAQ5. Following a 15 min incubation, this was replaced with 175µl of warm HBSS, and the cells transferred to an

Inhibitor	Main targets (reported *in vitro* IC50)	Concentrations used
Wortmannin	Non-specific PtdIns3-K inhibitor (2-4nM)	100nM, 200nM
LY294002	Non-specific PtdIns3-K inhibitor (1.4μM)	10μM, 20μM
PI-103	p110α (4nM), p110β (8nM), p110δ (>500nM), DNA-PK (2nM), mTORC1 (20nM), mTORC2 (80nM)	100nM, 200nM
TGX-221	p110β (5nM), p110δ (100nM), p110α (5μM), p110γ (3.5μM)	100nM, 1μM
MK-2206	Akt1 (8nM), Akt2 (12nM), Akt3 (65nM)	100nM, 1μM

Table 2.9. PtdIns3-K inhibitors used in this study. Inhibitor stock solutions were made up in DMSO, and then added to media to the final concentrations listed above. Final DMSO concentrations did not exceed 0.2%. The IC50 values were obtained from the relevant datasheets. (IC50: half maximal inhibitory concentration)

Eclipse Ti-E fluorescence microscope (Nikon, Tokyo, Japan), with heated chamber and automated stage. A single position was acquired per well, and imaged in both green (EGFP) and far-red (DRAQ5) channels. Each imaging position was saved, thus enabling further imaging loops of the same positions to be performed. Imaging was performed with the 20X objective. NIS Elements software was used for all image acquisition (Nikon) and 2 x 2 binning was applied. The cells were then returned to the tissue culture hood where PtdIns3-K inhibitors (table 2.9) were added to the final concentrations indicated. The nuclear export inhibitor (Ratjadone A) was used as a control at a final concentration of 5nM or 10nM. The cells were then immediately returned to the microscope chamber. Each well was imaged 5 minutes after the addition of inhibitor and every 5 minutes thereafter. Focus was maintained over the course of the experiment using PFS (Perfect Focus System, Nikon). Approximately 90 minutes after addition of the inhibitor, the media containing inhibitor was removed and replaced with 1X HBSS. The cells were then imaged for a further 60 minutes.

2.4.2.2 Procedure for Translocation screen and deconvolution

FKHRL1-U2OS cells were transfected with siRNA as described in section 2.1.3.2. 48 hours after transfection, the media was removed and the cells

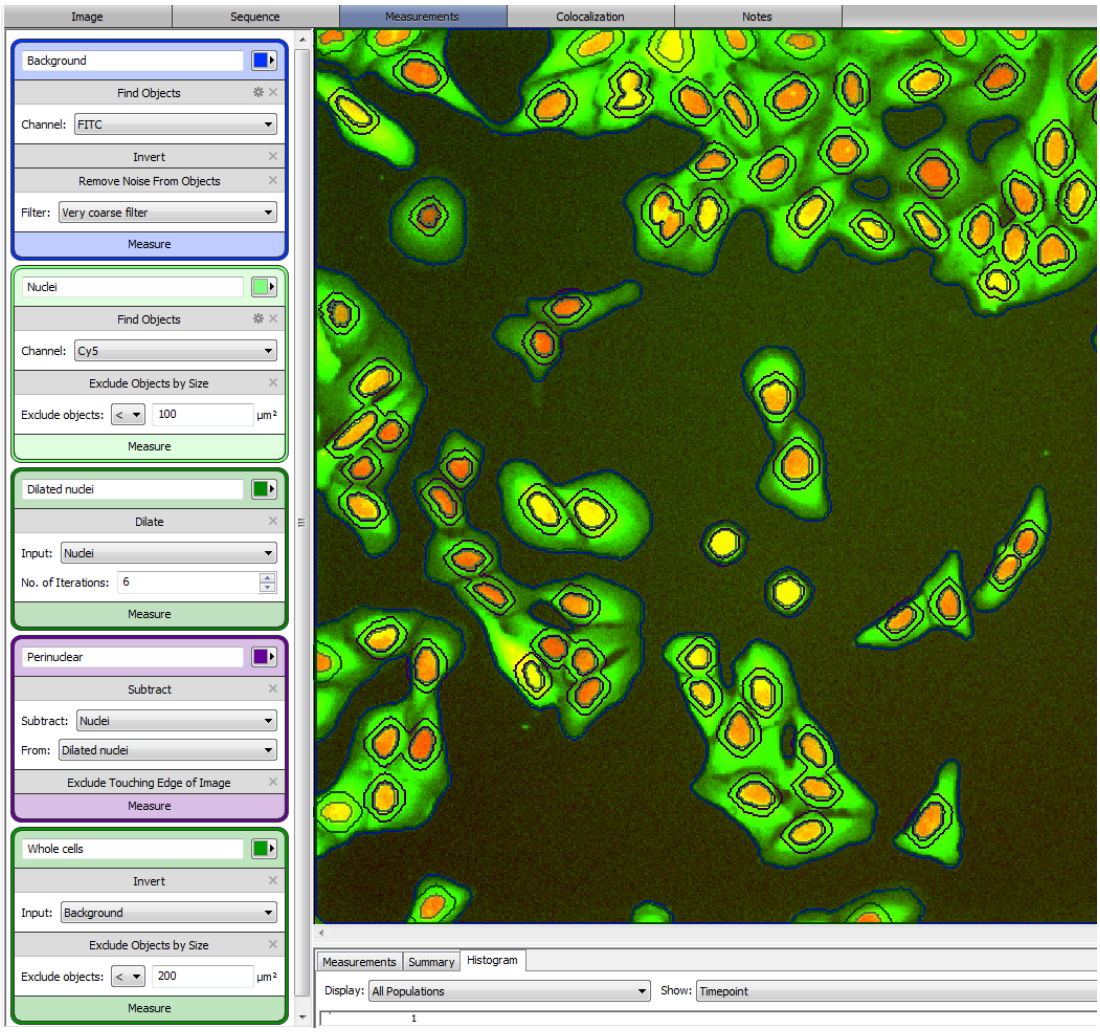

Fig 2.2. Image segmentation using Volocity version 6. A screenshot is shown highlighting the protocol employed to segment images into different compartments for further analysis. Objects were identified using automatic thresholding, which was then manually adjusted to maximise discrimination. The perinuclear torus was defined by dilating the nuclei by 6 iterations (pixels), and then subtracting the nuclear compartment from the dilated nuclei. (FOXO3-EGFP and DRAQ5 fluorescence was detected in the green [FITC] and far-red [CY5] channels respectively).

washed prior to the addition of HBSS containing 2.5µM DRAQ5, after which the cells were replaced in the incubator for 15 min. The media was then replaced with 150µl of fresh warm HBSS and the cells imaged as described in section 2.4.2.1. The cells were transferred to a cell culture hood, and PI-103 added to a final concentration of 100nM, after which the plate was immediately replaced and further imaging performed as described in section 2.4.2.1.

2.4.2.3 Image analysis

Image analysis was performed using Volocity version 6 software (PerkinElmer, Massachusetts, USA). In the nuclear translocation screen, this allowed segmentation of images into different compartments (fig 2.2) and hence quantification of FOXO3-EGFP distribution. Mean FOXO3-EGFP fluorescence in each cellular compartment was calculated and corrected for background fluorescence by subtraction of the mean FOXO3-EGFP level in the background compartment. Accurately outlining the cytoplasm proved impossible in certain cases due to changes in cell morphology and low-level fluorescence in the cytoplasm, such as occurred following profound nuclear translocation (fig 4.1A). In view of this, a perinuclear torus was defined for each cell (fig 2.2), and fluorescence within this compartment used to reflect cytoplasmic FOXO3-EGFP levels. As shown in fig 4.1, this allowed the calculation of a nuclear/cytoplasmic ratio, which reflected FOXO3-EGFP translocation in response to PtdIns3-K inhibition.

2.4.3 Live-cell assessment of synthetic lethality

2.4.3.1 Experimental procedure

Cell culture, transfections and imaging were generally performed as described in section 2.4.4, however imaging was performed every hour rather than every 5 minutes. While initial experiments used morphological changes to identify dead or dying cells, latterly DRAQ7 was used for this purpose. Here, the media was changed to HBSS containing 3μM DRAQ7 and PtdIns3-K inhibitor at the desired concentration. The cells were then placed in the microscope chamber and imaged every hour for the duration of the experiment. At the end of the experiment, the media was changed to fresh HBSS containing 5μM DRAQ5, the cells incubated for 15-20 minutes and imaged a final time.

Interaction between PtdIns3-K inhibition and the Hybrigenics inhibitors was performed as follows. A 96 well plate was seeded with 8000 cells per well in full media and incubated overnight. The media was then replaced with HBSS

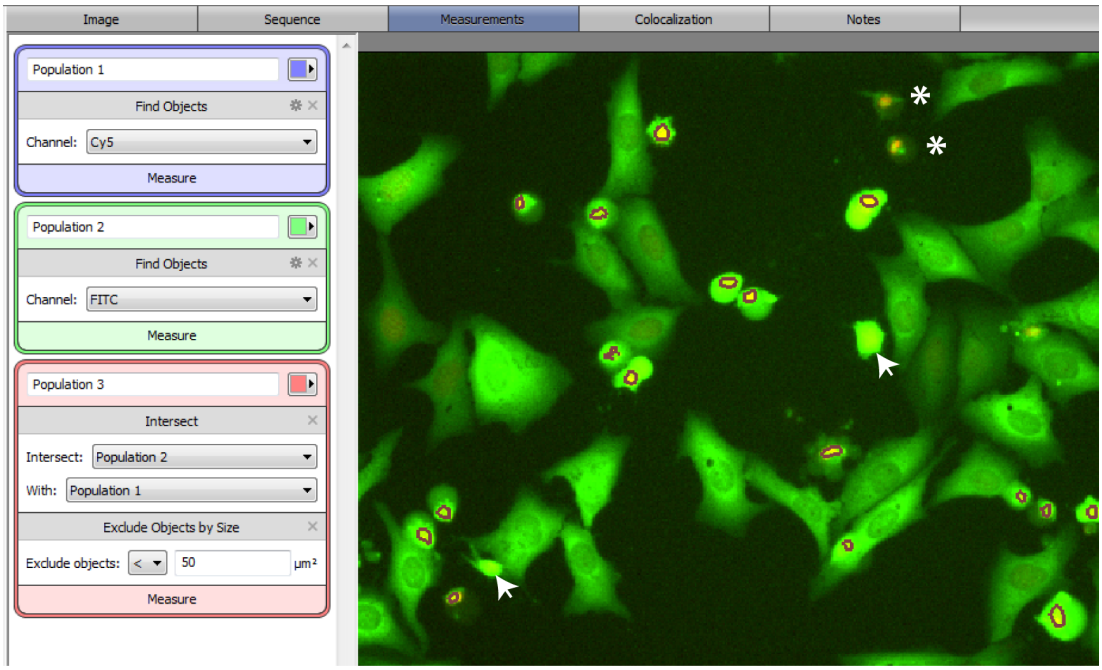

Fig 2.3 Quantification of cell death using changes in morphology and fluorescence. Changes in cell morphology (rounding up and associated increase in intensity of both FOXO3-EGFP and DRAQ5 fluorescence) indicated probable cell death (section 5.2)**.** Counting of these cells was facilitated by Volocity software. The cells were identified by thresholding in both channels, in each case thresholds were manually set to maximise discrimination between live and dead cells. Cell populations 1 and 2 were identified in the far-red (Cy5) and green (FITC) channels respectively. Population 3 was defined as the intersection between populations 1 and 2 and contained cells which exhibited intense fluorescence in both compartments; these were counted and exported. Cell fragments were excluded by size (<50µm^2). As indicated by the arrowheads, it was not always possible to identify all dead/dying cells by thresholding. Additionally, some cells that had died earlier in the experiment began to fragment leading to loss of fluorescence (indicated by an asterisk), and these cells were also difficult to identify using Volocity. Both latter cell populations were therefore manually counted and added to the Volocity count.

containing 3µM DRAQ7 and replaced in the incubator. Meanwhile serial dilutions of PI-103 and the Hybrigenics inhibitors were prepared in warm HBSS. These were then added to each well such that each row had a different concentration of PI-103, and each column a different concentration of HBX90,397 or HBX90,659. The cells were then imaged as described above.

2.4.3.2 Quantification of cell death

In section 5.2, dead or dying cells were identified as brightly fluorescent, rounded up cells. These were identified in Volocity using both the green (FITC) and far-red (Cy5) channels, using fluorescence thresholds that were manually adjusted to only include cells that exhibited the above changes (fig 2.3). The number of cells identified in this manner could then be counted using Volocity. However, it was not possible to set thresholds that identified all dead/dying cells, and any such cells that were not identified by Volocity, were counted manually and added to the Volocity count (fig 2.3). The number of dead cells was then divided by the total number of cells, which was obtained by counting the number of nuclei (in the far-red channel), to provide an estimate of cell death. This method was however observer dependent, and also included a small population of dividing cells which underwent similar morphological changes. As described in sections 2.4.3.1 and 5.3, latter experiments used a different method to enumerate cell death. DRAQ7 is a far-red fluorescent dye that is only taken up by dead or dying cells. DRAQ7 positive cells were therefore counted using Volocity and expressed as a percentage of the total number of cells. The latter was quantified from the number of cells taking up DRAQ5, which was added at the end of the experiment, as it emits light of a similar wavelength to DRAQ7.

2.5 Data analysis

Data sets were all plotted and analysed in Microsoft Excel 2008. All error bars reflect standard deviation. Where reported statistical tests utilised a two tailed student's t-test. In the translocation screen, the rate of nuclear translocation was estimated using the slope of the linear regression of the nuclear/cytoplasmic ratio between timepoints 2 and 5. This utilised Excel's slope function, and is defined as the 'vertical distance divided by the horizontal distance between any two points on the line'

Chapter 3

Identifying DUB regulators of the abundance of PtdIns3-K pathway components.

3.1 Introduction

The phosphatidylinositol 3-kinase (PtdIns3-K) signalling pathway is subject to multiple regulatory mechanisms including phosphorylation, acetylation and ubiquitylation (sections 1.5.2 and 1.5.4). The latter is an extremely versatile post-translational modification, and recent work has begun to uncover the multiple functions that ubiquitylation plays in PtdIns3-K signalling, including examples of regulation of protein stability, localisation and activity (section 1.5.4). Ubiquitin's ability to regulate multiple aspects of protein function is enabled through differing chain structures [377], and through the activity of deubiquitylating enzymes (DUBs), which provide reversibility ([80] and section 1.3). However, the role of DUBs in the PtdIns3-K pathway remains poorly defined (section 1.5.4).

The principal aim of this project was to employ a systematic approach to the identification of DUBs involved in the PtdIns3-K pathway. Two main strategies were employed, here the first of these is described; utilising immunoblotting to assay the protein expression levels of components of the PtdIns3-K pathway following a DUB siRNA screen.

As discussed in section 1.5, several components of the PtdIns3-K pathway are known to be degraded through the ubiquitin-proteasome system (UPS), and it is conceivable that deubiquitylation, through the action of DUBs, may rescue proteins thus destined for degradation. Depletion of a DUB acting in this manner would lead to increased degradation of its substrate, with a concomitant decrease in its protein level in the cell. This in turn can be detected by immunoblotting, which I have therefore employed as a readout in these screens. Notably, in addition to directly removing ubiquitin chains

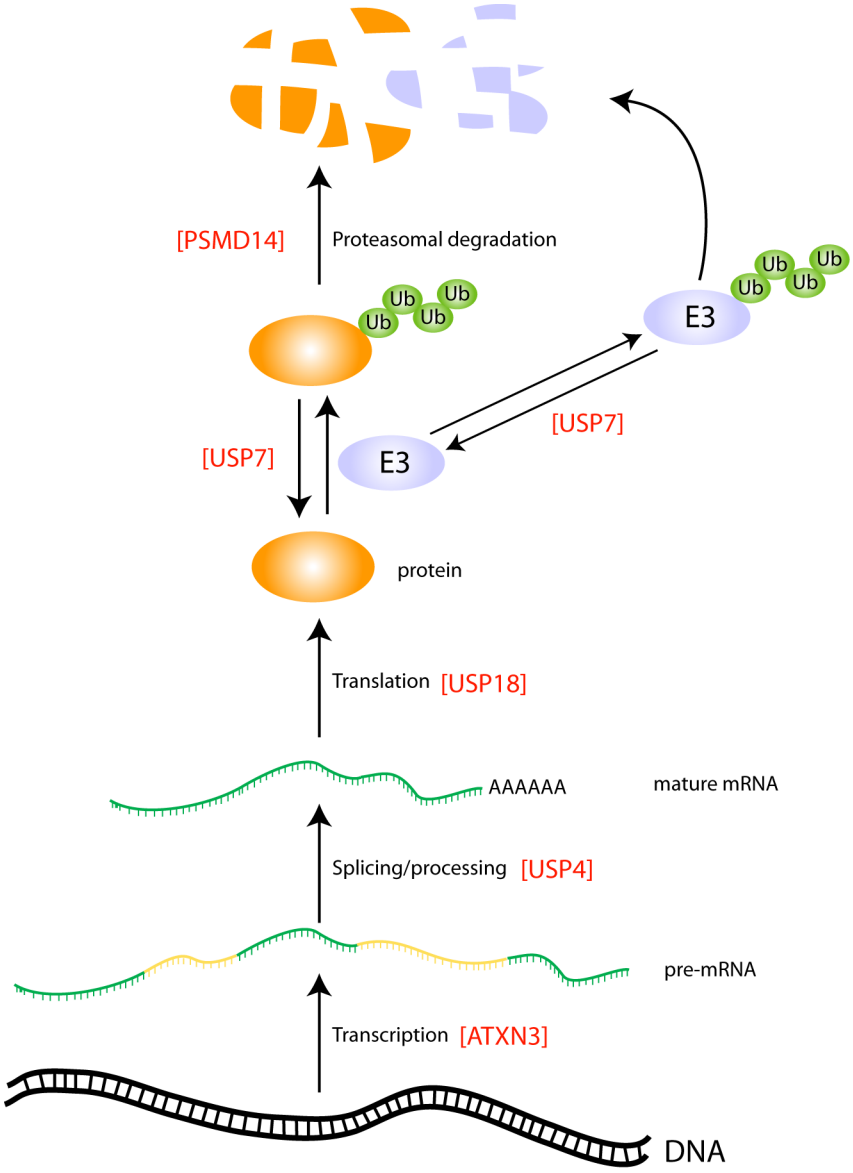

Fig 3.1. DUBs regulate multiple steps in protein synthesis and degradation. Protein abundance is determined by a balance between synthesis and degradation, each of which involves several steps. An example of a DUB involved in each step is given in parentheses and these are referred to in references [199, 209, 378-381]. (The green ovals depict K48 polyubiquitin chains, yellow and green mRNA segments respect introns and exons respectively.)

from proteins and thus leading to their stabilisation, DUBs may also have the opposite effect on proteins through stabilisation of the cognate E3 ligase (fig 3.1). The abundance of a protein is moreover dependant on several other factors, such as transcription and translation, which may equally be influenced by DUB depletion (fig 3.1). DUBs are also involved in the regulation of lysosomal degradation [382], and have recently been implicated

in autophagy [383]. Immunoblotting not only will reflect any of these mechanisms that affect protein levels but also has the potential advantage of detecting either mono- or polyubiquitylated forms of the proteins, which may indicate non-proteolytic regulation. Previous DUB screens have successfully utilised immunoblotting; an example being the identification of USP1 in the regulation of FANCD2, where USP1 depletion stabilised a monoubiquitylated form of FANCD2 [384].

3.2 DUB screening strategy and workflow

In this chapter I set out to screen for DUB regulators of the abundance of fourteen components of the PtdIns3-K pathway, namely p110α, p110β, p110γ, p85α, p170, PTEN, Akt1, Akt2, Akt3, mTOR, PDK1, FOXO1, FOXO3 and FOXO4 (fig 3.2, section 1.5.2). In order to generate sufficient protein lysate to immunoblot for each of these targets, a colleague (Han Liu) and I utilised a DUB siRNA library consisting of pools of siRNA oligonucleotides directed at each of 92 DUB targets (section 2.1.1 and Appendix A) to generate a library of lysates each derived from cells depleted of a different DUB (fig 3.3). Both non-targeting siRNA and mock-transfected controls were included. The work was performed in A549 cells grown under constant full-serum conditions. Serial lysis buffers were employed to provide crude fractionation of lysate (section 2.1.4.2). The lysates from each fraction were arrayed in multiple storage plates, each consisting of lysates from every DUB depletion and control. These plates were then stored and used when required for this and other projects (fig 3.3).

DUB RNAi libraries have previously been employed in the identification of DUB regulators of several different cellular processes in our laboratory and elsewhere [125, 192, 384-386]. This strategy has several potential advantages over a genome wide approach. These are partly practical, concerning the amount of reagents and manpower required. In addition some readouts would be difficult to use in a genome wide screen. For example, it would be impractical to perform immunoblotting for several different targets on all the lysates from

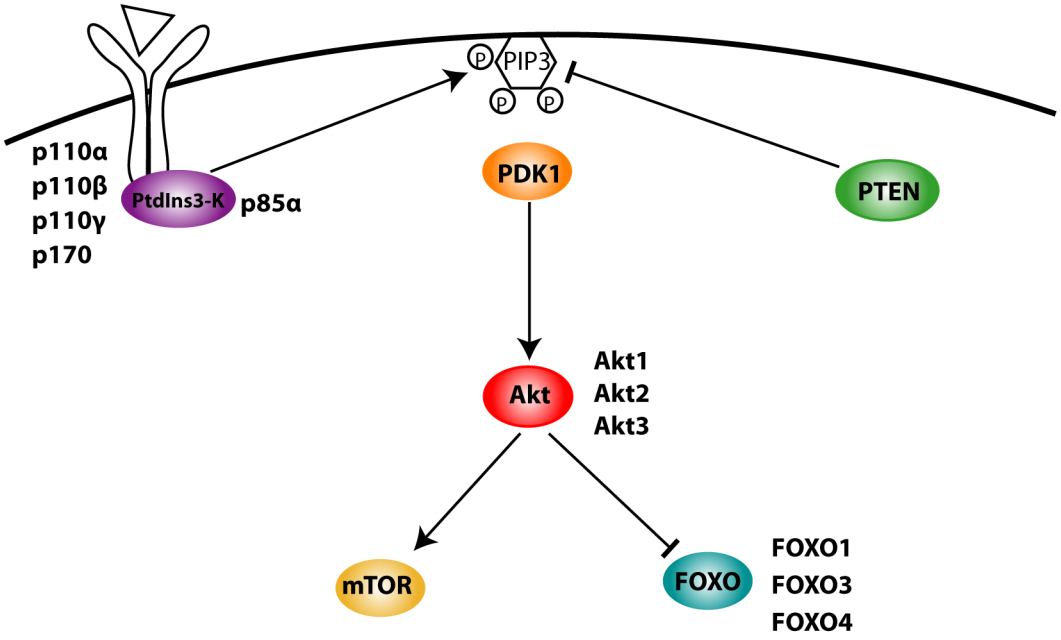

Fig 3.2. Components of the PtdIns3-K pathway selected for DUB siRNA screening. DUB siRNA screens were performed on a subset of components, which were selected on the basis of their involvement in malignancy. Where multiple isoforms of proteins exist, those chosen for investigation are shown next to the protein. Catalytic and regulatory PtdIns3-K subunits are shown on the left and right respectively.

a genome wide screen. A focused screen also allows a greater proportion of hits to be validated, and harnesses local expertise and availability of reagents relating to a specific area of research, in this case the DUBs. Furthermore, this approach promotes experience relating to a specific RNAi library, and an appreciation of the overall knockdown efficiency and the likelihood of both false-positives and false negatives. A potential disadvantage on the other hand, relates to as yet unidentified DUBs, which would be covered in a whole genome screen.

Off-target effects are a frequent source of false-positive results in siRNA screens, and may be controlled for by use of either redundancy or rescue experiments [387, 388]. In this study, hits from the screens were validated by deconvolution of the oligonucleotide pool (fig 3.3iv). This involved transfecting with each of the four, redundant, siRNA oligonucleotides from the pool separately; recapitulation of the effect observed with the pool by

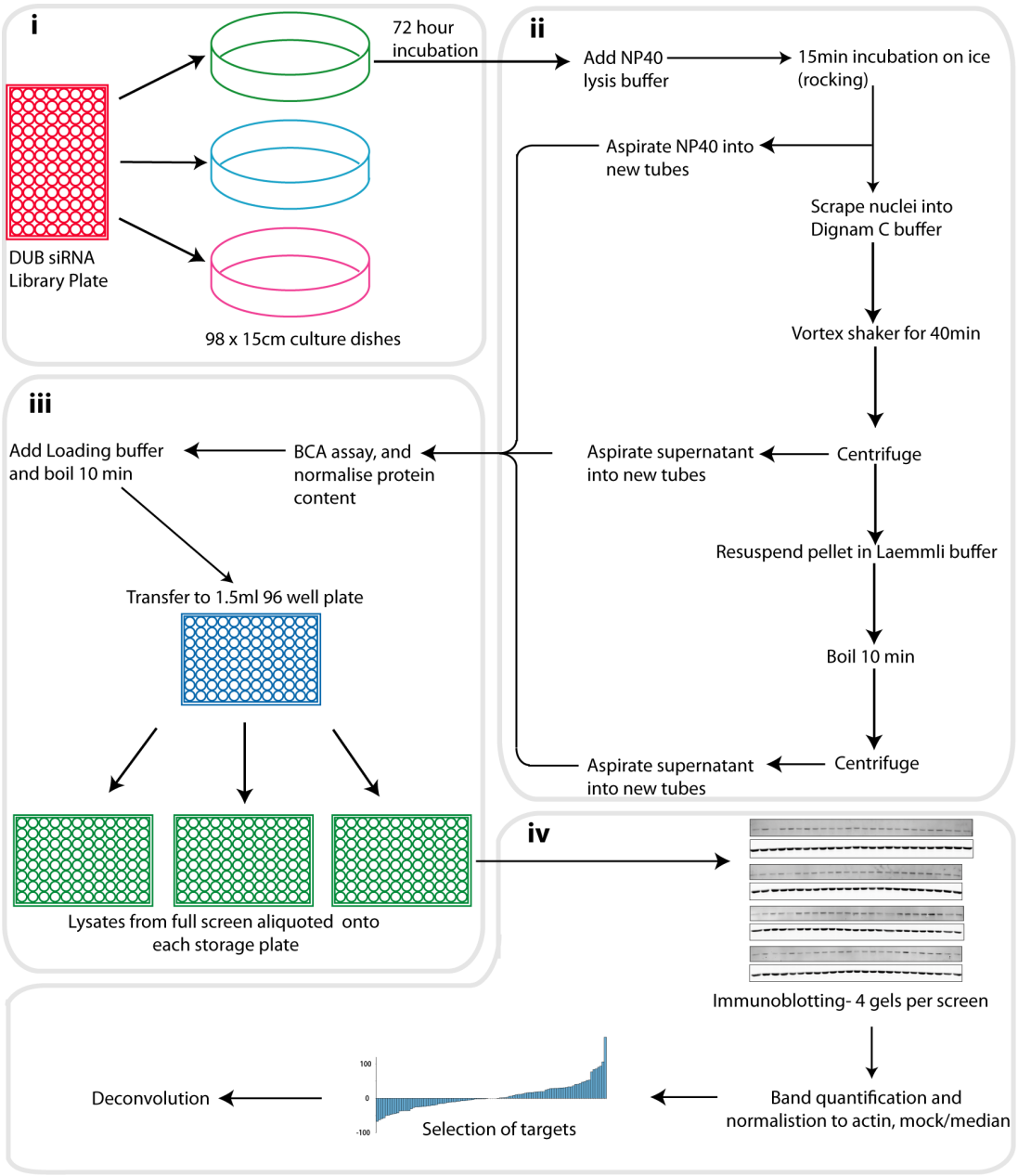

Fig 3.3. Immunoblot screening for DUB modulators of the PtdIns3-K pathway. **i**. A549 cells were seeded in 15cm dishes and either mock-transfected or transfected with siRNA directed at 92 DUBs or non-targeting siRNA (Qiagen). **ii**. Following a 72-hour incubation, the cells were lysed using a sequence of three buffers leading to crude fractionation of lysate. **iii.** For each fraction, the protein concentration of lysates was assayed, adjusted to a set same concentration, loading buffer added and the lysate boiled for 10 minutes. The lysates were arrayed on 96 well plates, with each plate containing extracts for the entire library in aliquots of equal volume and concentration. **iv**. Lysates were then run on SDS-PAGE gels and immunoblotted for proteins of interest, and reference protein. Detection was performed using an infrared scanner (Odyssey, LiCor), and quantification of bands (integrated intensity) was performed using Odyssey software. Initial validation of hits was performed through deconvolution of the oligonucleotide pool.

multiple individual oligonucleotides increases the likelihood the effect is on-target [388]. Knockdown with two or more oligonucleotides resulting in a change of protein level by 20% or more, in the same direction as the screen, was taken as confirmatory. Knockdown with the siRNA pool was usually performed alongside the single siRNA transfections to confirm the effect seen in the screen.

A complementary method involved the use of endoribonuclease-prepared short interfering RNA (esiRNA). This is an alternate method of RNAi, which has been developed relatively recently and which potentially reduces off-target effects [389]. JiaLih Wong in our laboratory has recently generated an esiRNA library against the majority of DUBs, a subset of which have been used for secondary validation in this study.

3.3 Quality control of DUB lysate library

Three main measures were employed for quality control. Firstly, examination of cells by light microscopy was performed prior to cell lysis. Depletion of most of the DUBs was associated with little visible toxicity. This was evidenced by an estimated confluency of between 70 and 90%, few floating cells in the media and healthy looking cells. Notable exceptions included USP1 and USP11 depletion, which both showed evidence of cellular toxicity. A reduced cell confluence of 40-50% with increased numbers of floating cells and an increased proportion of cells with granular/foamy cytoplasm was observed for both. Depletion of several other DUBs (USP42, YOD1, OTUD7B, USP51 and PRPF8) was also associated with cell toxicity, albeit to a lesser degree than USP1 and USP11.

The microscopy findings were supported by an assay of the protein concentration of lysates (fig 3.4). This reflects the protein yield following cell lysis and is a crude surrogate measure for cell number. The median protein concentration was 2.6 µg/µl, with an interquartile range of 2.4 – 3.0 µg/µl

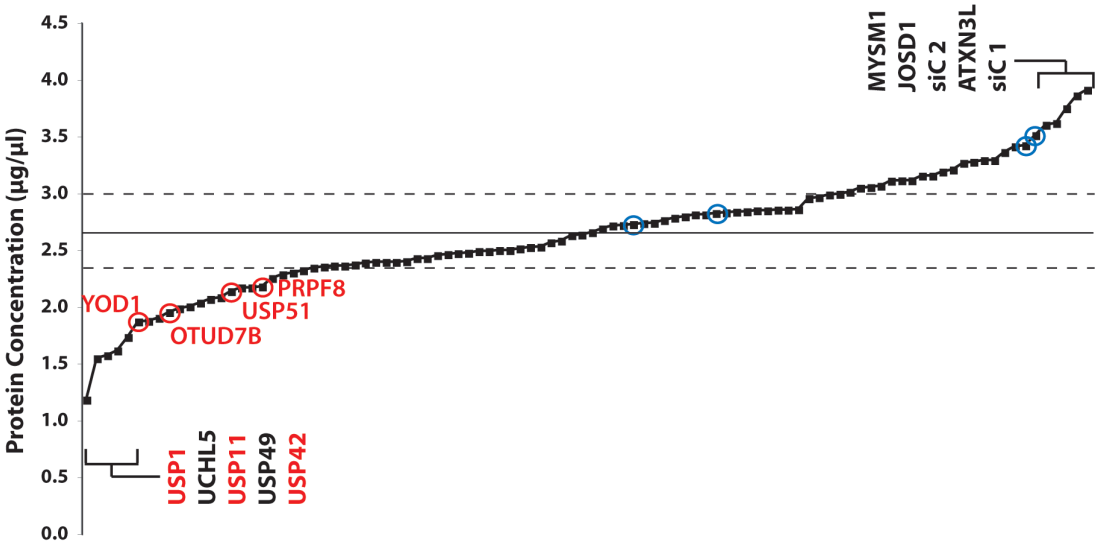

Fig 3.4. Protein concentration of DUB lysate library. A549 cells were transfected with siRNA from a library consisting of pools of oligonucleotides against 92 DUB targets, incubated for 72 hours and lysed as described in Fig 3.3. The protein concentration of each lysate was assayed; here the concentration of the NP40 fraction is shown ranked from low to high. The five top and bottom ranked DUBs or controls are indicated. DUBs whose depletion resulted in cellular toxicity as evidenced by light microscopic changes are highlighted in red. Mock controls are circled in blue. siC1 and siC2: technical replicates transfected with non-targeting siRNA control. The horizontal line represents the median, and the two dotted lines the 1st and 3rd quartiles. (n=1).

indicating relatively little variability. However, the six control lysates (4 mock-transfections and 2 with a non-targeting siRNA) are all located above the median (fig 3.4). This suggests that depletion of many DUBs may be detrimental to cell viability and/or proliferation. While this is likely to be subtle for the majority, depletion of a small subset of DUBs resulted in particularly low protein concentrations (fig 3.4).

A third measure employed for quality control of the lysate library was the assessment of knockdown efficiency for selected DUBs (fig 3.5). USP15 depletion resulted in an 82% reduction in USP15 protein level (fig 3.5i,ii). Similarly a knockdown efficiency of 72%, 94% and 79% was obtained for USP33, USP47 and PSMD14 respectively (fig 3.5iii,iv). Quantification of the USP15 blots (fig 3.5ii) also indicated extensive variability in USP15 at the protein level in samples depleted of other DUBs (+/- 60% from the mock).

This is likely to be due in part to experimental variability as well as cellular regulatory and compensatory mechanisms. As discussed in section 1.3.2, USP15 is closely related to several other members of the USP family of DUBs (fig 1.3). Despite these similarities, siRNA oligonucleotides against USP11 or USP19 did not significantly reduce USP15 protein levels (fig 3.5Ai,ii), indicating that the oligonucleotides pools are not cross-reactive. While USP4 depletion appeared to increase USP15 protein level on quantification (fig 3.5ii), this was not visually compelling (fig 3.5i) and is likely to represent experimental variation. On the other hand, depletion of the USP33 paralogue, USP20, strongly upregulated USP33 (fig 3.5iii). This has previously been described in our laboratory and is likely to represent an example of paralogue compensation [390]. This will be discussed further in chapter 6.

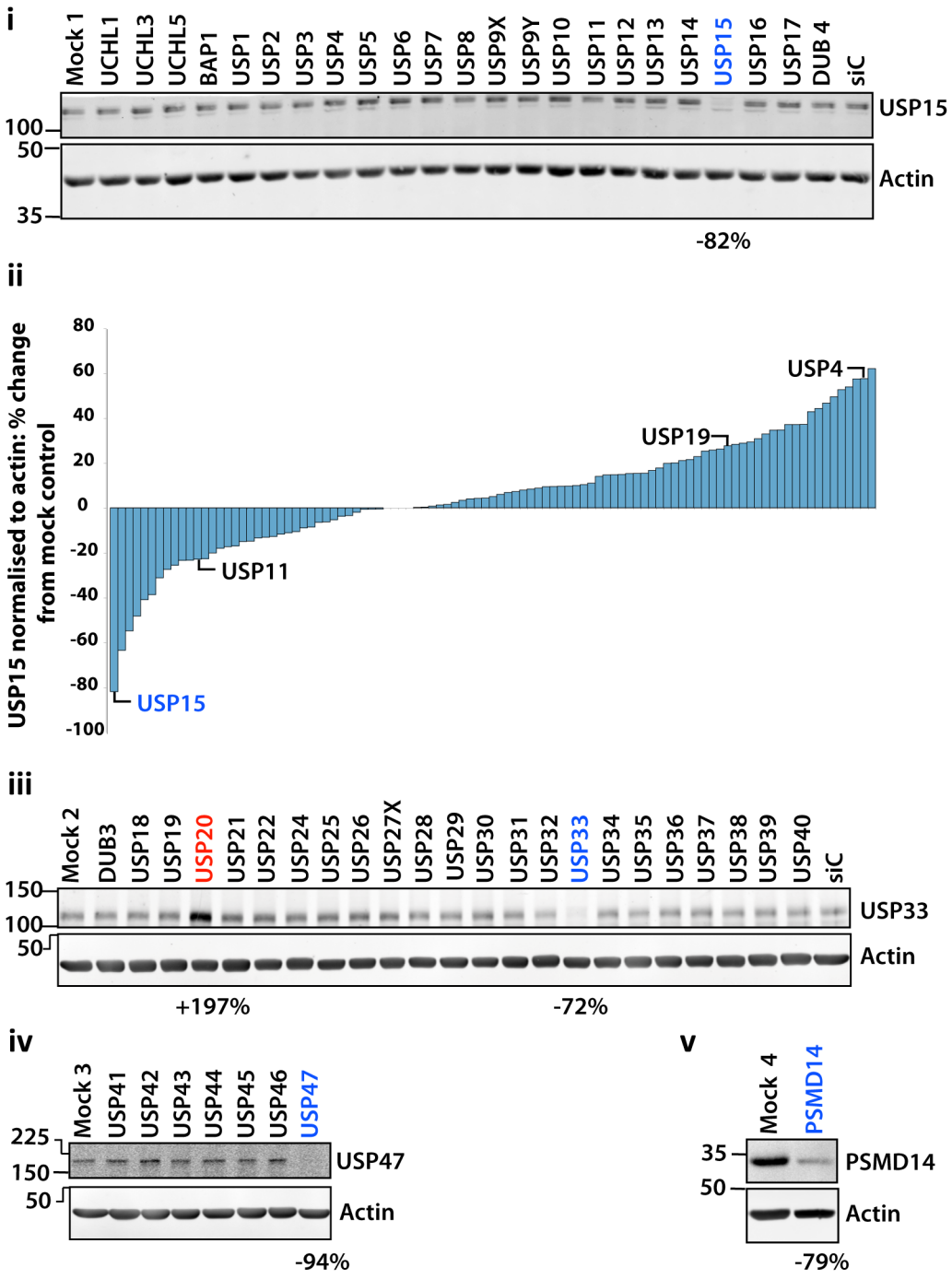

Fig 3.5. Validation of knockdown efficiency in the DUB lysate library. Equal amounts of NP40 protein lysates from the DUB siRNA screen (fig 3.3) were run on SDS-PAGE gels and immunoblotted for the indicated proteins. Imaging and quantification was performed using an Odyssey (LiCor) infrared scanner and software. **i.** Immunoblotting for USP15; one of four blots is shown. **ii**. Quantification of USP15 screen. The USP15 signal for each DUB knockdown was normalised to actin then ranked relative to the mock. **iii, iv, v**. Immunoblotting for USP33, USP47 and PSMD14 respectively using relevant screen lysates. The percentage knockdown compared to the mock is shown under each blot. Upregulation of USP33 by USP20 depletion is also indicated. (siC- non-targeting siRNA control)

3.4 PTEN abundance is regulated by several deubiquitylases.

Through its function as a lipid phosphatase, PTEN inactivates phosphatidylinositol 3,4,5 triphosphate ($PtdInsP_3$), thus acting as a negative regulator of the PtdIns3-K pathway (section 1.5.2). PTEN may be either polyubiquitylated or monoubiquitylated, leading to its degradation through the proteasome [335, 360] or nuclear localisation [57] respectively (section 1.5.4). The latter is essential for full tumour suppressor function of PTEN [57, 391]. The E3 ligases WWP2, NEDD4.1 and XIAP have been implicated in the ubiquitylation of PTEN [335, 336, 359, 360], while USP7 (also known as HAUSP) has been shown to cleave monoubiquitylated PTEN thus regulating its cellular localisation in response to oxidative stress [203]. No other DUBs regulating PTEN have been described thus far.

Identifying DUBs involved in regulating this vital tumour suppressor would be of significant scientific interest, and moreover would have potential relevance in clinical practice, particularly as post-transcriptional modification of PTEN appears to be a common mechanism by which malignancies lose PTEN function [335, 336] (section 1.5.3). I therefore set out to identify potential DUB regulators of PTEN protein level using lysates from the DUB lysate library.

Immunoblotting of NP40 lysates was performed for PTEN and blots are shown in fig 3.6. Marked changes in the level of PTEN can be seen for knockdown of several DUBs, most notably UCHL3, USP20 and YOD1 which decrease PTEN abundance. In contrast, OTUD4 and STAMBPL1 depletion increased PTEN levels. The integrated intensity of infrared fluorescence for each band was quantified using Odyssey (LiCor) software. For each sample, the PTEN signal was normalised to that of actin. A second normalization was applied to allow comparison of data from the four different blots. Two different methods were employed, firstly each band was normalised to the mock control from the same blot (fig 3.7i), in the second the median of the dataset from each blot was used for normalisation (fig 3.7ii). Normalising to a single value (e.g. the PTEN level in the mock control) can readily shift the

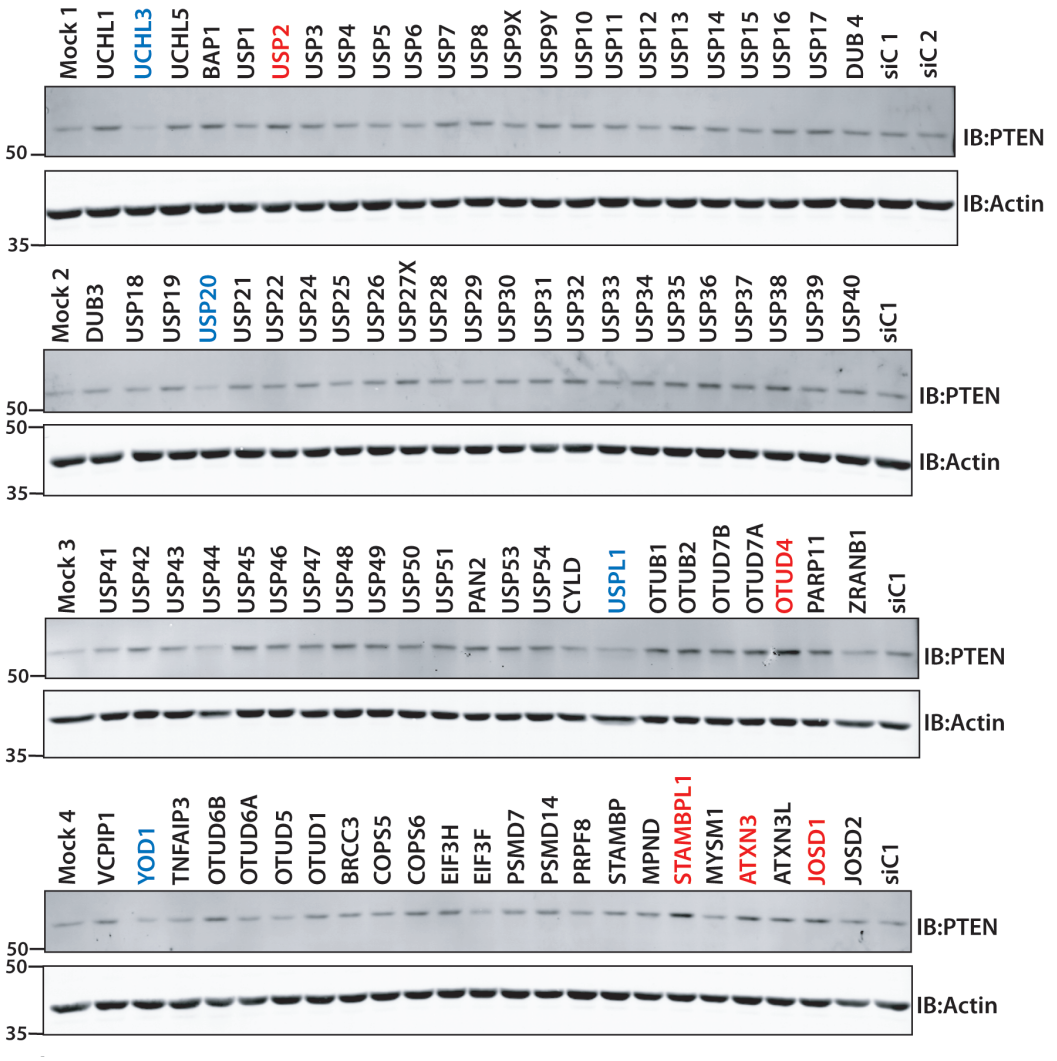

Fig 3.6. An immunoblot screen for DUB regulators of PTEN abundance. NP40 lysates from the DUB screen (fig 3.3) were run on four SDS-PAGE gels. Each blot included a mock-transfected and a non-targeting siRNA (siC) control. The blots were probed for PTEN and actin and imaged by infrared scanner (Odyssey, LiCor). Candidate DUBs selected for deconvolution are highlighted in red (upregulated) or blue (downregulated). (n=1)

entire dataset up or down, if the mock is abnormally low or high. This is seen in fig 3.7i, and the left hand panel of fig 3.7C, where a low value for PTEN in the mock controls has shifted the dataset for each blot upwards. In the screen, the mock and non-targeting controls were run on the extreme left and right respectively, of each gel. The low values for the mock control in each case may therefore reflect an edge effect, due to uneven protein transfer. Normalising to the median relative PTEN level for each blot results

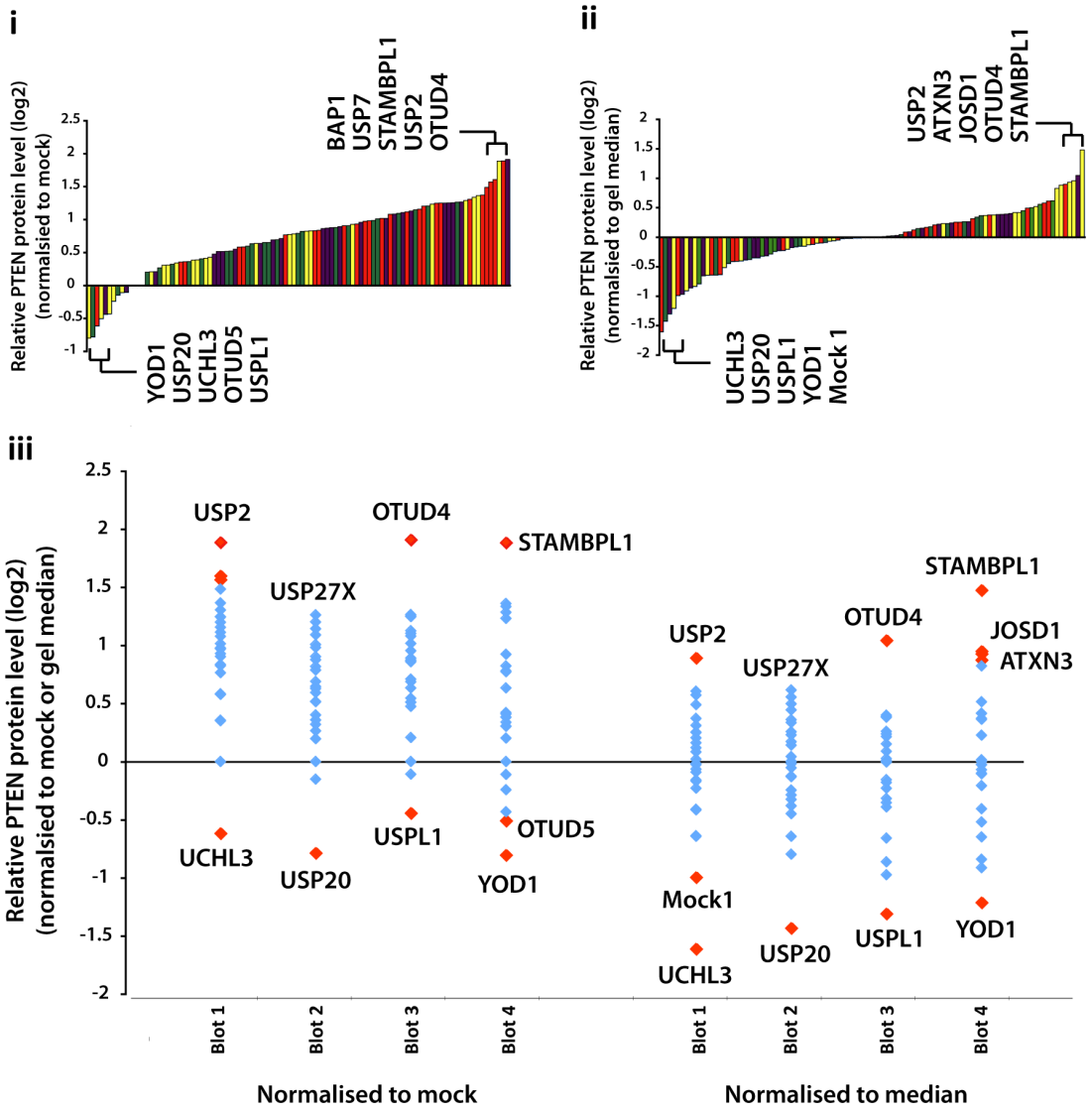

Fig 3.7. Identification of candidate DUBs from a screen for modulators of PTEN abundance. Immunoblotting for PTEN and actin was performed and is shown in fig 3.6**. A.** PTEN bands were quantified (Odyssey, LiCor), normalised to actin and then to the mock control of each blot. **B.** Alternatively the second normalisation was performed to the median PTEN/Actin of each blot. The four different colours indicate the different blots of origin (red- blot 1, green- blot 2, purple- blot 3, yellow- blot 4). **C.** A comparison of the data normalised in these two different manners is plotted separately for each blot. The 5 top and bottom ranked hits are highlighted in each panel. (n=1).

in a more symmetrical distribution (fig 3.7ii,iii). Although this appears to be biased towards blot 4, subsequent deconvolution was successful for three candidates from this blot (fig 3.8). Normalisation to the blot median has been employed as the primary approach in the quantification of subsequent screens.

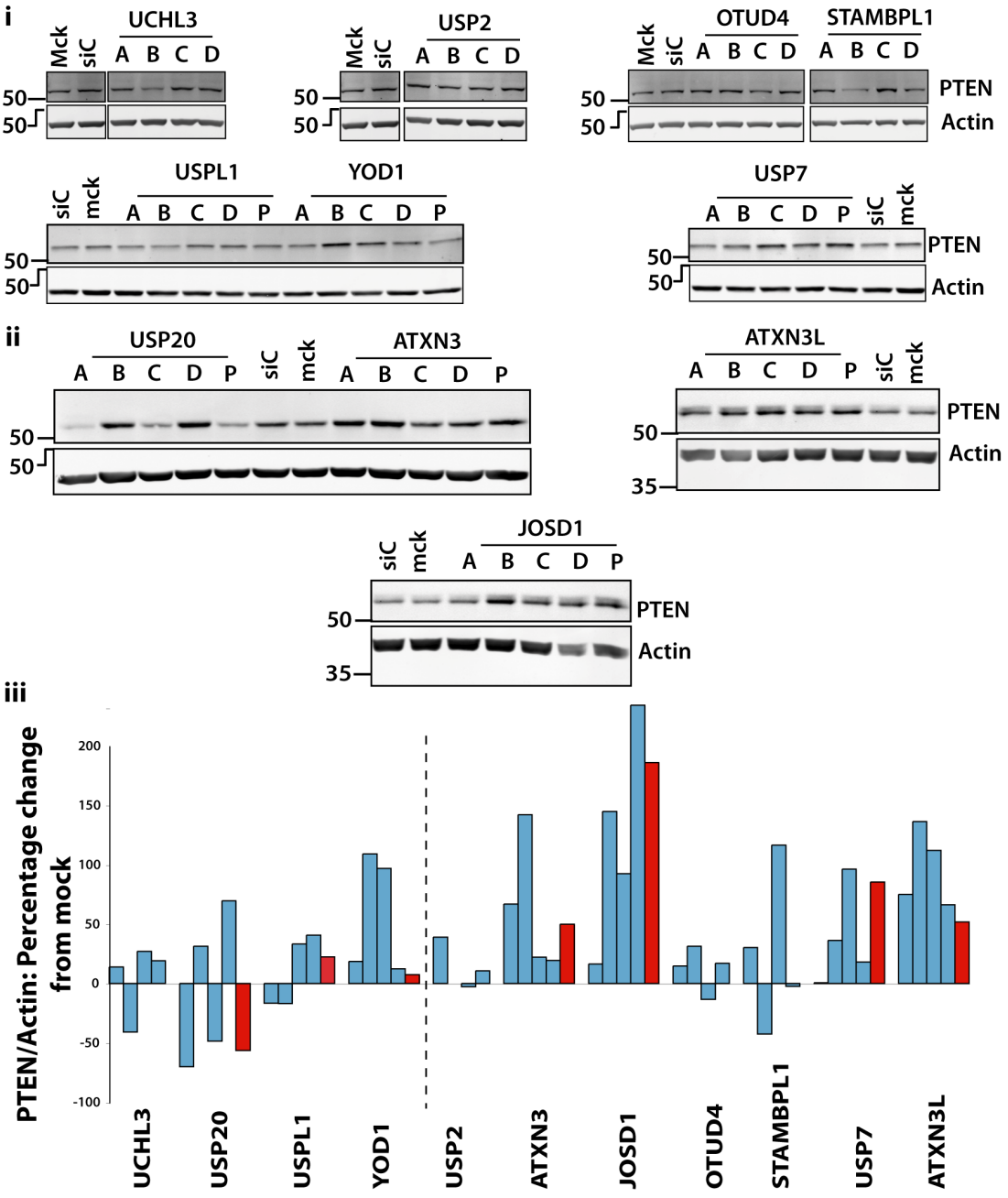

Fig 3.8. Deconvolution supports a role for several DUBs in the regulation of PTEN. **i,ii.** A 72-hour siRNA knockdown of DUBs identified in the PTEN screen was performed in A549 cells using individual oligonucleotides from each pool (designated A to D). Equal amounts of lysate for each sample were immunoblotted for PTEN and actin. siRNA transfections for the first set of DUBs (**i**) was performed using 20nM siRNA and oligofectamine (Invitrogen), while in the second (**ii**), 10nM siRNA and RNAiMax (Invitrogen) were employed. **iii**. Quantification of PTEN signal was performed, which was then normalised to the actin signal and compared to the mock. For each target, oligonucleotides A-D are depicted from left to right, pools (P) where included are shown in red. Targets to the left of the dotted line resulted in downregulation of PTEN in the screen, those on the right upregulated PTEN. (Detection and quantification performed on Odyssey infra-red scanner [LiCor]. siC- non-targeting siRNA control).

In all screens, the top and bottom 5 hits were picked for further validation, representing approximately 10% of the dataset. However, if one of the controls fell within the top or bottom 5 (for example in fig 3.7ii), then only four candidates were followed up. In this screen for DUB regulators of PTEN, the hits are thus STAMBPL1, OTUD4, JOSD1 (Josephin domain containing 1), ATXN3, and USP2 whose knockdown leads to an increase in PTEN level and UCHL3, USP20, USPL1, and YOD1 whose knockdown had the opposite effect. Deconvolution of these hits is shown in figure 3.8. USP7, which was 9th from the top of the dataset using the median of the blot for normalisation, and 4th using the mock, was also included due to its known role in deubiquitylation of PTEN. Deconvolution of ATXN3L, which was 7th from the top, and which shares extensive sequence homology with ATXN3, was also performed.

A summary of the deconvolution is provided in table 1. All candidates (with the exception of ATXN3L) were also depleted using esiRNA (fig 3.9). This was performed as a second validation step. However, while the experiment supported the findings of the deconvolution for ATXN3 and USP20, the degree of change in PTEN protein level was less marked, and esiRNA depletion of the other candidates did not significantly alter PTEN levels (fig 3.9). This may partly reflect reduced knockdown efficiencies for the esiRNA, however this was not investigated.

ATXN3, ATXN3L and JOSD1 were all successfully deconvoluted. Interestingly, while two siRNA oligonucleotides against USP20 resulted in downregulation of USP20 protein levels, the other two had the opposite effect. Further validation of ATXN3, ATXN3L, JOSD1 and USP20 will be discussed in chapter 6.

Depletion of STAMBPL1 (also known as AMSHLP) by two out of the four siRNA oligonucleotides resulted in upregulation of PTEN. However one of the two oligonucleotides had a much greater effect than the other. In addition, depletion by a third oligonucleotide had an opposing effect and

DUB	A	B	C	D	Deconvolution conclusion	esiRNA
UCHL3	-	+ ↓	- ↑	-	No	+ ↓
USP20	++↓	-	+↓	-	Yes	+ ↓
USPL1	-	-	- ↑	- ↑	No	-
YOD1	-	- ↑	- ↑	-	No	-
USP2	+ ↑	-	-	-	No	-
ATXN3	++↑	++↑	-	-	Yes	++↑
JOSD1	-	++↑	++↑	++↑	Yes	-
OTUD4	-	+ ↑	-	-	No	+↑
STAMBPL1	+ ↑	- ↓	++↑	-	Yes	-
USP7	-	+ ↑	++ ↑	-	Yes	- ↓
ATXN3L	++↑	++↑	++↑	++↑	Yes	ND

Table 3.1. Summary of deconvolution for candidate DUBs from the PTEN screen. DUBs whose depletion decreased or increased PTEN protein levels in the screen are indicated in blue and red respectively. Changes in protein level of more than 20% are indicated by an arrow in the direction of change. A change in protein level of 20 - 50% (in the same direction as the pool) is indicated by +, greater than 50% by ++, while less than 20% change (or a change in the opposite direction) is indicated by a - sign. Deconvolution was deemed successful if at least two siRNA oligonucleotides recapitulated the results of the pool. (ND- Not done).

resulted in PTEN downregulation. Depletion of STAMBPL1 by esiRNA did not result in upregulation of PTEN (fig 3.9). Depletion of STAMBPL1 was also performed using 4 alternative siRNA oligonucleotides (fig 3.10). Only one of the four siRNA oligonucleotides upregulated PTEN protein level to any degree (fig 3.10). In view of these results, which show a marginal upregulation of PTEN at best, STAMBPL1 was not followed up further.

USP7 was also successfully deconvoluted, with two out of the four oligonucleotides recapitulating the effect of the pool. The degree of increase in PTEN protein levels was however less pronounced than occurred following depletion of ATXN3, ATXN3L or JOSD1. As discussed above,

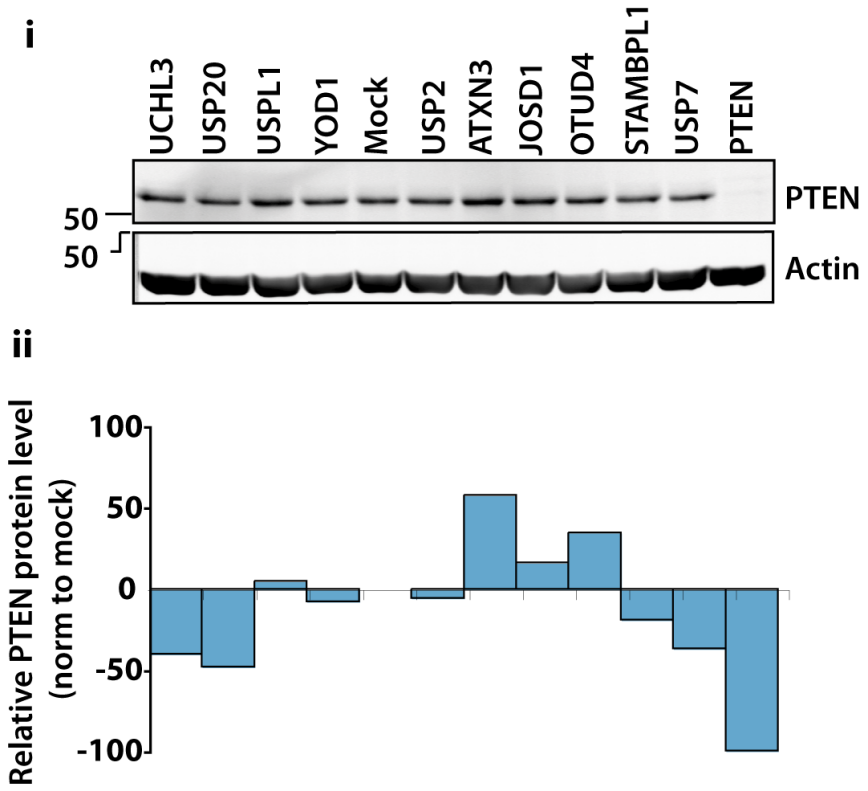

Fig 3.9. Depletion of ATXN3 and USP20 by esiRNA supports a role in regulating PTEN. i. A549 cells were transfected with esiRNA against the indicated DUBS, siRNA against PTEN, or mock transfected. Following a 72-hour incubation the cells were lysed using NP40. Equal amounts of lysate were immunoblotted for PTEN and actin. ii. Quantification of PTEN signal was performed, which was then normalised to the actin signal and compared to the mock. Detection and quantification performed on Odyssey infrared scanner [LiCor].

USP7 has previously been shown to be involved in the regulation of PTEN localisation [203], and I therefore prioritised the other three DUBs for further investigation.

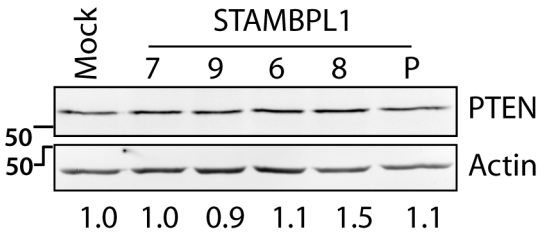

Fig 3.10. Depletion of STAMBPL1 does not significantly upregulate PTEN. A. A 72-hour siRNA knockdown of STAMBPL1 was performed in A549 cells using the indicated siRNA oligonucleotides (Dharmacon) and pooled oligonucleotide (P). Equal amounts of lysate were immunoblotted for PTEN and actin. Quantification of PTEN signal normalised to the actin signal and compared to the mock is shown below the blot. (Detection and quantification performed on Odyssey infrared scanner [LiCor]).

3.5 Screening for DUB regulators of PtdIns3-Kinase isoforms

The phosphoinositide 3-kinases are a family of lipid kinases, which regulate the key survival pathway bearing their name. PtdIns3-K isoforms are divided into three classes (I-III) on the basis of lipid substrate preference and structural features (section 1.5.1).

To date, there have been no reports of DUBs regulating any of the PtdIns3-K classes. In this section, I therefore set out to identify DUB regulators of the protein level of PtdIns3-K class I catalytic subunits (p110α, p110β, p110γ), the class I regulatory subunit, p85α, and the class II catalytic subunit, p170. These subunits were selected predominantly for their known association with cancer. Class I, and particularly p110α, is the predominant class associated with malignancy, although there have been reports of involvement of other classes, notably IB [392] and II [393], for which screens were therefore included. In mass spectroscopy experiments carried out in the host laboratory, p110β was found to be the most abundant PtdIns3-K catalytic subunit in A549 cells (M Clague, personal communication), and it was therefore also included.

3.5.1 Identifying DUB regulators of p110 isoform abundance

I first investigated the influence of DUB knockdown on three class I catalytic subunits; p110α and p110β (class IA), and p110γ (class IB) using NP40 lysates from the library described in fig 3.3. Representative immunoblots and signal quantification for the p110α, p110β and p110γ screens are shown in figs 3.11-13 respectively. Three technical replicates of the immunoblotting stage were performed for p110α and p110β, while two were performed for p110γ. In each figure the five lowest and highest ranked candidate DUBs are highlighted (fig 3.11-13). A comparison of the results of all three screens is provided in fig 3.14.

All three screens showed extensive variability between immunoblotting replicates, with the p110α screen the most affected. This particularly affected identification of DUBs whose depletion resulted in upregulation of the p110 isoforms, where the candidates identified on quantification generally did not appear convincing on examination of the blots. Exceptions included depletion of PSMD14 and/or PSMD7, which showed evidence of upregulation of all three isoforms (fig 3.11-13). While p110α upregulation is less obvious on PSMD7 or PSMD14 depletion, a higher molecular weight form of p110α becomes apparent (fig 3.11), that might represent polyubiquitylated p110α. PSMD7 and PSMD14 are integral components of the proteasome [394, 395] and their depletion is likely to mimic the effects of proteasome inhibition. These findings therefore support regulation of all three p110 isoforms by the proteasome (section 3.10).

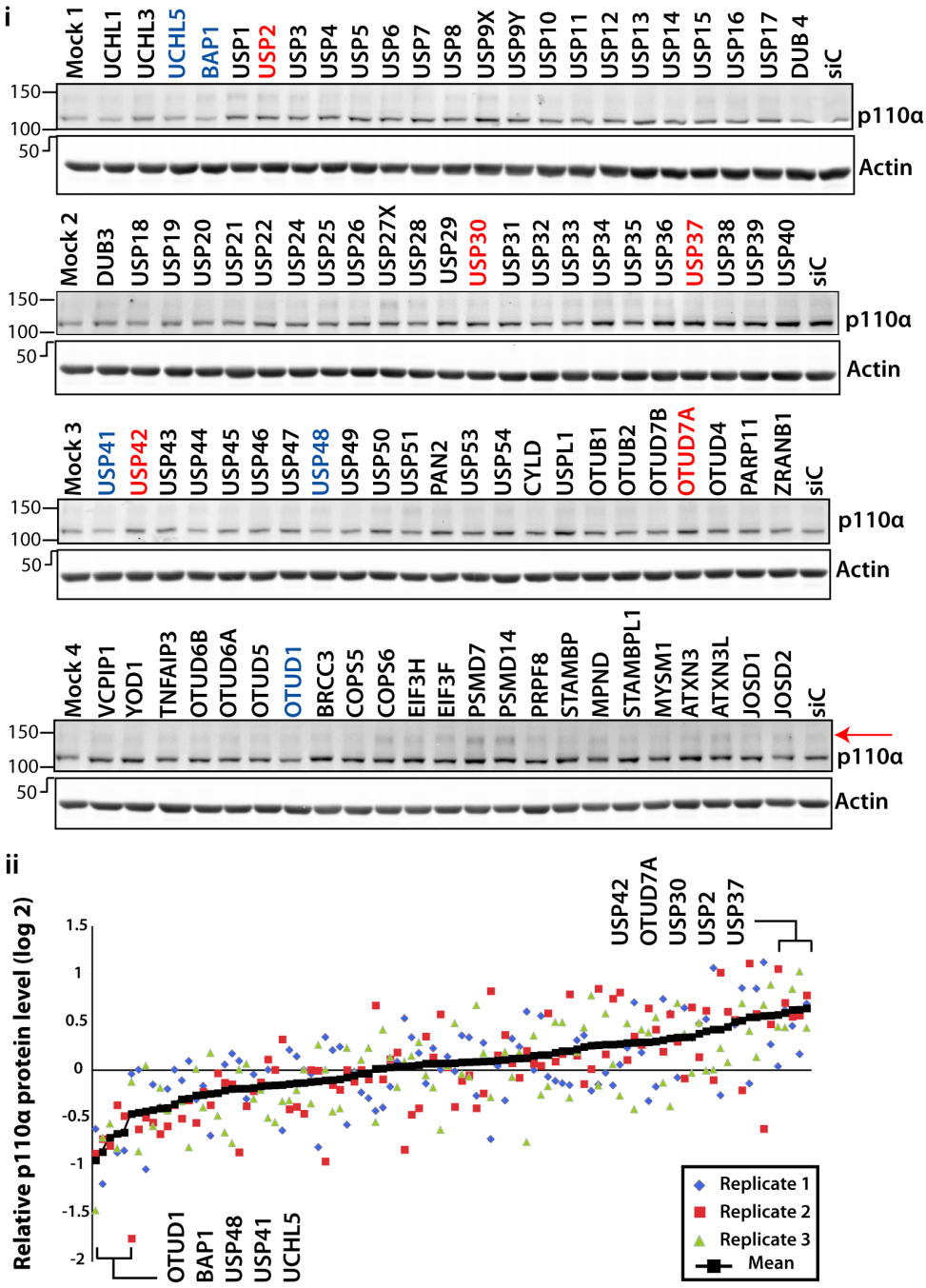

Fig 3.11. Screening for DUB regulators of p110α. i. NP40 lysates from the DUB screen (fig 3.3) were run on four SDS-PAGE gels. Each blot included a mock-transfected and non-targeting siRNA (siC) control. The blots were probed for p110α and actin, and imaged by infrared scanner (Odyssey, LiCor). Immunoblotting of lysates was performed three times and representative blots from one of the three runs are shown. The red arrow indicates a higher molecular weight band, which is most apparent on knockdown of PSMD7 or PSMD14. **ii.** Quantification of band intensity was performed using Odyssey (LiCor) software and the signal in each case normalised to actin and the median of each blot. The five lowest and highest ranked candidates are indicated and also highlighted in **i** (in blue and red respectively).

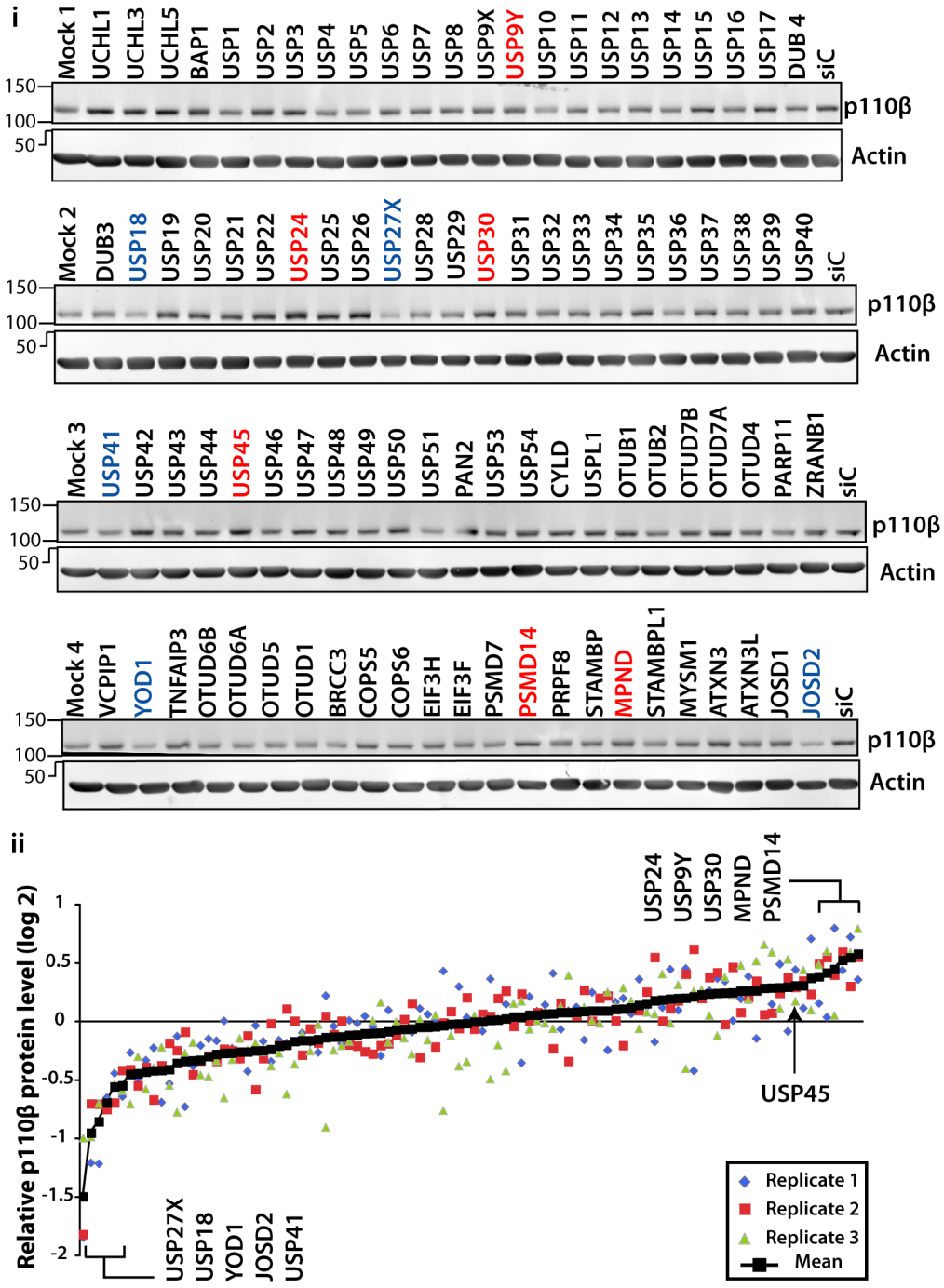

Fig 3.12. Screening for DUB regulators of p110β. A. NP40 lysates from the DUB screen (fig 3.3) were run on four SDS-PAGE gels. Each blot included a mock-transfected and non-targeting siRNA (siC) control. The blots were probed for p110β and actin, and imaged by infrared scanner (Odyssey, LiCor). Immunoblotting of lysates was performed three times and representative blots from one of the three runs are shown. **B.** Quantification of band intensity was performed using Odyssey (LiCor) software and the signal in each case normalised to actin and the median of each blot. The five lowest and highest ranked candidates are indicated and also highlighted in **A** (in blue and red respectively). USP45 which was ranked 9th from the top is also highlighted (see text).

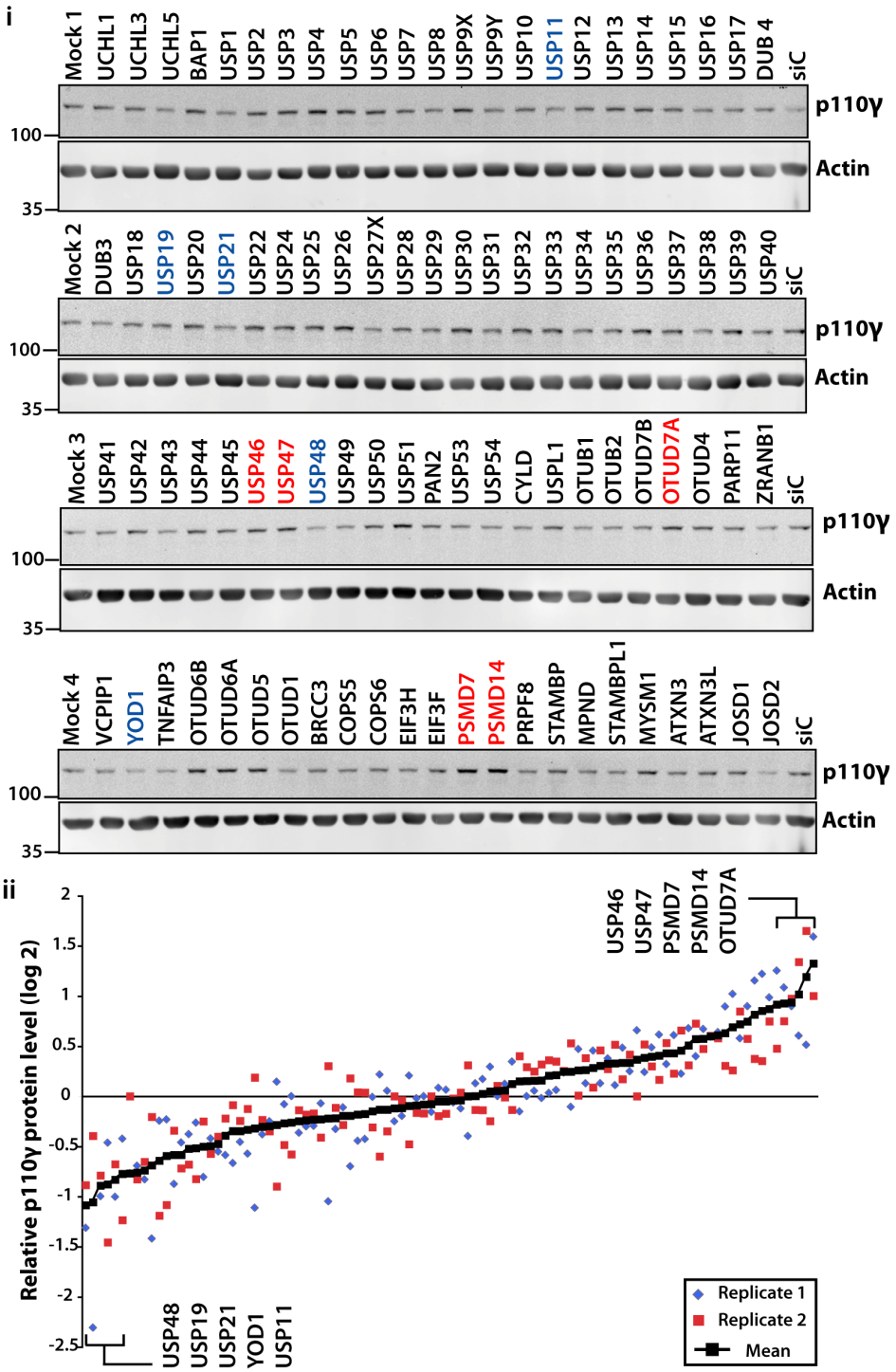

Fig 3.13. Screening for DUB regulators of p110γ. A. NP40 lysates from the DUB screen (fig 3.3) were run on four SDS-PAGE gels. Each blot included a mock-transfected and non-targeting siRNA (siC) control. The blots were probed for p110γ and actin, and imaged by infrared scanner (Odyssey, LiCor). Immunoblotting of lysates was performed twice and representative blots from one of the runs are shown. **B.** Quantification of band intensity was performed using Odyssey (LiCor) software and the signal in each case normalised to actin and the median of each blot. The five lowest and highest ranked candidates are indicated and also highlighted in **A** (in blue and red respectively).

OTUD7A depletion resulted in upregulation of both p110α and p110γ, and was consistent between replicates. USP45 depletion resulted in upregulation of p110β (fig 3.13); while this was only ranked 9th highest, it was relatively convincing on all immunoblot replicates. As will be discussed in chapter 4, USP45 was also subsequently identified in a functional screen for modulators of PtdIns3-K activity.

Candidate DUBs whose depletion downregulated p110 isoforms appeared more consistent between replicates. These included USP48, USP41 and YOD1, which were all identified in more then one of the p110 screens (fig 3.11-13). USP27X knockdown resulted in at least a 50% reduction in p110β levels in all three technical replicates (fig 3.12) and had a more modest effect on the other two isoforms (fig 3.11, 3.13).

Comparison of the datasets for the three p110 isoforms showed generally good concordance in the effects of DUB depletion on the regulation of p110 isoforms (fig 3.14) However, three DUBs were identified whose depletion resulted in different effects on p110α and p110β/p110γ protein levels. These are YOD1, USP1 and BAP1 (fig 3.14).

Due to time constraints, deconvolution of the p110 isoforms has not been performed as yet. Our intention is to collaborate with Marco Falasca's lab, who have a particular interest in p110γ (and p170, see section 3.7) for further investigation of p110γ targets.

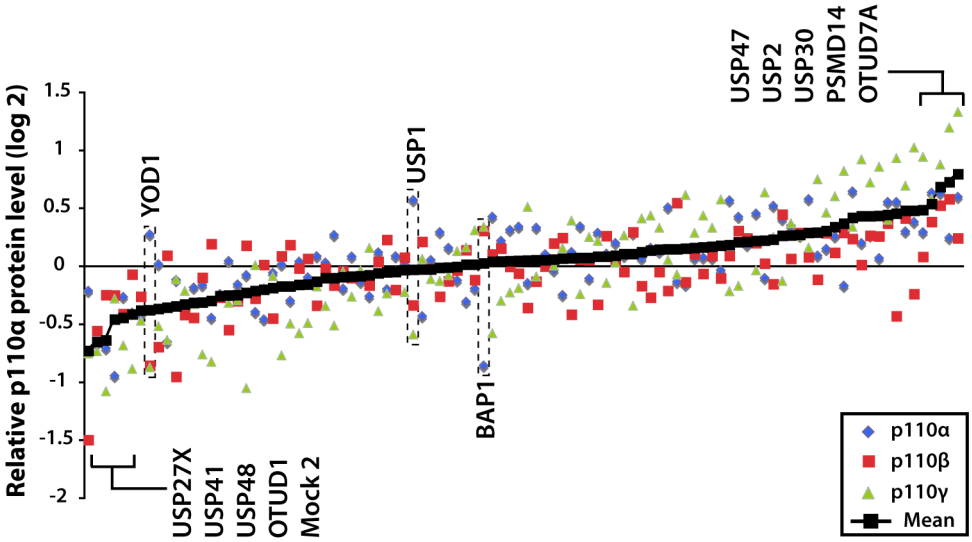

Fig 3.14. Identification of candidate DUBs whose depletion concordantly regulates p110 isoforms. The quantitative results from the p110α, p110β and p110γ screens (fig 3.12-14) were combined and are shown here. For each DUB depletion, the mean of the three p110 isoform screens was obtained and ranked (black). The mean results of the screens for each p110 isoform are plotted in blue, red and green. The 5 lowest and highest ranked candidates are highlighted, and examples where discordance between the three screens was observed.

3.5.2 Identifying DUB regulators of p170 abundance

I also investigated the role of deubiquitylases in regulating the protein abundance of the class II PtdIns3-kinase catalytic subunit, p170 (PIK3C2A), which has been implicated in hepatocellular carcinoma [393]. Unfortunately only a very weak signal was obtained with this antibody (BD611046), which also showed extreme variability across blots and between runs. Example blots are shown for two immunoblotting replicates (fig 3.15). In view of the variability across blots and the weak signal, attempts were not made to quantify the bands.

However, depletion of several of the DUBs showed a reproducible effect on p170 levels. Depletion of either PSMD7 or PSMD14 resulted in a higher molecular weight smear indicating probable p170 polyubiquitylation (fig 3.15), and thus proteasomal regulation. The most marked reduction in the p170 protein level was observed with USP48 knockdown, however depletion of

YOD1, USP27X or COPS6 also resulted in a reproducible reduction in p170. On the other hand, depletion of either USP47 or OTUD6A led to upregulation of p170 protein level.

Interestingly, the majority of the above candidates (USP48, YOD1, USP27X and USP47) were also identified in the p110 screens, which could suggest that the protein abundance of multiple catalytic PtdIns3-K isoforms may be co-regulated. An alternative explanation would be that the siRNAs against these DUBs (or the DUBs themselves) have generic effects on protein levels. However, USP48, USP27X and USP47 were only identified in screens for regulators of p110 or p170, which suggests that their effects may be specific to PtdIns3-K. YOD1 on the other hand, was additionally identified in screens for regulators of PDK1 (section 3.4) and mTOR (section 3.8). Candidates from the p170 screen are yet to be validated.

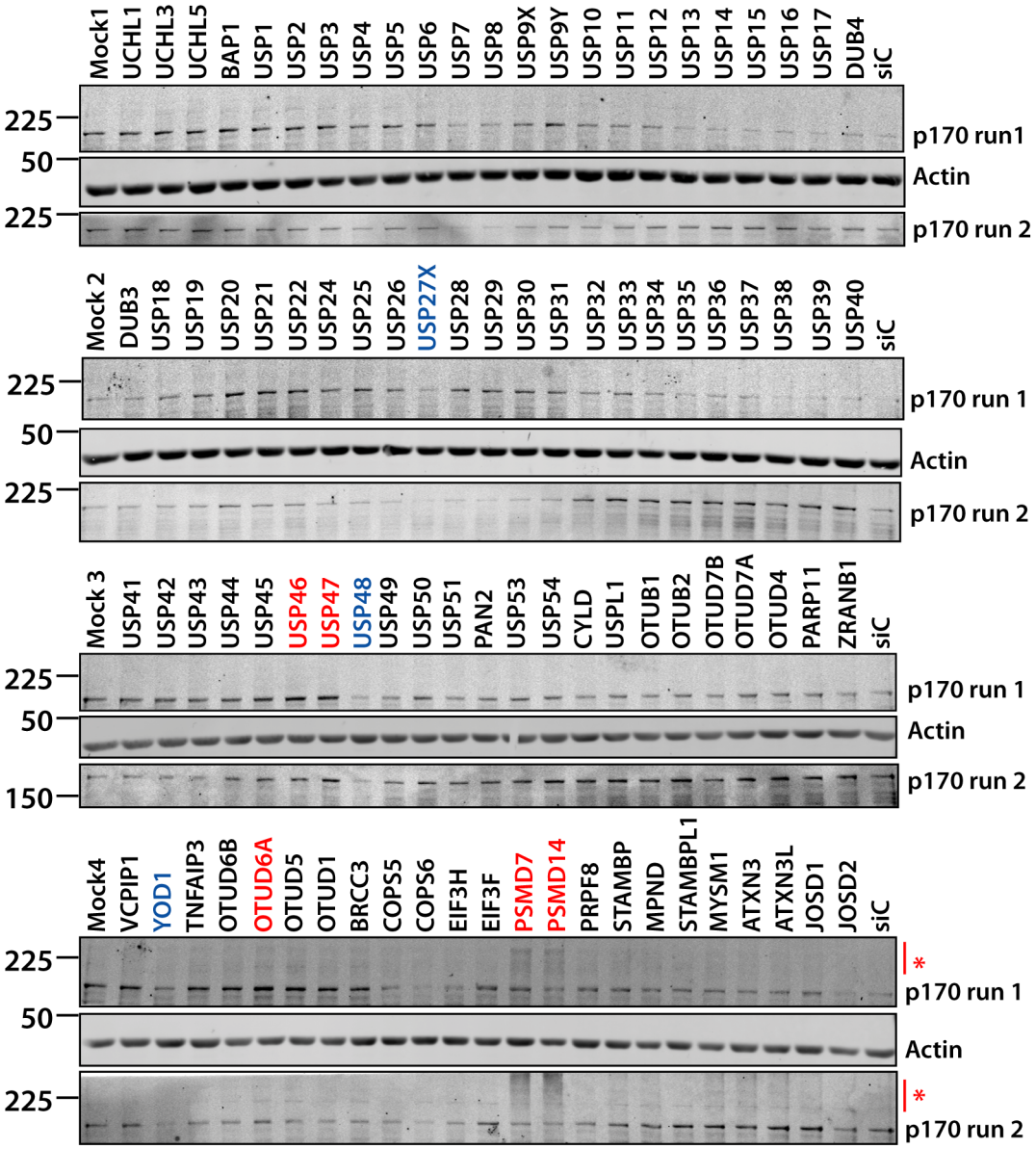

Fig 3.15 Depletion of either PSMD7 or PSMD14 leads to polyubiquitylation of p170. NP40 lysates from the DUB screen (fig 3.3) were run on four SDS-PAGE gels. Each blot included a mock-transfected and non-targeting siRNA (siC) control. The blots were probed for p170 and actin, and imaged by infrared scanner (Odyssey, LiCor). Immunoblotting of lysates was performed twice and blots from both runs are shown. The actin blot from the first run only is shown. A higher molecular weight smear is observed (red asterisk) on PSMD7 or PSMD14 knockdown.

3.5.3 Identifying DUB regulators of p85α abundance

The class IA regulatory subunit, p85α, was the next target we investigated. p85α has previously been shown to be polyubiquitylated, leading to its degradation [396], but to date no DUBs have been associated with its regulation. We therefore probed NP40 lysates from our screen for p85α (fig 3.16i), and quantified the signal as previously described (fig 3.16ii). The p85α signal was relatively unaffected by DUB knockdown, and no obvious candidates were identified visually. Subtle changes in p85α were however observed on quantification of the signal. Depletion of OTUD6A marginally increased p85α signal (by ~30%), but was also identified in the p170 screen where, although not quantified, its effects appeared more visually obvious.

3.6 A DUB screen for regulators of PDK1

PDK1 occupies a key position in the PtdIns3-K pathway, phosphorylating Akt in response to the generation of the second messenger $PtdInsP_3$ (section 1.5.2). It additionally phosphorylates and activates several other AGC kinases (reviewed in [260]). PDK1 auto-phosphorylates itself and is constitutively active [263]. A recent study has shown that PDK1 is monoubiquitylated in a variety of cell lines, and that this is reversed by overexpression of USP4 [358]. However, in this study depletion of USP4 did not alter monoubiquitylated PDK1, which suggests that other DUBs may be involved [358]. In addition, there are no known DUBs that regulate the stability of PDK1. I therefore set out to look at the effects of DUB depletion on PDK1 protein level.

3.6.1 PDK1 antibody comparison and characterisation

An initial PDK1 screen performed utilizing a PDK1 antibody (with an extensive bibliography) from Cell Signaling (3062) had to be abandoned when it became apparent that the principal band was non-specific. We therefore assessed several other antibodies including s682 (Dundee

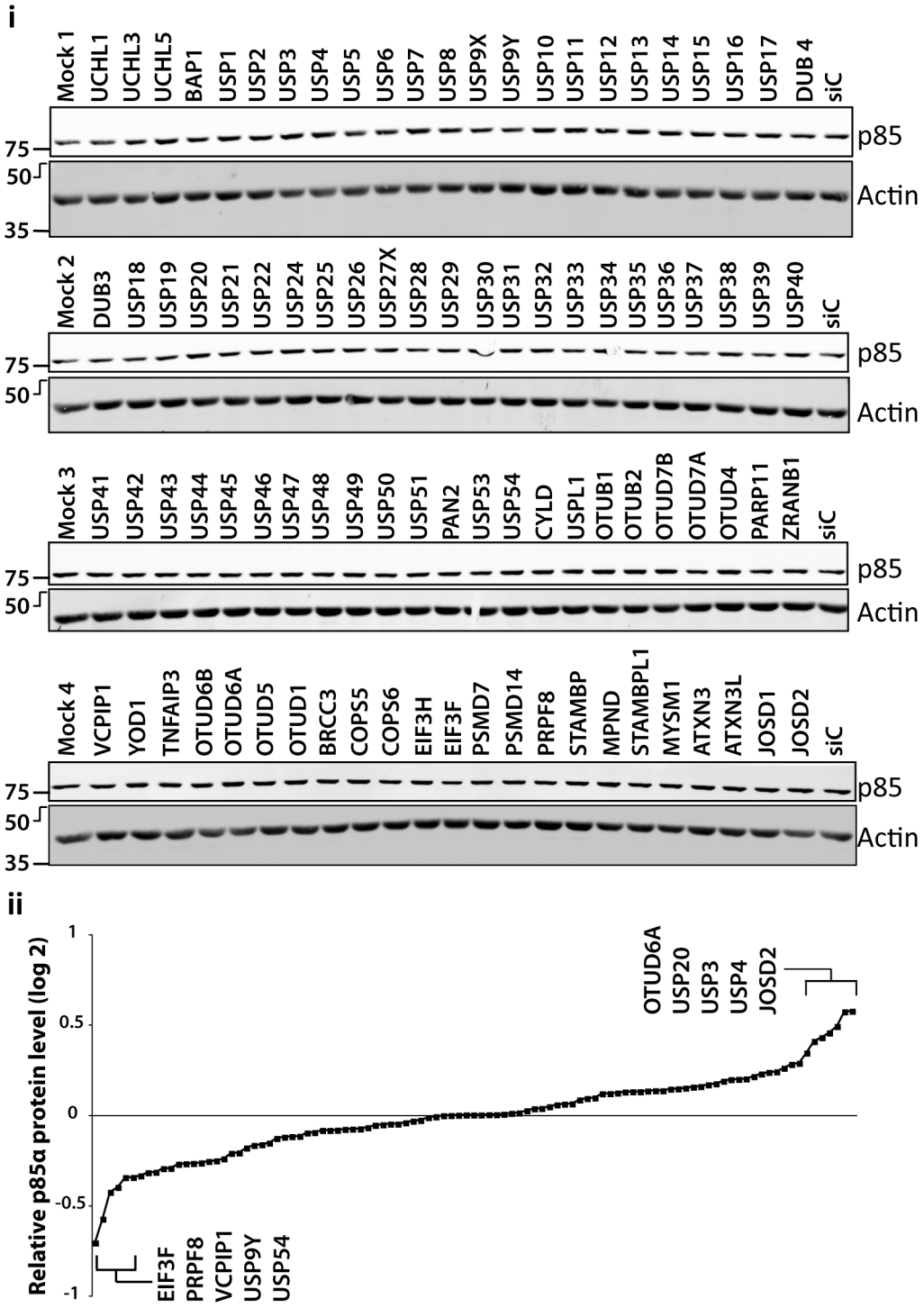

Fig 3.16. A screen for DUB regulators of p85α. i. NP40 lysates from the DUB screen (fig 3.3) were run on four SDS-PAGE gels. Each blot included a mock-transfected and non-targeting siRNA (siC) control. The blots were probed for p85α and actin, and imaged by infra-red scanner (Odyssey, LiCor). **ii**. Quantification of p85α and actin was performed and the p85α signal normalised to actin, then the blot median, and ranked as shown. The five lowest and highest ranked candidate DUBs are highlighted. (Detection and quantification was performed using an Odyssey infrared scanner).

phosphorylation unit), a gift from Dario Alessi (data not shown), BD611071 from BD Biosciences, a phospho-PDK1 antibody from Cell signaling (3061), and latterly a different production lot of 3062 from Cell Signaling (3062 lot 10) as well as a monoclonal antibody in development (5662). A summary of the antibody assessment is shown in fig 3.17i-iv. PDK1 has multiple described and predicted splice isoforms, principal examples of which are illustrated in fig 3.17v. In view of this, I felt the BD antibody most closely correlated with the expected band structure on immunoblots, with the principal band on immunoblotting correlating with isoform 1. This antibody was therefore used for further screens.

3.6.2 PDK1 protein level is regulated by multiple deubiquitinases

NP40 lysates from the DUB library (fig 3.3) were run on four SDS-PAGE gels per screen and immunoblotted for PDK1. Two technical repeats of the immunoblotting stage were performed for PDK1 and representative blots are shown in figure 3.18. Both the main splice-variant and all PDK1 immunoreactive bands detected between 50 and 70kDa were quantified. Intra-sample normalisation to actin and intra-blot normalisation to the median was performed. Results for quantification of both the main splice-variant and all detected variants are shown in fig 3.19. While there was significant variability between the two immunoblots for the screen, a number of hits were reproducible. Depletion of PRPF8, TNFAIP3, OTUD1, USP34, USP18 or USP32 all reproducibly downregulated either the main PDK1 band or all of the detected PDK1 bands. USP6 was also selected for deconvolution as it was ranked 6th for both quantifications, and is a paralogue of USP32 [397]. Candidates upregulating PDK1 were less consistent between replicates and only UCHL3, JOSD1 and CYLD were selected for deconvolution. Knockdown of both YOD1 and JOSD2 resulted in the appearance of an extra band at approximately 50kDa, and both were therefore also subjected to deconvolution.

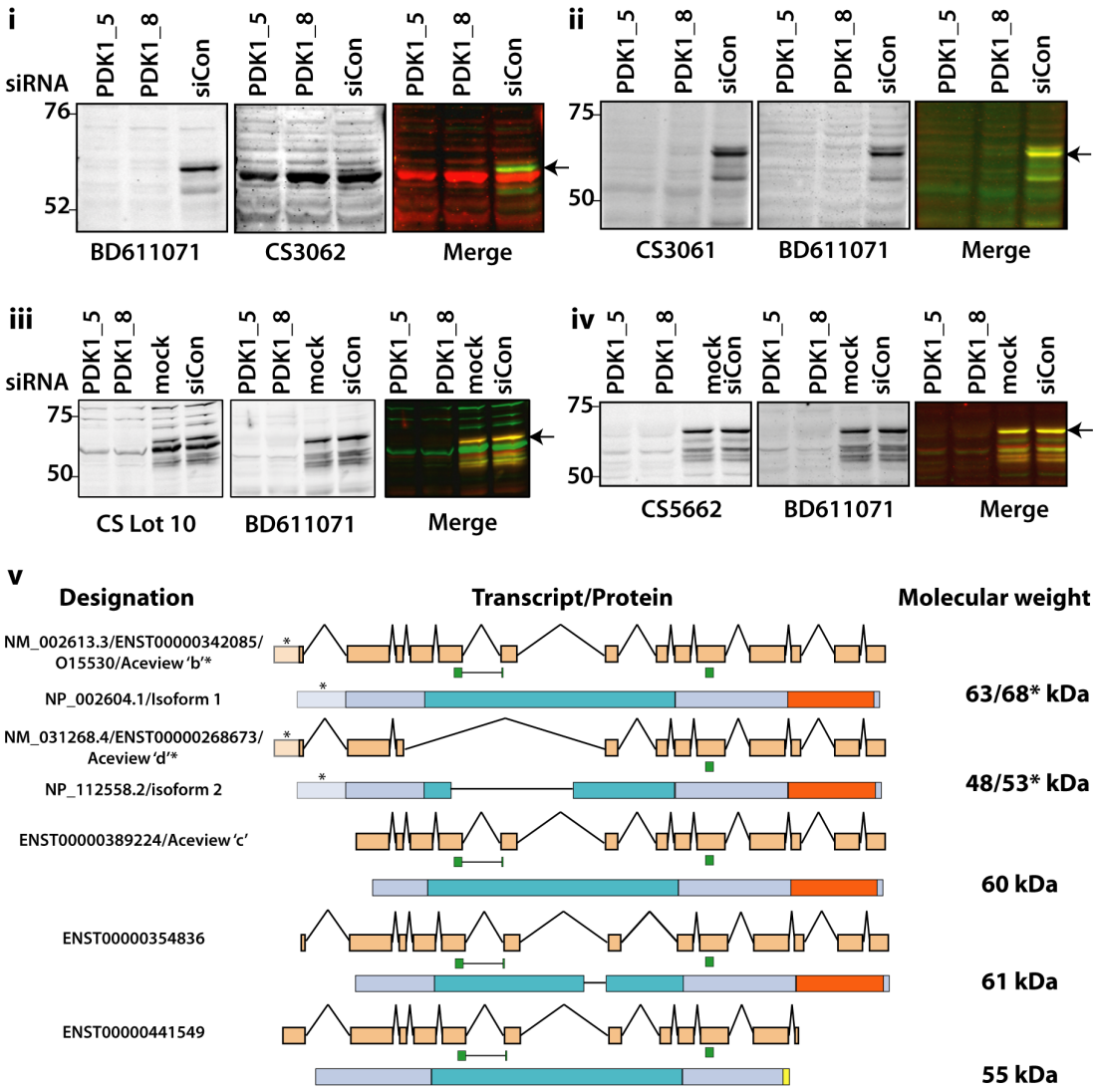

Fig 3.17. BD611071 is a specific PDK1 antibody and detects multiple splice variants. Comparison of the BD mouse PDK1 monoclonal antibody BD6111071 with a Cell Signalling antibody CS3062 (**i**), a phospho-PDK1 antibody from cell signalling, CS3061 (**ii**), a replacement lot of CS3062 (**iii**) and a monoclonal antibody CS5662 (**iv**). In each case the image in the left hand panel was detected using the green (800) channel of the Odyssey scanner while that in the right hand panel was detected with the red (680) channel. PDK1 was knocked down with two siRNA oligos as indicated. The arrow indicates the predominant isoform identified by BD611071. **v**. The reference sequence transcripts and proteins for PDK1, as well as principle examples from the Ensembl, Uniprot and Aceview databases are shown here, with the predicted protein molecular weights given to the right. Alternative start codons account for the differences in size described in different databases for the first two sequences (the asterisks indicate the longer Aceview sequences). The kinase domain is indicated in turquoise, and the PH domain in orange. The green boxes indicate the positions of the two siRNA sequences (PDK1_5 on the left and PDK1_8 on the right).

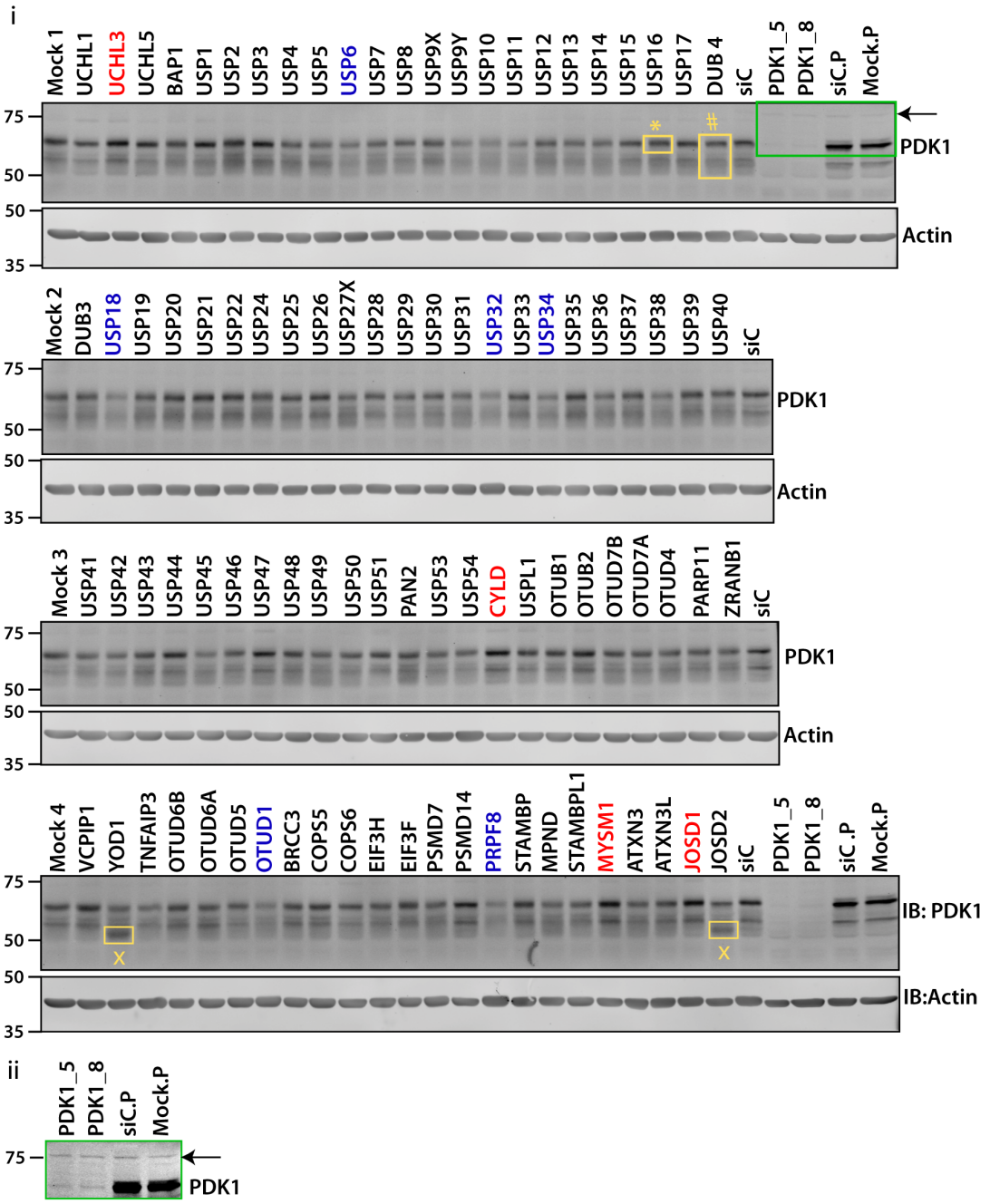

Fig 3.18. A screen for DUB regulators of PDK1. i. NP40 lysates from the DUB screen (fig 3.3) were run on four SDS-PAGE gels. Each blot included a mock-transfected and non-targeting siRNA (siC) control. A 72-hour knockdown of PDK1, using two siRNA oligonucleotides, was performed separately from the screen and samples (including independent controls, designated siC.P and Mock.P) run alongside the screen lysates on blots 1 and 4. The blots were probed for PDK1 and actin, and imaged by infrared scanner (Odyssey, LiCor). Immunoblotting of lysates was performed twice and representative blots are shown. Both the main band (*) and all the PDK1 immunoreactive bands detected between approximately 50 and 70kDa (♯) were quantified. A prominent band (x) just above 50kDa was also seen with YOD1 and JOSD2 knockdowns. A very faint band of approximately 75kDa is indicated by an arrow and is shown also in **ii**, where the contrast has been increased.

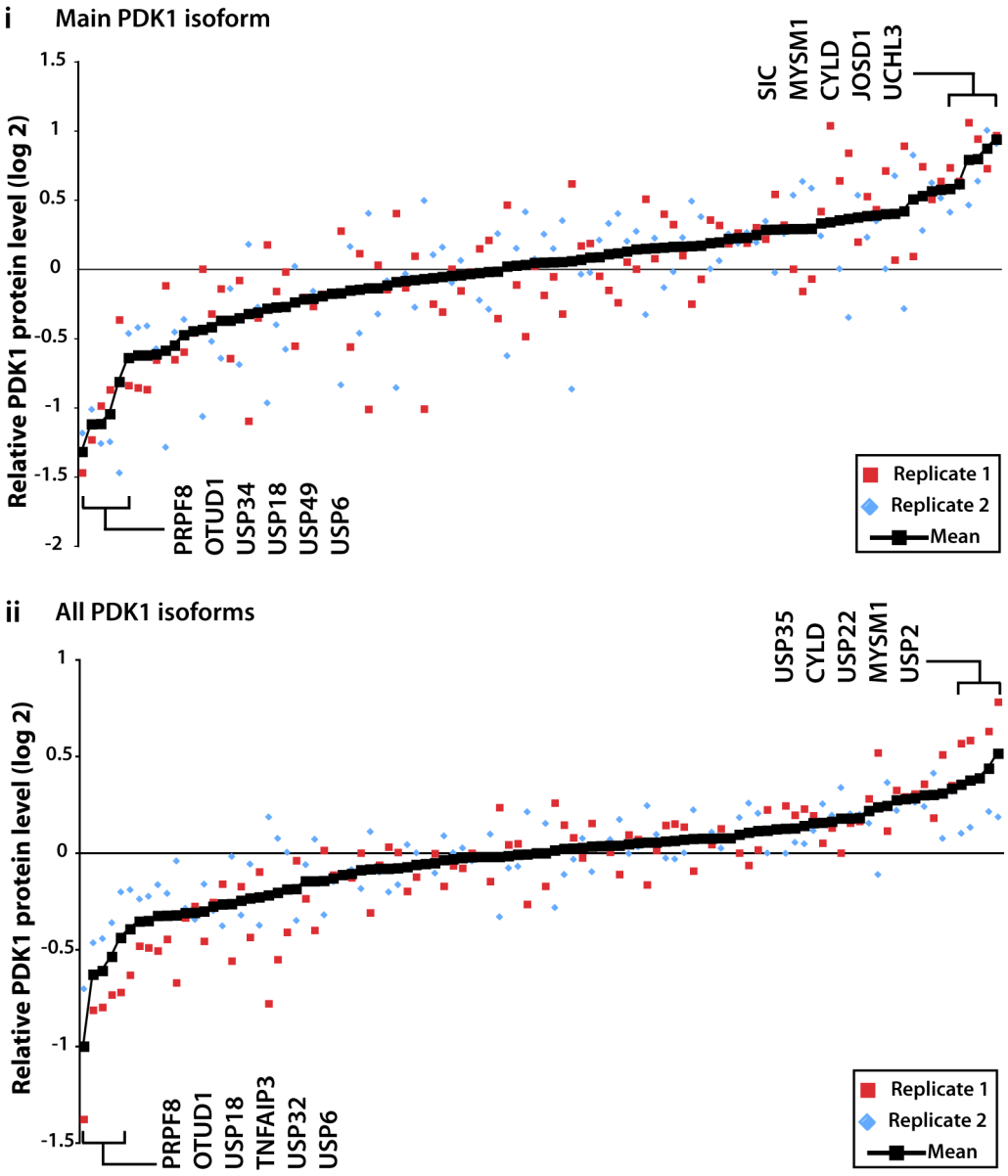

Fig 3.19. Multiple DUBs are candidate regulators of PDK1. Immunoblotting for PDK1 and actin was performed and is shown in fig 3.19**. i.** The predominant PDK1 bands were quantified (Odyssey, LiCor), normalised to actin and then the median of each blot. **ii.** Alternatively all the PDK1 bands between 50 and 70kDa were quantified, normalised to actin and the blot median. The two replicate screens are depicted in red and green, with the mean in black. The six bottom, and five top ranked candidates are highlighted in both i and ii.

In view of the study which showed that PDK1 may be monoubiquitylated [358], I also examined the blots for higher molecular weight PDK1 immunoreactive bands. While a very faint band of approximately 75kDa was

seen, this was not downregulated by PDK1 depletion (fig 3.18i,ii), and therefore most likely represents a non-specific band.

Deconvolution of the selected candidates (fig 3.20 and table 3.2) identified several DUBs for which more than one oligonucleotide recapitulated the effect of the pool. These included PRPF8, TNFAIP3, OTUD1, USP34 and USP32, which decreased PDK1 protein level, and UCHL3, which increased it. On the other hand USP18, USP6, CYLD and JOSD1 failed to validate through deconvolution. A combined depletion of USP6 and USP32 was also performed to assess whether depletion of these closely related DUBs would have additive effects on PDK1 protein levels. This resulted in a similar reduction in PDK1 protein level to USP32 depletion alone, further indicating that USP6 does not regulate PDK1 protein levels. The lower molecular weight band seen with YOD1 and JOSD2 knockdown was not recapitulated in deconvolution.

A subset of candidates from the PDK1 screen were further investigated through QPCR (fig 3.21). Depletion of either PRPF8 (pre-mRNA processing factor 8) or TNFAIP3 using any of the individual oligonucleotides or pooled oligonucleotide resulted in a reduction in PDK1 transcript level. In the case of USP32, two of the individual USP32 oligonucleotides, and the pool, led to a reduction in PDK1 transcripts. There was a good correlation between the effects of USP32 oligonucleotides on PDK1 mRNA and protein level (fig 3.21ii), suggesting that USP32's effects on PDK1 may similarly be mediated through transcription. However, in the case of OTUD1, there was no correlation between PDK1 mRNA and protein suggesting that its effects on PDK1 are post-transcriptional, with alterations in mRNA occurring through compensatory mechanisms.

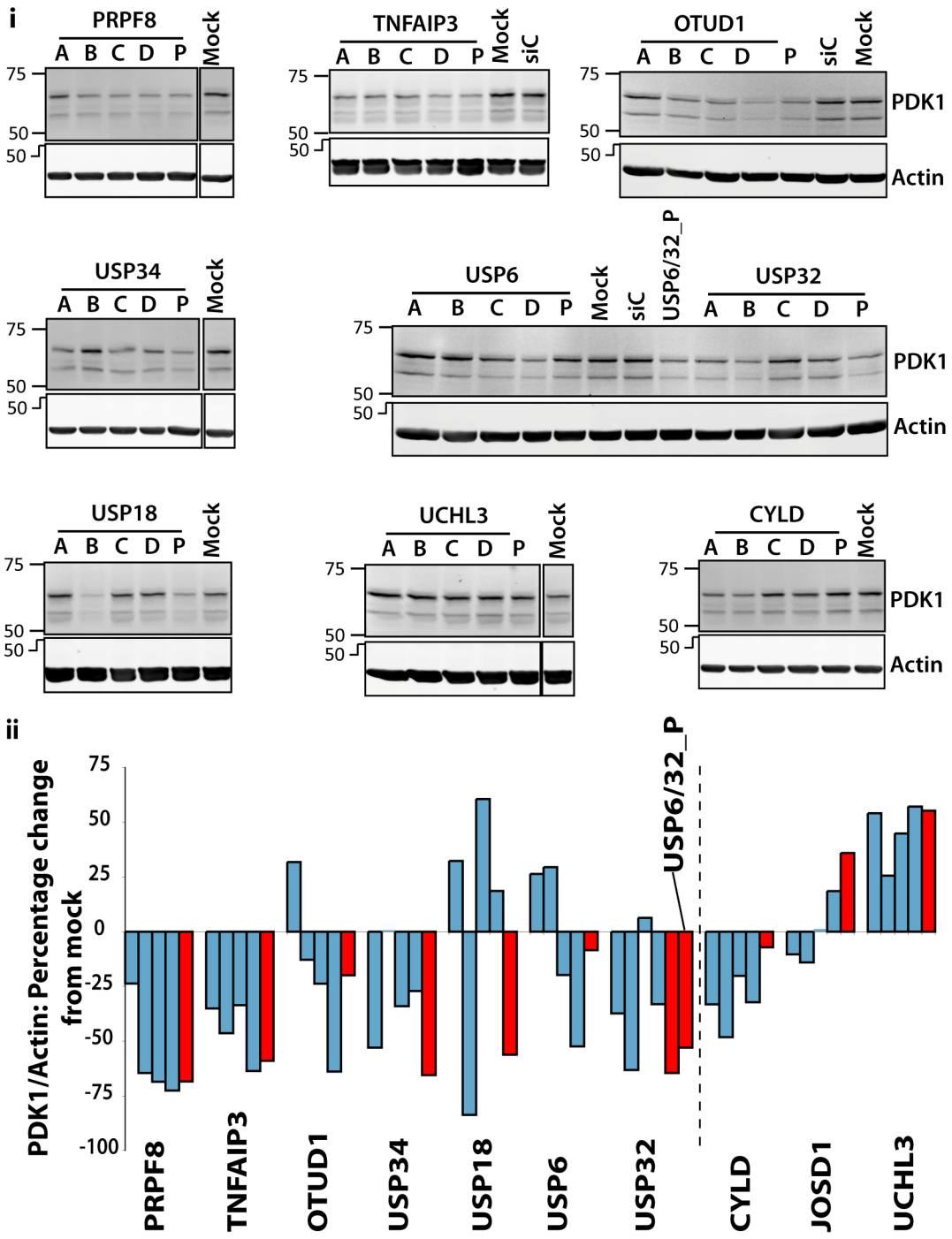

Fig 3.20. Deconvolution reveals multiple DUB regulators of PDK1 protein level. i. Target DUBs were knocked down separately with each of the four individual oligonucleotides from the pool (designated A-D in each case) as well the pool (P), cells were incubated for 72 hours, lysed with NP40, and lysates immunoblotted for PDK1. **ii.** The predominant PDK1 isoform was quantified, normalised to actin. Change in PDK1 level is shown here as a percentage of the mock control. For each DUB, the four oligos are shown from left to right with the pools shown in red. Knockdown of DUBs to the left of the line resulted in decreased PDK1 stability in the screen, while those to the right increased PDK1 levels. The data represent the means of two experiments (siC- non-targeting siRNA control, USP6/32_P- combined depletion of USP6 and USP32 using oligonucleotide pools for both).

DUB	A	B	C	D	Deconvolution conclusion
PRPF8	+ ↓	++ ↓	++ ↓	++ ↓	Yes
TNFAIP3	+ ↓	+ ↓	+ ↓	++ ↓	Yes
OTUD1	- ↑	-	+ ↓	++ ↓	Yes
USP34	++ ↓	-	+ ↓	+ ↓	Yes
USP18	- ↑	++ ↓	- ↑	-	No
USP6	- ↑	- ↑	-	+ ↓	No
USP32	+ ↓	++ ↓	-	+ ↓	Yes
CYLD	- ↓	- ↓	- ↓	- ↓	No
JOSD1	-	-	-	-	No
UCHL3	++ ↑	+ ↑	+ ↑	++ ↑	Yes

Table 3.2. Deconvolution of hits from PDK1 screen. DUBs whose depletion decreased or increased PDK1 protein levels in the screen are indicated in blue and red respectively. Changes in protein level of more than 20% are indicated by an arrow in the direction of change. A change in protein level of 20 - 50% (in the same direction as the pool in the original screen) is indicated by +, greater than 50% by ++, while less than 20% change (or a change in the opposite direction) is indicated by a - sign. Deconvolution was deemed successful if at least two siRNA oligonucleotides recapitulated the results of the pool.

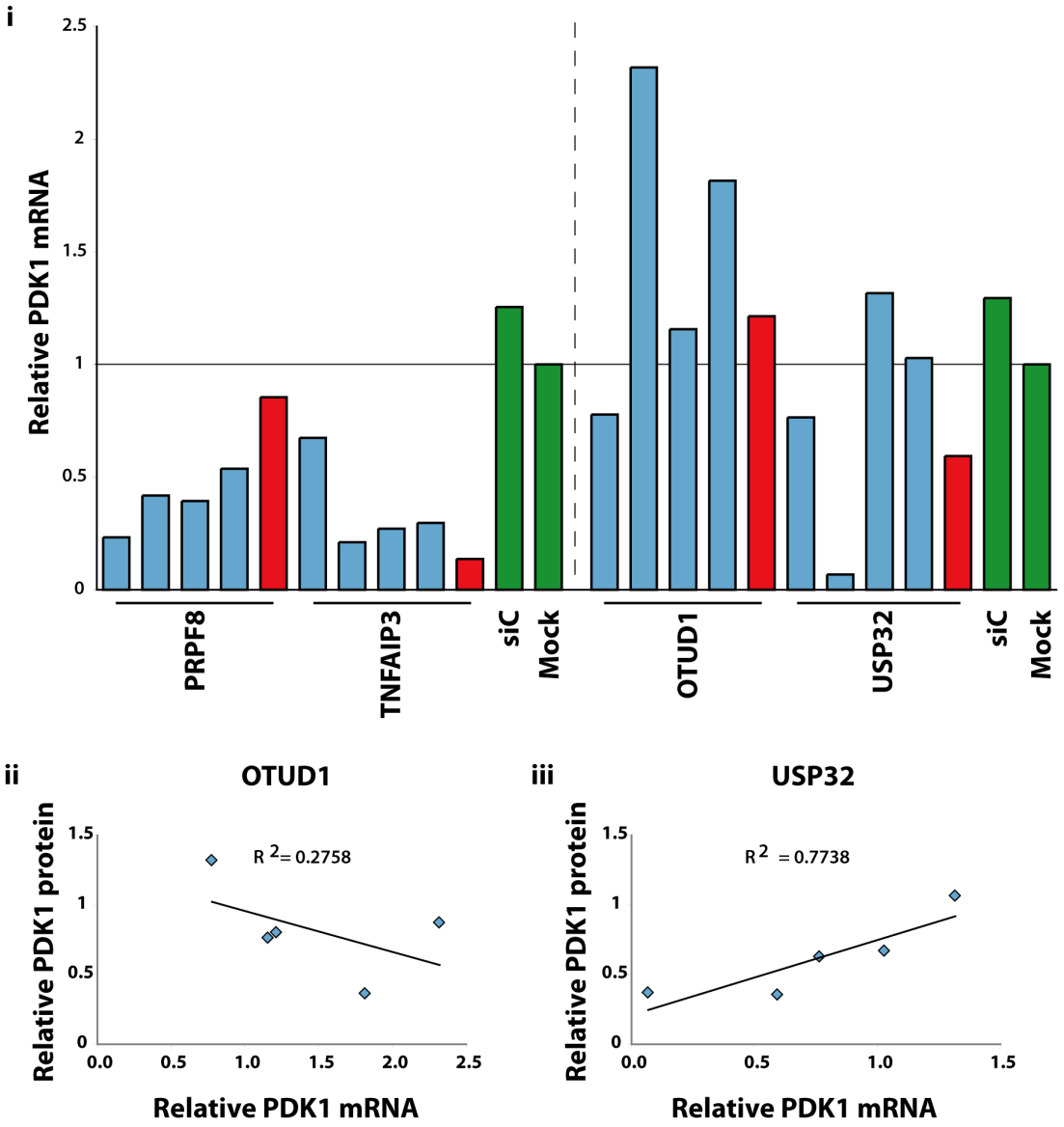

Fig 3.21. PRPF8, TNFAIP3 and USP32 depletion decreases PDK1 transcript levels. **i**. A549 cells were transfected with siRNA oligonucleotides against the indicated targets and incubated for 72 hours after which total RNA was extracted. cDNA was prepared by reverse transcription, after which QPCR was performed using an iQ5 Real-Time PCR detection system and SYBER green mastermix (BioRad) using actin as the reference gene. The knockdowns were performed in two separate experiments, respectively shown to the left and right of the dotted line, with independent controls. In each case mRNA level was calculated with reference to the mock control. For each target, oligonucleotides A-D are shown from left to right and the pools in red. The controls are in green. **ii,iii.** Correlation between relative mRNA level as assayed by QPCR and protein level assayed previously by immunoblotting (fig 3.20) for USP32 and OTUD1 respectively. (siC- non-targeting siRNA control)

3.7 Screening for modulators of Akt protein level

The next component of the pathway to be investigated was Akt. Activation of Akt requires two phosphorylation events (section 1.5.2). The first site (T308) is phosphorylated by PDK1 [261], while phosphorylation of the second (S473) is mediated by mTORC2 [264]. Akt in turn is a master kinase, with a host of downstream effectors (section 1.5.2).

Akt is known to be polyubiquitylated through both K48 and K63 linkages (section 1.5.4) with the latter modification leading to membrane localisation and activation of Akt [351]. Depletion of the DUB UCHL1 has been shown to increase proteasomal degradation of Akt ([353] and section 1.5.4). However no attempts have been made to my knowledge to systematically identify DUBs that may be involved in Akt regulation.

3.7.1 Akt antibody characterisation

Three isoforms of Akt are encoded by separate genes, all of which have been implicated in malignancy (reviewed in [398]). In this study, I used an antibody from Cell Signalling (CS9272), which detects all three isoforms; Akt1, Akt2 and Akt3. Although the three isoforms are of very similar molecular weight (~56kDa), it is possible to distinguish them to an extent by immunoblotting (fig 3.22, left). However it is feasible that phosphorylation of Akt isoforms may shift the apparent molecular weight, making analysis of the band structure less clear (fig 3.22, right). The Akt3 band in particular is less clear after treatment with EGF.

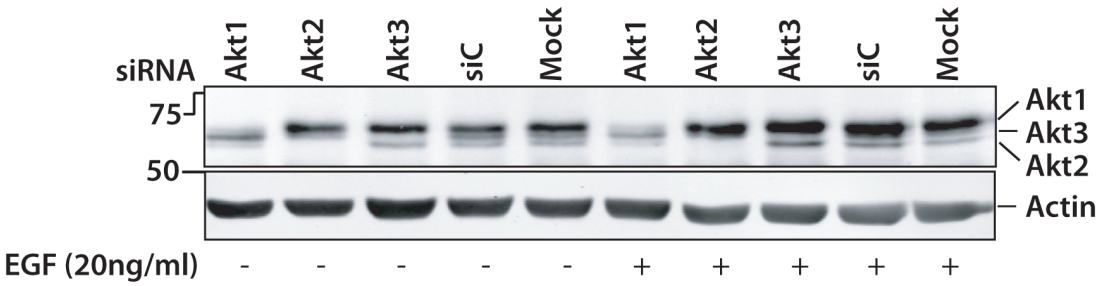

Fig 3.22. Antibody CS9272 detects, and discriminates between, the three Akt isoforms. Knockdown of individual isoforms was performed, and A549 cells were either directly lysed in hot SDS-buffer, or pre-treated with EGF for 15min prior to harvesting. Lysates were run on 8% SDS-PAGE and immunoblotted for Akt and actin. (siC- non-targeting siRNA control).

3.7.2 Akt screen

NP40 lysates from the DUB screen were immunoblotted for Akt (fig 3.23). Three runs (technical replicate gels) were performed and blots from a single replicate are shown in Fig 3.23. It proved impossible to quantify the individual Akt isoforms separately, and although there were visual indications that certain DUB knockdowns affected specific bands disproportionately, these were not consistent between runs and have not been pursued further.

Partly due to the complex band structure, there was extensive variability between runs (fig 3.24i) and the data was therefore also plotted in an alternative fashion to allow comparison (fig 3.24ii) of each datapoint with its neighbours. This allowed an assessment of both the reproducibility between replicates and any gel bias. The five lowest ranked candidates were relatively reproducible between replicates (fig 3.24ii). However, the highest ranked candidates were biased by replicate run 3. USP44, USP46 and USP47 are all from a contiguous section of blot, and there was little correlation with the other blots. Akt quantification for USP15 depletion was similarly biased by one of the three runs, while in the case of OTUD6B depletion, Akt was only marginally elevated in a second screen. Only DUBs whose depletion

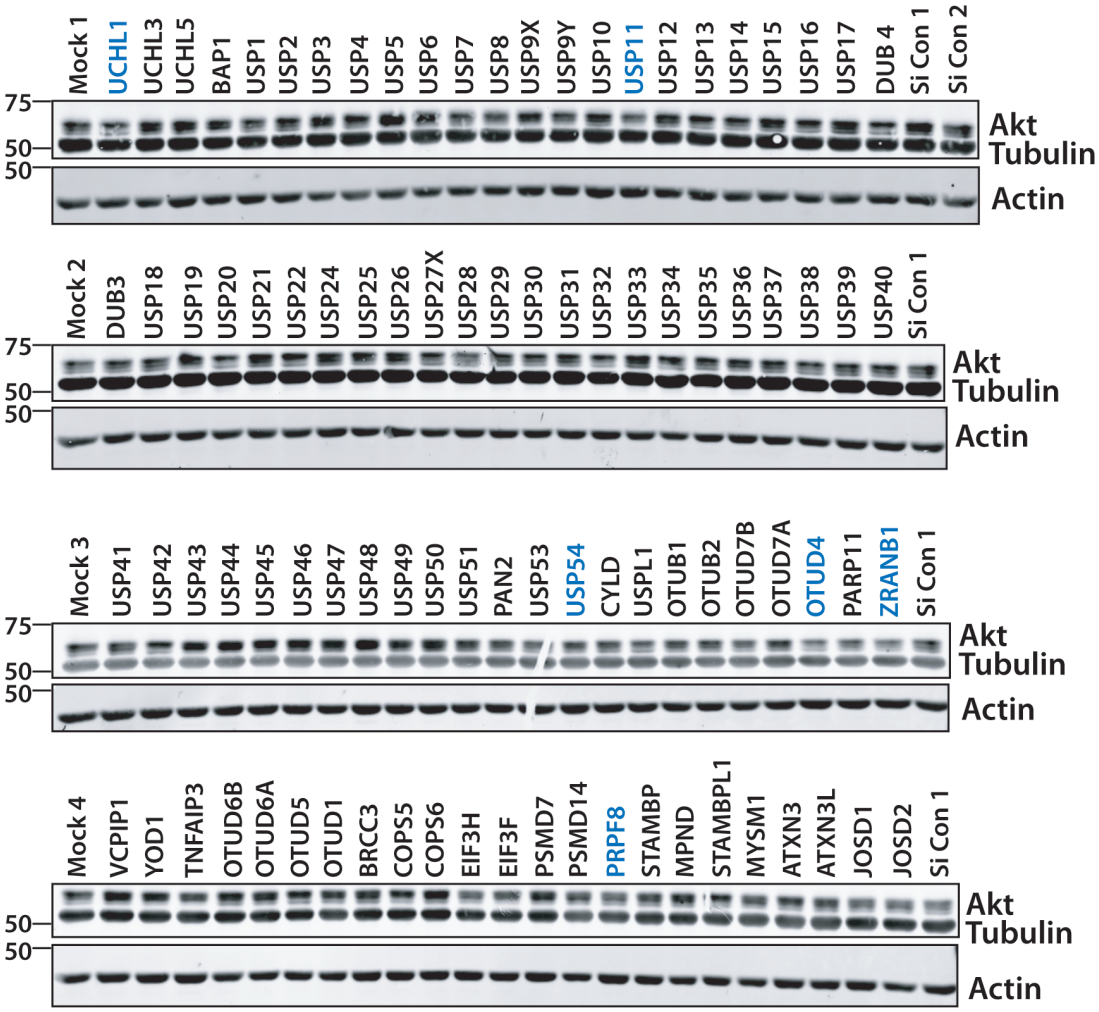

Fig 3.23. An siRNA screen for DUB regulators of Akt level. NP40 lysates from the DUB screen (fig 3.3) were run on four SDS-PAGE gels. Each blot included a mock-transfected and non-targeting siRNA (siC) control. The blots were probed for Akt and actin, and imaged by infrared scanner (Odyssey, LiCor). Immunoblotting of lysates was performed three times and blots from one of the three replicates are shown. Candidate DUBs to be considered for validation are highlighted in blue.

downregulated Akt will be considered for validation, these are: PRPF8, USP54, OTUD4, ZRANB1 and USP11. Depletion of UCHL1 has been reported to reduce Akt stability and thus abundance [353]. In the screen UCHL1 depletion did affect Akt protein level in the expected direction. However UCHL1 was only ranked 14th for the downregulation of Akt protein level, and with limited reproducibility between screens (fig 3.24). Due to the lack of reproducibility between replicates, deconvolution of the Akt screen was not prioritised and has not yet been performed.

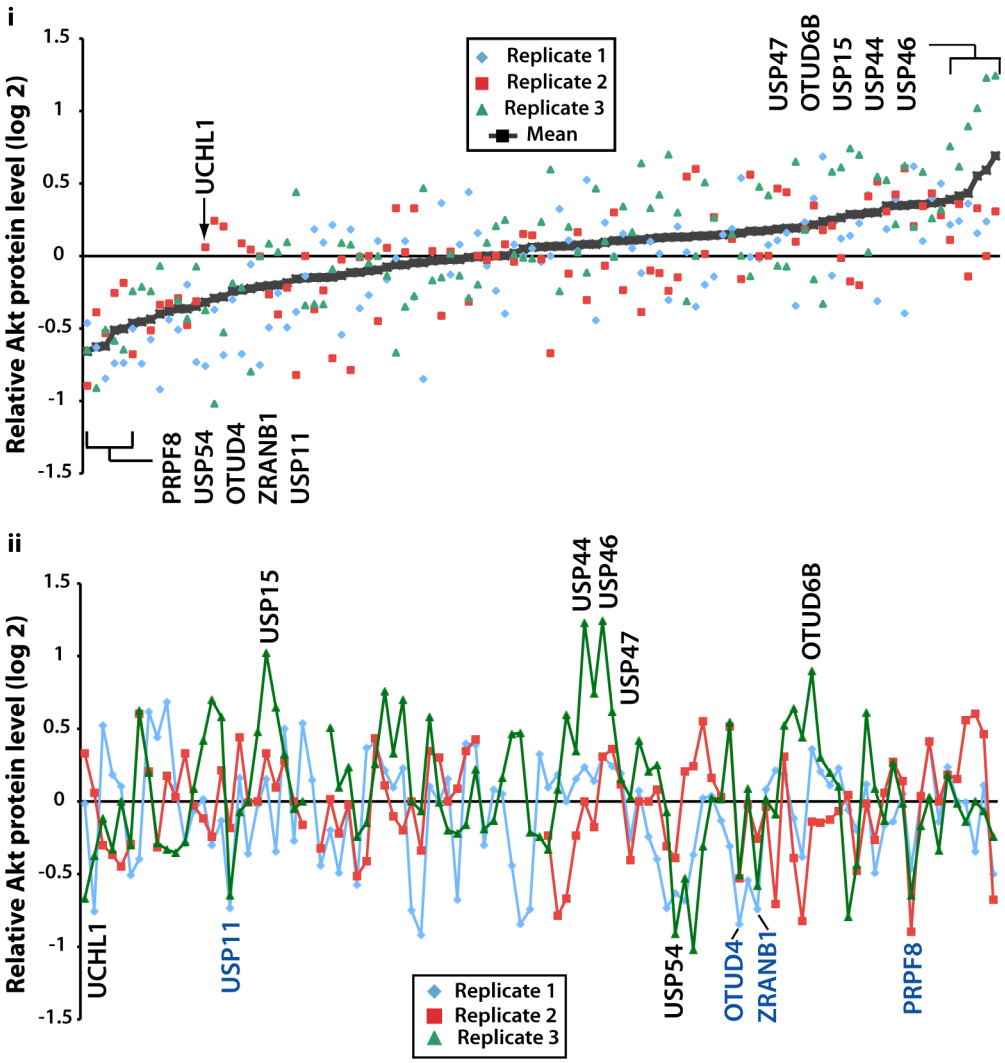

Fig 3.24. Quantification of Akt blots identifies several candidate DUBs whose knockdown decreases Akt protein level. Immunoblotting for Akt and actin was performed and is shown in fig 3.23. **i.** Akt bands were quantified (Odyssey, LiCor), normalised to actin and then the median of each blot. The mean of 3 immunoblotting replicates was ranked from low to high. The 5 top and bottom ranked candidates are highlighted. UCHL1, ranked 14th from the bottom, is highlighted. **ii**. Here the data are not ranked on quantification, but are plotted according to their position on the gel, enabling each data point to be compared with its neighbours.

3.8 Identifying DUB modulators of mTOR

The mammalian target of rapamycin (mTOR) is a key component of two multiprotein complexes in PtdIns3-K signalling (section 1.5.2). The first of these (mTORC1) is a key effector of the pathway [399], while the second (mTORC2) is responsible for the second phosphorylation event leading to full activation of Akt [264]. The recent introduction of mTOR inhibitors into clinical practice has generated further interest in the regulation of this key protein, particularly as mTOR inhibition drives activation of the PtdIns3-K pathway through a feedback loop [400, 401]. Ubiquitylation by the E3 ligase and tumour suppressor FBXW7 has been shown to promote degradation of mTOR and cell lines harbouring mutations in FBXW7 have been shown to be particularly sensitive to mTOR inhibitors [402]. However, no DUBs have been shown to regulate mTOR function.

NP40 lysates from the DUB library were immunoblotted for mTOR. Three technical replicates of the immunoblotting were performed. Unfortunately the signal was very variable across blots and inconsistent between replicates such that quantification was not informative. However, a striking reduction in the protein level of mTOR following YOD1 knockdown was observed in all replicate runs, and an example of one of these blots is shown in fig 3.25i. This effect of YOD1 depletion on mTOR was however only recapitulated by one of the four oligonucleotides from the original siRNA pool (fig 3.25ii). This does not appear to be due to differences in YOD1 depletion efficiency between oligonucleotides, as all generated satisfactory depletion of YOD1 as shown in fig 3.25iii.

Depletion of two other DUBs, namely OTUD5 and TNFAIP3, also had reproducible effects on mTOR in the three technical repeats, increasing the mTOR protein level in all cases (fig 3.25i). Deconvolution of these two candidates has not yet been performed.

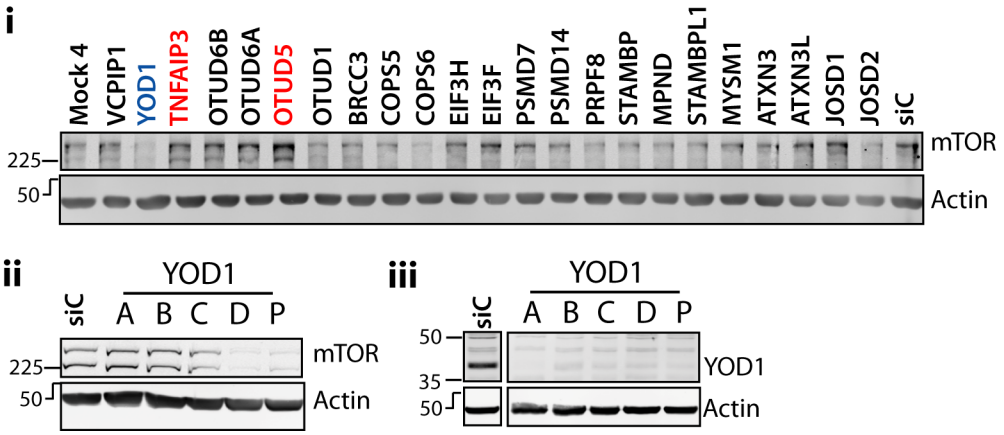

Fig 3.25. Knockdown of YOD1 reduces mTOR protein level through a potential off target effect. NP40 lysates from the DUB screen (fig 3.3) were run on four SDS-PAGE gels. Each blot included a mock-transfected and non-targeting siRNA (siC) transfected control. The blots were probed for mTOR and actin, and imaged by infrared scanner (Odyssey, LiCor). Immunoblotting of lysates was performed three times. **i.** Example of one of the blots showing effects of depletion of several DUBs on mTOR protein level. **ii,iii**. A 72-hour knockdown of YOD1 was performed with each of the four oligonucleotides from the original pool (designated A-D) and the pool (P), the cells were lysed with NP40, and lysates immunoblotted for mTOR (ii) or YOD1 (iii).

3.9 A549 cells express low levels of FOXO1, FOXO3 and FOXO4 protein

The FOXO family of transcription factors are key effectors of the PtdIns3-K pathway, and are known to be subject to both poly- and monoubiquitylation (section 1.5.4). In the case of FOXO4 (and FOXO3), monoubiquitylation has been shown to be reversed through the action of USP7 [205]. I had intended to systematically investigate the role of DUBs in the regulation of the FOXO family members in both cytosolic (NP40) and nuclear (Dignam C) fractions. However, the signal obtained with several different antibodies (against FOXO1, 3 and 4) using either fraction or the whole cell lysate was extremely low, indicating low expression levels and thus precluding an immunoblotting-based screen in this cell line.

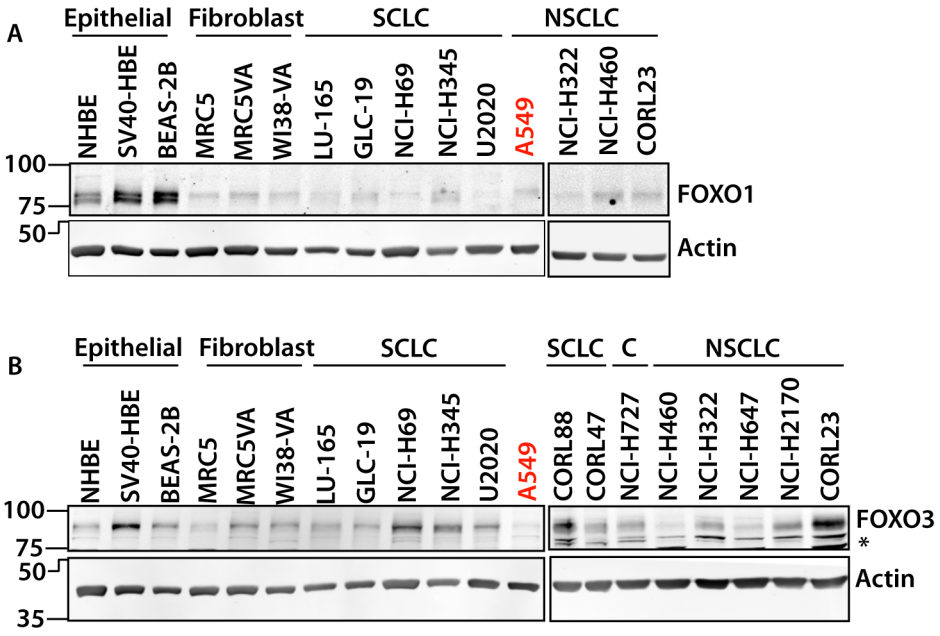

Fig 3.26. Low FOXO1 protein expression in lung cancer cell lines. A panel of cell lines were maintained under normal, basal culture condition. Whole cell lysis of cells was performed with hot SDS buffer. Equal amounts of lysate were immunoblotted for FOXO1 (**i**) or FOXO3 (**ii**) and actin. The first three 'normal' cell lines were derived from bronchial epithelium, while the other three normal cell lines were derived from lung fibroblasts. (asterisk indicates non-specific bands, SCLC- small cell lung cancer, NSCLC- non-small cell lung cancer, C- carcinoid).

FOXO protein expression was also assessed in a panel of cell lines derived from small cell lung cancer (SCLC), non-small cell lung cancer (NSCLC) and normal lung fibroblasts or epithelial cells (Fig 3.26), to identify alternative cell lines which may be used in future screens for modulators of FOXO abundance. Lysates from these cell lines had been prepared previously by J. Coulson and M. Faronato. FOXO1 expression was virtually undetectable in all of the SCLC and NSCLC lines (fig 3.26i). Interestingly, 3 cell lines derived from lung epithelium (non-malignant) showed higher FOXO1 expression, while three cell lines derived from normal lung fibroblasts did not (fig 3.26i). FOXO3 expression was more variable across the panel, with a proportion of both SCLC and NSCLC cell lines expressing higher protein levels (fig 3.26ii), and it may therefore be feasible to perform a screen for DUB regulators of FOXO3 abundance in one of these cell lines in future.

In chapter 4, I will describe a second screening approach to identifying DUB regulators of the PtdIns3-K pathway, in which translocation of stably expressed FOXO3-EGFP was employed as a read out. This also provided the opportunity to identify DUBs that regulated the abundance of overexpressed EGFP-tagged FOXO3, which will be discussed in section 4.4.

3.10 Discussion

In this chapter I have described a systematic approach to investigating the role of DUBs in the regulation of the protein level of nine components of the PtdIns3-K pathway (fig 3.27). This led to the identification and initial validation of several novel regulators of two core components, PTEN and PDK1 (fig 3.27), and in addition has identified lead candidates for the regulation of other components of the pathway (listed in table 3.3).

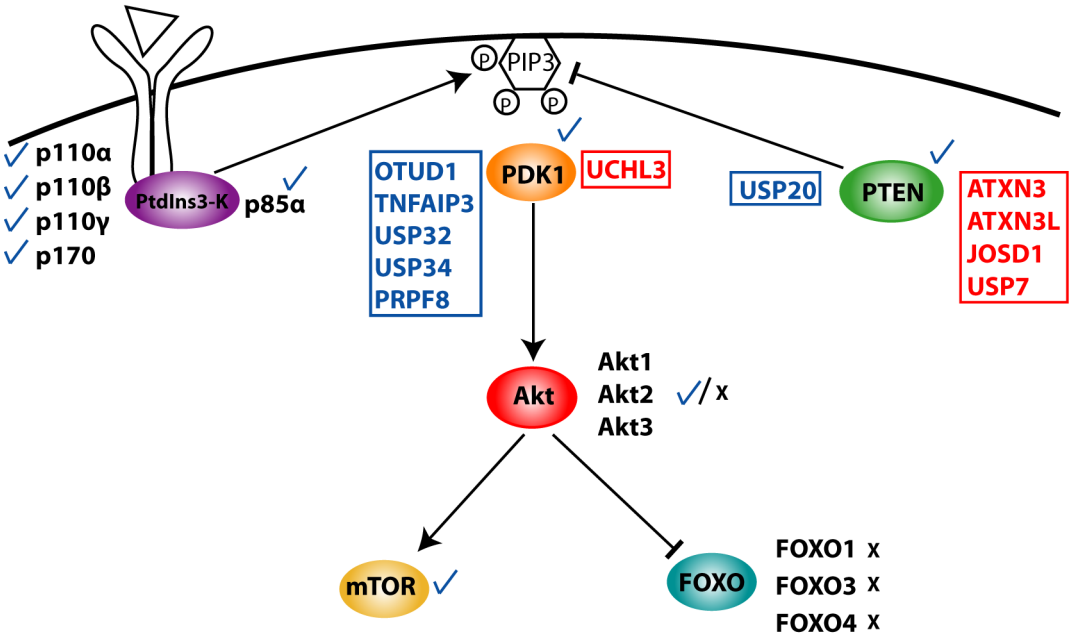

Fig 3.27. Graphical summary of a systematic investigation into the role of DUBs in the regulation of the PtdIns3-K pathway. Ticks denote components of the pathway that were successfully investigated through immunoblotting, while those marked with a cross were not. Isoforms of PtdIns3-K, Akt and FOXO included in this study are listed. Assessment of the individual Akt isoforms was not feasible, and a combined quantification of all three isoforms was therefore performed. The boxes highlight candidate DUBs which were successfully validated through deconvolution. (red and blue indicate DUBs whose depletion respectively leads to upregulation or downregulation of the target protein).

DUB	PTEN	p110α	p110β	p110γ	p170	p85α	PDK1	Akt	mTOR
UCHL3	D1						**U1**		
USP20	**D2**					U4			
USPL1	D3								
YOD1	D4		D3	D4	D				D
STAMBPL1	U1								
OTUD4	U2							D3	
JOSD1	**U3**						U2		
ATXN3	**U4**								
USP2	U5								
ATXN3L	**U7**								
USP7	**U9**								
OTUD1		D1					**D3**		
BAP1		D2							
USP48		D3		D1	D				
USP41		D4	D5						
UCHL5		D5							
USP37		U1							
USP2		U2							
USP30		U3	U3						
OTUD7A		U4		U1					
USP42		U5							
USP27X			D1		D				
USP18			D2				D4		
JOSD2			D4			U1			
PSMD14		*	**U1**	**U2**	**¶**				
MPND			U2						
USP9Y			U4			D4			
USP24			U5						
USP19				D2					
USP21				D3					
USP11				D5				D5	
PDMD7		*		**U3**	**¶**				
USP47				U4	U				
USP46				U5	U				
OTUD6A					U	U5			
EIF3F						D1			
PRPF8						D2	**D1**	D1	
VCPIP1						D3			
USP54						D5		D2	
USP4						U2			
USP3						U3			
TNFAIP3							**D2**		U
USP34							**D3**		
USP6							D4		
USP32							**D5**		
CYLD							U3		
ZRANB1								D4	
OTUD5									U

Table 3.3 Summary of candidate DUBs affecting the stability of selected PtdIns3-K components. DUBs identified in each screen are listed. D and U indicate down and up-regulation respectively, and the number in each case represents the ranking. For example D1 represents the candidate DUB whose depletion most strongly downregulated the abundance of the respective PtdIns3-K component. The p170 and mTOR screens were not quantified for technical reasons, and so candidates are not ranked. Candidate DUBs which were successfully deconvoluted are highlighted in green, while those which were not are in orange. The remainder have not been deconvoluted. The two proteasomal components (PSMD14 and PSMD7) are highlighted in bold. The asterisk refers to upregulation of a higher molecular weight species of p110α on depletion of either PSMD14 or PSMD7. The ¶ refers to a higher molecular weight smear of p170 observed on depletion of the same DUBs.

The siRNA transfections and lysate production were performed on a large scale, thus allowing assessment of protein stability for multiple targets within the PtdIns3-K pathway, and providing a valuable resource for other projects in the laboratory. Knockdown efficiency has only been determined for a selection of targets, but where assessed appears satisfactory (fig 3.5).

Notably, RNAi screening methodology is subject to both false positive negative discovery rates ([387, 388] section 3.2). In the screens I performed in this work, several steps were taken to minimise both false positives and negatives. Firstly, the library I employed utilised pools of four siRNA oligonucleotides against each DUB target rather than single oligonucleotides. This would be expected to compensate for potential poor knockdown efficiencies of individual oligonucleotides, and thus reduce false negative results [403]. Interestingly, recent work suggests that increasing pool complexity may also reduce off-target effects (and thus false positives), at least at the mRNA level [389]. Although increasing the number of siRNA oligonucleotides would likely increase the number of other transcripts affected, the concentration of each siRNA oligonucleotide in the pool is decreased thus reducing the magnitude of its off-target effects [389].

Both false positive and negative results may be reduced by experimental repeats and technical replication [404]. However, due to time and practical constraints, the initial generation of a library of DUB knockdown lysates was performed only once. Multiple technical replicates of the immunoblotting step were however performed for the majority of screens. While immunoblotting is an extremely well established methodology, and the only feasible method for studies such as this, it is subject to several limitations which may cause variability between replicate immunoblotting of the same sample [405]. Additionally, due to the number of samples in the lysate library, several large blots were run per screen, which increased the likelihood of variability across screens, and introduced a further step (and thus source of error) to enable comparison across blots. The use of multi-strip immunoblotting has been proposed as an alternative strategy, to minimise such variability [406] and may be an option for further work.

A relatively large proportion of the hits (approximately 10%) were selected for further investigation, in order to reduce the likelihood of false negatives. In two of the screens, these candidates have been refined by deconvolution. This was deemed successful if at least two of the individual oligonucleotides making up the pool recapitulated the effects seen in the screen. Approximately half of the candidates subjected to deconvolution met the criteria set. The remainder of the screens have not been subject to deconvolution experiments to date, due to time constraints.

Five DUB regulators of PTEN protein level were identified, and validated by deconvolution. They include USP7, which has been shown to reverse monoubiquitylation of PTEN, and thus promote its nuclear exclusion [203]. While the study did not address the effects of USP7 on PTEN stability, PTEN nuclear localisation has been shown elsewhere to result in its protection from polyubiquitylation and thus degradation [57]. It is thus possible that USP7 depletion would lead to increased monoubiquitylation of PTEN, its nuclear localisation and hence stabilisation, which would fit with the results seen in my screen. Nuclear localisation of PTEN following USP7 depletion has not been assessed. However in other experiments, PTEN was almost entirely extracted in the NP40 fraction (see fig 6.7). While this may reflect a true cytosolic localisation of PTEN, it may alternatively be due to extraction of nuclear PTEN in the NP40 fraction. This has not been investigated further, and USP7 was not prioritised for further study.

Depletion of ATXN3, ATXN3L or JOSD1 also increased PTEN protein level, and this was confirmed in each case by more than one siRNA oligonucleotide. The effects of USP20 depletion were less clear. Depletion by two out of four siRNA oligonucleotides resulted in a decrease in PTEN protein level, thus recapitulating the effect of the pool. However, the other two oligonucleotides had the opposite effect and led to an increase in PTEN level. Regulation of PTEN by any of these four DUBs has not been described previously.

ATXN3 was first identified due to its role in Machado-Joseph disease. Subsequently it has been shown to have multiple functions, including regulation of retrotranslocation of substrate in endoplasmic reticulum associated protein degradation (ERAD) [407] and transcriptional repression [378]. Recently, increased longevity was described in *C. elegans* worms deficient in ATXN3 and p97 [408]. Interestingly this appears to be mediated through IGF signalling [408]. Another potential link between ATXN3 and PtdIns3-K signalling is suggested by a proteomic study of the EGF induced ubiquitin network, which included ATXN3 and JOSD1 [409]. No functions have been ascribed to JOSD1.

The host laboratory has previously shown a role for ATXN3L in hepatocyte growth factor-induced scattering of epithelial cells [385], but no other functions have been described to date. USP20 on the other hand stabilises HIF-1α [92], regulates β2-adrenergic receptor recycling [91] and is a negative regulator of NFκB signalling [93].

Six candidates DUBs were identified that regulate PDK1 (fig 3.27). Four of these were assessed by QPCR, which showed that depletion of PRPF8, TNFAIP3 or USP32 decreased PDK1 mRNA levels, suggesting that their effects on PDK1 are manifested through regulation of transcript levels. The effects of OTUD1 on PDK1 protein level on the other hand appeared to be independent of transcript level.

PRPF8 is a member of the JAMM/MPN+ family of DUBs, although it is catalytically inactive [410]. It is however a core component of the spliceosome [411], suggesting that its effects on PDK1 may be mediated through defects in splicing. This is supported by the finding that PRPF8 depletion reduced PDK1 mRNA levels. PRPF8 depletion also reduced p85α and Akt levels, however neither of these findings has been validated.

TNFAIP3 is a well-established negative regulator of the NFκB pathway. It has both DUB and E3 ligase activity allowing it to act through a ‘ubiquitin-editing‘ mechanism whereby K63 ubiquitin chains are removed from key mediators of

the pathway, and replaced with K48 chains leading to their degradation [185]. There is extensive cross talk between NFκB and PtdIns3-K signalling [412, 413]. Moreover RIP1 (a TNFAIP3 substrate) has been shown to downregulate PTEN and mTOR at a transcriptional level [414]. Similar indirect mechanisms may explain the effects that I observed of TNFAIP3 on PDK1 mRNA level.

No functions have been ascribed to OTUD1 in the literature as yet. OTUD1 has however been shown to interact with USP11 [415], another DUB that has been shown to be involved in NFκB signalling [416]. Intriguingly CYLD, which was also identified in this screen (although it did not validate through deconvolution), is a further DUB classically associated with NFκB signalling [126, 127].

The other two DUBs whose depletion led to decreased protein levels of PDK1 were USP32 and USP34. USP32 has been shown to be overexpressed in breast cancers [417], but no substrates have been described. USP34 on the other hand regulates the stability of axin, and thus wnt/β-catenin signalling [195]. Depletion of the final candidate, UCHL3, led to increased PDK1 protein levels. Significantly, UCHL3 has previously been implicated in insulin signalling and adipogenesis [418]. In that study, decreased activation of the PtdIns3-K pathway was observed in response to insulin signalling in mouse embryonic fibroblasts derived from UCHL3 knockout mice [418]. While these results appear contrary to the results in my screen, this may indicate cell type dependence, or represent a feedback mechanism.

Interestingly, depletion of one or other of two proteasomal DUBs, PSMD14 and PSMD7, altered protein levels all four PtdIns3-K catalytic subunits (table 3.3). Both are integral components of the proteasome [394, 395] and their depletion would be expected to phenocopy proteasomal inhibition, leading to protein stabilisation and the accumulation of polyubiquitylated species. Protein levels of p110β and p110γ were both increased by PSMD14 and/or PSMD7 depletion, while higher molecular weight species are seen in the

p110α and p170 screens. These findings suggest that turnover may be relatively rapid for these proteins, and supports further investigation into the role of DUBs in their regulation. Confirmation by proteasomal inhibition has yet to be performed.

In this chapter, I identified several novel DUB regulators of PTEN and PDK1, which are both core components of the PtdIns3-K pathway. Further investigation into the PTEN regulators, USP20, ATXN3, ATXN3L and JOSD1, will be described in chapter 6. Additionally several interesting candidate DUBs were identified for other components of the PtdIns3-K pathway and the study also provided evidence of proteasomal regulation of PtdIns3-K catalytic subunits. Due to time constraints, these latter findings have not been followed up as yet.

Chapter 4

A functional RNAi screen for DUB regulators of the PtdIns3-K pathway

4.1 Introduction

The FOXO group of transcription factors regulate a variety of cellular processes including differentiation, stress response, cell cycling and apoptosis [419]. Activation of the PtdIns3-K pathway leads to Akt-dependent phosphorylation of FOXO resulting in transcriptional inactivation, translocation to the cytoplasm and binding to 14.3.3 ([297, 302, 420], section 1.5.2). Subcellular localization of FOXO is thus dependent on activity of the PtdIns3-K pathway, and provides a readout that has previously been employed in screens for small molecule inhibitors of this pathway [421, 422].

Ubiquitylation is a versatile post-translational modification, involved not only in the regulation of protein stability, but also in the subcellular localization and activity of substrates, including components of the PtdIns3-K pathway (discussed in section 1.6). In chapter 3, immunoblotting was employed to identify deubiquitylases involved in regulating the protein level of several components of the PtdIns3-K pathway. Here I describe an alternative, and complementary approach, in which subcellular localization of FOXO3-EGFP is employed as a marker of downstream activation of the PtdIns3-K pathway. Live cell imaging enabled the design of a dynamic screen, in which the effects of DUB knockdown on the rate and extent of FOXO3-EGFP translocation in response to PtdIns3-K inhibition were followed. Regulation of FOXO3-EGFP abundance by DUBs was also assessed in this screen as a secondary output.

4.2 FOXO3-EGFP screen development and workflow

To facilitate the assessment of nuclear to cytoplasmic shuttling of FOXO, I obtained a human osteosarcoma cell line stably expressing a FOXO3 (FKHRL1)-EGFP construct (FKHRL1-U2OS, Fisher). FOXO3-EGFP is predominantly cytoplasmic under normal cell culture conditions, and as expected translocates to the nucleus on PtdIns3-K inhibition using either a non-selective (LY294002) or selective class IA (PI-103) inhibitor (fig 4.1i). Under basal conditions, FOXO3-EGFP constantly shuttles between the cytoplasmic and nuclear compartments, as indicated by accumulation in the nucleus when export is blocked using Ratjadone A (fig 4.1i). The use of a live cell nuclear counterstain enables FOXO3-EGFP localization to be assayed through image segmentation and analysis (fig 4.1ii). As described in section 2.4, cytoplasmic fluorescence was measured in a perinuclear torus defined by dilating the nuclei. This was used in preference to measuring the whole cytoplasm, which was difficult to define in certain cases due to changes in cell morphology and low-level fluorescence in the cytoplasm, such as occurred following profound nuclear translocation (section 2.4 and fig 4.1ii). The ratio of nuclear to cytoplasmic FOXO3-EGFP was utilised as a single quantitative measure of subcellular localisation (Box 1, Fig 4.1iii).

Live cell imaging of FOXO3-EGFP in FKHRL1-U2OS cells where nuclei were counterstained with a vital dye enables translocation of FOXO3-EGFP to be followed in real time, as shown in fig 4.1iii-v. Treatment of cells with either LY294002 or PI-103 led to a dose-dependant nuclear translocation of FOXO3-EGFP (fig 4.1iv). This is reflected by the ratio of nuclear to cytoplasmic FOXO3-EGFP, which started to increase from about 5 minutes after addition of inhibitor. From 10-25 minutes the increase in ratio was essentially linear after which the rate of change decreased and the ratio reached a plateau at approximately 50 minutes (fig 4.1iv). Both LY294002 and PI-103 are reversible inhibitors of PtdIns3-K, and FOXO3-EGFP rapidly translocates back to the cytoplasm on washout of the inhibitor (fig 4.1iii,iv).

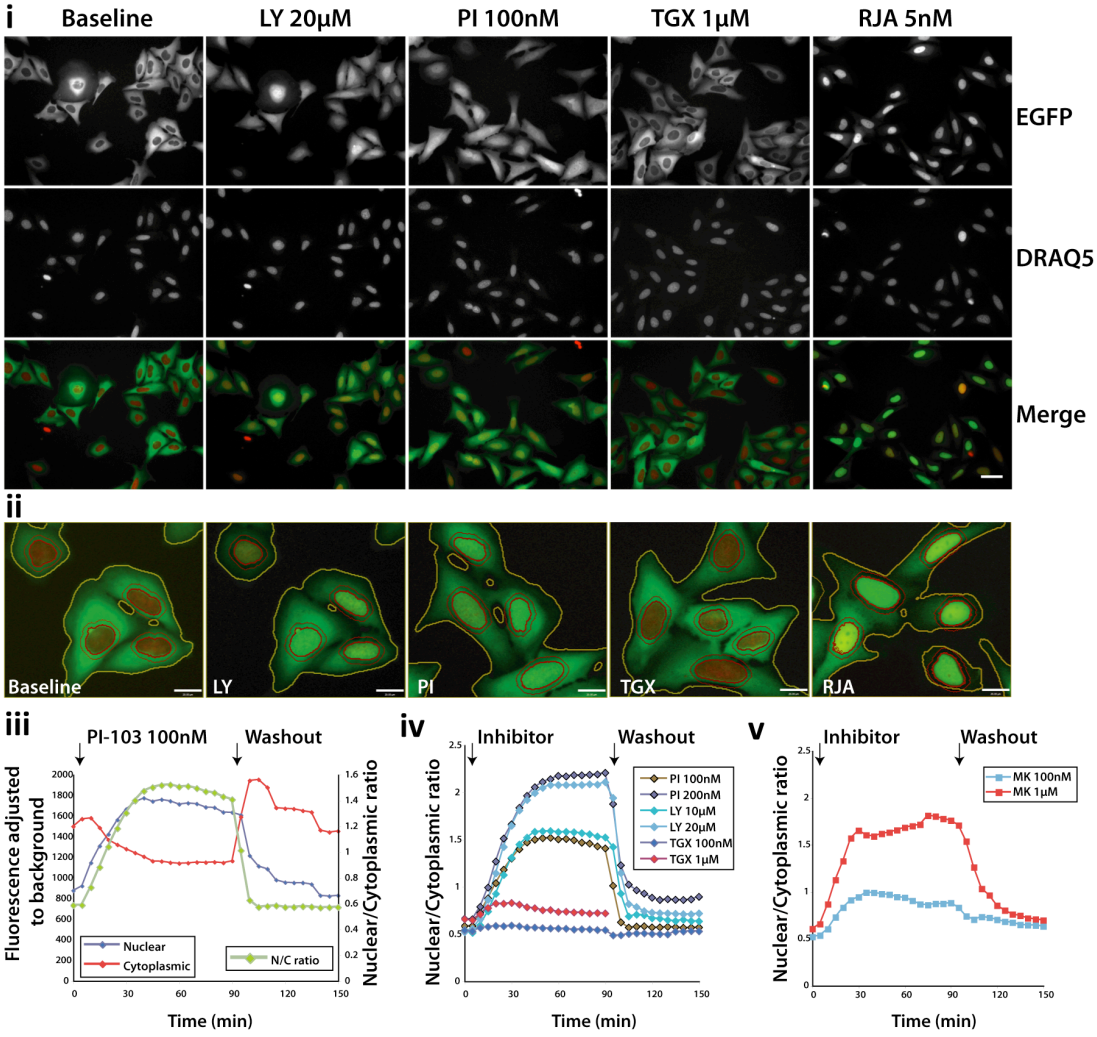

Fig 4.1 FOXO3-EGFP subcellular localization is responsive to inhibition of the PtdIns3-K pathway. FKHRL1-U2OS cells were seeded in a 96 well plate and incubated overnight. The cells were stained with 2.5μM DRAQ5 in phenol red free DMEM for 15 min, after which the media was removed and replaced with HBSS. Fluorescence imaging of each well was performed using a Nikon Ti-E automated microscope. Approximately 20-30 cells were imaged per well. The plate was removed, inhibitors added at the described concentration in Hank's Buffered Saline Solution and imaging performed every 5 minutes for 90 minutes, after which the inhibitors were removed and replaced with fresh HBSS. Cells were then imaged for a further hour. **i**. Representative images taken at baseline (left-hand panel) or 60 minutes after addition of inhibitors. (scale bar: 50μm) . **ii.** Image segmentation and quantification was performed using Volocity (PerkinElmer) software. Nuclei are outlined in a thick red line, the perinuclear torus in a thin red line and the cytoplasm in yellow. (scale bar 20μm). **iii**. Timecourse of mean nuclear and cytoplasmic GFP fluorescence, and nuclear/cytoplasmic ratio following addition of 100nM PI-103. **iv,v**. Timecourse of FOXO3-EGFP translocation in response to indicated inhibitors. Following 1μM TGX-221 treatment, the cells were washed off when the inhibitor was removed. (LY: LY294002, PI: PI-103, TGX: TGX-221, RJA: Ratjadone A, MK: MK-2206, N/C nuclear/cytoplasmic).

Box1. FOXO3-EGFP nuclear/cytoplasmic ratio
The FOXO3-EGFP nuclear/cytoplasmic ratio was the primary output for the screen described in this chapter. The mean intensity of GFP fluorescence in the nuclear (n) and cytoplasmic (c) compartments was measured as described in section 2.4. Subtraction of mean background GFP intensity (b) was performed to obtain corrected nuclear (N) and cytoplasmic (C) fluorescence. The ratio of corrected nuclear to cytoplasmic (N/C) FOXO3-EGFP is thus a measure that integrates changes in fluorescence in both compartments, and acts as a robust indicator of translocation.

Treatment with TGX-221, which is a selective p110β inhibitor with ~1,000 fold selectivity over p110α [423], resulted in minimal translocation (fig 4.1iv) even at a concentration well in excess of the IC50 (5nM against the purified kinase). This suggests p110β is not involved in PtdIns3-K signalling under these conditions, and supports instead a role for p110α and/or p110δ, which are inhibited by PI-103 with an IC50 of 8nM and 48nM respectively. Inhibition of signalling downstream of PtdIns3-K, using the allosteric Akt inhibitor, MK-2206 [424] on the other hand, also resulted in nuclear translocation of FOXO3-EGFP (fig 4.1v), thus demonstrating that FOXO3-EGFP translocation is responsive to perturbation of the PtdIns3-K/Akt signalling axis at multiple levels.

The above findings confirm that the localisation of FOXO3-EGFP in FKHRL1-U2OS cells is responsive to alterations in PtdIns3-K signalling, and provides a readout of activation status of the pathway. Moreover, live cell imaging provides the ability to follow FOXO3-EGFP translocation in response to PtdIns3-K inhibition. This in turn allowed the design of a dynamic RNAi screen to identify DUB regulators of the pathway, not only under basal conditions, but also following its perturbation by the addition of a PtdIns3-K inhibitor (fig 4.2). This has potential benefits as follows. Firstly, depletion of proteins by siRNA (over a period of 48 hours here) may allow cellular adaptation, through upregulation of redundant proteins for example. However in the presence of stress, a partially compensated functional deficit may then be unmasked. Secondly, this approach would favour discovery of

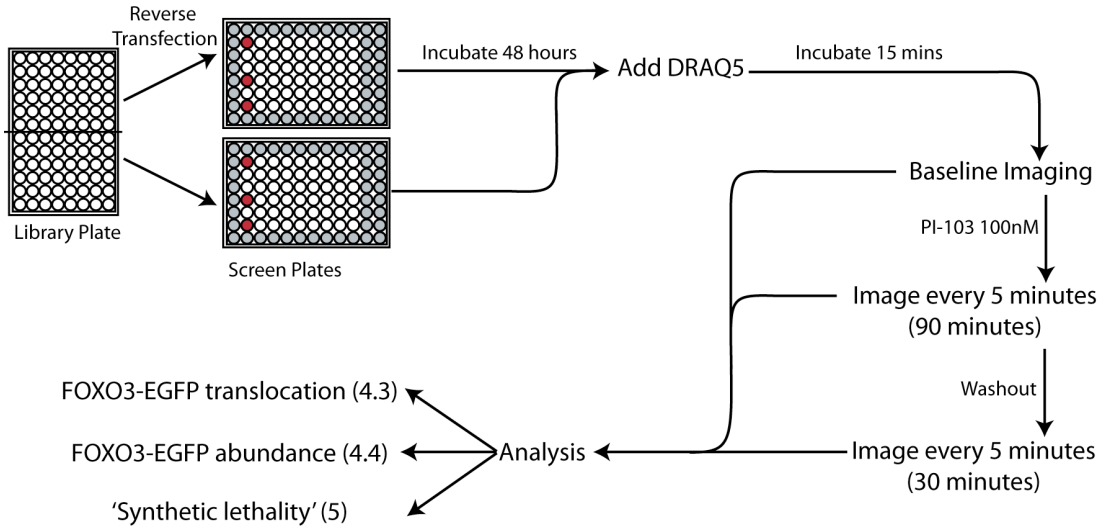

Fig 4.2. Schematic of an siRNA screen for DUB modulators of the PtdIn3-K pathway. FKHRL1-U2OS cells were transfected with siRNA directed at 92 DUBs in 96 well plates. Targets were split equally between 2 plates. 2 mock controls and a non-targeting siRNA control were included on each plate (red). The outermost wells were not utilised for cell culture, and instead filled with PBS to minimise edge effects. After a 48 hour incubation, the cells were counterstained with 2.5μM DRAQ5 and imaged using a Nikon automated microscope as outlined. A single position was selected for each well, and the same position imaged at each timepoint. Image segmentation and quantification of fluorescence was performed using Volocity (Perkin Elmer) software. Three main parameters were analysed, the first two are discussed in this chapter, while the third is discussed in chapter 5.

regulators of the PtdIns3-K pathway, over those of other pathways known to affect FOXO translocation (such as oxidative stress [425]). Additionally, FOXO3-EGFP was predominantly cytoplasmic at baseline suggesting constitutive activation of the PtdIns3-K pathway in these cells, thus reducing the chances of identifying DUBs whose depletion increases PtdIns3-K activity. However, following PtdIns3-K inhibition, FOXO3-EGFP localisation becomes predominantly nuclear, and it would be expected that DUB depletion leading to increased activity of the PtdIns3-K pathway would antagonise this translocation. In the screen, PI-103 was employed at a concentration of 100nM (fig 4.2). At this concentration, PI-103 had been shown to result in sub-maximal translocation of FOXO3-EGFP (fig 4.1iv), thus allowing for measurement of both potentiation or inhibition of the response with each DUB siRNA.

Notably, the predominantly cytoplasmic localisation of FOXO3-EGFP under basal conditions also precluded the reverse approach to a dynamic screen, in which cytoplasmic translocation of FOXO3-EGFP is assayed following stimulation of the PtdIns3-K pathway.

4.3 Identifying DUBs that modulate FOXO3-EGFP localisation

4.3.1 Nuclear translocation screen

Three independent screens were performed for assessment of translocation as outlined in fig 4.2. In each, the ratio of nuclear/cytoplasmic FOXO3-EGFP was assayed for every well once every 5 minutes following the addition, and then washout of 100nM PI-103, using live cell imaging and subsequent quantitative image analysis. Due to the time taken to image all the wells on a 96-well screen plate (approximately 4 minutes), there were slight differences in the timing of imaging between wells after the addition of inhibitor, although each well was imaged at exactly 5-minute intervals. The timepoint for each imaging loop was therefore reported, rather than the absolute time from the addition of the inhibitor.

Trajectories of response to PI-103 treatment (fig 4.3) predominantly followed a similar pattern to that seen in preliminary experiments (fig 4.1), with an initial linear increase in the nuclear/cytoplasmic ratio, followed by a plateau phase and a rapid reduction in the nuclear/cytoplasmic ratio following washout of the inhibitor.

To determine the effects of DUB knockdown, data were analysed at several timepoints; namely at baseline, on reaching plateau, and then pre- and post-washout of inhibitor. The rate of nuclear translocation was estimated by the slope of the linear regression of the ratio between timepoints 2 and 5 (fig 4.3). In each case, data were normalized to the mean of the dataset, then results from the three screens averaged and ranked as shown in fig 4.4i-v.

Alterations to the mean nuclear/cytoplasmic ratio following DUB depletion were modest. At baseline a maximum increase of 39%, and decrease of 14%

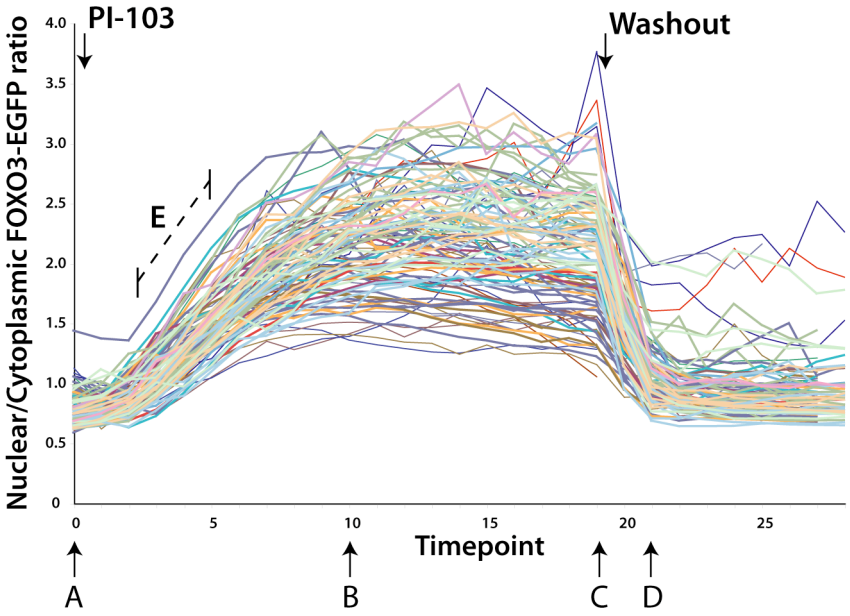

Fig 4.3. Effects of DUB depletion on the timecourse of FOXO3-EGFP nuclear translocation following PI-103 treatment. Three screens were performed, data from one of which are represented here. 48 hours after transfection with a DUB siRNA library, the cells were stained with 2.5μM DRAQ5 in phenol red free DMEM for 15 min, after which the media was removed and replaced with HBSS. A single position in each well was imaged at baseline and then at 5-minute intervals (timepoints) following treatment with 100nM PI-103, and then washout of inhibitor as indicated. Imaging was performed using a Nikon Ti-E automated microscope, and a median of 137 cells were imaged per well (range 49-137). Image analysis was performed for each timepoint using Volocity software (PerkinElmer) and the nuclear/cytoplasmic (N/C) ratio calculated as described in Box 1. The arrows beneath the plot indicate timepoints (baseline [A], plateau [B] and pre- [C] and post [D] washout) at which data from the three experiments were collated for further analysis. The rate of change in nuclear/cytoplasmic ratio between timepoints 2 and 5 (E) was similarly estimated.

were observed following knockdown of USP1 and UCHL3 respectively, while at plateau the maximum increase and decrease (for OTUD1 and USPL1) were 26% and 35% respectively. However, depletion of several candidate DUBs resulted in changes to the nuclear/cytoplasmic ratio that were maintained over multiple timepoints (fig 4.4i-iv) thus shifting the entire curve upwards or downwards (fig 4.4vi). Examples include OTUD1 whose knockdown increased the nuclear/cytoplasmic ratio, and UCHL3 and USP32 whose knockdown decreased it (fig 4.4vi). This is also illustrated in

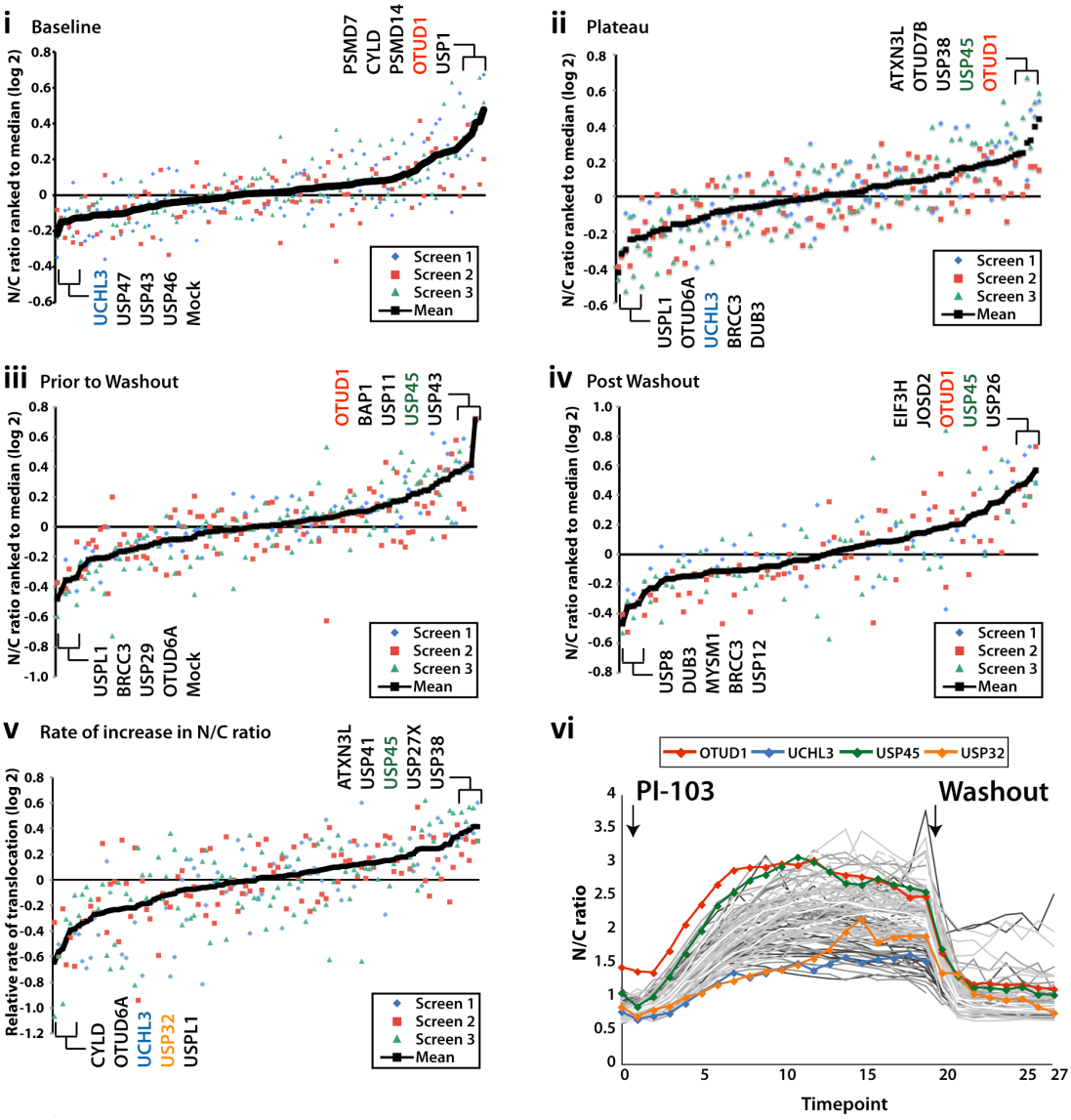

Fig 4.4. Identification of candidate DUBs whose knockdown modulates FOXO3-EGFP translocation in response to PtdIns3-K inhibition. Three independent screens were performed as described in figure 4.3. The first two screens were imaged at 20X and the final screen at 10X magnification. Median (range) of cells imaged per condition were 29 (11-56), 40 (20-71), and 137 (49-238) for screens 1, 2 and 3 respectively. The nuclear/cytoplasmic ratio at baseline **(i),** plateau **(ii)** and pre- **(iii)** and post **(iv)** washout (see fig 4.3) for each screen (blue, red and green respectively) was normalised to the median. The mean of the three screens (black) was ranked as shown. The rate of change in the nuclear/cytoplasmic ratio following treatment with PI-103 (fig 4.3) is similarly ranked in **v**. In each case, the 5 highest and lowest ranked candidates are highlighted. **vi.** Trajectories for OTUD1 (red), UCHL3 (blue), USP45 (green) and USP32 (orange) are overlaid on the dataset from the third screen.

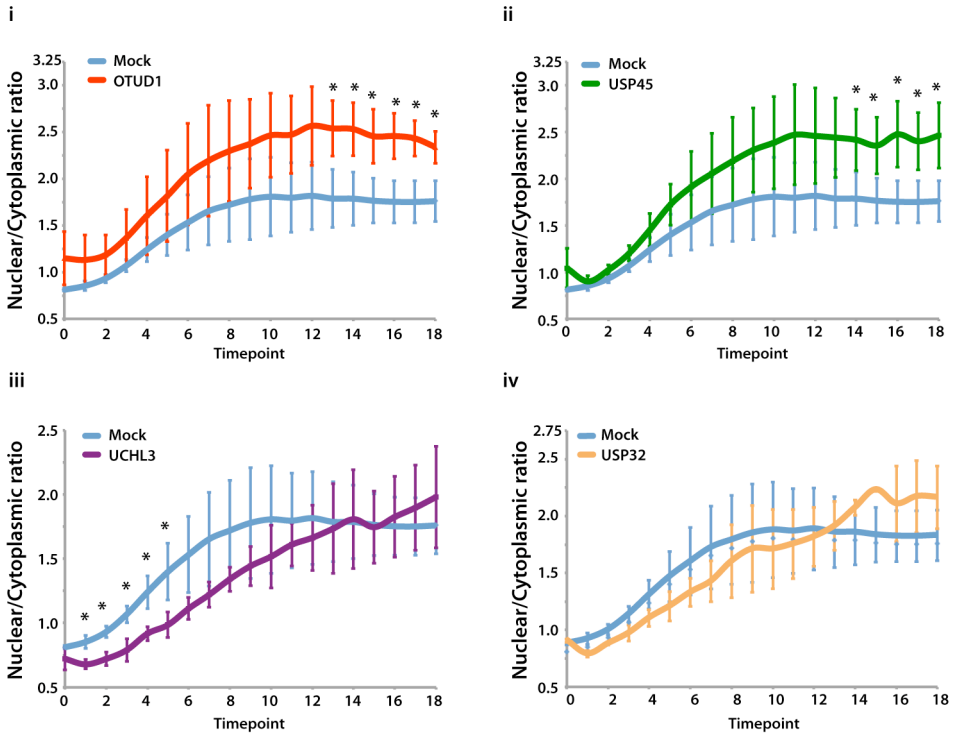

Fig 4.5. Depletion of OTUD1 or USP45 increases nuclear translocation of FOXO3-EGFP. Three independent screens were performed as described in fig 4.4. Changes to the FOXO3-EGFP nuclear/cytoplasmic (N/C) ratio following treatment with PI-103 in cells depleted of OTUD1 (i), USP45 (ii), UCHL3 (iii) or USP32 (iv) are shown in comparison to mock-transfected cells. Similar results were seen on comparison with the non-targeting siRNA control (data not shown). Error bars represent the standard deviation. n=3 with the exception of (iv) where n=2. A student's t-test was used to compare each siRNA depletion with the mock control, the asterisk indicates $p < 0.05$.

fig 4.5, which contrasts the trajectories of selected DUB depletions with the mock controls. Depletion of some of the DUBs altered the rate of nuclear translocation following treatment with PI-103. For example, USP45 depletion increased the rate of nuclear translocation (fig 4.5ii), while depletion of either UCHL3 and USP32 flattened the response (fig 4,5iii,iv).

Unfortunately, several technical factors led to a loss of datapoints, particularly at later time points. These included; focus slippage, poor nuclear staining leading to difficulties segmenting images, and loss of cells during media change. In certain cases there was also evidence of cell death, and

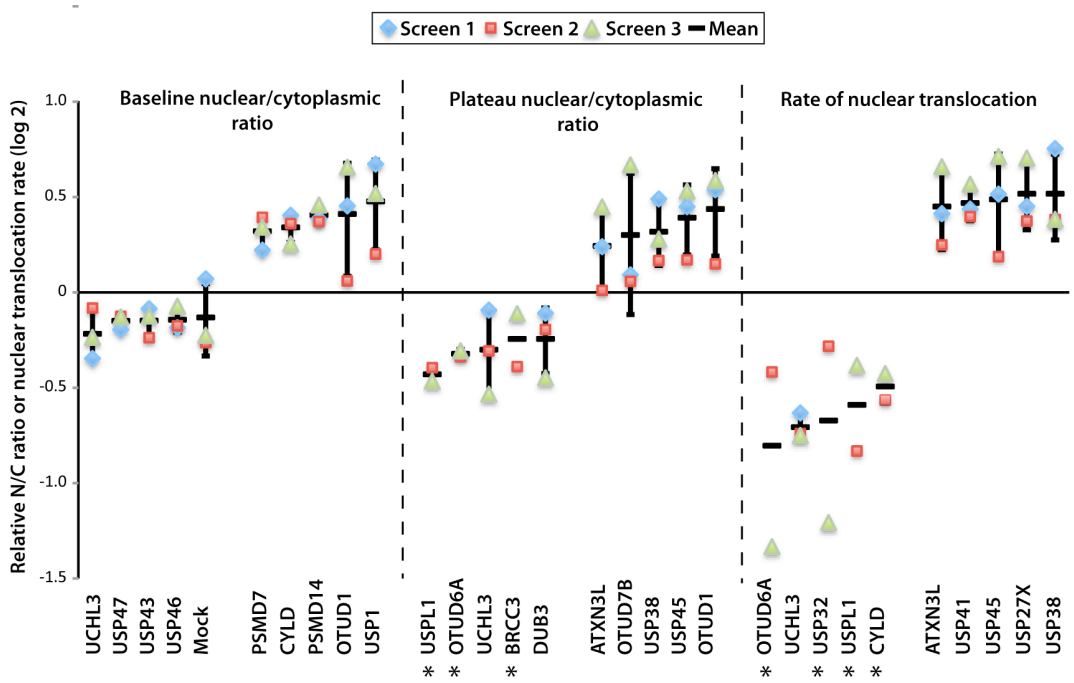

Fig 4.6. Selection of targets for deconvolution. The 5 top and bottom ranked targets from three screens for DUB modulators of the PtdIns3-K pathway (figure 4.4) are shown here in more detail. Candidates altering baseline or plateau nuclear/cytoplasmic ratio, and rate of nuclear translocation are shown from left to right. (Black bar indicates the mean of the three screens, error bars the standard deviation. n=3 with the exception of DUB knockdowns marked with an *, where n=2).

this is discussed further in chapter 5. Due to these factors, deconvolution was limited to candidates identified in the early timepoints only (baseline and plateau nuclear/cytoplasmic ratio, rate of nuclear translocation) for which data were available from at least 2 screens. Exceptions were USP1 and USP43, where data were available from only one experiment for plateau ratio and rate of translocation.

The top and bottom ranked candidates from these timepoints are shown in more detail in figure 4.6. USP47, USP43 and USP46 were not selected for deconvolution, as their effects were very small (less than 10% mean reduction in baseline nuclear/cytoplasmic ratio). OTUD7B was also excluded, as it had minimal effects in two of the three screens. The rest of the candidates were deconvoluted as described below.

4.3.2 Deconvolution of nuclear translocation screen

Deconvolution was performed in triplicate in a similar manner to the original screen (fig 4.2). However the washout step was not performed and cells were only imaged for 55 minutes (11 timepoints) after addition of PI-103. For each candidate DUB, knockdown was performed using the four individual siRNA oligonucleotides that constituted the original pool, which was also used for comparison. Results from the deconvolution experiments are shown in figure 4.7. Deconvolution was deemed successful if two or more single oligonucleotides recapitulated the effects of the siRNA pool. This was defined as a minimum change of 20% from the negative controls. Out of 16 candidate DUBs, 8 (50%) were successfully deconvoluted for at least one parameter (table 4.1).

4.3.3 USP45 and USP32 depletion respectively increase and decrease the nuclear translocation of FOXO3-EGFP in response to PI-103 treatment

USP45 depletion increased both the rate of nuclear translocation and the nuclear/cytoplasmic ratio at plateau in the FOXO3-EGFP translocation screen (fig 4.6). These findings were recapitulated in deconvolution (fig 4.7 ii,iii), which also showed a modest increase in the nuclear/cytoplasmic ratio at baseline following USP45 depletion by two of the siRNA oligonucleotides (and the pool) (fig 4.8i). A timecourse of the nuclear/cytoplasmic ratio following PI-103 treatment is shown in fig 4.8ii. The increase in nuclear accumulation of FOXO3-EGFP is clearly visible 50 minutes after addition of 100nM PI-103 in USP45 depleted cells (fig 4.8iii).

The findings for USP32 depletion in the screen (fig 4.6) were also recapitulated on deconvolution of the siRNA pool, where depletion of USP32 by three out of four oligonucleotides resulted in a reduced rate of translocation (fig 4.7iii). Examination of the timecourse (fig 4.9i) shows that two of the four siRNA oligonucleotides (A and D), had the most marked effect with a persistently reduced gradient of the curve compared with the controls. Following depletion of USP32 using either of these oligonucleotides, a large

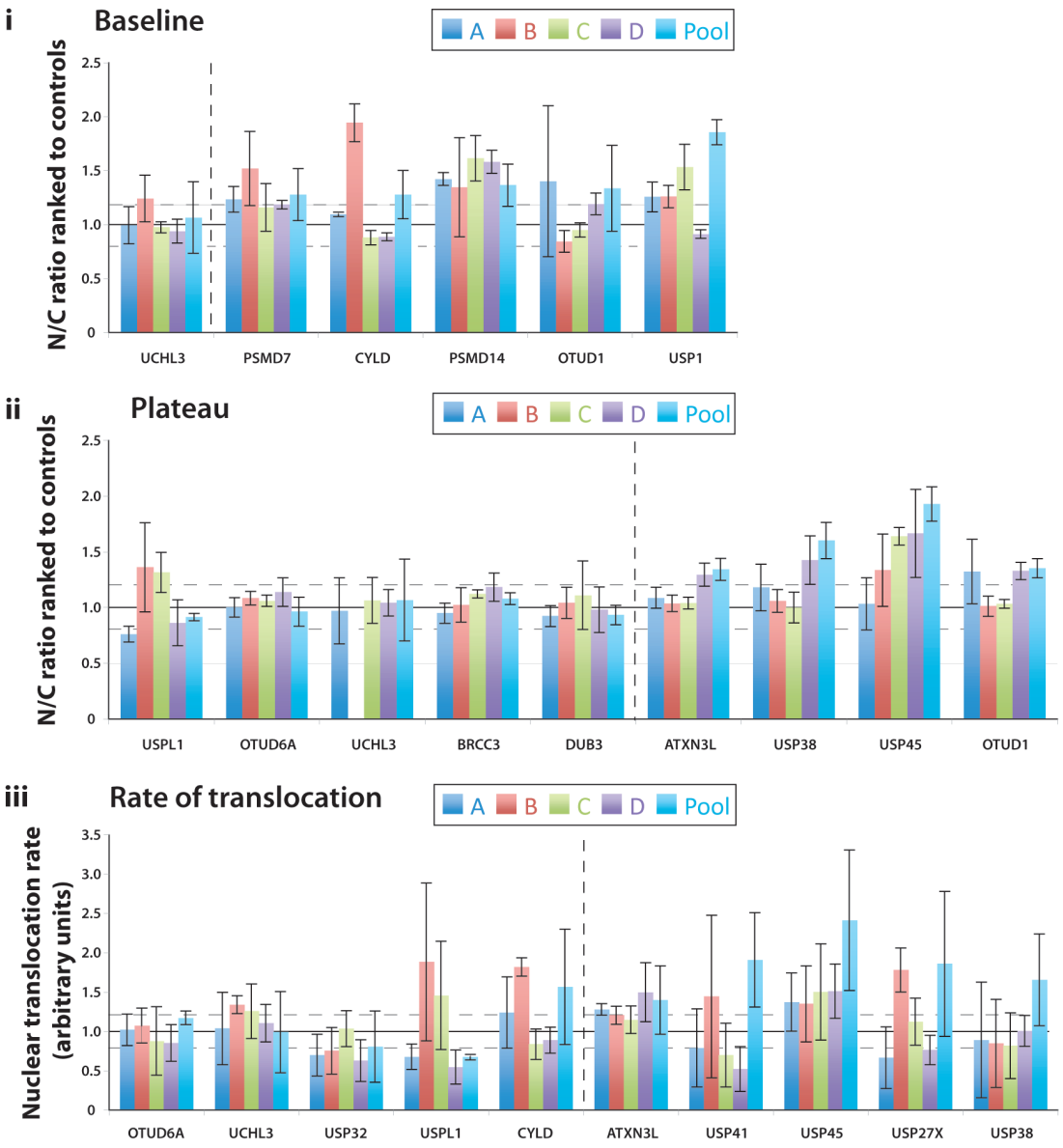

Fig 4.7. Deconvolution of the nuclear translocation screen candidates. FKHRL1-U2OS cells were transfected with four independent siRNA oligonucleotides (A-D) and pooled (P) oligonucleotide against each target. 48 hours after transfection, each well was imaged at baseline and then at 5-minute intervals (timepoints) for 55 minutes following addition of 100nM PI-103 using a Nikon Ti-E automated microscope. A median (and range) of 126 (28-292) cells were imaged per well. Image analysis was performed using Volocity (PerkinElmer) software, and the nuclear/cytoplasmic ratio at baseline and time 10 (plateau) calculated as described in Box 1. The rate of translocation between timepoints 2 and 5 was estimated by the slope of the linear regression. Each datapoint was normalised to the mean of the controls. Deconvolution for baseline and plateau N/C ratio, and rate of increase in N/C ratio are shown in (**i-iii**) respectively. For each oligonucleotide and parameter the mean +/-SD is shown. Horizontal dotted lines indicate +/- 20% change compared to controls. Candidates to the left of the vertical dotted line were downregulated in the screen, while those on the right were upregulated.

DUBs whose knockdown:	↓ Baseline N/C Ratio	↑ Baseline N/C Ratio	↓ Plateau N/C Ratio	↑ Plateau N/C Ratio	↓ Rate of Translocation	↑ Rate of Translocation
UCHL3	1 (N)		3 (N)		3 (N)	
USP1		1 (Y)				
OTUD1		2 (Y)		1 (Y)		
PSMD14		3 (Y)				
CYLD		4 (N)			1 (N)	
PSMD7		5 (Y)				
USPL1			1 (N)		5 (Y)	
OTUD6A			2 (N)		2 (N)	
BRCC3			4 (N)			
DUB3			5 (N)			
USP45				2 (Y)		3 (Y)
USP38				3 (N)		1 (N)
ATXN3L				5 (N)		5 (Y)
USP32					4 (Y)	
USP27X						2 (N)
USP41						4 (N)

Table 4.1 Summary of deconvolution of DUB candidates from the translocation screen. Candidate DUBs selected for deconvolution are shown here with numbers indicating ranking in the original screen (fig 4.4). Deconvolution of candidate DUBs was considered to have been successful where two or more single oligonucleotides recapitulated the effects of the siRNA pool. This was defined as a minimum change of 20% from the negative controls. Deconvolution results are shown in parentheses (Y- Yes, N- No), and successfully deconvoluted candidates are shown in blue (down regulation) or red (up regulation). (N/C- nuclear/cytoplasmic)

proportion of cells showed a persistent cytoplasmic localisation of FOXO3-EGFP despite PI-103 treatment (fig 4.9ii).

OTUD1 was also deconvoluted according to the criteria set, with two of the four siRNA oligonucleotides increasing the nuclear/cytoplasmic ratio at both baseline and plateau. However, only one of the siRNA oligonucleotides resulted in a reproducible increase in all three experiments, and the phenotype was marginal (fig 4.7). Similarly, while three siRNA

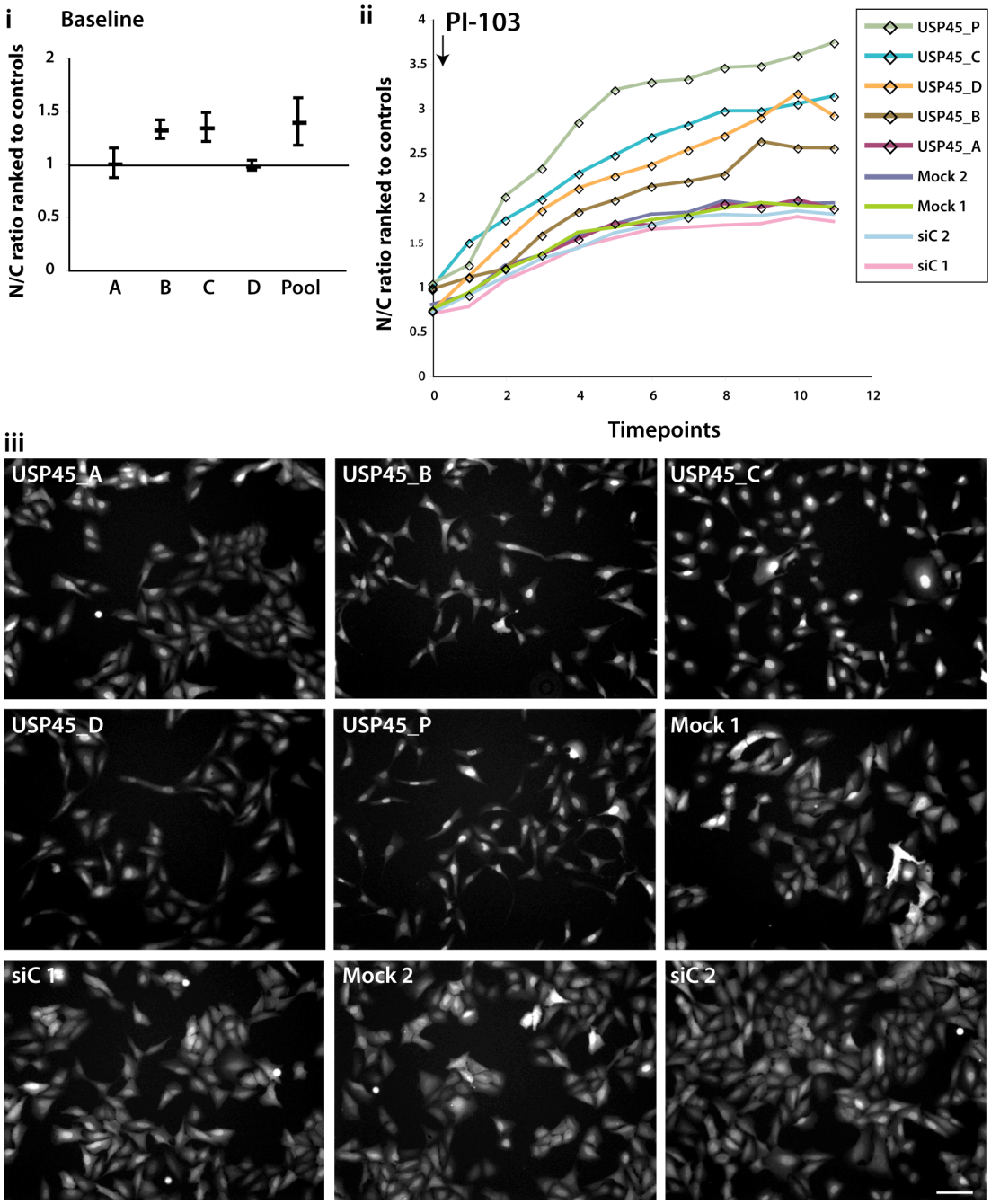

Fig 4.8 USP45 knockdown increases nuclear translocation of FOXO3-EGFP in response to PI-103 treatment. Data for USP45 knockdown from three deconvolution experiments (fig 4.6) are highlighted here**. (i).** Baseline nuclear/cytoplasmic (N/C) ratio following knockdown with 4 individual siRNA oligonucleotides (A-D) and pooled oligonucleotides. The ratio in each case was normalised to the mean of 4 negative controls (2 mock and 2 non-targeting siRNA [siC]). The black bars show the mean of three experiments, and the error bars show the standard deviation. **(ii)** Timecourse of nuclear/cytoplasmic ratio following addition of 100nM PI-103. The data represent the mean of three experiments for each timepoint **(iii)**. Representative greyscale FOXO3-EGFP fluorescence images from timepoint 10 (50 minutes). (scale bar represents 100μm)

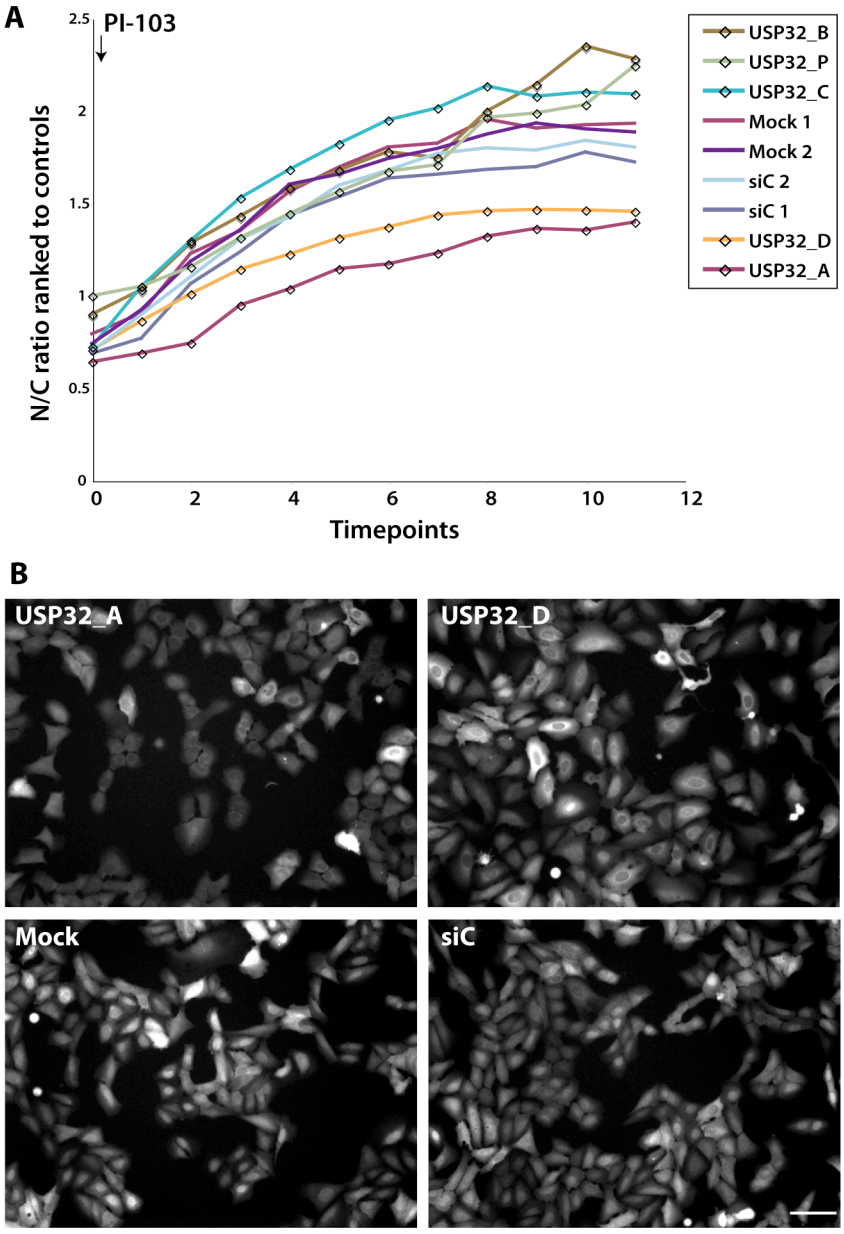

Fig 4.9. USP32 depletion decreases the nuclear translocation rate of FOXO3-EGFP in response to PI-103 treatment. Data for USP32 knockdown from three deconvolution experiments (fig 4.6) are highlighted here. In each experiment knockdown of USP32 was performed with 4 individual siRNA oligonucleotides (A-D) and pooled oligonucleotides. The nuclear/cytoplasmic ratio for each timepoint was calculated as described in Box 1. The ratio in each case was normalised to the mean of 4 negative controls (2 mock and 2 non-targeting siRNA [siC]). i. A timecourse of the nuclear/cytoplasmic ratio following addition of 100nM PI-103 is shown here. The data represent the mean of three experiments for each timepoint. ii. Representative greyscale FOXO3-EGFP images. Scale bar represents 100µm.

oligonucleotides against ATXN3L increased the rate of translocation, only one did so convincingly (fig 4.7C).

In the original screen, UCHL3 depletion reduced the nuclear/cytoplasmic ratio at baseline and at plateau, as well as reducing the rate of translocation (fig 4.6). These effects were not deconvoluted with individual oligonucleotides, and the effect of the pool was also not reproduced (fig 4.6).

USP1, USPL1, and the proteasomal subunits PSMD7 and PSMD14, were also successfully deconvoluted. However, depletion of these DUBs also affected the overall abundance of FOXO3-EGFP (see section 4.4), making it difficult to interpret their effects on nuclear-translocation of FOXO3-EGFP, and this has not been pursued further at present.

4.4 Screening for DUB regulators of FOXO3-EGFP abundance

4.4.1 FOXO3-EGFP fluorescence

A secondary output from the screen was a measure of the total cellular level of FOXO3-EGFP fluorescence indicating changes to the abundance of FOXO3-EGFP. Here, mean total cellular fluorescence was determined at baseline (i.e. in the absence of PtdIns3-K inhibition), corrected for background, normalized to the mean of the dataset and ranked (fig 4.10i). Knockdown of the five top ranked DUB candidates increased FOXO3-EGFP abundance by between 1.5 and 2-fold while depletion of the bottom ranked five candidates decreased FOXO3-EGFP abundance by about half on average (fig 4.10ii). The effects of depletion of those candidates (particularly those reducing FOXO3-EGFP fluorescence) was relatively consistent between experiments (fig4.10ii).

Several DUBs whose depletion affected FOXO3-EGFP abundance, also altered its translocation (USP1, PSMD7, PSMD14 and OTUD6A) and were therefore deconvoluted as described in fig 4.7. In view of the potential utility of stabilizing FOXO3 in cancer therapy, I additionally selected the remainder of the five candidates which upregulated FOXO3-EGFP in the screen for

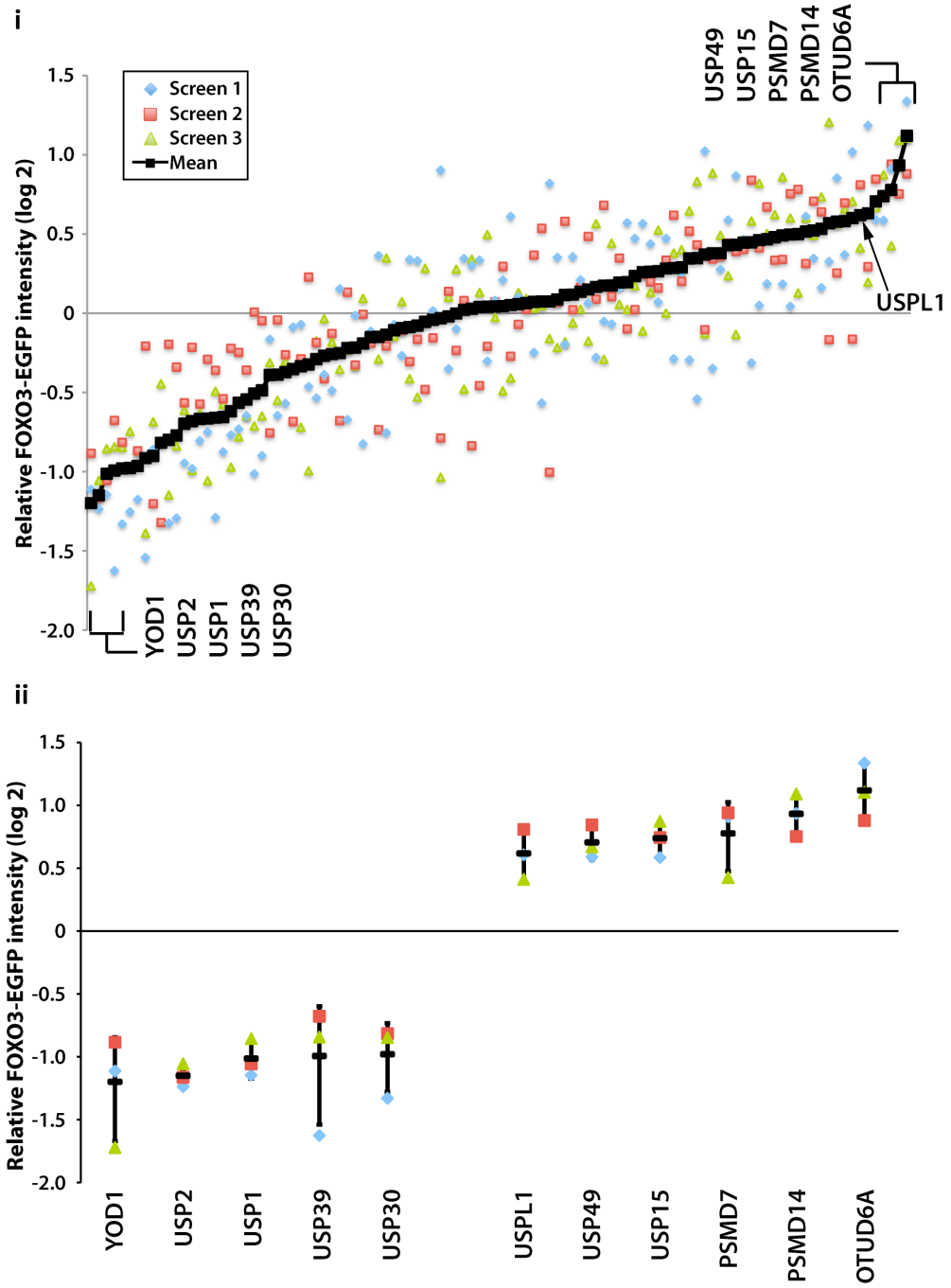

Fig 4.10. Screening for DUB regulators of total cellular FOXO3-EGFP fluorescence. Three independent screens were performed as described in figs 4.3 and 4.4. Here analysis of the mean intensity of FOXO3-EGFP fluorescence at baseline is shown**.** The periphery of the cells were outlined, and mean intensity of GFP fluorescence within cells determined and corrected to background. Results from each screen were normalised to the median. **i.** For each DUB knockdown, the mean of the three screens was ranked and plotted as shown. The top and bottom 5 candidates are highlighted, and shown with error bars in **ii**. Median (range) of cells imaged per condition were 29 (11-56), 40 (20-71), and 137 (49-238) for screens 1, 2 and 3 respectively). Error bars represent standard deviation.

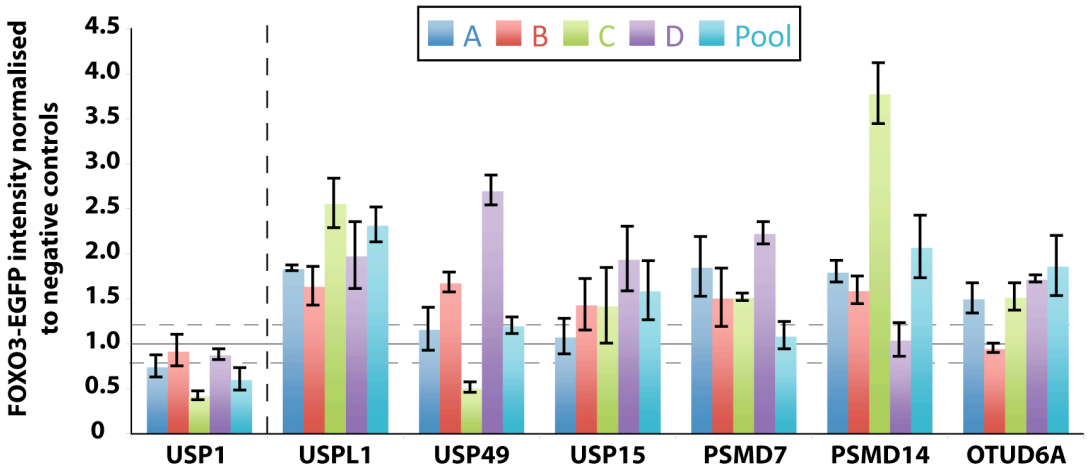

Fig 4.11. Deconvolution of candidate DUBs from the FOXO3-EGFP abundance screen. Candidate DUBs were deconvoluted as described in fig 4.6, and here data for whole cell FOXO3-EGFP fluorescence at baseline (prior to addition of PI-103) are shown, which was calculated as described in fig 4.9. For each candidate DUB, knockdown was performed using 4 individual siRNA oligonucleotides (A-D) and pooled oligonucleotides. Results for each DUB knockdown were normalised to the mean of four negative controls (2 mock and 2 non-targeting siRNA). A median (and range) of 105 (35-246), 98 (28-234), 126 (28-292) cells were imaged per condition in the first, second and third experiments respectively Candidates up and down regulating FOXO3-EGFP in the screen are separated by the vertical dotted line. (Horizontal dotted lines indicate +/- 20%, error bars show SD. n=3)

deconvolution. USPL1, which had also been identified in the translocation screen, was ranked seventh in the abundance screen and was therefore also included in the deconvolution, the results of which are summarised in fig 4.11.

Similarly to the translocation screen, deconvolution was deemed successful if at least two single oligonucleotides recapitulated the effects of the siRNA pool. This was defined as a minimum change of 20% from the negative controls, and all candidate DUBs were deconvoluted successfully by these criteria (fig 4.11).

Both PSMD7 and PSMD14 are integral components of the 19s proteasome, and as discussed in section 3.11, their depletion would be expected to interfere with the proteasomal degradation of proteins thus potentially leading

to their stabilisation. This is supported by the findings here, with depletion of either PSDM7 or PSMD14 resulting in an increase in FOXO3-EGFP fluorescence in the screen, an effect that was recapitulated by 4 and 3 individual siRNA oligonucleotides respectively.

Depletion of USPL1 similarly increased FOXO3-EGFP fluorescence in the screen. This was supported by deconvolution experiments in which depletion of USPL1 by each of the four individual oligonucleotides, or the pool, resulted in an increase in fluorescence, ranging from approximately 50 to 150% (fig 4.11). Representative images for two of the oligonucleotides and two controls are shown in fig 4.12i. This increase in FOXO3-EGFP abundance was further investigated in an independent experiment, in which FOXO3-EGFP was assayed by immunoblotting for either FOXO3 or EGFP (fig 4.12ii). Both the FOXO3 and EGFP antibodies detected the same fusion protein species, and showed similar upregulation following USPL1 depletion (fig 4.12ii). In addition, the results of immunoblotting assay for FOXO3-EGFP abundance were similar to those of the fluorescence experiment (fig 4.12iii).

USP15, OTUD6A or USP49 depletion also resulted in an increase in FOXO3-EGFP fluorescence. All three DUBs were successfully deconvoluted according to the criteria set, however confirmation by immunoblotting has not been performed for these candidates.

Depletion of USP1, on the other hand, resulted in a decrease in FOXO3-EGFP fluorescence. On deconvolution, all four of the oligonucleotides reduced FOXO3-EGFP fluorescence, although this was most appreciable for two of the four (fig 4.11, 4.13i). Confirmation of the effects of USP1 depletion on FOXO3-EGFP abundance was performed by immunoblotting for EGFP and FOXO3 (fig 4.12ii) for which results were very similar to fluorescence microscopy (fig 4.12iii).

Interestingly, USP1 knockdown was also quite toxic, and resulted in a noticeable reduction in cell number at 48 hours post transfection (fig 4.12i). In the three deconvolution experiments, a mean of 47, 63, 69, 126 and 63 cells

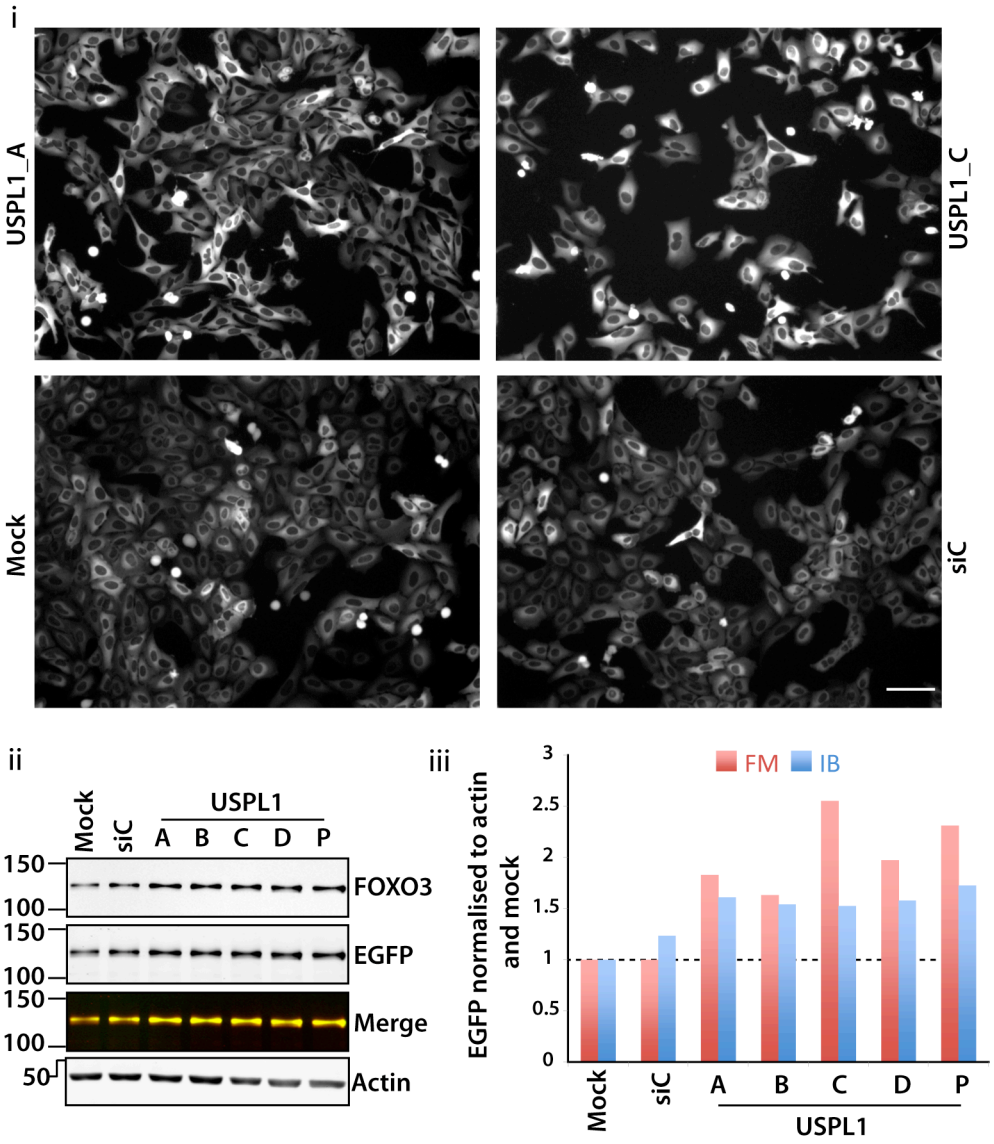

Fig 4.12. Depletion of USPL1 increases FOXO3-EGFP abundance. i. Representative images from the deconvolution experiments described in fig 4.10. **ii.** A 72-hour knockdown of USPL1 was performed using the indicated oligonucleotides, cells were lysed with NP40 and immunoblotted for the indicated proteins. Imaging was performed using an infrared scanner (Odyssey [LiCor]). FOXO3 and EGFP were detected using the green and red channels respectively, and a merge of the results from the two is shown in the third panel from the top. **iii**. Comparison of fluorescence imaging and immunoblotting for EGFP. In each method normalised EGFP signal was compared to the mock control. (A-D: individual siRNA oligonucleotides, P: pool, siC: non targeting siRNA control, FM: fluorescence microscopy, IB: immunoblotting, scale bar represents 100µm, n=1)

were counted per microscopy field following USP1 knockdown using oligonucleotides A-D and the pool respectively, compared to a mean of 163 cells for the negative controls.

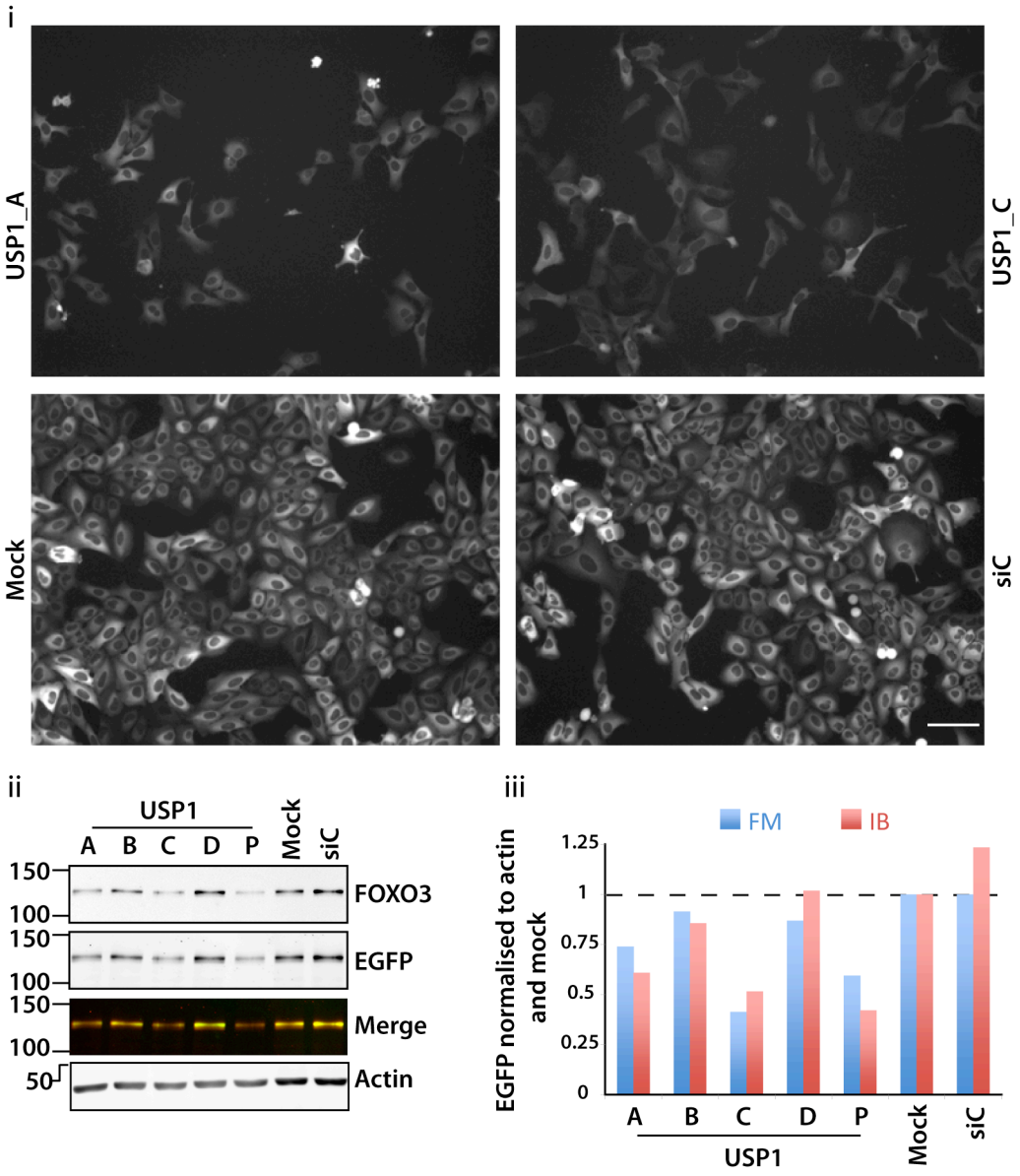

Fig 4.13. Depletion of USP1 decreases FOXO3-EGFP abundance. i. Representative images from the deconvolution experiment described in fig 4.10. **ii.** A 72-hour knockdown of USP1 was performed using the indicated siRNA oligonucleotides, cells were lysed with NP40 and immunoblotted for FOXO3 and EGFP as indicated. Imaging was performed using an infrared scanner (Odyssey [LiCor]). FOXO3 and EGFP were detected using the green and red channels respectively, and a merge of the results from the two is shown in the third panel from the top. **iii.** Comparison of fluorescence imaging and immunoblotting for EGFP. In each method normalised EGFP signal was compared to the mock. (A-D: individual siRNA oligonucleotides, P: pool, siC: non targeting siRNA control, FM: fluorescence microscopy, IB: immunoblotting, scale bar represents 100μm, n=1)

4.4.2 Immunoblotting for FOXO3-EGFP

As described in section 4.4.1 above, quantification of the effects of USP1 and USPL1 depletion on FOXO3-EGFP abundance using immunoblotting for either FOXO3 or EGFP gave very similar results to its determination by quantification of fluorescence imaging. This therefore provided an alternative assay for an siRNA screen seeking to identify DUBs whose depletion altered FOXO3-EGFP abundance (fig 4.14).

A simplified version of the screening strategy described in chapter 3 was employed here, in which the cells were grown in 96 well plates, lysed *in situ*, then prepared directly for immunoblotting, without prior normalisation of protein concentration. This led to considerable variability in protein loading between lanes as demonstrated by immunoblotting for actin (fig 4.14i). However, normalisation to actin allowed comparison of samples, as shown in fig 4.14ii. Three of the five candidates whose depletion downregulated FOXO3-EGFP, were similarly among the candidates identified using fluorescence microscopy.

However, correlation between the two screens was less good for DUBs whose depletion increased FOXO3-EGFP, with only one of the top 5 candidates by immunoblotting (USP15) also identified in the fluorescence screen. The coefficient of correlation for the whole dataset was 0.403 (fig 4.14iii). Interestingly, USP7, which has been shown to be involved in nuclear localisation of FOXO4 [205], was identified as one of the candidates upregulating FOXO3-EGFP levels. However, USP7, and other candidates identified in this screen, have not been subject to further validation thus far.

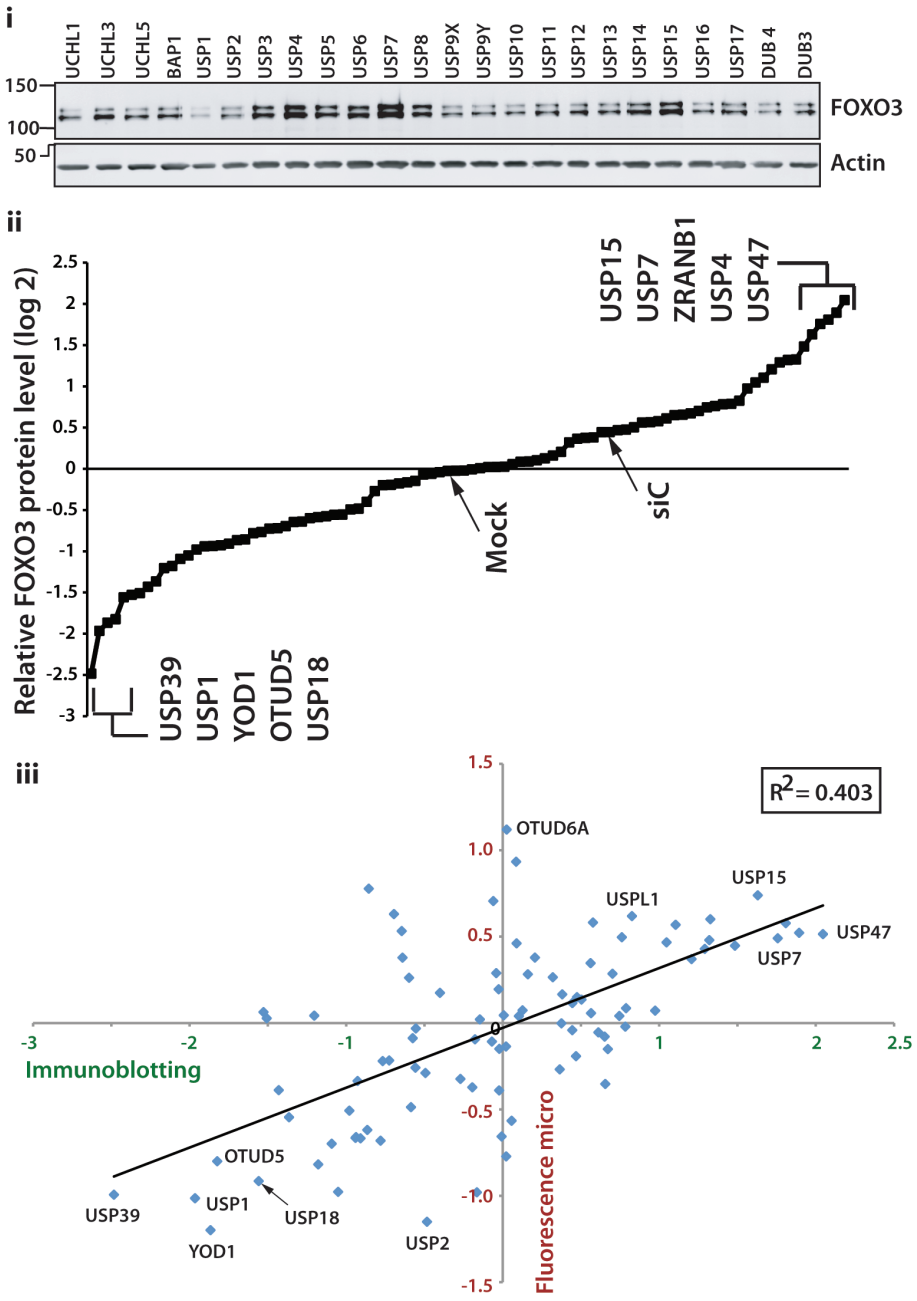

Fig 4.14 An immunoblotting screen for DUB regulators of FOXO3-EGFP. A 48-hour knockdown with pooled oligonucleotides directed at 92 DUBs was performed in U2OS-FKHL1 cells grown in two 96 well plates. Mock and non-targeting siRNA (siC) controls were also included. Lysis was performed directly on the plates using NP40 buffer. Loading buffer was then added to each well, following which the lysate was transferred to a new 96 well plate, which was sealed, and the lysate boiled. Samples were then directly run out on four SDS-PAGE gels and immunoblotted for FOXO3 and actin. **i.** Representative blot. **ii.** The FOXO3 signal was normalised to actin and the median of each blot, then ranked as shown. **iii**. Plot of the results of the immunoblotting screen compared to the fluorescence screen described in section 4.4.1. (Imaging and analysis of blots was performed on an odyssey [LiCor] infrared scanner, n=1).

4.5 Discussion

In this chapter I have described an siRNA screen for DUB modulators of downstream PtdIns3-K activity which utilised PtdIns3-K dependent translocation of FOXO3-EGFP as a readout for pathway activity. The screen used live cell imaging to follow the effects of DUB depletion on FOXO3-EGFP translocation following PtdIns3-K inhibition, thus increasing both the scope and dynamic range of the screen as discussed in section 4.2.

The effects of DUB depletion on FOXO3-EGFP localisation in cells under normal growth conditions and following PI-103 treatment, as well as the rate of nuclear translocation after PI-103 treatment were assessed. In general, depletion of single DUBs only resulted in modest changes to each of these parameters. Interpretation of the data from this screening strategy was also complicated by marked variability between the three replicate screens. However, of the five top and five bottom ranked candidate DUBs, half were successfully validated for at least one parameter (table 4.2) by deconvolution of the original oligonucleotide pool.

As described in section 3.9, low endogenous expression of the FOXO family precluded immunoblot screening for DUBs affecting endogenous FOXO protein level in A549 cells. In the current screen, using cells in which FOXO3-EGFP was stably overexpressed, I observed significant variations in overall fluorescence (reflecting FOXO3-EGFP abundance) following knockdown of several DUBs, and therefore utilized fluorescence intensity as a secondary output from the screen. Seven DUB candidates whose depletion upregulated or downregulated FOXO3-EGFP fluorescence were subject to deconvolution, which was successful in all cases (table 4.2). For two of the candidates (USP1 and USPL1), the effects on FOXO3-EGFP abundance have been further validated by immunoblotting.

Depletion of several DUBs identified in the screen resulted in particularly compelling phenotypes, and these are further discussed here. USP45 knockdown resulted in an increased rate of translocation of FOXO3-EGFP

DUB whose knockdown:	Decreases nuclear localisation	Increases nuclear localisation	Decreases total cellular fluorescence	Increases total cellular fluorescence
USPL1	✓			✓
USP32	✓			
USP1		✓	✓	
OTUD1		✓		
PSMD7		✓		✓
PSMD14		✓		✓
USP45		✓		
ATXN3L		✓		
OTUD6A				✓
USP15				✓
USP49				✓

Table 4.2 Summary of successfully deconvoluted DUB candidates. The first two columns include DUBs affecting either baseline or plateau nuclear/cytoplasmic ratio or rate of translocation. Deconvolution was deemed successful if two or more single oligonucleotides recapitulated the effects of the siRNA pool, which was defined as a minimum change of 20% from the negative controls.

into the nucleus, and an increased degree of nuclear localization as the response plateaued. No substrates or functions have been ascribed to USP45 to date. However, several USP45 interactors have been described in a mass spectroscopy based screen [415]. Interestingly, these include PIK3CG (PtdIns3-K p110γ). In my (previously described) screen for DUB regulators of the protein level of PtdIns3-Kinases (section 3.4), USP45 knockdown resulted in a small reduction (~10%) in the protein level of p110γ. On the other hand, USP45 knockdown upregulated the protein level of both p110β and p110α and was ranked 9th and 13th respectively for these two screens. While the changes in protein level were modest, the increase in p110β and p110α, may represent compensatory changes in response to alterations in p110γ level or activity.

Knockdown of USP32 led to reduced nuclear accumulation of FOXO3-EGFP in response to PtdIns3-K inhibition. This was only apparent for two out of the four individual siRNA oligonucleotides, which may reflect differential knockdown efficiency or alternatively different effects on USP32 splice variants, and will require further investigation.

USP32 is closely related to the human proto-oncogene USP6 [397], and in one study was found to be overexpressed in 50% of breast cancer cell lines (9/18) and 22% (9/41) of primary breast cancers [417]. As previously discussed, USP32 knockdown results in a decrease in the protein level of PDK1 (section 3.4). However, this is unlikely to explain the data seen here, as loss of PDK1 would be expected to decrease activation of Akt, and thus favour nuclear accumulation of FOXO3. This suggests that USP32 regulates other components of the PtdIns3-K pathway. Several USP32 interactors have described [415], but none of these is directly related to PtdIns3-K signalling.

As demonstrated by Ratjadone A treatment (fig 4.1), nuclear export inhibition results in rapid and profound nuclear accumulation of FOXO3-EGFP suggesting it is continuously shuttling between the cytoplasm and nucleus. While USP45 and USP32 were successfully deconvoluted, further validation will be required to prove that the effects on nuclear translocation were due to modulation of PtdIns3-K downstream activity, and not due to general effects on nuclear import or export. This may include the use of a cell line expressing a GFP labelled protein with a strong nuclear export signal, such as is described by Zanella et al [426]. Their study employed a GFP tagged Rev protein which is almost exclusively cytoplasmic at steady state, but accumulates rapidly in the nucleus on inhibition of nuclear export.

Depletion of USPL1 and USP1 respectively increased and decreased the abundance of FOXO3-EGFP, which was assessed by both fluorescence microscopy and immunoblotting. However, as endogenous FOXO3 was not detectable in these cells, the findings may reflect regulation of the tagged protein only, and not reflect that of endogenous untagged protein. To

address this, further validation would involve investigating the effects of depletion of both DUBs in cell lines with relatively high FOXO3 expression, examples of which include non-small cell lung cancer cell lines such as H1299, H1650 [427], or CORL23 (section 3.9). In addition, further work will include determining whether depletion of these DUBs alters FOXO3-EGFP synthesis, or its degradation. Depletion of either USPL1 or USP1 also appeared to alter nuclear localisation of FOXO3-EGFP, however interpretation of this data was difficult in view of the considerable differences in FOXO3-EGFP abundance in these DUB depletions compared to the controls.

USPL1 has been shown to be a specific SUMO isopeptidase and to lack activity against ubiquitin [428], however no functional roles have been described. SUMOylation, unlike ubiquitylation is not a degradative signal *per se*, but like ubiquitin may influence activity, localisation or stability of its substrate [429]. SUMOylation and ubiquitylation are known to cross talk, and in certain instances the same residue may be either SUMOylated or ubiquitylated (an example being PCNA which may be either ubiquitylated or SUMOylated at position K164 [56]). It is therefore feasible that depletion of USPL1 could lead to increased SUMOylation of FOXO3, thus preventing degradative ubiquitylation, and leading to FOXO3 stabilisation. However, SUMOylation of FOXO factors has not yet been reported in the literature and analysis of the FOXO3 sequence using the SUMOylation prediction programme SUMOplot, identified only motifs with low probability for SUMOylation.

Several USPL1 interactors have been identified including ANKFY1 (ankyrin repeat and FYVE domain-containing protein 1) [415], which in turn interacts with the PtdIns3-K class II catalytic subunit PIK3C2A (p170) [430]. While knockdown of USPL1 did not significantly alter p170 protein level in my screen (section 3.7), this clearly does not preclude a role for USPL1 in its regulation.

USP1 is known to deubiquitylate FANCD2 [384] and PCNA [431] and is implicated in the DNA damage response. USP1 has also recently been shown to regulate the phosphorylation status of Akt by altering the stability of PHLPP1 [432]. In a separate study, a small molecule inhibitor of USP1 was shown to reverse cisplatin resistance and decrease proliferation in a non-small cell cancer cell line [214]. This small molecule inhibitor may be useful in determining the effects of USP1 on FOXO3 in future. Notably, USP1 depletion resulted in a decrease in cell number of both cell lines used in this thesis. In this chapter I show reduced cell number after a 48 hour knockdown of USP1 in FKHRL1-U2OS cells (section 4.4.1), while in section 3.2 I described a visual assessment of toxicity, which correlated with a greater than 50% reduction in protein yield, following a 72 hour depletion of USP1 in A549 (non-small cell lung cancer) cells.

In previous studies, USP7 was shown to be involved in the regulation of FOXO subcellular localization [205]. Oxidative stress resulted in the mono-ubiquitylation of FOXO4 (and FOXO3), leading to its nuclear localisation, and this was reversed by USP7 in 293T cells [205]. However, USP7 was not identified as a regulator of FOXO3 localisation in the current screen. This may indicate that USP7 involvement is limited to oxidative stress response, that it is cell type dependent, or it may represent a false negative result from the screen. Interestingly though, USP7 depletion did alter FOXO3-EGFP abundance in the immunoblotting screen (fig 4.14), although this finding has not been confirmed by deconvolution.

In summary, I have described the identification of several DUBs whose knockdown either modulates FOXO3-EGFP nuclear accumulation in response to inhibition of PtdIns3-K or alters FOXO3-EGFP abundance. While further validation is required, these findings suggest a vital role for several new deubiquitylases in regulating the PtdIns3-K pathway.

Chapter 5

Depletion of USP8 sensitises to PI-103 induced cell death

5.1 Introduction

Synthetic lethality refers to the interaction of two or more mutations, each of which is not in itself lethal, but which in combination cause cell death. First described in *Drosophila* over 60 years ago [433, 434], synthetic lethality has been extensively investigated in yeast [435] and other model systems. The term is now also used when one of the mutations is replaced by loss of gene function through RNAi or pharmaceutical inhibition. The latter has provided novel therapeutic opportunities, and potentially allows the targeting of malignancies in which tumour suppressors are inactivated. The best-established example is the use of PARP (poly ADP ribose polymerase) inhibitors in BRCA mutant breast cancers, where the homozygous loss of BRCA (1 or 2) in the cancer bestows sensitivity to PARP inhibitors [436].

Synthetic lethality screens have now become established as valuable tools in drug discovery, and provide insights into the mechanisms of drug action and resistance [437]. While the FOXO3-EGFP translocation screen described in chapter 4 was not designed as a synthetic lethal screen, it provided the opportunity to observe synthetic effects between DUB depletion and treatment with the PtdIns3-K (and mTOR) inhibitor PI-103. The depletion of three DUBs was observed to potentiate cell death on addition of PI-103, and initial validation for one of these candidates, USP8, is described here.

5.2 Depletion of USP8, OTUD4 or DUB4 increases PI-103 dependent cell death

The screen for regulators of PI-103 dependent nuclear translocation of FOXO3 (FKHRL1)-EGFP is described in section 4.2. In brief, FKHRL1-U2OS

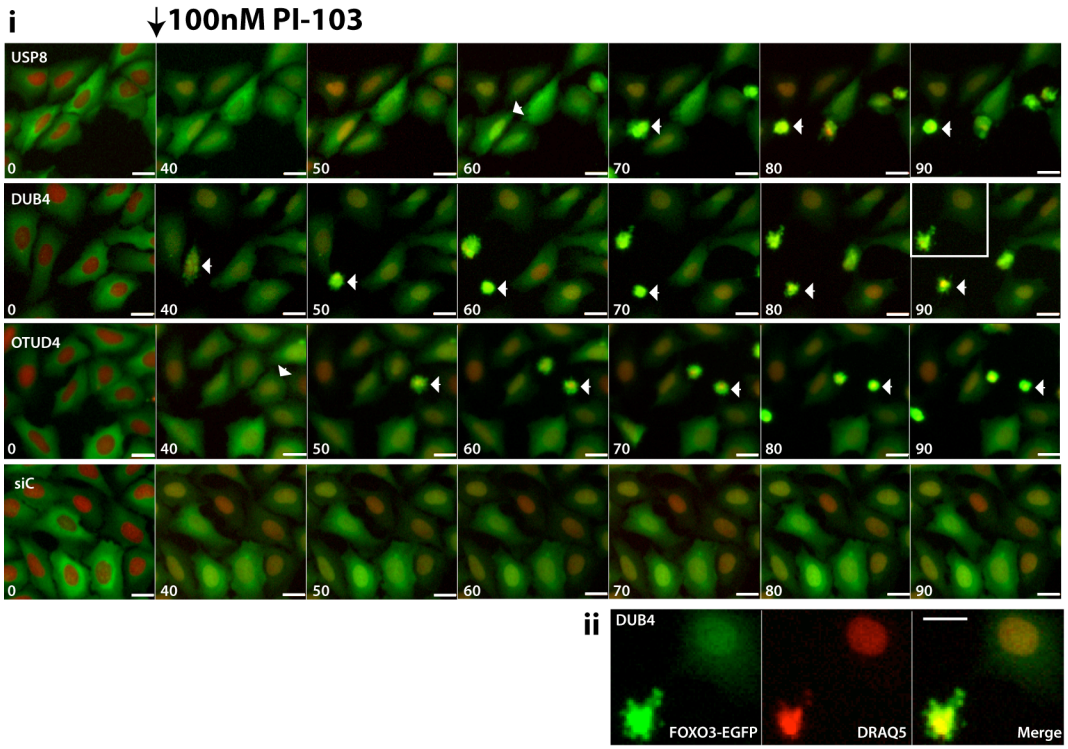

Fig 5.1. Knockdown of USP8, DUB4 and OTUD4 leads to increased cell death on PI-103 treatment. Data shown here are from one of three screens performed as described in fig 4.3. Following a 48-hour siRNA knockdown in FKHRL1-U2OS cells, cells were imaged at baseline and then every 5-minutes following addition of 100nM PI-103. **i**. Representative cropped images for cells transfected with USP8, DUB4, OTUD4 and non-targeting (siC) siRNA oligonucleotides. Merged FOXO3-EGFP (green) and DRAQ5 (red) images are shown. Time after addition of 100nM PI-103 (minutes) is shown in the bottom left-hand corner. In the top three panels an example of a cell undergoing cell death is indicated by an arrowhead. **ii.** Magnified view of inset from DUB4 panel, with separate FOXO3-EGFP and DRAQ5 channels. (scale bar represents 25μm).

cells were transfected with a DUB siRNA library, incubated for 48 hours and imaged every 5 minutes following the addition of 100nM PI-103. While a low level of cell death was observed over the time course of the screen in all conditions, this was most pronounced and reproducible following depletion of USP8, DUB4 or OTUD4. Approximately 40 to 50 minutes after the addition of PI-103, a proportion of cells began to round up and progressively exhibit an increased intensity of GFP and DRAQ5 fluorescence (fig 5.1i,ii). In addition, the cellular margins became irregular, and finally there was evidence of nuclear fragmentation (fig 5.1ii).

These data suggested that depletion of USP8, DUB4 or OTUD4, sensitises FKHRL1-U2OS cells to death following treatment with PI-103. In order to confirm this observation, a 48-hour knockdown of these three DUBs was performed in FKHRL1-U2OS cells, which were then imaged at baseline and hourly following the addition of 100nM PI-103 (fig 5.2). The media conditions employed in the original translocation screen were retained, however vehicle (DMSO) treatment was included as a control. In addition to a mock-transfected control, three other members of the DUB library, which had not caused increased cell death in the screens (USP9X, DUB3 and PARP11), were included as controls. These were contiguous to USP8, DUB4 and OTUD4 respectively in the DUB library plate, and were selected in this manner to reduce bias. An estimate of cell death was obtained by counting cells with increased EGFP and DRAQ5 fluorescence intensity (section 2.4.3), and this was expressed as a percentage of total cells.

Basal cell death, prior to the addition of PI-103 or DMSO, provided an estimate of the toxicity that could be directly ascribed to a given DUB depletion in this assay. Of the three DUBs identified in the screen, only DUB4 depletion led to an increase in basal toxicity, compared to the mock control.

An assessment of cell death was made at 1 and 2 hours following addition of PI-103 or DMSO. Treatment of mock-transfected cells with vehicle alone did not result in any quantifiable cell death over the course of the experiment, while treatment with PI-103 resulted in less than 5% cell death after 2 hours (fig 5.2). Depletion of two of the three DUBs randomly selected from the DUB library (USP9X and PARP11) did not induce cell death compared to the mock-transfected cells. DUB3 depletion on the other hand did increase PI-103 induced cell death, albeit to a lesser degree than the DUBs identified in the screen, and this only became evident at the two-hour time point.

Similarly to observations made during the screen, depletion of USP8, DUB4 or OTUD4 increased PI-103 induced cell death (fig 5.2). In DUB4 depleted cells, greater than 60% cell death was observed 2 hours after adding PI-103

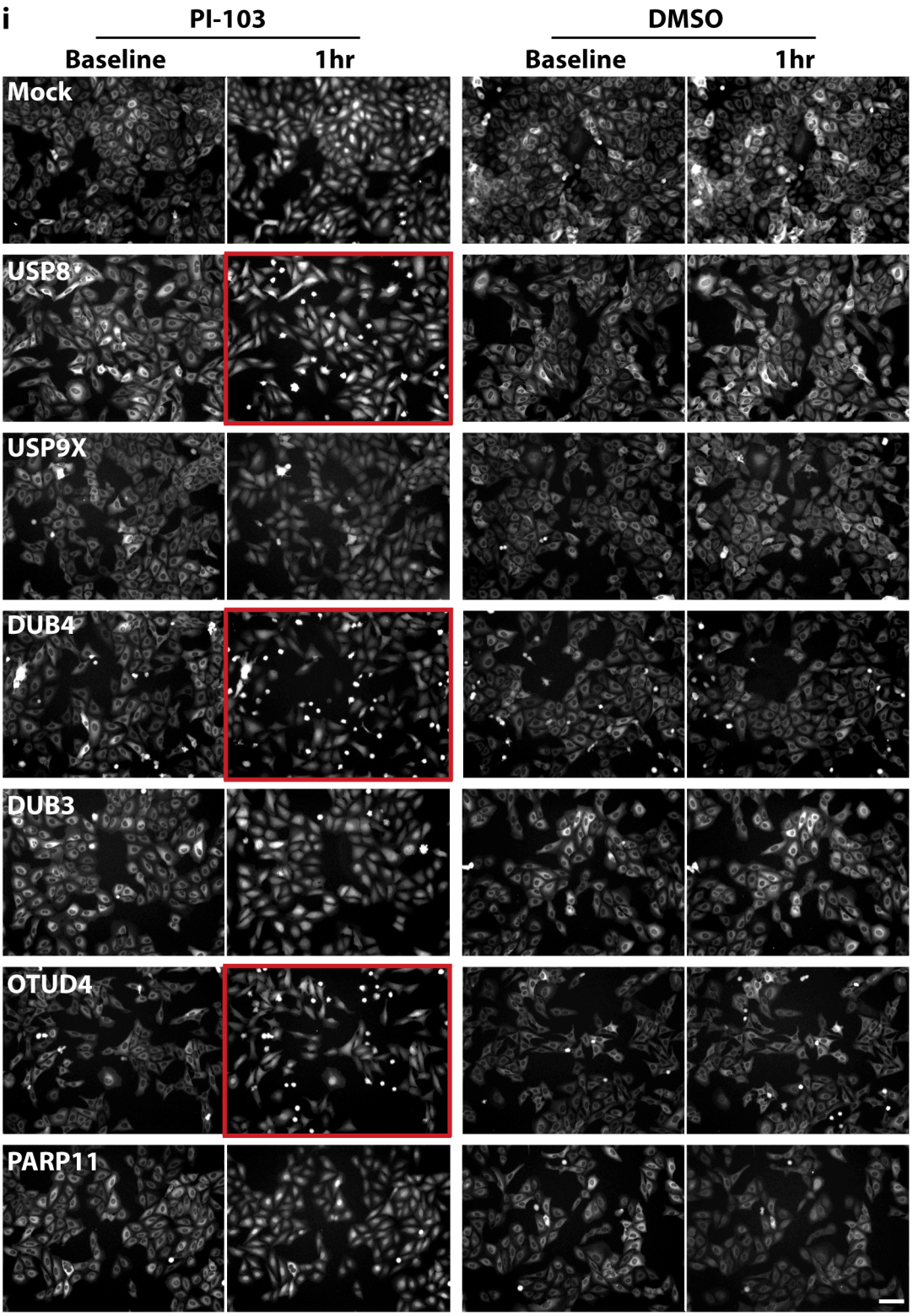

Figure 5.2 (continued overleaf)

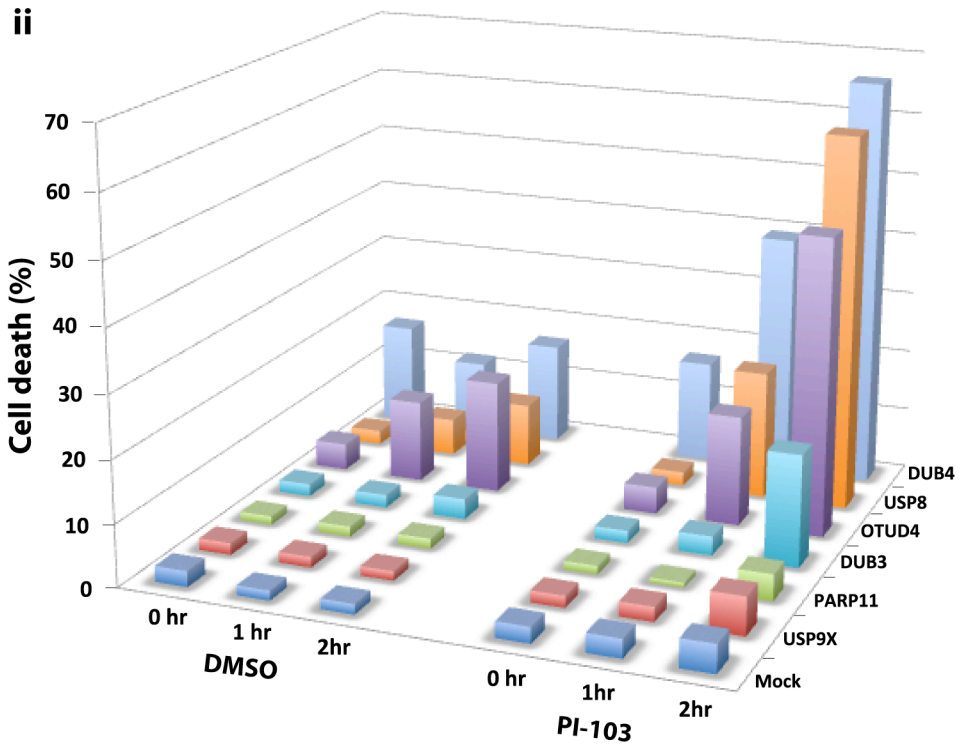

Fig 5.2. Loss of USP8, DUB4 or OTUD4 increases PI-103 induced cell death. FKHRL1-U2OS cells were transfected in a 96 well plate with siRNA oligonucleotide pools directed at the indicated genes, or mock transfected. Following a 48-hour incubation, the cells were stained with DRAQ5, and then the media changed to serum-free Hanks Buffered Saline Solution (HBSS) containing either 100nM PI-103 or vehicle (DMSO). Imaging was performed hourly by automated microscopy. **i.** Representative grey-scale FOXO3-EGFP fluorescence images of cells at baseline and an hour after addition of PI-103 or DMSO. (scale bar represents 100μm) **ii**. An estimate of cell death was obtained by counting the number of cells with both high intensity GFP and DRAQ5 fluorescence using Volocity (PerkinElmer) software. The number of dead cells is expressed as a percentage of total cells at baseline. A median of 156 (range 62-365) cells were imaged in each well (one position) at baseline. Three replicates were performed per condition and the mean of the three is reported.

(fig 5.2ii). While basal cell death was increased to about 15% of cells, no further cell death was observed after 2 hours of DMSO treatment (fig 5.2ii).

On the other hand, USP8 or OTUD4 depletion did not increase baseline cell death (fig 5.2), but was associated with increased cell death after 1 or 2 hours of PI-103 treatment (fig 5.2B). Depletion of either USP8 or OTUD4 also increased cell death following treatment with DMSO, though to a lesser extent. The differential in cell death between PI-103 and DMSO treated cells

was more marked following depletion of USP8, where cell death of approximately 60% and 10% respectively was observed.

These results support the observations made in the screen, and indicate that all three DUBs are worthy of further study in the context of interaction with PI-103 inhibition. However, the most convincing of these was USP8, whose depletion did not cause direct toxicity, but increased sensitivity to PI-103 significantly more than to vehicle. Previous studies have also linked USP8 to the PtdIns3-K pathway (discussed in section 5.8), supporting its study in this context. Additionally, USP8 has been the subject of other projects in the host laboratory, and reagents (including an antibody and inhibitors) were therefore available. For these reasons, investigation of USP8 was prioritised over the other candidates.

5.3 Assessment of cell death using DRAQ7 provides further evidence for a role for USP8 depletion in PI-103 sensitivity.

The first validation step undertaken was deconvolution of the USP8 pool (figs 5.3 and 5.4). This utilised an alternative assay to measure cell death. In the previous section, cell death was estimated based on morphological changes that led to an increase in the intensity of EGFP and DRAQ5. This was, however, open to observer bias (section 2.4.3). Furthermore, the small proportion of cells undergoing mitosis exhibited a similar appearance to those scored as undergoing cell death. I therefore designed an assay with which to specifically follow cell death during live cell imaging (fig 5.3). This employed DRAQ7 (Biostatus), a nuclear dye that is only taken up by dead cells, and is non-toxic to live cells [438]. DRAQ7 has previously been employed in flow cytometry to count the proportion of dead cells [439], however to my knowledge no publications have previously reported the use of DRAQ7 in microscopy time lapse assessment of cell death in monolayer culture.

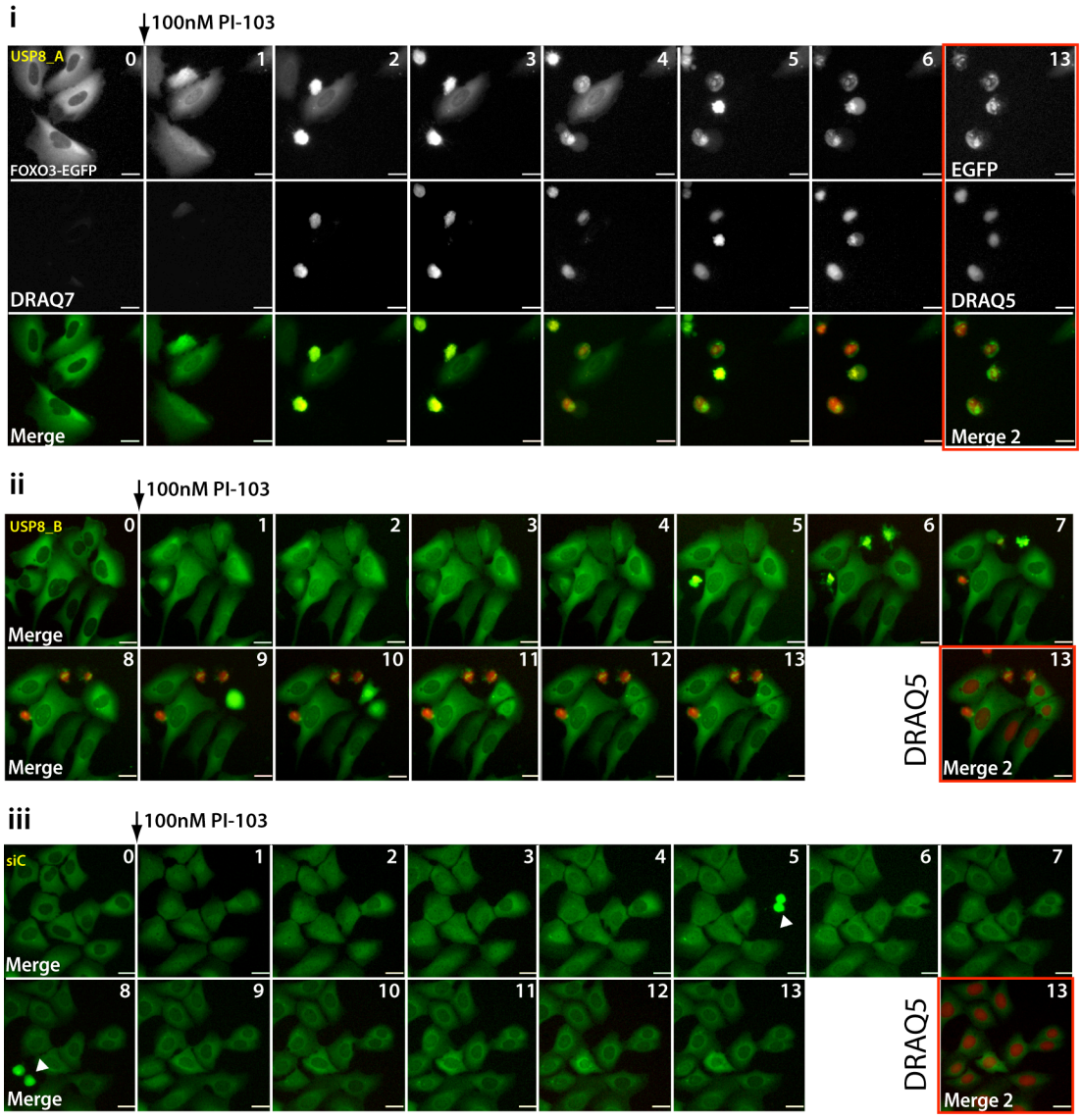

Fig 5.3. DRAQ7 staining enables the identification of cell death during live cell imaging. FKHRL1-U2OS cells were transfected in a 96 well plate with the indicated siRNA oligonucleotides against USP8, or non-targeting siRNA control (siC). Following a 48-hour incubation, the media was changed to serum-free HBSS, containing 3μM DRAQ7 and either 100nM PI-103 (PI), 1μM MK2206 (MK) or vehicle (DMSO), and imaging was performed hourly by automated microscopy for 13 hours after which DRAQ5 was added to a concentration of 5μM, cells were incubated a further 20 minutes and a final image taken. **i.** Representative cropped images (FOXO3-EGFP, DRAQ7 and merge) from baseline and first 6 hours following treatment with 100nM PI-103. Right-hand panel contains final images (FOXO3-EGFP, DRAQ5 and merge 2). **ii-iii**. Timelines for merged (FOXO3-EGFP and DRAQ7) cropped images, the final panel was stained with DRAQ5. (Merge 2: FOXO3-EGFP and DRAQ5, scale bar represents 25μm, the arrowhead indicates mitotic cells)

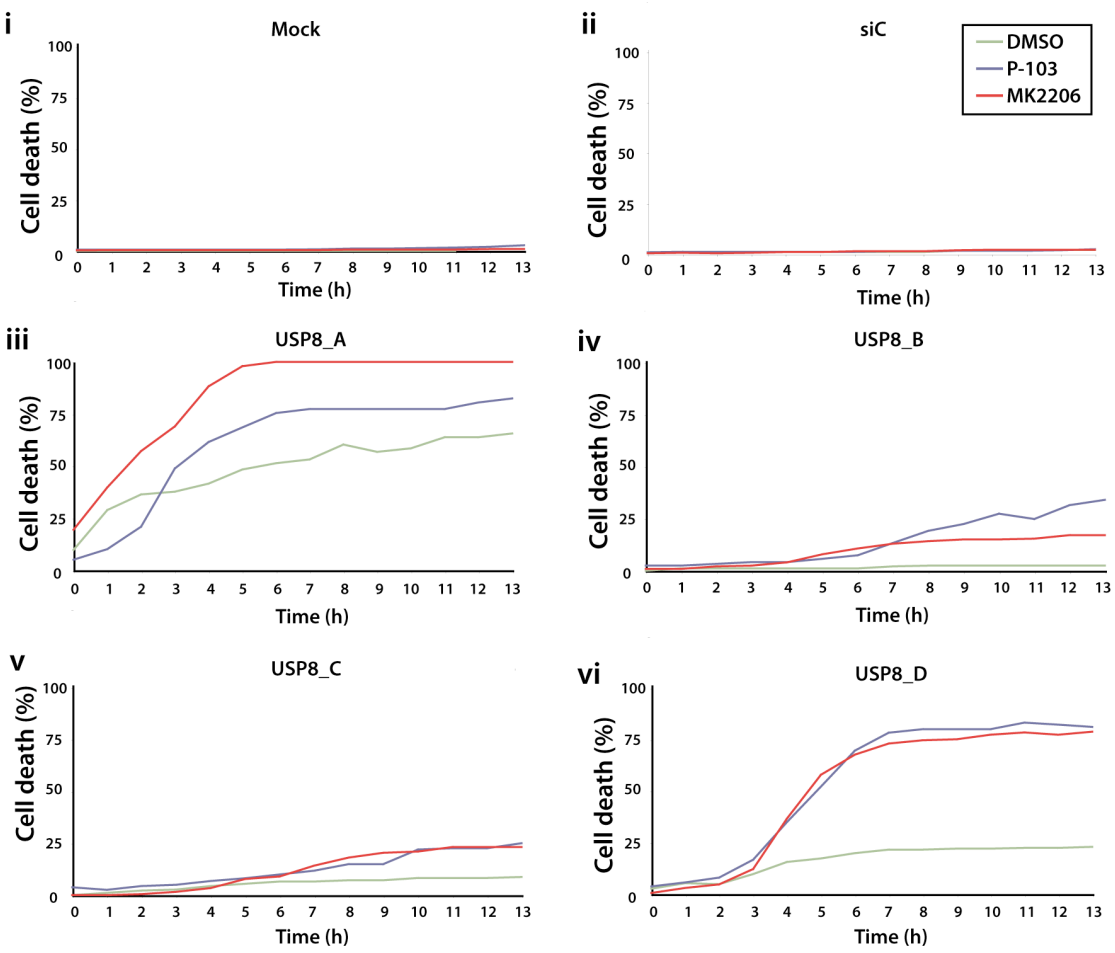

Fig 5.4. USP8 depletion sensitises FKHRL1-U2OS cells to PtdIns3-K inhibition. FKHRL1-U2OS cells were transfected with siRNA oligonucleotides against USP8 (A-D), mock transfected or transfected with non-targeting siRNA (siC), incubated for 48 hours and treated with 100nM PI-103 (PI), 1μM MK2206 (MK) or vehicle (DMSO) as described in fig 5.3. Cells taking up DRAQ7 were counted using Volocity (PerkinElmer) and expressed as a percentage of total cells, which were counted following staining with DRAQ5, which was performed after the last timepoint. A single position was imaged per well and a median of 105 (range 19-256) cells were imaged per condition.

In fig 5.3, representative images of cells following a 48-hour transfection with USP8 siRNA (using oligonucleotides A and B) or control siRNA are shown. Cells undergoing the changes scored previously as indicative of cell death (rounding up, increased EGFP intensity), also took up DRAQ7 (fig 5.3i,ii), while the remainder of cells were not stained by DRAQ7 (fig 5.3i-iii). Cells transfected with control siRNA showed no evidence of DRAQ7 uptake (and thus cell death), and indeed continued to divide (fig 5.3iii). Depletion of USP8

using either oligonucleotide resulted in the death of a proportion of cells, this being most marked with USP8_A (fig 5.3i-iii).

At the end of the experiment, the cells were stained with DRAQ5 to allow a total cell count, and DRAQ7 positive (dead) cells at each timepoint were then expressed as a percentage of total cells (Fig 5.4i-vi). Minimal cell death was observed in either the mock-transfected or non-targeting siRNA controls (fig 5.4i,ii). On the other hand, depletion of USP8 by all 4 siRNA oligonucleotides resulted in increased cell death following treatment with either PI-103 or MK2206 (fig 5.4iii-vi). Overall cell death was most marked following depletion of USP8 with oligonucleotide A, however for this oligonucleotide, significant cell death was also seen on treatment with vehicle alone (fig 5.4iii). Depletion of USP8 with the other three oligonucleotides in all cases resulted in substantially more cell death following treatment with either PI-103 or MK2206, over vehicle alone.

In this experiment, the findings of the original screen, in which USP8 depletion sensitised cells to PI-103 dependent cell death, were successfully validated by deconvolution of the oligonucleotide pool. In addition, inhibition of Akt using MK2206 resulted in very similar effects to PI-103 treatment, indicating that depletion of USP8 may generally sensitise cells to inhibition of the PtdIns3-K pathway.

5.4 The USP8 inhibitors HBX 90,397 and HBX 90,659 increase sensitivity to PI-103 treatment.

Two USP8 inhibitors developed by Hybrigenics [440] were available in the host laboratory following a previous collaboration. Table 5.1 summarises their activity against a panel of deubiquitylases, and shows their selectivity for USP8. These compounds were utilised to further investigate the effects of USP8 loss of function on sensitivity to PI-103 in FKHRL1-U2OS cells.

Firstly, FKHRL1-U2OS cells were treated with varying concentrations of either USP8 inhibitor in the absence of PI-103 and imaged hourly for 12

Inhibitor	Designation in Colombo et al [440]	IC50 (μM)				
		USP8	USP7	USP5	UCHL1	UCHL3
HBX 90,397	22c	0.559	>100	>100	>100	10
HBX 90,659	22d	0.850	>100	>100	>100	>100

Table 5.1. USP8 inhibitors used in this work. Adapted from Colombo, M et al [440], and Colland, F (unpublished).

hours. Representative images following treatment with HBX 90,659 are shown in fig 5.5. At the lowest concentration used (1.25μM), no significant changes were observed and there was no evidence of increased cell death compared to cells treated with vehicle alone (fig 5.5i). Treatment with 2.5μM HBX 90,659 however, resulted in several effects commencing approximately 5 hours after addition of inhibitor. These included a proportion of cells where FOXO3-EGFP translocated to the nucleus (fig 5.5i,ii). However, more apparent was a tightly localized accumulation of FOXO3-EGFP within the nucleus forming a brightly fluorescent spot, which was observed in most cells. In addition, the cytoplasm appeared more granular, with dendritic like extensions, and a proportion (<10%) became permeabilised to DRAQ7, indicating cell death (fig 5.5i,ii).

At the highest concentration of HBX 90,659 (5μM), marked nuclear translocation of FOXO3-EGFP was observed (fig 5.5i,iii). This commenced approximately 3 hours after addition of inhibitor, and by six hours of treatment, essentially all cells showed a predominantly nuclear localization of FOXO3-EGFP. Nuclear translocation was generally preceded by a localised accumulation within the nucleus (data not shown), as described above for cells treated with 2.5μM inhibitor. The cells also developed small vacuoles in the perinuclear region, and dendritic-like cytoplasmic extensions. Interestingly, cell death was not apparently increased, with no evidence of DRAQ7 staining.

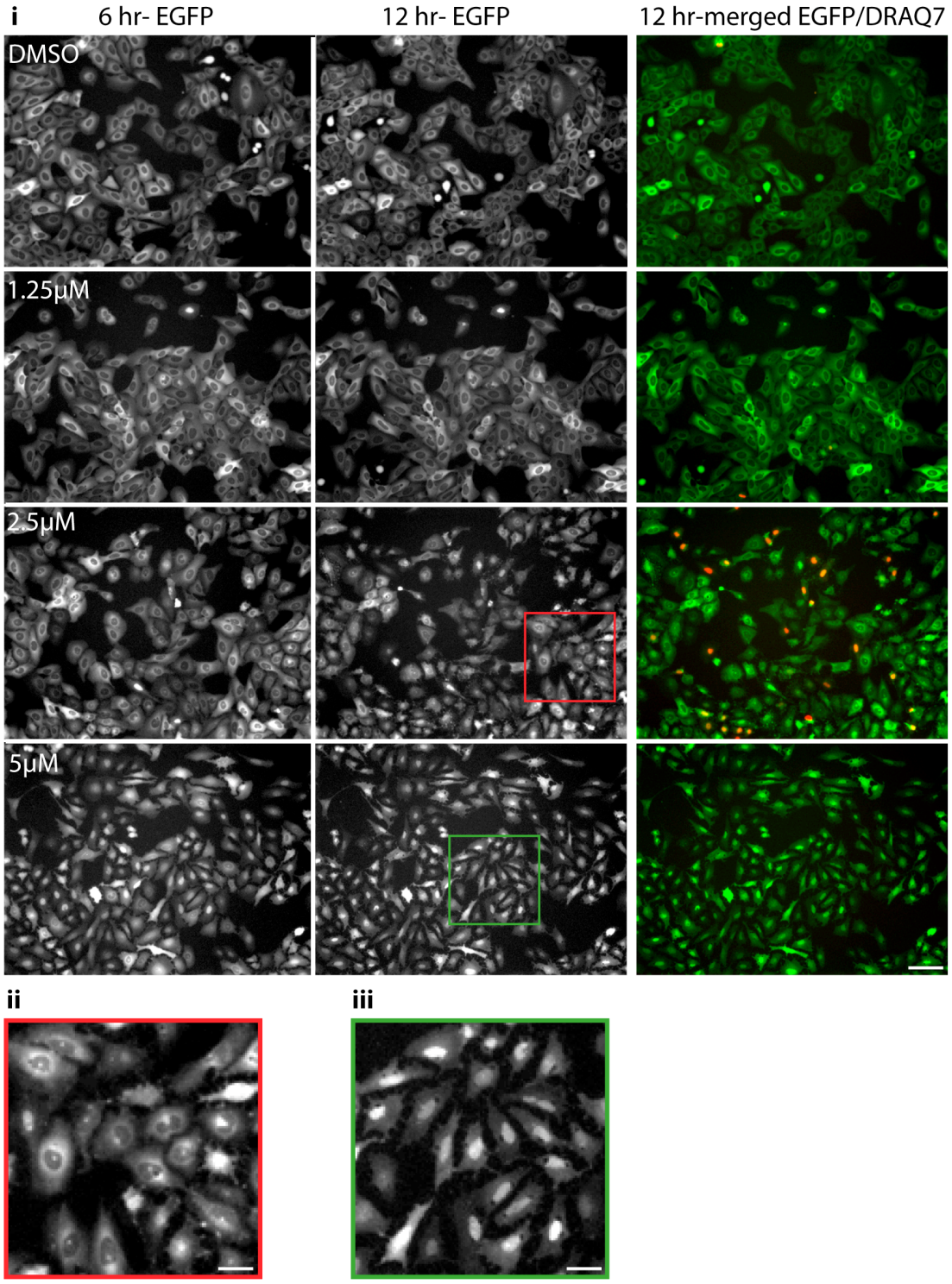

Fig 5.5. HBX 90,659 promotes nuclear localisation of FOXO3-EGFP. FKHRL1-U2OS cells were seeded in a 96 well plate and incubated overnight. The following day, media was changed to HBSS containing 3μM DRAQ7 and the indicated concentrations of HBX 90,659, and hourly imaging performed by automated fluorescence microscopy. **i.** Representative FOXO3-EGFP images after 6 or 12 hours are shown in the first 2 panels, while the final panel shows merged EGFP/DRAQ7 images from the 12-hour timepoint. (scale bar-100μm) **ii,iii**. Cropped images of cells treated for 12 hours with 2.5μM or 5μM HBX90,659 respectively. (scale bar 25μm).

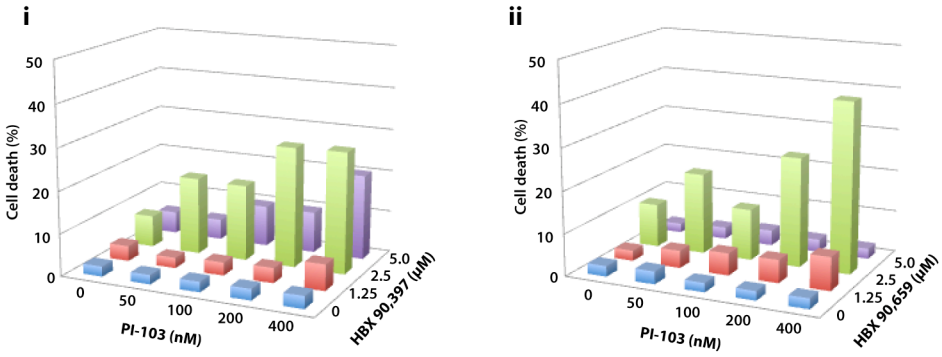

Fig 5.6. The USP8 inhibitors HBX 90,397 and 90,659 sensitise cells to PI-103 induced cell death. FKHRL1-U2OS cells were seeded in a 96 well plate, allowed to attach overnight and treated with the indicated inhibitors in HBSS containing 3μM DRAQ7. The cells were imaged hourly by automated microscopy (Nikon), and after 13 hours, DRAQ5 was added, cells were incubated a further 20 minutes and final imaging performed. Dead and total cells were counted using the DRAQ7 and DRAQ5 images respectively using Volocity (PerkinElmer) software. **i,ii** Percentage dead cells following 12 hour treatment with indicated inhibitors. The results represent the mean of two experiments. One well, and a median (range) of 190 (103-354) cells were imaged per condition.

Inhibition of USP8 with the second USP8 inhibitor (HBX 90,397) resulted in similar effects (data not shown). Both inhibitors therefore promoted the nuclear translocation of FOXO3-EGFP, particularly at the highest concentration of inhibitor. However, this translocation was less rapid than that following direct inhibition of the PtdIns3-K pathway with LY294002 or PI-103, which was essentially complete within 45-50 minutes. The nuclear translocation was also frequently preceded by a focal accumulation of FOXO3-EGFP within the nucleus, which was not seen following direct PtdIns3-K inhibition, indicating that it is unlikely to be due to a direct effect on the PtdIns3-K pathway. While USP7 depletion has been shown to promote the nuclear accumulation of FOXO4, the concentration of either inhibitor in the experiment was substantially lower than the IC50 for USP7 (table 5.1), suggesting this is not the mechanism.

I next quantitatively investigated the effects of combining USP8 inhibition with PI-103 treatment (fig 5.6). Treatment with of U2OS-FKHRL1 cells with PI-103 alone did not result in increased cell death over the timecourse of the experiment, even at the highest concentration (400nM) (fig 5.6). Treatment

with either USP8 inhibitor alone resulted in minimal cell death at either the lowest (1.25μM) or the highest concentration (5μM), although slightly more cell death was observed with HBX 90,397. However, at the intermediate concentration of 2.5μM, both USP8 inhibitors increased cell death by three to four fold, compared to DMSO treatment (fig 5.6).

In the presence of either USP8 inhibitor at a concentration of 1.25μM, co-treatment with PI-103 exhibited a dose-dependent effect on cell viability. This was more striking in the presence of 2.5μM of the USP8 inhibitors. In view of the lack of sensitivity of the cells to PI-103 alone, this supports the findings of the USP8 depletion experiments, indicating that inhibition of USP8 sensitises these cells to PI-103 induced toxicity.

Interestingly, the highest dose of both USP8 inhibitors (5μM) resulted in less cell death. Only HBX 90,397 induced dose-dependent cell death following PI-103 treatment at this dose. One plausible explanation is that a quiescent or senescent state may be induced at this concentration, and is discussed further in section 5.7.

5.5 The effects of USP8 depletion are partially dependent on media conditions

The experiments described so far in this chapter were all performed in Hank's buffered saline solution (HBSS), which had initially been chosen to optimize imaging conditions. The HBSS contained glucose, and was supplemented with glutamate, pyruvate and HEPES, but did not contain essential amino acids or serum. I therefore repeated the experiment described in Fig 5.4, in serum-free DMEM (fig 5.7). This experiment employed new batches of the siRNA oligonucleotides against USP8, which were purchased to replace those from the library. As discussed in appendix B, oligonucleotides 2, 5, 1 and 3 appear to correspond to the library oligonucleotides A, B, C and D respectively. This experiment also titrated the PI-103 concentration.

Significantly more toxicity was observed following transfection with the mock and non-targeting siRNA controls when FKHRL1-U2OS cells were grown in serum-free DMEM (fig 5.7i,ii), than in the previous experiment in which the cells were grown in HBSS (fig 5.4i,ii). PI-103 again increased cell death compared to that seen with vehicle alone, however a differential cell kill was only clearly apparent after approximately 6 hours of treatment.

Depletion of USP8 by all four oligonucleotides resulted in increased cell death, compared to the controls (fig 5.7), however this was less marked than that observed in HBSS (fig 5.3). Furthermore in DMEM the difference in cell death in USP8 depleted cells between PI-103 treated and DMSO treated cells was less pronounced, and for one of the four oligonucleotides (USP8_1) was only apparent at higher PI-103 concentrations (200 and 400nM).

I next employed immunoblotting for cleaved PARP, which is upregulated in apoptosis, to investigate the cause of cell death, and to compare the effects of PI-103 treatment in HBSS and serum free DMEM. A 48-hour depletion of USP8 was followed by a 12-hour treatment with 200nM PI-103 or vehicle alone (fig 5.8). Only two USP8 siRNA oligonucleotides (USP8_1 and

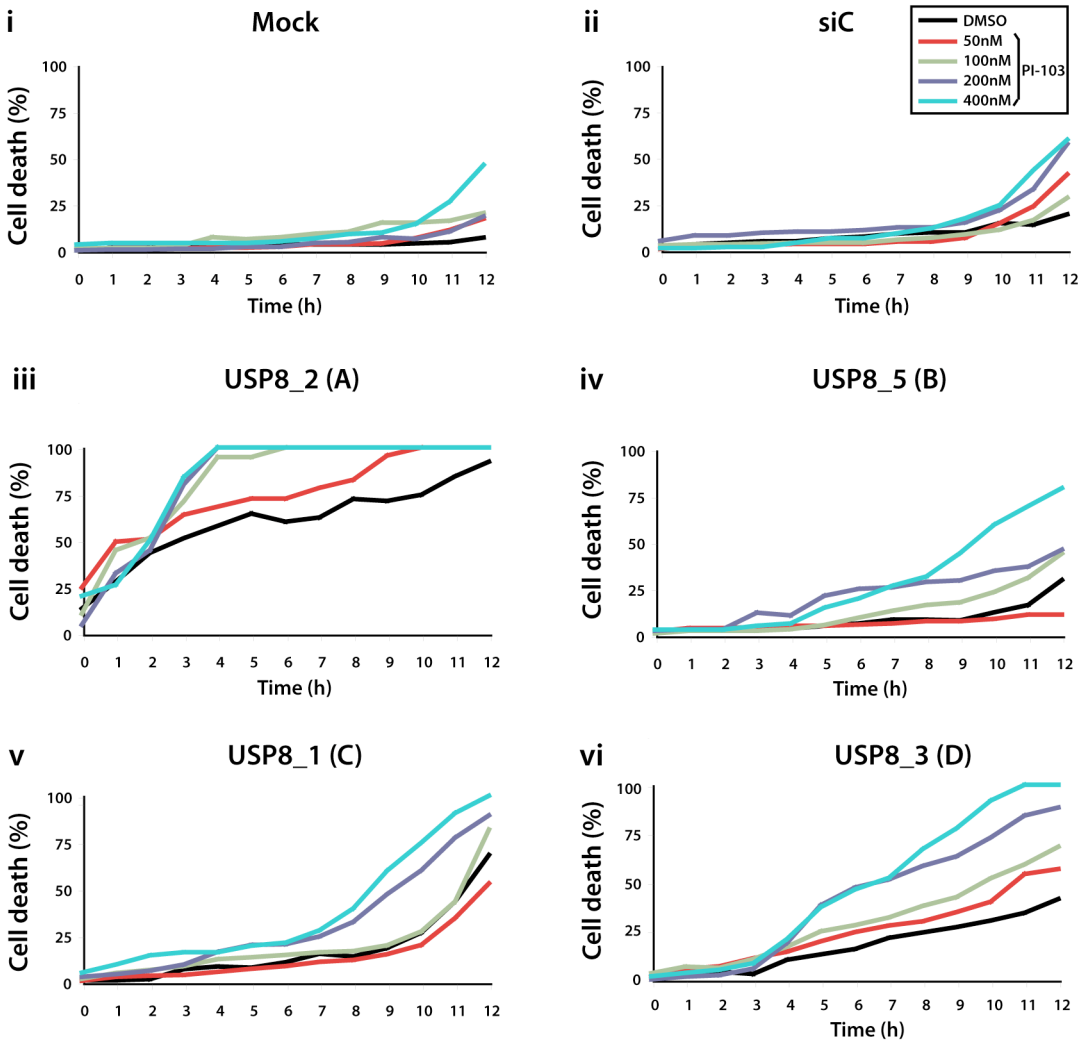

Fig 5.7. Culture in serum free DMEM reduces sensitisation to PtdIns3-K inhibition following USP8 depletion. i-vi. FKHRL1-U2OS cells were transfected in a 96 well plate with the indicated siRNA oligonucleotides against USP8 (1,2,3,5), non-targeting siRNA (siC) or mock transfected. The letters in parentheses refer to the numbering of the original (library) siRNA oligonucleotides. Following a 48-hour incubation, the media was changed to serum free DMEM (HEPES buffered, with no phenol red), containing vehicle (DMSO) or varying concentrations of PI-103 (legend, top right), and 3μM DRAQ7. Imaging was performed hourly by automated microscopy for 12 hours after which DRAQ5 was added to a concentration of 5μM, cells were incubated a further 20 minutes and a final image taken. Cells taking up DRAQ7 were counted using Volocity (PerkinElmer) and expressed as a percentage of total cells, which were counted using DRAQ5 on completion of experiment. A single well and position were imaged per condition, with a median (range) of 144 (50-298) cells imaged.

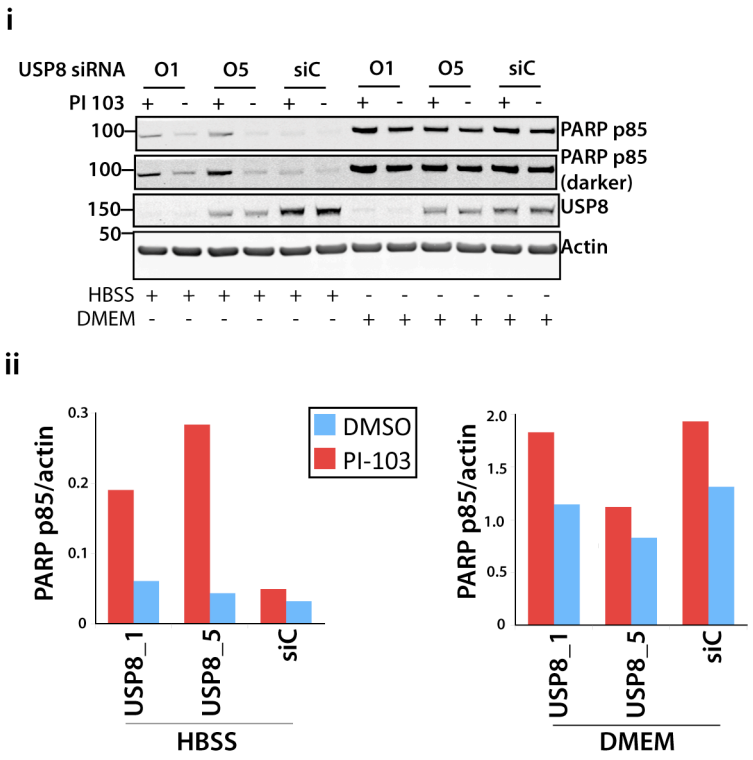

Fig 5.8. USP8 depletion does not increase PI-103 dependent apoptosis in serum free DMEM. FKHRL1-U2OS cells were transfected with the indicated USP8 siRNA and incubated for 48 hours, following which they were treated with 200nM PI-103 or DMSO in either HBSS or serum free DMEM for 12 hours **i.** The cells were lysed with NP40, and equal volumes of lysate were run on NuPAGE 4-12% gels and immunoblotted for PARP p85, USP8 and Actin. **ii.** Quantification of bands was performed using Odyssey (LiCor), and the cleaved PARP p85 was normalized to actin. (siC- non-targeting siRNA control, n=1).

USP8_5) were employed, due to the excessive toxicity observed with the other two oligonucleotides.

Cells transfected with non-targeting siRNA and cultured in HBSS, exhibited little evidence of apoptosis on treatment with DMSO and this was only marginally increased by treatment with PI-103 (fig 5.8i,ii). However in USP8 depleted cells, PI-103 treatment resulted in substantially more PARP cleavage than following DMSO treatment (fig 5.8i,ii), indicating USP8 depletion leads to increased sensitivity to PI-103 induced apoptosis.

Control cells cultured in serum free DMEM exhibited significantly more PARP cleavage than those cultured in HBSS, and this was increased by approximately 50% on PI-103 treatment over vehicle only (fig 5.8i,ii). USP8 depleted cells responded similarly to PI-103 treatment, and there was no evidence of sensitization to PI-103 induced cell death (fig 5.8i,ii).

These results indicate that FKHRL1-U2OS cells undergo more apoptosis when cultured in serum free DMEM, than those cultured in HBSS. This is in accordance with the previous live cell experiments, where more cell death was observed in the controls when the experiment was performed in serum free DMEM (fig 5.7) than when it was performed in HBSS (fig 5.4).

However, the differential induction of PARP cleavage in USP8 depleted cells treated with PI-103 or DMSO was less reflective of the results from the live cell experiments. Depletion of USP8 did not significantly increase apoptosis over controls, and PI-103 induced PARP cleavage was not significantly different between USP8 depleted and control cells (fig 5.8). In the live cell experiments in serum free DMEM however, some differential in cell death between USP8 depleted cells and controls was observed, and PI-103 induced cell death was also increased in USP8 depleted cells (fig 5.7). The latter was however less marked at later timepoints, where PI-103 induced cell death was also observed in controls. Lysing cells at earlier timepoints may therefore better reflect the findings of the live cell experiments. The differences in the results from the two methodologies may also partly reflect the contribution of non-apoptotic cell death, which would not be detected using immunoblotting for PARP cleavage.

Akt dependent phosphorylation of USP8 has previously been shown to increase its stability in 293T cells [441], while in a second study, which was performed in glioblastoma cell lines, activation of Akt decreased USP8 protein level [442]. No changes to USP8 protein level following PtdIns3-K inhibition were seen in my experiments (fig 5.8). This may indicate cell line specific differences or reflect time dependent changes, as only a single timepoint was assessed here. Interestingly however, the USP8 protein level

did appear to be altered by media conditions with less USP8 seen in the DMEM cultured cells, than in those cultured in HBSS.

Overall, these findings indicate that the effects of USP8 depletion on PI-103 induced cell death are at least partly dependent on specific media conditions. Further investigation into this would include the identification of specific media conditions that promote the sensitisation of cell death by USP8 depletion, however this has not been performed due to time constraints.

5.6 USP8 depletion affects PI-103 sensitivity in U2OS parental cells.

All the experiments reported above were performed in U2OS cells stably transfected with FOXO3-EGFP. FOXO3 is pro-apoptotic, and its overexpression would be expected to increase sensitivity to apoptotic cell death. I therefore investigated whether the effects of USP8 depletion on sensitizing cells to PI-103 depletion were restricted to cells expressing FOXO3-EGFP. In this experiment, parental U2OS cells were transfected with USP8 siRNA, incubated for 48 hours and then treated with PI-103 or vehicle (fig 5.9 and 5.10). This experiment was performed under the same media conditions to the original screen.

The use of DRAQ7 enabled cell death to be followed in label-free cells (fig 5.9). As previously, DRAQ7 positive cells were counted at each timepoint and divided by the number of DRAQ5 cells at the final timepoint to give the percentage of dead cells (fig 5.10). Overall, less cell death occurred in this experiment (fig 5.10), compared to the same experiment performed with FKHRL1-U2OS cells (fig 5.4). The non-targeting siRNA, and mock-transfected cells did not show an increase in cellular death following PI-103 treatment over the course of the experiment (fig 5.10i,ii). On the other hand, depletion with three of the four USP8 siRNA oligonucleotides resulted in increased sensitivity to PI-103 treatment (fig 5.10iii,iv,vi), and this was partially dose-dependent. The fourth oligonucleotide, USP8_1 (fig 5.8F) was an exception, in which DMSO treatment resulted in similar cell death to cells

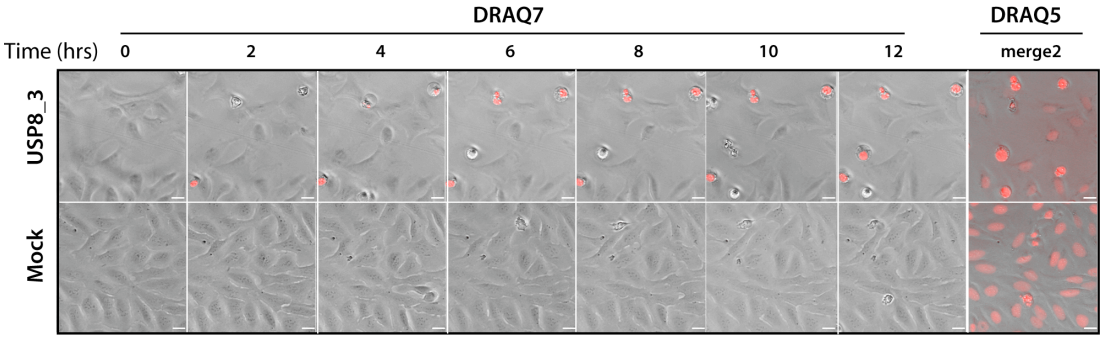

Fig 5.9. USP8 depletion sensitizes parental U2OS cells to PI-103 induced cell death (1). U2OS cells were transfected in a 96 well plate with siRNA oligonucleotides against USP8, non-targeting siRNA (siC) or mock transfected. Following a 48-hour incubation, the media was changed to HBSS, containing vehicle (DMSO) or varying concentrations of PI-103, and 3μM DRAQ7. Imaging was performed hourly by automated microscopy for 12 hours after which DRAQ5 was added to a concentration of 5μM, cells were incubated a further 20 minutes and a final image taken. Representative cropped images following 100nM PI-103 treatment of cells transfected with USP8_3 siRNA, or mock-transfected are shown here. The panels show a merge of DRAQ7 (red) and light microscopic images, with the exception of merge 2 (far right panel) in which the red represents DRAQ5 stained cells. (scale bar- 25μM).

treated with the highest concentration of PI-103. However, treatment at the other dose levels resulted in cell death that was dose dependent, indicating possible aberrant results from the DMSO treated well. This experiment suggests that interaction between USP8 depletion and PI-103 treatment is not limited to cells overexpressing FOXO3. However increased cellular levels of FOXO3 may potentiate the effects of their cross-talk.

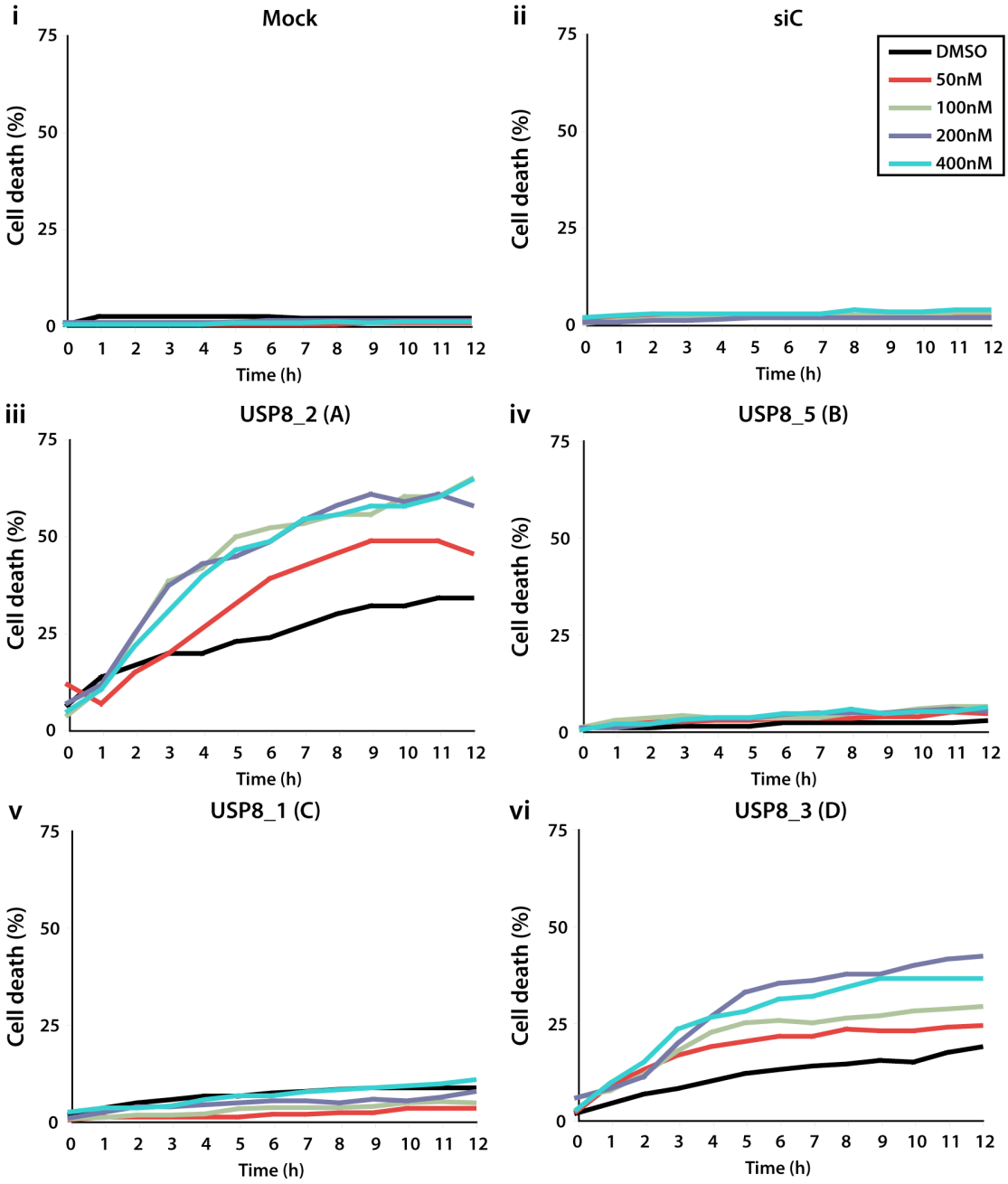

Fig 5.10. USP8 depletion sensitizes parental U2OS cells to PI-103 induced cell death (2). U2OS cells were transfected with the indicated siRNA oligonucleotides against USP8 (1,2,3,5), non-targeting siRNA (siC) or mock transfected, incubated for 48 hours, treated with varying concentrations of PI-103 (legend top right) and imaged as described in fig 5.9. The letters in parentheses refer to the numbering of the original (library) siRNA oligonucleotides. Cells taking up DRAQ7 were counted using Volocity (PerkinElmer) and expressed as a percentage of total cells, which were counted following staining with DRAQ5 on completion of the experiment. A single position, and median (range) of 206 (62-397) cells were imaged per condition (n=1).

5.7 Discussion

In the screen described in chapter 4, I set out to investigate the effects of DUB depletion on PtdIns3-K dependent translocation of an EGFP tagged FOXO3 fusion protein. This provided the additional, and originally unanticipated, opportunity to observe synthetic effects between depletion of DUBs and treatment with the PtdIns3-K inhibitor (PI-103), which I have described here.

The depletion of three DUBs (namely DUB4, OTUD4 and USP8) was observed to increase cell death on treatment with PI-103. As described in section 5.2, several factors led to the prioritization of USP8 for further investigation, including the presence of local expertise and reagents, and established links between USP8 and PtdIns3-K signaling. USP8 is known to be involved in the downregulation of several receptors, including EGFR [443], ErbB2 [444], ErbB3 [441], which lie upstream of the PtdIns3-K pathway, and is itself phosphorylated by Akt [441]. In the latter study, Akt dependent phosphorylation led to USP8 stabilisation in 293T cells [441]. However, in a different study, which utilised a glioblastoma multiforme cell line, the USP8 protein level was decreased by Akt activation [442]. This suggests the effects of Akt on USP8 may be cell line or context dependent, and in the work presented in this chapter, PtdIns3-K inhibition did not cause obvious alterations to USP8 protein level. The second study also showed that USP8 promotes TRAIL-induced apoptosis [442]. These studies taken together indicate that USP8 both influences, and is influenced by, PtdIns3-K signaling, and may be involved in apoptotic pathways.

Initial validation of USP8 synthetic lethality with PI-103 was performed by deconvolution of the oligonucleotide pool. Knockdown with the four oligonucleotides resulted in markedly different degrees of cell death in the absence of PI-103; this is likely to represent a combination of off-target effects as well as differing knockdown efficiencies and dynamics. However all four increased sensitivity to PI-103 induced cell death. In addition to sensitising the cells to PI-103 induced cell death, USP8 depletion also

increased cell death in response to the Akt inhibitor MK2206. While this supports a general interaction between USP8 depletion and inhibition of the PtdIns3-K pathway, it is feasible that USP8 depletion increases sensitivity to stress, rather than specific PtdIns3-K inhibition. This would be partly supported by the cell death seen in USP8 depleted cells treated with DMSO only. However, as the cells in these experiments were serum-starved, they would be anticipated to have decreased signalling through the PtdIns3-K pathway, and thus in effect partial PtdIns3-K inhibition. Further (non PtdIns3-K) inhibitors could be assessed in future to determine if the effects on cell death are PtdIns3-K dependent.

Further validation of the interaction between USP8 and PI-103 was obtained through the use of two USP8 inhibitors. Hybrigenics had identified USP8 as a potential drug target on the basis of a screen for USPs whose depletion altered cell viability or proliferation [445] and its known key involvement in the regulation of receptor endocytosis and trafficking [443], and had previously collaborated with the host laboratory in investigating the activity of two USP8 inhibitors. Both of these compounds increased sensitivity to PI-103 induced cell death (fig 5.6).

Interestingly, while both the inhibitors increased cell death at a concentration of 2.5μM, this was less apparent at the highest concentration used (5μM). At this concentration, profound nuclear localisation of FOXO3-EGFP was observed, even in the absence of PtdIns3-K inhibition, clearly linking their effect to this pathway. The FOXO family of transcription factors are known to induce both apoptosis and cellular senescence [446], and it is feasible that the high levels of nuclear translocation of FOXO3-EGFP seen at the highest dose of the USP8 inhibitors led to the senescence rather than apoptosis. In future this could be tested by the use of a senescence assay, an example being a β-galactosidase assay [447].

Neither inhibitor has been exhaustively investigated, and it is also feasible that at higher concentrations, they inhibit other factors that may prevent the activation of apoptotic pathways. Interestingly, a recent study has shown that

β-catenin translocation to the nucleus can confer resistance to PtdIns3-K inhibitors and can subvert FOXO3a to promote metastasis rather than to act as a tumour suppressor [448]. It is possible that the USP8 inhibitors used in my study promote nuclear translocation of β-catenin in these cells, in addition to FOXO3-EGFP, although this has not been assessed.

The mechanism driving nuclear translocation of FOXO3-EGFP on treatment with the USP8 inhibitors is unknown. While USP7 depletion has been shown to promote FOXO4 and FOXO3 translocation into the nucleus, the concentrations of both inhibitors used were over an order of magnitude lower then the IC50 for USP7 [440]. Inhibition of USP8 itself may lead to FOXO translocation. While this is not supported by the experiments in which USP8 was depleted using siRNA, it is feasible that this is due to differing effects of the acute or chronic loss of USP8 function obtained with inhibitors or siRNA transfection respectively. Alternatively, sufficient residual USP8 may remain after siRNA dependent depletion to influence FOXO3 translocation. While specificity against a limited panel of DUBs has been checked, wider effects on other DUBs (or indeed other enzymes) have not been established, and it is therefore possible that their effects here may have been mediated through inhibition of other targets.

Immunoblotting experiments supported the live cell imaging experiments and indicated that the synthetic lethality between loss of USP8 activity and PI-103 was at least partially due to apoptosis. However, all the above experiments were conducted in HBSS, which had originally been used to optimize fluorescence imaging. Repeating the USP8 knockdown in serum free DMEM resulted in increased cell death in the controls using live cell imaging, and increased overall apoptosis measured by immunoblotting for cleaved PARP. Under these media conditions, the effects of USP8 depletion on PI-103 sensitivity were less apparent on live cell imaging and absent on immunoblotting.

In both media conditions, the cells were serum starved. FKHRL1-U2OS cells grew well in full serum DMEM, suggesting the cell death in serum free

DMEM was due to serum starvation. However, cells grown in HBSS appeared to have been relatively protected from serum starvation. While the role of different media components have not been fully elucidated, two likely possibilities are the presence of amino acids and pH. The HBSS was not supplemented with amino acids, which may have been protective, potentially through the induction of autophagy. Secondly the pH of the HBSS was approximately 7- 7.2, and fell to 6.8- 6.9 at the end of a 12-hour incubation, and it is possible that this altered pH (compared to 7.4 in DMEM) may have altered response to PtdIns3-K inhibition. Interestingly, the lower pH observed in cells cultured in HBSS may be more reflective of the pH within tumours, which are frequently acidotic [449], and these findings may therefore prove to have clinical relevance. Further experiments to dissect out the relevant constituents are yet to be performed.

The other two DUBs that induced PI-103 dependent cell death may also be worthy of further investigation. The first of these, DUB4 is a member of the USP17 subfamily of DUBs, which consists of multiple, closely related members that arose through ancestral gene duplication and several of which exist within a tandemly repeated block on chromosome 4 [83]. While neither a substrate nor function has been ascribed to DUB4, the closely related USP17 has been shown to be involved in Ras signalling [450, 451], and regulation of HDAC activity [452]. Moreover, another member of the family, DUB3, has been shown to rescue cdc25A from proteasomal degradation, and promote growth on soft agar; its depletion retarded growth of tumour xenografts in mice [453]. Interestingly, DUB3 was not identified in the screen, but it was noted to cause increased cell death at a later time point in the follow-up experiment, where it had been included as a control (fig 6.2). The final DUB that exhibited synthetic lethality with PI103 was OTUD4. Substrates for OTUD4 have not been described as yet, although it has been implicated in BMP signalling during Zebrafish development [454]. Several interactors have been identified including the autophagy protein ATG12 [455].

The findings in this chapter are both exploratory and preliminary. However, they are potentially of significant scientific and clinical interest. Further investigation into the interaction between depletion of the three DUBs and PI-103 induced cell death may provide valuable insights into the cellular roles of these DUBs, while the combinatorial inhibition of one or other of these DUBs with inhibition of the PtdIns3-K pathway may prove a useful therapeutic strategy.

Chapter 6

USP20, ATXN3, ATXN3L and JOSD1 regulate PTEN protein level

6.1 Introduction

Ubiquitylation has been shown to influence both the stability [335, 359, 360, 456] and subcellular localization [57, 359] of the tumour suppressor PTEN (section 1.5.4). The deubiquitylase USP7 may reverse the monoubiquitylation of PTEN, and promote its nuclear exclusion [203]. However, no DUBs regulating the stability of PTEN have yet been identified.

In chapter 3, I described the identification of five deubiquitylases whose knockdown influenced PTEN protein level. These were USP20, depletion of which downregulated PTEN, and USP7, ATXN3, ATXN3L and JOSD1 for which depletion upregulated PTEN. All five were successfully validated by deconvolution, by the criterion that at least two individual oligonucleotides recapitulated the effects of the pool. However, USP7 depletion only modestly increased PTEN levels. In addition, USP7 has previously been shown to regulate monoubiquitylation of PTEN [203], and it was therefore not followed up further in this study. Here I will describe initial investigations into the mechanisms by which the other four DUBs may regulate PTEN cellular abundance.

6.2 USP20 depletion alters PTEN protein level

In the original siRNA screen, depletion of USP20 using a pool of siRNA oligonucleotides resulted in a reduction in the PTEN protein level (figs 3.6 and 3.7). The effects of the pool were recapitulated by two of the four siRNA oligonucleotides that made up the original pool (figs 6.1i and 3.8). However, USP20 depletion by the other two oligonucleotides did not have the same effect on PTEN, and USP20_D actually led to an increase in PTEN level (Fig 6.1i).

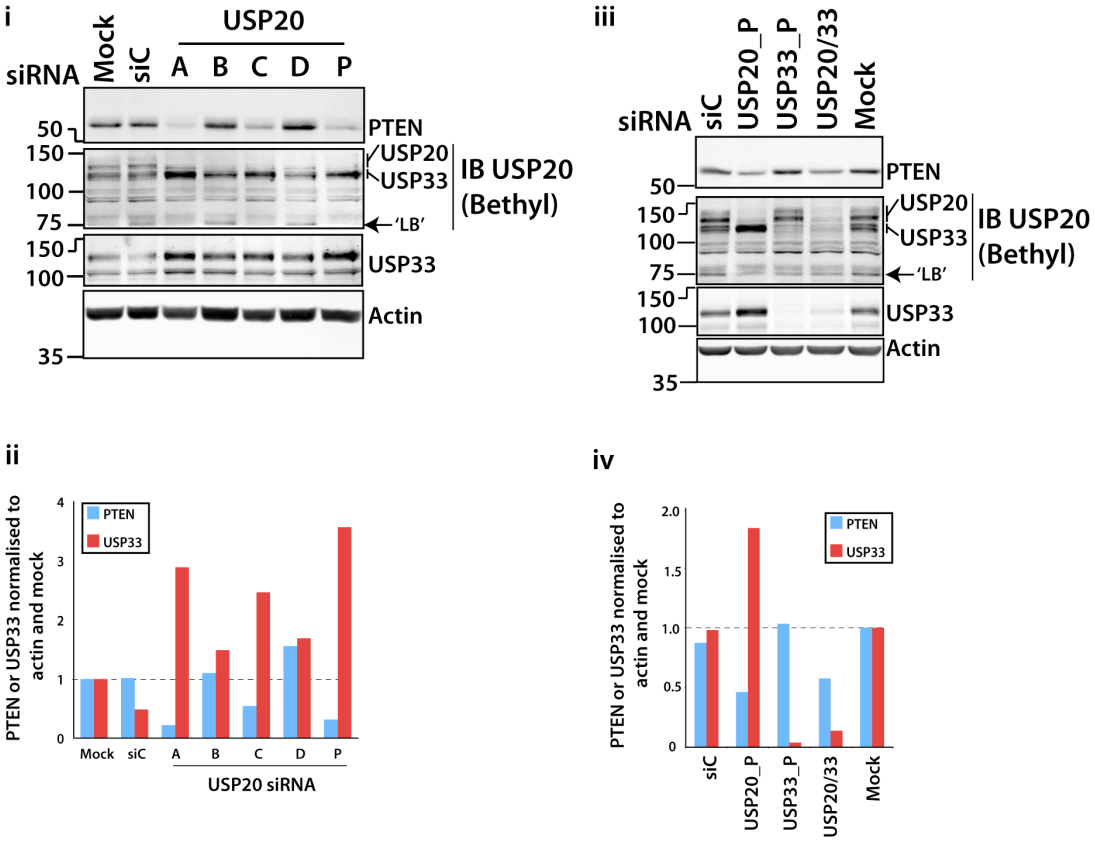

Fig 6.1. The effects of USP20 depletion on PTEN protein level inversely correlate with USP33 induction. i,ii. A549 cells were transfected with siRNA, incubated for 72 hours and lysed in NP40 buffer. Equal amounts of each lysate were immunoblotted as indicated. **iii,iv.** PTEN and USP33 bands were quantified, normalized to actin and then compared to the mock control. Imaging and quantification were performed using an infrared scanner and associated software [Odyssey, LiCor]. (A-D: individual USP20 siRNA oligonucleotides, P: pooled oligonucleotides, USP20/33: dual depletion with USP20 and USP33 pools, 'LB': lower molecular weight band. n=1)

I first set out to investigate if these differences in phenotypic effect on PTEN correlated with knockdown efficiency using immunoblotting for USP20 (fig 6.1i). For this, I initially employed a polyclonal antibody from Bethyl (A301-189A), which was raised against an epitope mapping to a region between amino acids 863 and 913 of human USP20 (fig 6.3iii). In this region, USP20 shares extensive sequence homology with its paralogue USP33, with a sequence identity of 57% (appendix B), and the A301-189A antibody thus detects both USP20 and USP33. As shown in figures 6.1i and iii, at least two bands of approximately 120-140kDa are depleted by all USP20 oligonucleotides, and a band of slightly lower molecular weight (~110-

120kDa) is depleted by USP33 siRNA. The three reference sequences for the USP20 transcript differ only in their untranslated regions and encode a protein with a predicted molecular weight of 102kDa (fig 6.3). It is feasible that unmodified USP20 is obscured by the USP33 band, although this ran at a higher molecular weight than 102kDa (fig 6.1i,ii). The USP20 bands that were depleted run at a higher molecular weight to that predicted, suggesting these may be modified forms of USP20. Due to the lack of specificity of this antibody, quantitative assessment of USP20 knockdown efficiency was not attempted for this experiment.

As discussed previously (section 3.3), depletion of USP20 is known to lead to upregulation of USP33, this representing an example of paralogue compensation [390]. This was again shown here, and interestingly there also appeared to be an inverse correlation between the effects of the USP20 siRNA oligonucleotides on PTEN protein level, and the degree of upregulation of USP33 (figs 6.1i,iii). This could suggest that USP20 depletion leads to USP33 upregulation, and this in turn leads to a reduction in PTEN protein level. In order to test this, I performed a dual knockdown of both USP20 and USP33 using pooled siRNA oligonucleotides in each case (fig 6.1ii,iv). The dual knockdown failed to abolish the effects of USP20 depletion on PTEN, indicating that upregulation of USP33 is not required for USP20 depletion to upregulate PTEN.

I speculated that the degree of USP33 upregulation may be acting as a surrogate marker for USP20 knockdown efficiency, which I had not been able to assess quantitatively with the Bethyl antibody. I therefore sought to better assess USP20 levels with a second commercially available antibody (Aviva, ARP59314), which is raised against an internal epitope of USP20 that shares limited homology with USP33 (sequence identity of 24%, appendix B). While a strong band was detected at just over 100kDa (fig 6.2i), which would be in keeping with unmodified USP20, this was not depleted by USP20 knockdown, and more closely resembled the band structure seen on blotting for USP33 (fig 6.2ii). While this band did not colocalise with the

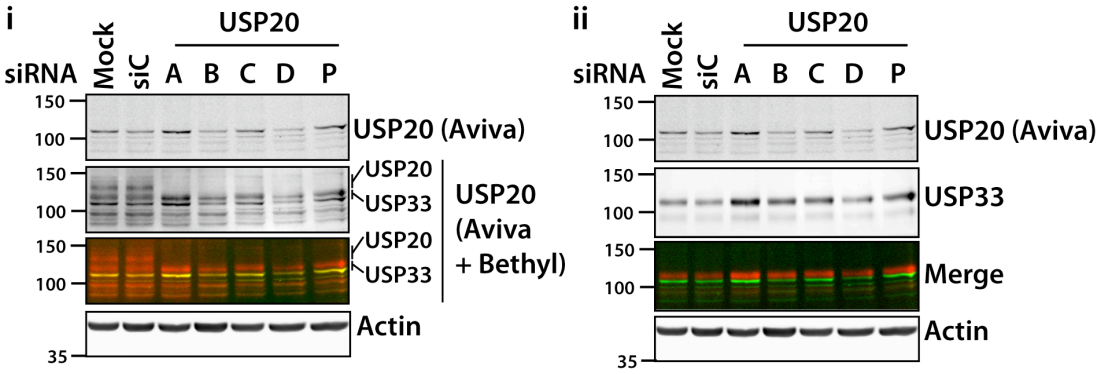

Fig 6.2. Antibody ARP59314 does not detect endogenous USP20. A549 cells were transfected with the indicated USP20 siRNA, non-targeting siRNA (siC) or mock transfected. Following a 72-hour incubation the cells were lysed in NP40 buffer. Equal amounts of each lysate were immunoblotted with the indicated antibodies. **i.** Immunoblotting for USP20 was performed using ARP59314 (Aviva-A) and A301-189A (Bethyl-B) sequentially (first two panels from the top). Both antibodies were raised in rabbits, and the second panel therefore represents a composite of the immunoreactive bands for both the antibodies. A merge of images immunoblotted with ARP59314 (green channel) and both antibodies (false coloured red channel) is shown in the third panel. **ii**. Immunoblotting was also performed for USP33, and a merge of the USP20 (Aviva in green) and USP33 signal (in red) is shown in the third panel from the top.

USP33 antibody (fig 6.2ii), it may still represent a splice variant of USP33 that is not recognized by the USP33 antibody.

None of the other bands detected by this antibody (ARP59314) were depleted by USP20 siRNA, and it does not appear to recognise the higher molecular weight USP20 bands detected by the Bethyl antibody, that were clearly depleted by the USP20 siRNA oligonucleotides (fig 6.2i). This suggests antibody ARP59314 does not detect endogenous USP20, and it has not been possible thus far to quantitatively assess USP20 depletion using immunoblotting.

The difference in effects of the different USP20 oligonucleotides on PTEN levels could also reflect differential effects on USP20 splice variants. Interestingly, a lower molecular weight band ('LB') of approximately 75kDa detected with the Bethyl USP20 antibody appeared to directly correlate with PTEN level (fig 6.1i). This was supported by an independent experiment,

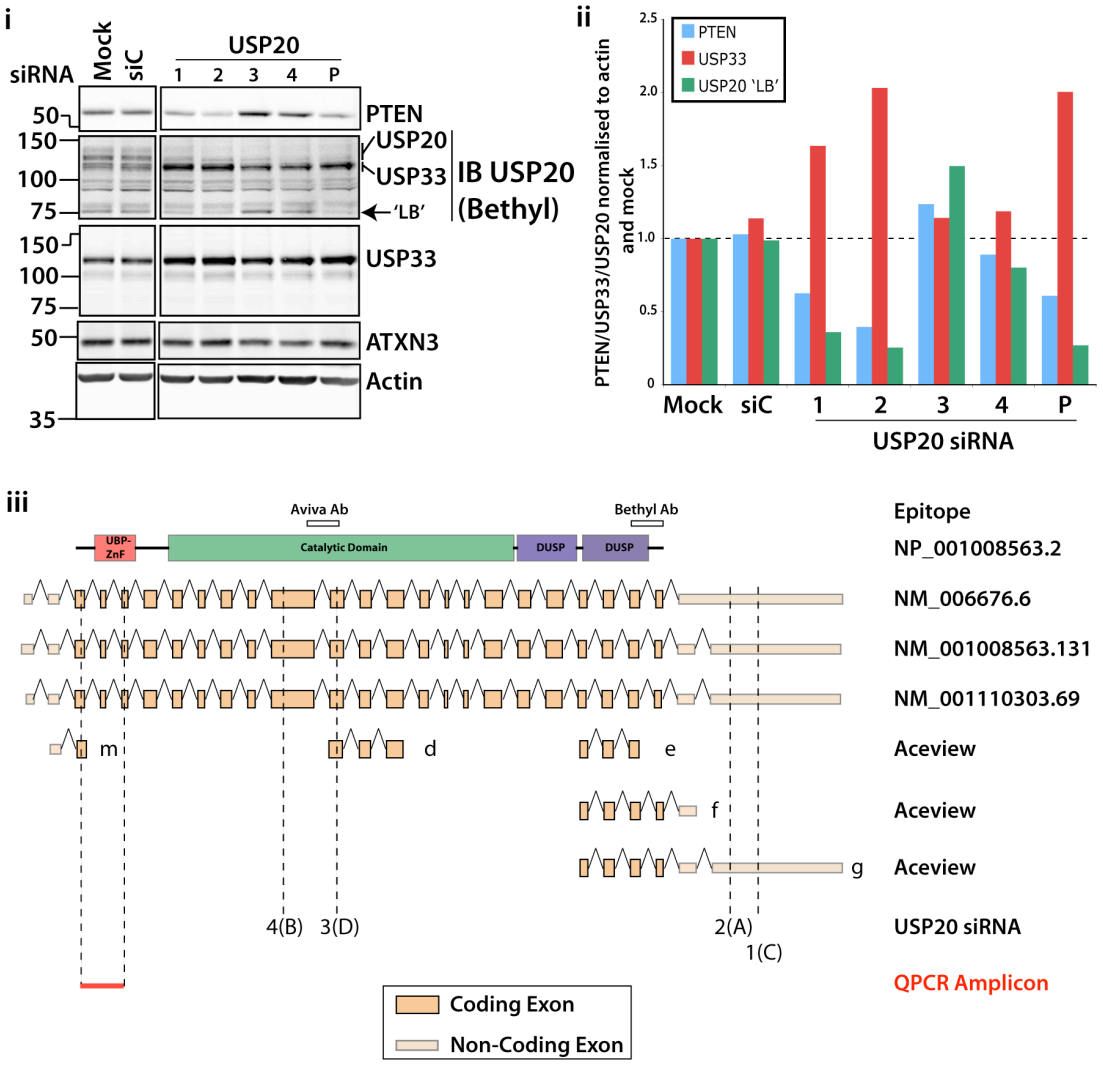

Fig 6.3. The effect of USP20 siRNA oligonucleotides on PTEN correlates with location on transcript. i,ii. A549 cells were transfected with the indicated USP20 siRNA, incubated for 72 hours and lysed in NP40 buffer. Equal amounts of each lysate were immunoblotted as indicated. PTEN, USP33, and a lower molecular weight band detected with the USP20 antibody 'LB', were quantified, normalized to actin and then compared to the mock control. Imaging and quantification were performed using an infrared scanner and associated software [Odyssey, LiCor]. (1- 4: individual USP20 siRNA oligonucleotides, P: pooled oligonucleotides.) **iii**. Schematic of USP20 protein and splice variants (named in right hand column). Location of USP20 siRNA oligonucleotides and QPCR primers is also shown. Bethyl Ab and Aviva Ab respectively refer to the epitopes detected by USP20 antibodies A301-189A (Bethyl) and ARP59314 (Aviva). (UBP-ZnF: UBP type Zinc Finger, DUSP: Domain of Ubiquitin Specific Protease. USP20 oligonucleotides 1, 2, 3 and 4 correspond to plates C, A, D and B respectively from the DUB siRNA library- see Appendix A.) The position of the QPCR amplicon is highlighted in red.

which employed four USP20 siRNA oligonucleotides that were purchased to replenish those in the original DUB siRNA library (fig 6.3i, ii). Both USP20 siRNA oligonucleotides which downregulated PTEN protein levels (and the 75kDa immunoreactive band detected using the USP20 antibody) were located at the 3' end of the USP20 transcript within the 3'UTR (untranslated region), while the other two sequences map internally within the coding region of the transcript (fig 6.3iii). This would suggest that oligonucleotides 1 and 2 may differentially affect alternative USP20 splice variants compared to oligonucleotides 3 and 4, providing a possible explanation for the effects these four USP20 oligonucleotides have on the 75kDa band.

However a search of multiple databases (ASD, ECgene, DOTS, Ensembl and Aceview), failed to identify any USP20 splice variants that would give rise to an alternative 75kDa isoform. Moreover this immunoreactive band also appears to be partially depleted by USP33 knockdown (fig 6.1ii). As this USP20 antibody also detects USP33, the band could represent an alternative splice variant of USP33, rather than USP20. While the band was not detected using the USP33 antibody (fig 6.3i), this does not rule out the possibility that the lower band represents a USP33 splice variant, as it could lack the epitope which is detected by the USP33 antibody.

As I had been unsuccessful in the assessment of USP20 knockdown efficiency using immunoblotting, I turned to QPCR instead (fig 6.4). This showed the knockdown efficiency of the four individual oligonucleotides and the pool ranged from approximately 65% - 85% (fig 6.4i). There was no evidence of correlation between the knockdown efficiency of the USP20 oligonucleotides and their effects on PTEN protein level (fig 6.4ii). This suggests that variation in USP20 siRNA oligonucleotide knockdown efficiency was not responsible for their differences in effect on PTEN protein.

In addition, this experiment allowed me to assess the effect of USP20 knockdown on PTEN mRNA levels (fig 6.4i). Depletion of USP20 using oligonucleotide USP20_1 or the USP20 siRNA pool led to a reduction in PTEN mRNA. On the other hand, USP20_3 led to an increase in PTEN

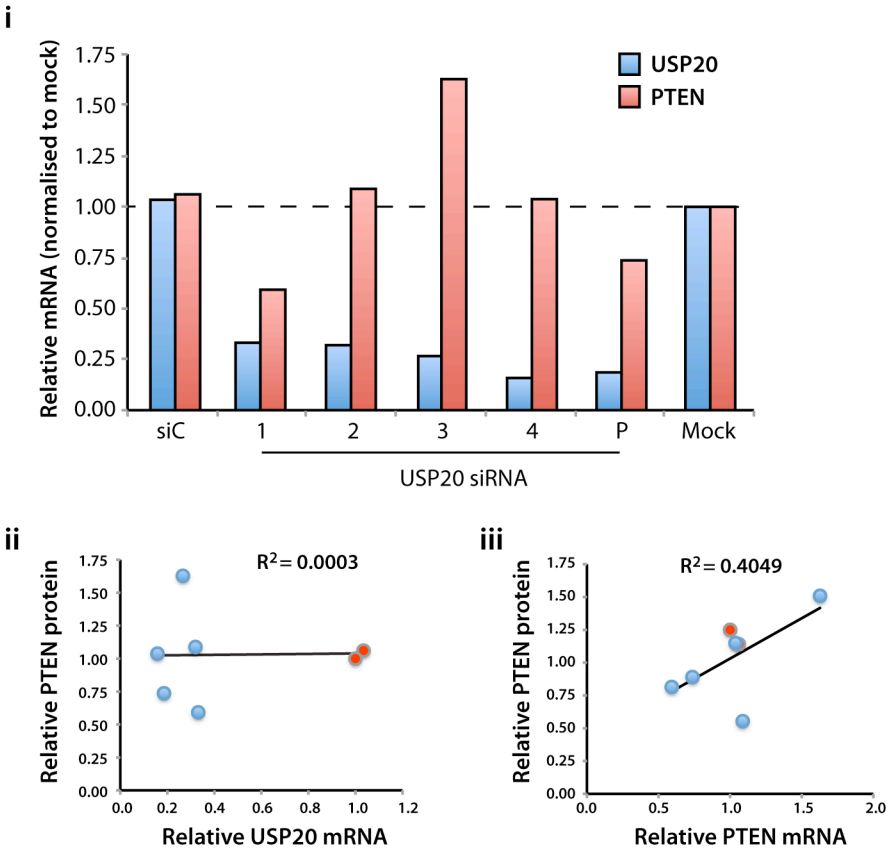

Fig 6.4. USP20 knockdown efficiency does not correlate with PTEN protein levels. i. A549 cells were transfected with the indicated USP20 siRNA, non-targeting siRNA or mock transfected, and incubated for 48 hours prior to preparation of total RNA. QPCR was performed for USP20 and PTEN using an IQ5 real time PCR detection system and SYBR green supermix (BioRad). Actin was employed as the reference gene and results were further normalized to the mock control. **ii, iii**. Scatterplots of the relative USP20 or PTEN mRNA levels compared to the PTEN protein levels observed in the experiment described in fig 6.3. The coefficient of correlation (R^2) is shown in the top right hand corner in both graphs. Controls are shown in red. (P: pooled siRNA oligonucleotide. 1,2,3 and 4: individual USP20 oligonucleotides. siC: Non-targeting siRNA control. The experiment was performed once.)

mRNA. Interestingly the effects of USP20 oligonucleotides on PTEN mRNA partly correlate with their effects on PTEN protein (fig 6.4iii), as assessed by immunoblotting in fig 6.3. These findings suggest that the effects of USP20 on PTEN may at least partly occur through regulation of its transcript level.

The experiments described in this section support the findings of the screen, and suggest depletion of USP20 can alter PTEN protein level. While

individual USP20 siRNA oligonucleotides had differential effects on PTEN, the most reproducible finding was a reduction in PTEN protein level with two out of the four oligonucleotides. The data do not provide a clear explanation for the differential effects of the siRNA oligonucleotides on PTEN, however one possibility is that they represent differential effects on USP20 splice variants. Further investigation into the potential role of USP20 splice variants was not prioritized, as the DUB screen also identified three DUBs whose depletion upregulated PTEN, and which may therefore represent potential drug targets (section 6.9).

6.3 Both ATXN3 and ATXN3L upregulate PTEN protein level

Depletion of ATXN3, ATXN3L or JOSD1 led to increased PTEN protein levels in the screen (figs 3.6 and 3.7). Interestingly all three are members of the Josephin family of deubiquitylases and share extensive sequence homology (fig 6.5). Only one member of the family, JOSD2, was not identified in the PTEN immunoblot screen. Although TAF1D (also known as JOSD3) is sometimes included in this DUB family [415], neither the catalytic Cys nor His are conserved ([415] and S Urbé, personal communication). Initial validation has focused on ATXN3 and ATXN3L, which share the greatest homology, and for which additional reagents were locally available.

Depletion of ATXN3 by any of the four siRNA oligonucleotides from the DUB library resulted in an increase in PTEN level (fig 3.8). Similar results were obtained with siRNA oligonucleotides purchased to replace the original library oligonucleotides (fig 6.6). A correlation between effects on PTEN level and ATXN3 knockdown efficiency is also noted (fig 6.6i,ii). Knockdown efficiency was in excess of 95% for three out of four oligonucleotides, each of which increased the PTEN protein level to at least 150% of control. Transfection with the fourth oligonucleotide (ATXN3_1) only depleted ATXN3 by 60%, and had marginal effects on PTEN level.

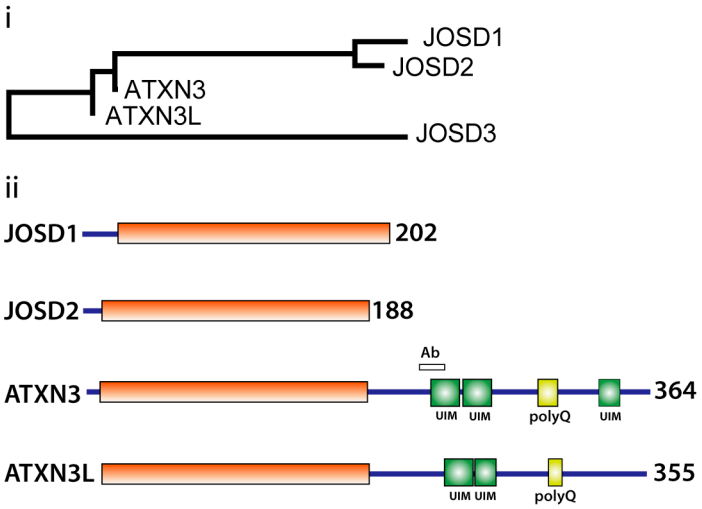

Fig 6.5 The Josephin family of deubiquitylases. i. A phylogenetic tree was constructed using the maximum likelihood method as described in figure 1.3. JOSD3 (TAF1D) lacks both the catalytic Cys and His and was not included in the DUB library**. ii.** A representation of the domain structure of the four Josephins that were included in this study. The domains of each protein are drawn to scale with the catalytic domains of each protein depicted in orange, the ubiquitin-interacting motif's (UIM) in green and polyglutamine tracts (polyQ) in yellow. Ab represents the binding site of the ATXN3 antibody (650401, BioLegend).

As discussed in section 6.2, depletion of USP20 (using pooled siRNA oligonucleotides) led to a reduction in PTEN protein level, thus regulating PTEN in the opposite direction to ATXN3. While these effects are most likely to be independent of each other (fig 6.6iii), two alternative models may be hypothesized in which one of the two deubiquitylases exerts its effects on PTEN through regulation of the other (fig 6.6iv,v). I therefore performed a dual knockdown of ATXN3 and USP20 to determine if depletion of either had a dominant effect on PTEN protein level (fig 6.6vi). This resulted in an intermediate PTEN protein level, which most likely indicates that the two deubiquitylases act independently (6.6iii).

Similarly to ATXN3, ATXN3L depletion also upregulated the PTEN protein level (fig 3.6 and 3.7). This effect of ATXN3L was also successfully deconvoluted, with all four siRNA oligonucleotides leading to an increase in PTEN protein level (fig 6.7i). ATXN3L is closely related to ATXN3 (fig 6.5) with which it shares an overall sequence identity of 72%, including 85%

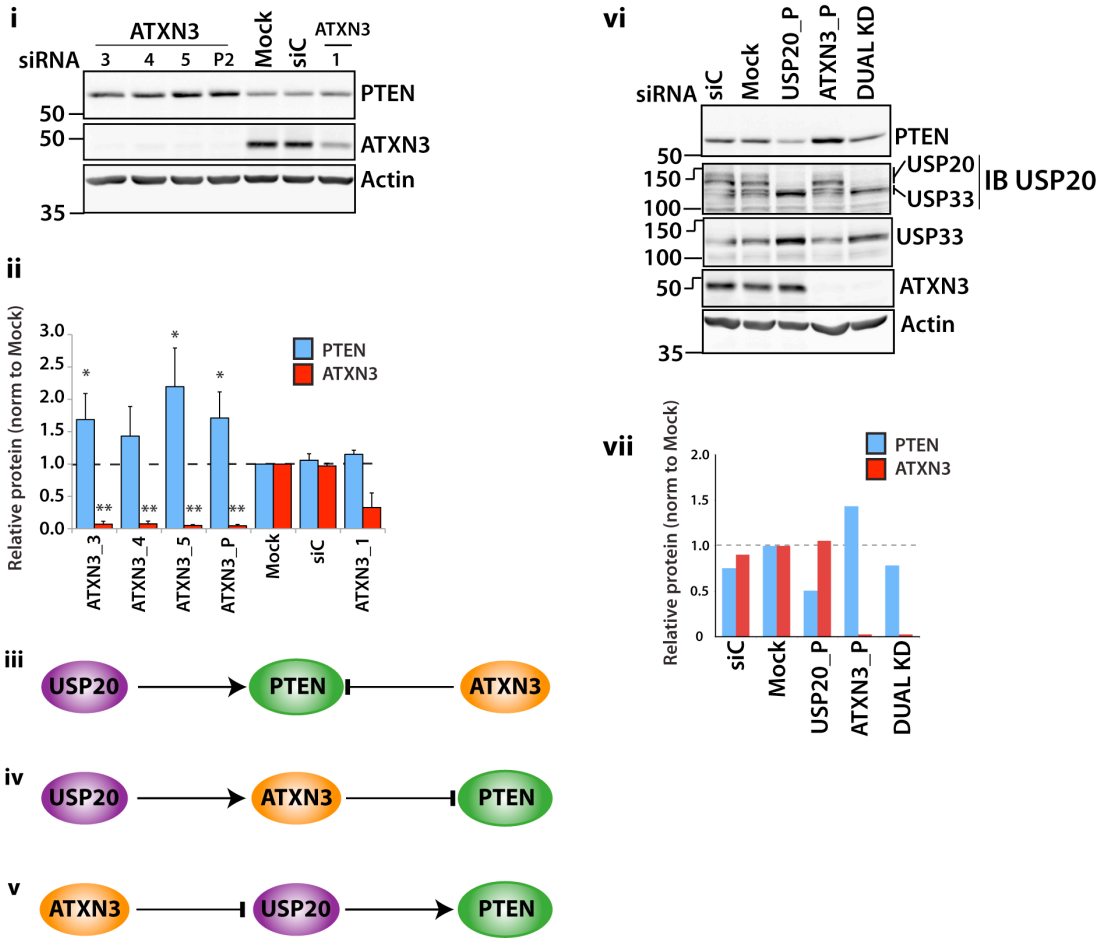

Fig 6.6. ATXN3 depletion upregulates PTEN protein level. i,vi. A549 cells were transfected with the indicated siRNA oligonucleotides, incubated for 72 hours and lysed in NP40 buffer. Equal amounts of each lysate were immunoblotted as indicated. **ii.** PTEN and ATXN3 were quantified, normalized to actin and then compared to the mock control. Mean data for three (ATXN3) or four (PTEN) experiments are shown. Students' t-tests compared PTEN or ATXN3 abundance in response to each siRNA to that with siC, *P<0.05, **P<0.001. Error bars show standard deviation. **iii,iv,v.** Models of interaction between USP20, ATXN3 and PTEN. **vii.** Quantification of dual USP20/ATXN3 depletion was performed, as described in ii, from a single experiment. (1, 3, 4, 5: individual ATXN3 siRNA oligonucleotides, P and P2: pooled ATXN3 oligonucleotides from the DUB siRNA library and replacement oligonucleotides respectively. DUAL: combined knockdown of ATXN3 and USP20 using pooled siRNA for both. Imaging and quantification were performed using an infrared scanner and software [Odyssey, LiCor]. n=1)

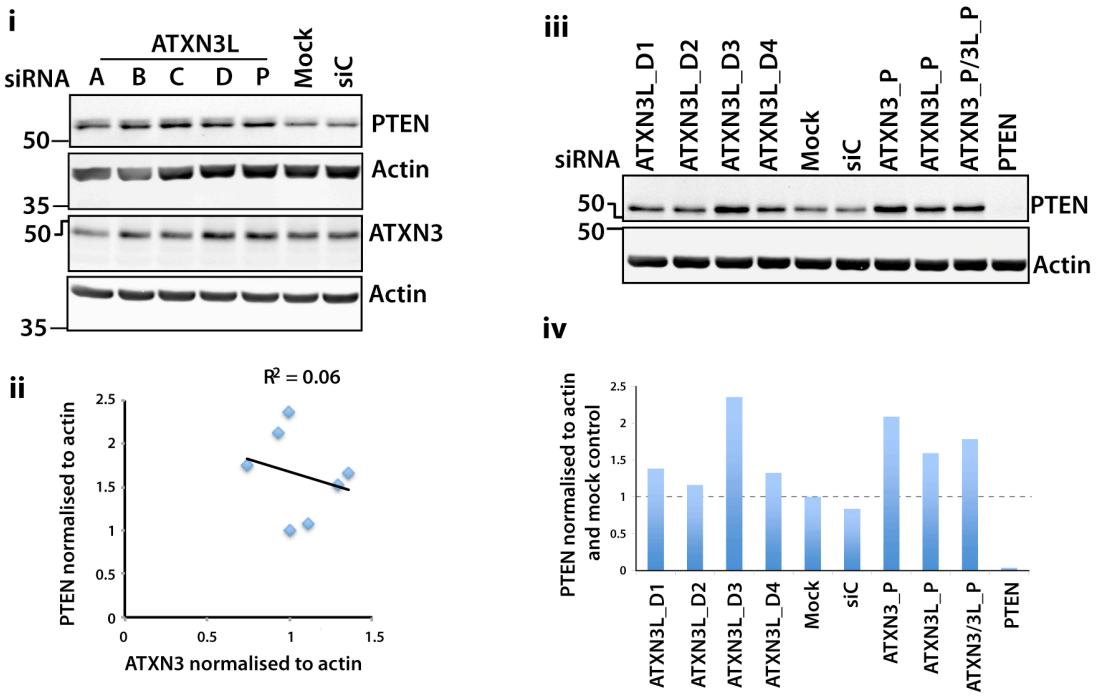

Fig 6.7. ATXN3L upregulates PTEN in an ATXN3-independent manner. i. Depletion of ATXN3L was performed as described in fig 3.8. Lysates were immunoblotted for ATXN3 and actin as shown in the first two panels; immunoblots for PTEN and actin from fig 3.8 are shown for comparison. **ii.** Scatterplot of ATXN3 and PTEN quantification normalized to actin and mock control. The coefficient of determination (R^2) is shown. **iii.** A549 cells were transfected with the indicated siRNA, incubated for 72 hours and lysed in NP40 buffer. Equal amounts of each lysate were immunoblotted as indicated. **iv.** PTEN was quantified, normalized to actin and then compared to the mock control. (A- D: individual ATXN3L siRNA oligonucleotides, P: pooled oligonucleotides, D1-D4 ATXN3L oligonucleotides (Dharmacon), ATXN3/3L: combined depletion of ATXN3 and ATXN3L. Imaging and quantification were performed using an infrared scanner and associated software [Odyssey, LiCor].)

homology in the catalytic domain [457]. Although the ATXN3L siRNA oligonucleotides were designed to be specific for ATXN3L and were not predicted to cross-react with ATXN3, this could not be ruled out. I therefore assessed the effects of ATXN3L siRNA on ATXN3 protein level (fig 6.7i). There was no evidence of ATXN3 depletion following knockdown of ATXN3L, and the ATXN3 level did not correlate with the PTEN protein level in this experiment (fig 6.7i,ii). It is therefore unlikely that the effects of the ATXN3L siRNA oligonucleotides on PTEN were mediated through off-target depletion of ATXN3. The lack of correlation between ATXN3 and PTEN protein levels

in the absence of direct ATXN3 depletion, is also in keeping with the findings in fig 6.6i, where partial depletion of ATXN3 with ATXN3_1 did not have significant effects on PTEN protein. This indicates that a profound loss of ATXN3 is required in order to upregulate PTEN.

The effects of ATXN3L depletion on PTEN levels in both the screen and deconvolution were further supported by depletion using another four independent siRNA oligonucleotides (Dharmacon), which had previously been used in our lab (fig 6.7iii,iv). All four of these siRNA oligonucleotides resulted in increased PTEN protein levels, albeit to a more modest degree for all oligonucleotides bar ATXN3L_D3. No ATXN3L antibody was available to assess ATXN3L depletion in this experiment, and the differences in effect on PTEN level may therefore reflect differing knockdown efficiencies.

In view of the similarity between ATXN3 and ATXN3L, I also sought to investigate the effects of a dual depletion of both (fig 6.7iii,iv). In this experiment, depleting both ATXN3 and ATXN3L did not appear to have additive effects on PTEN protein level (fig 6.7ii,iv). This suggests that both may have functions within the same pathway, such that depletion of either leads to disruption of the pathway and produces a similar phenotype.

6.4 USP20 or ATXN3 depletion alter overall PTEN protein levels

In addition to negatively regulating the PtdIns3-K pathway, PTEN has well established nuclear roles including the regulation of the APC-CDH1 complex [458]. PTEN nuclear shuttling is regulated by ubiquitylation [57], which may be reversed by USP7 [203]. I therefore set out to investigate whether depleting either USP20 or ATXN3 led to alterations in the distribution of PTEN rather than the overall protein levels. A549 cells were lysed with a series of buffers to crudely fractionate proteins into cytosolic (NP40), nuclear (Dignam C) and chromatin bound (Laemmli) fractions (fig 6.8). PTEN was only detected in the NP40 fraction, despite loading a relatively high proportion of nuclear to cytosolic lysate (fig 6.8). This may indicate either that

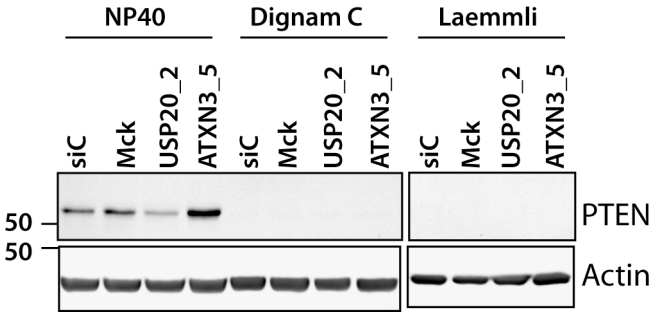

Fig 6.8. USP20 and ATXN3 regulate overall PTEN protein level. A549 cells were transfected with the indicated siRNA, incubated for 72 hours and lysed sequentially with NP40, Dignam C and Laemmli buffers to obtain crude cytoplasmic, nuclear and chromatin bound fractions. Lysates were immunoblotted for PTEN and actin as indicated. 15µg of NP40 and 5µg of Dignam C and Laemmli lysates were loaded respectively. This represents a higher proportion of protein from either Dignam C or Laemmli fractions than was extracted (approximately ten times as much protein was extracted with NP40 than with Dignam C or Laemmli). Imaging was performed using an infrared scanner [Odyssey, LiCor].

PTEN was almost exclusively localized to the cytoplasm, or that nuclear PTEN was being extracted in the NP40 fraction. Discrimination between the two would require fluorescence microscopy and/or the use of alternative lysis buffers [203], neither of which have been performed. However, in the absence of any detectable PTEN in the other cellular fractions, the changes in PTEN level in the NP40 fraction do reflect changes in total cellular PTEN. While the effects of ATXN3L and JOSD1 depletion on PTEN level in other cellular fractions were not assessed, depletion of either DUB led to an increase in PTEN in the NP40 fraction and, in view of the absence of PTEN detected in the nuclear fraction here (fig 6.8), this most likely also reflects an increase in overall cellular PTEN protein levels.

6.5 ATXN3 depletion does not alter the rate of PTEN degradation

Here, I investigated the effects of ATXN3 and USP20 depletion on turnover of PTEN protein. Cells were lysed at successive timepoints following treatment with cycloheximide, which was employed to inhibit translation of new protein (fig 6.9). As previously, USP20 and ATXN3 depletion

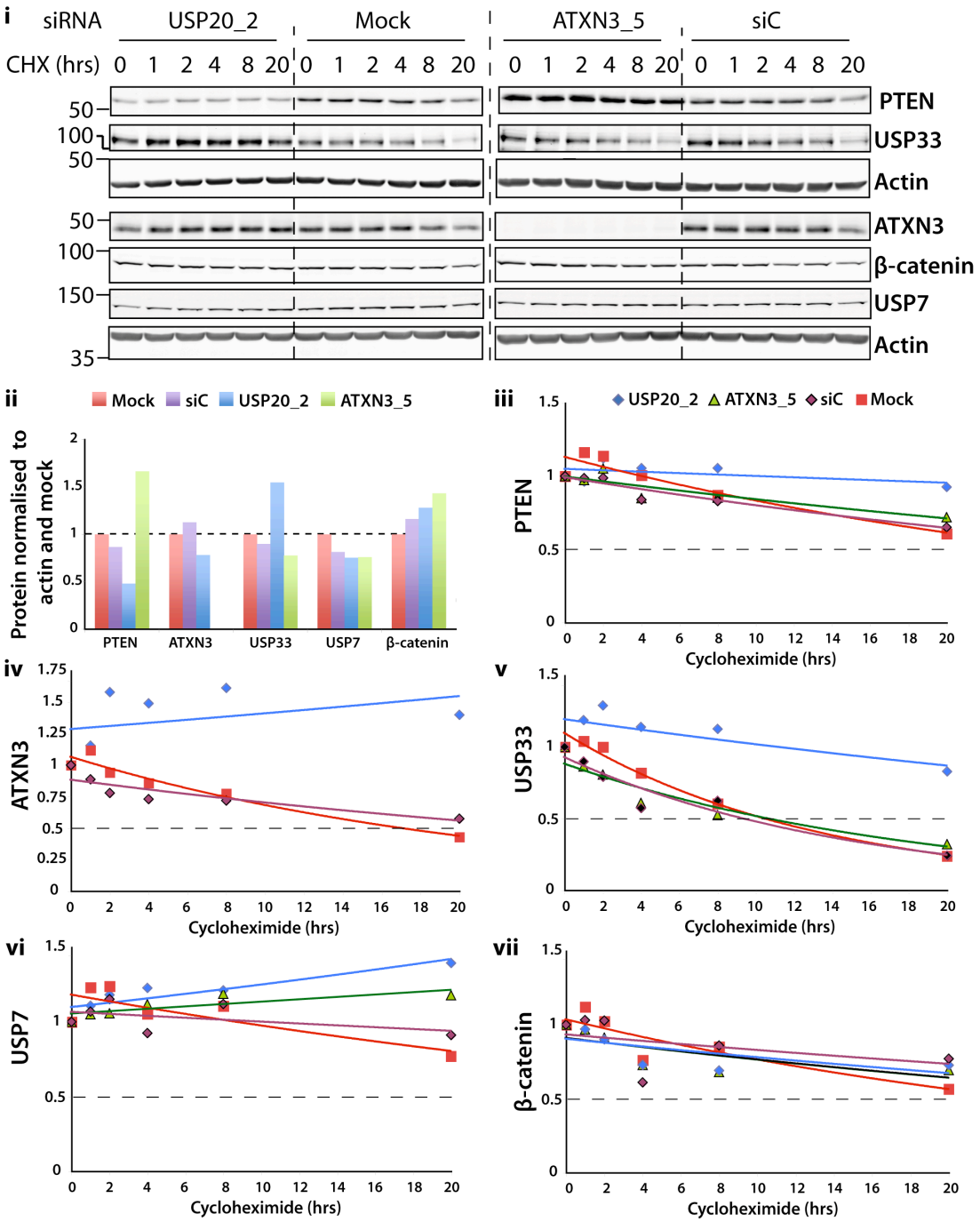

Fig 6.9. USP20 depletion stabilizes ATXN3 and USP33. A549 cells were transfected with the indicated siRNA oligonucleotides or mock transfected. Cells were incubated for a total of 72 hours, and prior to lysis were treated for the indicated duration with 100µg/ml cycloheximide (CHX). Cells were lysed with NP40 and equal volumes of lysate were immunoblotted as indicated. Imaging and quantification were performed on an infrared scanner and associated software (Odyssey, LiCor). **i**. Immunoblots. **ii**. Quantification prior to CHX addition. **iii-vii**. Each protein was quantified, normalized to actin and baseline level, and plotted as shown. USP20_2, ATXN3_5, siC (non-targeting siRNA) and Mock are represented in blue, green, purple and red respectively. The half-life is indicated by a dotted line. (n=1).

respectively decreased and increased the PTEN protein level prior to cycloheximide addition (fig 6.9i,ii). However PTEN was relatively stable, exhibiting a half-life in excess of 20 hours (fig 6.9iii). Previous studies have reported a wide range for PTEN's half-life, ranging from 10 to more than 72 hours in different cell lines [364, 459, 460].

ATXN3 depletion did not affect the rate of PTEN protein degradation (fig 6.9iii). Interestingly, while USP20 depletion had decreased PTEN protein level by approximately 60% at baseline, the degradation rate of the residual PTEN in the presence of cycloheximide was slowed (fig 6.9iii). This indicates that USP20 may have two effects on PTEN, potentially altering both its transcription and degradation.

I wondered whether USP20 may have broader effects on protein degradation. The effects of USP20 depletion on rates of degradation of ATXN3, USP33 and USP7 (fig 6.9iv,vi) were also assessed. In all three cases, USP20 depletion stabilized the protein and decreased the rate of degradation, although this was less apparent for USP7.

While this may represent a specific effect on a subset of deubiquitylases, it could alternatively reflect more general effects on protein degradation. I therefore assessed the effects of USP20 depletion on β-catenin degradation, as an example of an unrelated protein, which is degraded by the proteasome (fig 6.9vii). The rate of β-catenin degradation was not influenced by USP20 depletion. However I did not assay the effects of USP20 depletion on the degradation of a wider range of proteins, and it remains feasible that USP20 has a generic role in protein degradation.

6.6 Crosstalk between ATXN3, ATXN3L and USP20

No commercial antibodies were available for ATXN3L or JOSD1, and as discussed in section 6.2, depletion of USP20 was impossible to quantitatively assess using either of the available antibodies. I therefore employed

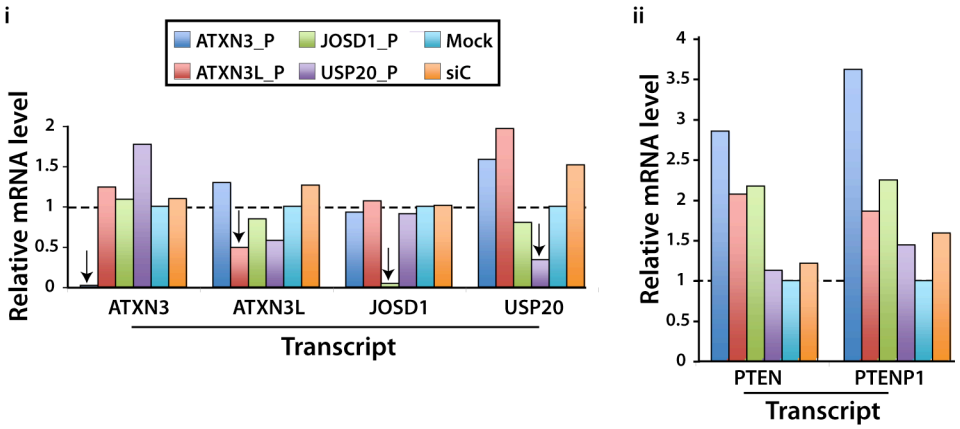

Fig 6.10 ATXN3, ATXN3L and JOSD1 transcriptionally regulate PTEN i.ii A549 cells were transfected with pooled siRNA oligonucleotides against the indicated targets and incubated for 72 hours prior to lysis, after which RNA was extracted and cDNA prepared by reverse transcription. QPCR was performed for ATXN3, ATXN3L, JOSD1, USP20, PTEN and PTENP1 using an IQ5 real time PCR detection system and SYBR green supermix (BioRad). Actin was employed as a reference gene and results were further normalized to the mock control. The arrowheads indicate direct effects of siRNA on their respective targets. (n=1).

quantitative RT-PCR (QPCR) to assess knockdown efficiency of these DUBs (fig 6.10i). Pooled siRNA oligonucleotides from the DUB library were used. A knockdown efficiency at the transcript level of 95% or greater was obtained for ATXN3 and JOSD1, while that for USP20 and ATXN3L was approximately 65% and 50% respectively. For ATXN3, this mirrors estimation of ATXN3 depletion by immunoblotting (fig 6.6). The relatively poor knockdown efficiency for USP20 however, did not appear to be reflected on immunoblotting (fig 6.1 and 6.2). This may be due to the presence of USP20 species that were not visualized due to lack of antibody specificity (section 6.2). In addition, the USP20 mRNA) knockdown efficiency was better when assessed after a 48-hour transfection (fig 6.4), and it is possible that at 72 hours the effects of the USP20 siRNA were beginning to decline.

ATXN3L knockdown efficiency at the transcript level was only approximately 50% (fig 6.10i). However I have not been able to assess this by immunoblotting, and have also not assessed either the differential effects of individual ATXN3L siRNA oligonucleotides or earlier experimental timepoints. Interestingly, the ATXN3L transcript was also much less abundant than that

for ATXN3, taking on average an additional eight cycles of amplification to cross the cycle threshold (Ct). This suggests that the ATXN3L transcript is approximately 250 fold less abundant than that of ATXN3.

Intriguingly, there were several indications of interplay between the four DUBs at the transcript level (fig 6.10i). USP20 depletion reduced ATXN3L transcripts to a similar degree to that which occurred following ATXN3L depletion. However, USP20 depletion had the opposite effect on ATXN3 transcripts, which it upregulated (fig 6.10i). On the other hand depletion of ATXN3L led to upregulation of the USP20 transcript (fig 6.10i). These findings could represent either feedback mechanisms. However, the experiment has only been performed once and these findings will firstly require confirmation in independent experiments.

6.7 ATXN3 regulates PTEN transcriptionally

As discussed in section 3.1, DUBs may have effects on protein level through multiple mechanisms. These include regulation of transcription, which was assessed here using QPCR. Depletion of ATXN3, ATXN3L or JOSD1 all increased PTEN mRNA transcript levels (fig 6.10ii). This was most marked for ATXN3 for which depletion resulted in an almost three fold increase in PTEN transcripts (6.10ii), while ATXN3L and JOSD1 depletion resulted in an approximately 2-fold increase in transcript levels. Depletion of USP20 using pooled oligonucleotide did not alter PTEN transcription (fig 6.10ii). However the earlier experiment described in figure 6.4 had shown a correlation between PTEN mRNA and protein levels. Further parallel experiments will be required to confirm this finding.

PTENP1 (PTEN pseudogene 1) is a pseudogene that has been shown to be involved in regulating PTEN level by acting as a decoy for miRNAs targeting PTEN [375]. I therefore also assessed transcript levels for PTENP1 (fig 6.10ii). This supported co-regulation of PTEN and PTENP1 transcription by ATXN3. While ATXN3L and JOSD1 depletion also upregulated the PTENP1

transcript level, this was to a more modest degree, and similar levels were seen with a non-targeting siRNA.

The data were most supportive for a role of ATXN3 at the PTEN and/or PTENP1 transcript level, and were in keeping with the experiment described in fig 6.9 in which ATXN3 depletion failed to alter PTEN protein degradation. This transcript level regulation of PTEN by ATXN3 was further supported by a correlation between PTEN protein and mRNA levels which were assessed in parallel (fig 6.11). The latter experiment utilized a 48-hour incubation to avoid cellular toxicity, which was observed with ATXN3 depletion at longer timepoints. Although induction of PTEN protein levels after 48 hours by ATXN3 depletion was less marked than by 72 hours, this clearly correlated with PTEN transcript levels (fig 6.11).

We next sought to determine if ATXN3 depletion leads to increased PTEN transcript levels through increasing transcription or by reducing transcript degradation. For this purpose, actinomycin D was used to inhibit *de novo* transcription, thus enabling determination of the half-life of relevant transcripts. mRNA half-lives were 1.9, 4.4 and >6 hours for PTENP1, PTEN and ATXN3 respectively (fig 6.12i). The relatively short half-life for PTENP1 transcript compared to that of PTEN is in keeping with its function as a decoy for miRNA directed at PTEN [375].

Depletion of ATXN3 led to an increase in the level but a decrease in the half-lives of both PTEN and PTENP1 transcripts. The half lifes of PTEN and PTENP1 were decreased from 4.1 to 1.7, and 1.7 to 0.7 hours respectively in ATXN3 depleted cells (fig 6.12ii).

Interestingly, degradation of PTEN mRNA was delayed and only began to occur after about half an hour, at which time PTENP1 levels had already decreased significantly; in the case of ATXN3 depleted cells by almost half. Between 30 and 90 min PTEN mRNA degradation was substantially accelerated in ATXN3 depleted cells while the rate of degradation at later time points was similar to that of the control (fig 6.12ii). The reduction in the

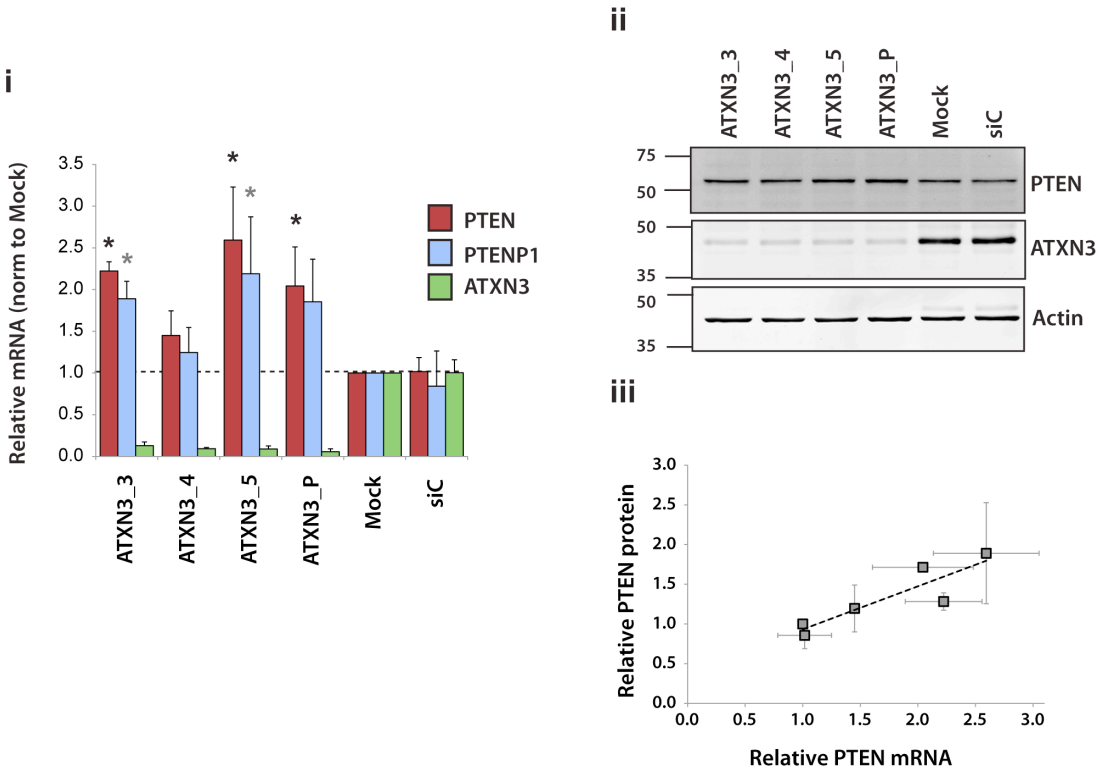

Fig 6.11. ATXN3 depletion regulates PTEN abundance by increasing the level of the PTEN and PTENP1 transcripts. i,ii. A549 cells were transfected with the indicated siRNA oligonucleotides for 48hrs prior to lysis. **i**. Total RNA was extracted and expression of ATXN3, PTEN and PTENP1 transcripts relative to actin were determined by QPCR. Mean values are shown normalised to mock transfected cells for three independent experiments, error bars show standard deviation. Student's t-test compares each siRNA with siC, *P<0.05, n=3. **ii**. In parallel, cells were lysed using NP40 and equal amounts of each lysate were immunoblotted. A representative blot is shown. PTEN protein levels were quantified relative to actin and normalised to the mock control (n=3). **iii.** A scatter plot correlating PTEN mRNA and protein expression for each ATXN3 siRNA. (error bars show standard deviation, R^2=0.797).

half-life of both PTEN and PTENP1 does not explain their increase in abundance following ATXN3 depletion, and most likely reflects a compensatory mechanism that is attempting to counteract increased expression. This experiment therefore indicates that ATXN3 depletion increases PTEN and/or PTENP1 transcription, rather than the degradation of these transcripts.

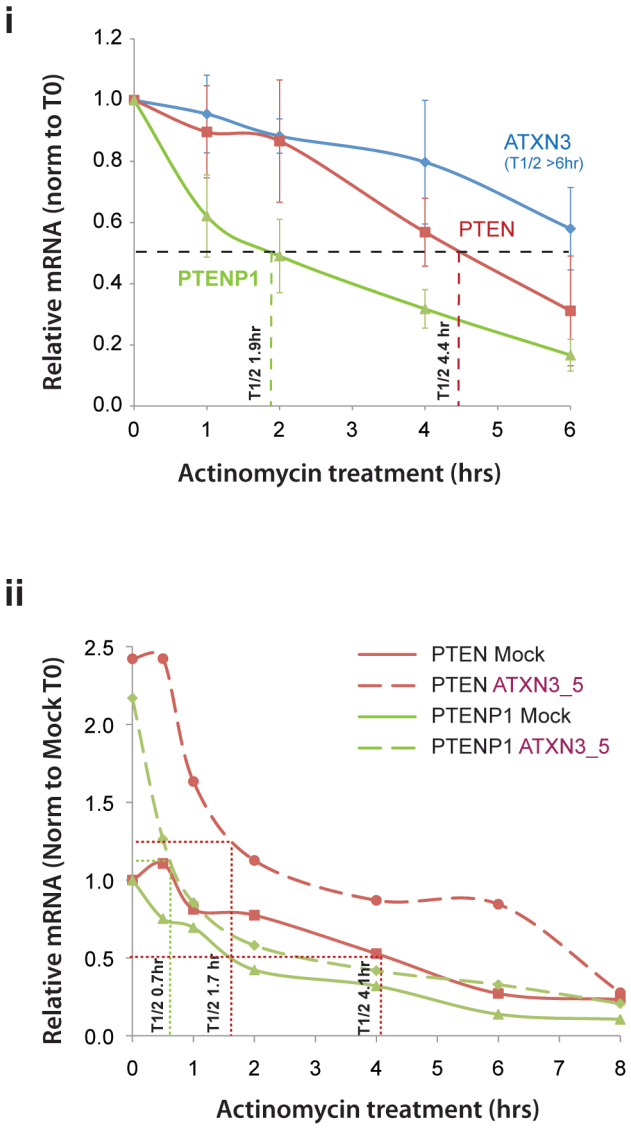

Fig 6.12. Depletion of ATXN3 does not enhance stability of the PTEN or PTENP1 transcripts. i. A549 cells were treated with actinomycin D for the indicated times prior to preparation of total RNA. Levels of the ATXN3, PTEN and PTENP1 transcripts were determined relative to that of actin by QPCR. Mean values, normalised to the expression level of each gene prior to addition of actinomycin D, are shown from three independent experiments. Error bars show standard deviation and the half-life is indicated by a dotted line. **ii.** A549 cells were transfected with a single siRNA targeting ATXN3 or with no oligonucleotide for a total of 48hrs; cells were treated with actinomycin D for the indicated times immediately prior to preparation of total RNA. The levels of ATXN3, PTEN and PTENP1 transcripts were determined relative to that of actin by QPCR. Mean values, normalised to the expression level of each gene in mock-transfected cells prior to addition of actinomycin D, are shown from two independent experiments. The half-life of each transcript following ATXN3 depletion is indicated by a fine dotted line. The half-life of PTEN in mock-transfected cells is similarly shown. PTENP1s half-life in mock-transfected cells is obscured by that of PTEN in ATXN3 depleted cells, and is similarly 1.7hrs.

6.8 ATXN3 depletion and HDAC inhibition have additive effects on PTEN transcript levels

ATXN3 is known to be involved in transcriptional repression through the modulation of histone acetylation status [378, 461], which suggested a possible mechanism by which ATXN3 could regulate PTEN. We therefore assessed the effects of the histone deacetylase inhibitor vorinostat, on PTEN, PTENP1 and ATXN3 transcript levels (fig 6.13). While PTEN transcript levels were increased by vorinostat, this was to a much lesser extent than that seen for the positive control SCG3 (fig 6.13i) which is known to be highly repressed in A549 cells [373], through an HDAC dependent mechanism (J. Coulson, unpublished data). SCG3 transcript levels increased linearly with increasing vorinostat concentrations (fig 6.13i). In contrast, maximum PTEN induction (3-fold) occurred in cells treated with 2μM vorinostat, while at higher drug concentrations PTEN levels declined to a plateau of approximately 2-fold induction. PTENP1 also exhibited an increase in transcript levels in cells treated with 2μM vorinostat, however this was less marked, representing an increase of only 50%, and at higher concentrations of vorinostat, PTENP1 transcript levels were similar to those in untreated cells (fig 6.13i). The ATXN3 transcript level was unaffected by vorinostat.

We next investigated the effect of combining ATXN3 depletion and vorinostat treatment (fig 6.13ii). In this experiment, depletion of either ATXN3 or vorinostat treatment resulted in an approximately 2.5-fold increase in PTEN transcript level, while combination of the two resulted in a 5-fold increase in transcript level. This represents an additive effect of the two interventions and suggests that ATXN3 depletion alters PTEN transcription independently of its previously reported role in modification of histone acetylation status.

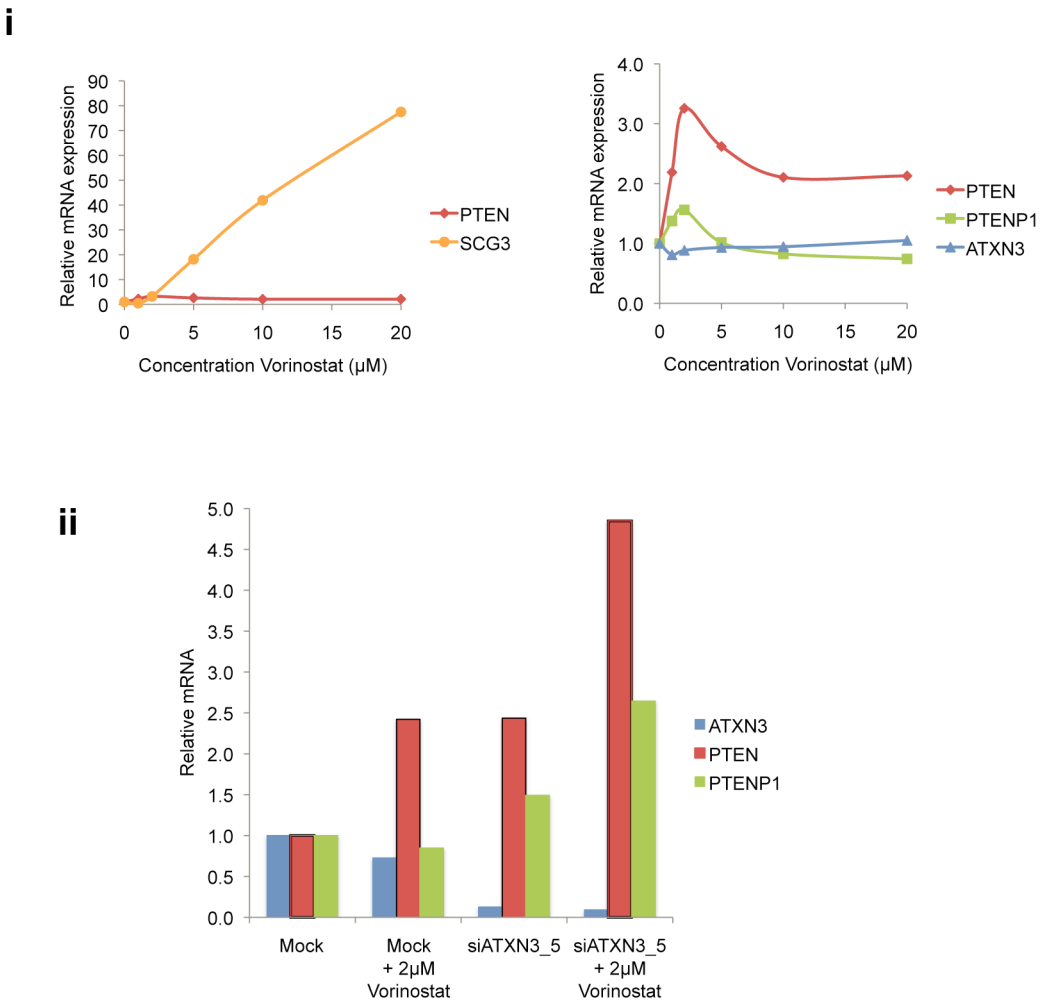

Fig 6.13. ATXN3 depletion and HDAC inhibition additively increase PTEN transcript levels. i. A549 cells were treated with the indicated concentrations of vorinostat for 16 hours prior to preparation of total RNA. Levels of the ATXN3, PTEN and PTENP1 transcripts were determined relative to that of actin by QPCR. **ii.** A549 cells were transfected with a single siRNA targeting ATXN3 or with no oligonucleotide for a total of 48hrs. For the last 16 hours, cells were treated with 2μM vorinostat. Total RNA was extracted and the levels of ATXN3, PTEN and PTENP1 transcripts were determined relative to that of actin by QPCR. (n=1)

The effects on PTENP1 transcripts were less clear, as vorinostat treatment did not affect PTENP1, while ATXN3 depletion and combined treatment resulted in 1.5-fold and 2.5-fold induction respectively. However, this experiment has only been performed once, and confirmation of these findings in an independent experiment will be required.

6.9 Discussion

In this chapter I have presented further confirmation that USP20, ATXN3, ATXN3L and JOSD1 are involved in the regulation of PTEN, and described preliminary investigations into the mechanisms by which this occurs.

USP20 has previously been shown to be involved in multiple cellular processes, including regulation of type II deiodinase [89, 90], β_2 adrenergic receptor recycling [91], VHL stability [92], and downregulation of NFκB signaling through deubiquitylation of TRAF6 and TAX [93]. Here I provide evidence suggesting USP20 is also involved in regulation of PTEN. The effects of USP20 depletion on PTEN protein level were however oligonucleotide dependent, with two siRNAs directed at the 3'-end of the transcript leading to a reduction in PTEN level, and the other two (which map internally on the transcript) leading if anything to a slight increase in PTEN level.

USP33 is a paralogue of USP20, and is upregulated on depletion of USP20 [390]. Intriguingly, the effects on PTEN inversely correlated with the extent of USP33 upregulation in response to USP20 depletion, though dual knockdown of USP33 and USP20 indicated that the upregulation of USP33 is not required for the effects of USP20 depletion on PTEN. This may indicate instead that upregulation of USP33 acts as a marker for the extent of depletion of USP20, which was otherwise difficult to assess. Quantitative assessment of knockdown efficiency at the protein level was unfortunately hampered by the absence of a specific antibody, and it is possible that subtle differences in residual USP20 may explain the differential effects on PTEN. This was not however supported by QPCR data, which showed similar knockdown efficiency between the four oligonucleotides.

Interestingly, a lower molecular weight protein was also detected with the USP20 antibody, and levels of this directly correlated with effects on PTEN. This may represent a splice variant or truncated version of either USP20 or USP33, however further investigation will be required establish its identity.

Following treatment with cycloheximide, PTEN appeared to be stabilized by USP20 depletion. This is contrary to the effects of USP20 depletion on steady-state PTEN protein levels, and may indicate two distinct effects of USP20 on PTEN. Alternatively this may suggest a separate role for USP20 in protein degradation in general. Indeed, USP20 depletion also stabilized ATXN3, USP33 and USP7 protein levels in the absence of ongoing translation. Although USP20 depletion failed to impact on stability of beta-catenin, a more general role for USP20 in protein degradation cannot be ruled out. Interestingly, in a proteomic screen for DUB interactors, Sowa et al identified several components of the 19S proteasome as USP20 interactors [415]. This suggests that USP20 may be involved in regulation of the proteasome and thus protein degradation. However this needs further investigation, particularly as the cycloheximide experiment was carried out with a single oligonucleotide that reduced PTEN levels and has not been performed using one of the other oligonucleotides that, if anything, increased the protein level of PTEN.

ATXN3 depletion upregulated PTEN protein level but did not affect its protein stability. This is consistent with the QPCR findings, which suggest ATXN3 influences PTEN transcription. Interestingly, ATXN3 depletion upregulates transcripts of both PTEN and its pseudogene PTENP1. Upregulation of the latter could augment effects on PTEN by acting as a decoy for miRNA against PTEN [375], thus protecting PTEN mRNA against degradation. However, degradation of PTEN transcripts was actually increased following ATXN3 depletion, which likely reflects a feedback mechanism to increased PTEN levels.

ATXN3 was first identified due to its role in Machado-Joseph disease. Subsequently it has been shown to have several functions, including regulation of retrotranslocation of substrate in endoplasmic reticulum associated protein degradation (ERAD) [407]. Recently, increased longevity was described in *C. elegans* worms deficient in ATXN3 and p97 [408], and this appears to be mediated through IGF signalling [408]. Another potential

link between ATXN3 and PtdIns3-K signalling is suggested by a proteomic study of the EGF induced ubiquitin network, in which ATXN3 was identified [409].

ATXN3 has previously been shown to modulate histone acetylation and to repress gene expression [378, 461]. In addition, PTEN transcript levels may be upregulated by histone deacetylase (HDAC) inhibition [347-349]. Upregulation of PTEN transcript levels by the HDAC inhibitor vorinostat was also seen in our study. Combining HDAC inhibition and ATXN3 depletion resulted in additive increases in PTEN transcript level. This suggests that ATXN3's effects on PTEN are not dependent on histone modulation, and that depletion or inactivation of ATXN3 may prove to be useful therapeutic intervention leading to upregulation of PTEN expression.

Depletion of the closely related ATXN3L similarly increased the PTEN protein level. This appears to be at least partly due to effects on PTEN transcription. Post-translational effects on protein degradation have not been examined, and it remains feasible that effects on PTEN protein level may be mediated through multiple mechanisms. Little is known of the cellular role for ATXN3L. However, in a study in A549 cells, ATXN3L depletion led to a decrease in HGF-dependent scattering as well as a decrease in wound healing [385], indicating a potential role in cell signaling. Crystallographic and enzymatic studies have shown ATXN3L is a more efficient enzyme than ATXN3 [457]. This is of interest as QPCR indicates very low ATXN3L expression as assessed at the mRNA level, which may result in a low cellular abundance of ATXN3L protein.

JOSD1, the third DUB which upregulated PTEN is also a member of the MJD family of deubiquitylases. While QPCR indicates some transcriptional regulation, investigation of effects on protein degradation have not yet been undertaken. JOSD1 was also identified in the study of the EGF induced ubiquitin network which included ATXN3 [409].

Interestingly JOSD3, which is a more distant relative of the Josephins (fig 6.5) and which was not included in the screen as it is an inactive DUB, is a bona fide transcriptional regulator [462]. This provides support to the findings of my study, which identified three Josephins that appear to transcriptionally regulate PTEN.

While the data presented in this chapter require further elaboration, they support a key role for deubiquitylases in the regulation of PTEN. In addition to providing insights into the regulation of a core tumour suppressor, these data have clear therapeutic implications. As discussed in section 1.5.3, PTEN is frequently silenced in cancer through non-genetic mechanisms. Its reactivation in these tumours would potentially lead to a reduction in activation of the PtdIns3-K signaling pathway, leading in turn to a reduction in cancer cell survival. Reactivation of PTEN could potentially be achieved through several mechanisms (section 1.5.3). However, research into this field is at a relatively early stage, and the identification here of three DUBs whose depletion leads to upregulation of PTEN, may provide new targets for pharmaceutical development.

Chapter 7

Final Discussion

The deubiquitylases are increasingly recognised as vital regulators of multiple cellular processes germane to cancer [9, 111], and are moreover attractive drug targets (section 1.4.7). Previous studies have shown that ubiquitylation plays a vital role in regulating PtdIns3-K signaling (section 1.5.4), which is a crucial survival pathway that is frequently dysregulated in malignancy (1.5.3). Several DUBs that regulate components of the PtdIns3-K pathway have been identified (1.5.4), however this had not been previously approached in systematic manner. In this thesis, I have described a series of siRNA screens, which were employed to identify previously undescribed DUB regulators of the PtdIns3-K pathway. Here I will summarise the main findings of this work and discuss their implications, as well as potential future work.

7.1 The PtdIns3-K pathway is extensively regulated by DUBs

The project was designed to approach the role of DUBs in this pathway systematically, and I therefore utilised two complementary screening strategies to maximise the chances of success. This involved assessing the effects of DUB depletion on both the protein level of PtdIns3-K components (chapter 3), and downstream activity of the pathway (chapter 4). The methodology employed a DUB siRNA library that had previously been designed by the host laboratory in collaboration with Qiagen. The library is comprehensive, consisting of siRNA oligonucleotides against 92 DUBs and covering all but one of the currently known, transcribed, DUBs (section 2.1).

The screens performed in this work led to the identification of candidate DUBs that regulate the protein level of nine PtdIns3-K components (p110α, p110β, p110γ, p85α, p170, PTEN, PDK1, Akt and mTOR), as well as DUBs that modulate the translocation of GFP-tagged FOXO3 in response to

PtdIns3-K inhibition. The planned assessment of the effects of DUB depletion on endogenous FOXO1, FOXO3 and FOXO4 transcription factors was not feasible due to low-level expression in A549 cells. However, the second screening approach, which utilised cells stably expressing an EGFP tagged form of FOXO3, allowed the identification of several DUBs that altered protein levels of this overexpressed form of FOXO3.

As discussed in sections 3.2 and 3.10, several measures were undertaken to minimise the false positive and negative rates in these screens. The main method for eliminating false positives involved deconvolution of the oligonucleotide pool, which was employed as a first validation step (section 3.2). Initial refining of candidates using deconvolution was performed for the translocation screen and two of the immunoblotting screens (PTEN and PDK1). More than half of all candidates subject to deconvolution were validated according to the criteria described (sections 3.2 and 4.3.2). The remainder of the immunoblotting screens were not subject to deconvolution due to time constraints.

Surprisingly, the screens failed in the main to identify DUBs previously known to be involved in regulating the PtdIns3-K pathway (1.5.4). A partial exception is USP7, depletion of which increased PTEN and FOXO3-EGFP protein levels (sections 2.4 and 4.4.2). Although in previous studies USP7 regulated PTEN and FOXO localisation rather than stability [203, 205] it is feasible that USP7 depletion may also influence their stability (discussed in sections 3.10 and 4.5).

Several factors may explain the lack of overlap between the results of my screens and published data. Firstly, the findings may be context specific. For example USP7 was shown to regulate FOXO4 (and FOXO3) monoubiquitylation under conditions of oxidative stress [205] rather than in response to PtdIns3-K modulation as was investigated here. Similarly, the role of UCHL1 in the regulation of Akt was described in the context of mechanical stress induced vascular injury ([353], section 3.7). Secondly, DUBs may have differential effects in different cell lines. The work

establishing a role for USP7 regulation of PTEN monoubiquitylation for example, was predominantly performed in a promyelocytic cell line [203]. Additionally, DUBs may have redundant effects, such that depletion of a single DUB is compensated for by other DUBs. For example, while overexpression of USP4 was recently shown to reduce monoubiquitylation of PDK1, its depletion did not impact on PDK1 ubiquitylation, suggesting that other DUBs may also be able to deubiquitylate PDK1 [358]. Similarly both USP1 and USP46 have been implicated in altering the stability of the Akt phosphatase PHLPP1 [356, 357] and it is feasible that depletion of either would be insufficient to alter signalling.

However the lack of overlap may also partly represent experimental false negatives, which are an inherent risk in siRNA screens (section 3.10). Several factors influence the false negative rate; experimental noise and the quality of the RNAi reagents being of particular importance [387, 463]. The former was clearly a concern in this project, as demonstrated by the degree of variation between replicates. However, the selection of a relatively large proportion (approximately 10%) of the DUB library from each screen for further investigation is likely to have minimised the chances of missing a candidate DUB whose depletion significantly altered the parameter under investigation. The second point, relating to the quality of RNAi reagents, may be partly assessed by knockdown efficiency. While this was greater than 70% for the four DUBs that were assessed in the DUB lysate library (section 3.3), USP20 and ATXN3L knockdown efficiency, as assessed by QPCR, was respectively only 60% and 50% (section 6.x). In addition, the degree of depletion required to produce a loss of function phenotype is likely to vary significantly between different proteins.

There was also limited overlap between DUBs identified in the immunoblotting and translocation screens. This likely results from similar factors to those described above. In addition, the translocation screen assayed the effects of DUB depletion on downstream PtdIns3-K signalling, and therefore reflects a synthesis of effects for all upstream components. This would be of relevance if a DUB has effects on more than one

component, which could antagonise each other. Notably the two screens were performed in different cell types (A549 and U2OS respectively). A549 cells in particular contain both homozygous K-Ras mutations and are LKB1 null [464], which would be expected to increase signalling through the PtdIns3-K axis. Interestingly, despite these mutations, A549 cells show minimal activation of K-Ras effectors (Akt and extracellular signal regulated kinase 1/2 [ERK1/2]) under non-stimulated conditions, and respond to EGF stimulation [465]. However, it is likely that PtdIns3-K signalling would be subtly different from that in U2OS cells, which do not contain these mutations.

Despite the above caveats, this study has significantly expanded the number of DUBs implicated in the regulation of the PtdIns3-K pathway. Several of these have been subject to initial validation, and examples of particular scientific and therapeutic potential are discussed further in sections 7.2-7.4.

7.2 PTEN is transcriptionally regulated by three members of the Josephin family of deubiquitylases

The immunoblot screen for regulators of the tumour suppressor PTEN identified four DUBs whose depletion upregulated its protein levels (section 3.4). USP7, which has previously been shown to alter monoubiquitylation of PTEN [203], was not followed up further. The remaining three (ATXN3, ATXN3L and JOSD1) were all members of the Josephin family of DUBs, which contains only two other members (fig 6.3). In view of the similarity between these proteins, I used QPCR to show that the siRNA oligonucleotides against ATXN3, ATXN3L and JOSD1 were not cross-reactive. In the case of ATXN3 for which I had an antibody, I was additionally able to show that ATXN3L depletion did not affect ATXN3 protein levels.

Depletion of all three DUBs increased the transcript levels of PTEN and its pseudogene PTENP1. ATXN3 depletion was additionally shown to have no effect on PTEN protein or transcript stability, supporting a role in the transcriptional regulation of PTEN. Previous studies have shown that ATXN3

interacts with modifiers of histone acetylation [378, 461]. However, in this study, depletion of ATXN3 and the use of histone deacetylase inhibitors resulted in an additive increase in PTEN protein levels suggesting that the role of ATXN3 in PTEN regulation is independent of histone modification.

PTEN is a key negative regulator of PtdIns3-K signaling and one of the most commonly mutated tumour suppressors in cancer (section 1.5). Studies in human cancers and model systems have shown that PTEN is a haploinsufficient tumour suppressor, with loss of a single PTEN allele being sufficient to promote cancer development ([319, 466], section 1.5.3). This is supported by work in mouse models, which showed that reducing PTEN expression by only 25% is sufficient to increase cancer risk [467].

PTEN is often silenced in tumours through non-genetic mechanisms, both at transcriptional and post-transcriptional levels ([197], section 1.5.3). In these tumours, development of drugs that lead to reactivation of PTEN may prove a valuable therapeutic strategy [197]. This could potentially be achieved in several different ways, for example inhibiting E3 ligases (XIAP, NEDD4.1, WWP2) that promote PTEN degradation, increasing the enzymatic activity of PTEN, or increasing PTEN transcription. However all of these strategies are at a relatively early stage, and the identification here of three DUBs whose depletion leads to an increase in PTEN level is therefore of potential clinical significance.

Several lines of investigation will be required to determine if one or other of these DUBs are indeed potential drug targets. Identification of the mechanism(s) by which these DUBs regulate PTEN level is not only of scientific interest, but would also enable a better understanding of the likely wider effects of their loss of function. In addition it would be important to determine if the mechanism is dependent on the catalytic activity of the DUBs as this may potentially be targeted through the use of small molecule inhibitors. Assessing the functional effects of their depletion on PtdIns3-K downstream signaling and viability/proliferation of different cell types would

also be vital in determining if the upregulation of PTEN is likely to translate into clinical effect.

7.3 Promoting FOXO3 nuclear translocation and/or stability

Similarly to the screen for regulators of PTEN, the translocation screen described in chapter 4 identified DUBs whose depletion could potentially be used to increase tumour suppressor function. The FOXO family of transcription factors are tumour suppressors that are often functionally silenced in cancer [468, 469]. This may occur through several different mechanism63s, including deletion [470], repression of expression by miRNAs [471, 472], proteasomal degradation [473] and Akt-dependent nuclear exclusion [297]. In this study, depletion of USP45 enhanced FOXO3-EGFP nuclear translocation in response to PtdIns3-K inhibition. Several DUBs were also identified whose depletion increased FOXO3-EGFP protein levels. These included USPL1, which was validated by deconvolution using both imaging and immunoblotting. Depletion of either USP45 or USPL1 may therefore potentially lead to increased FOXO3 function, the former through increased nuclear localisation and the latter through an increase in abundance. However, as discussed in section 4.5, several steps are required to validate these findings, which would firstly involve demonstrating that these DUBs also regulate endogenous FOXO.

7.4 DUBs, PI-103 and synthetic lethality

Intriguingly, the translocation screen identified three DUBs (USP8, OTUD4 and DUB4) whose depletion was synthetically lethal with PI-103 treatment (chapter 6). Validation was confined to USP8, which showed the most convincing effect, and for which reagents were available. The effects of USP8 depletion on sensitisation to PI-103 induced cell death were confirmed on deconvolution of the siRNA pool, and were also replicated in parental U2OS cells and with an Akt inhibitor. In addition, similar results were obtained using immunoblotting for cleaved PARP p85 as a readout for cell death. Furthermore, two USP8 inhibitors similarly sensitised cells to PI-103

induced cell death. However, all these findings were observed when cells were cultured in HBSS, and the differential in cell death was less marked in DMEM. The reason for this difference has not been deciphered but may relate to either the absence of amino acids or the lower pH in the HBSS (section 5.8). If the latter is the case, the findings here may remain clinically relevant, as tumours are frequently acidotic [449]. In addition, the interaction between USP8 depletion and PtdIns3-K inhibition may also provide an opportunity to identify novel functions for USP8.

7.5 Concluding remarks

The work described in this thesis led to the identification of several, previously undescribed, DUB modulators of the PtdIns3-K pathway. In this chapter, I have focused on candidates for which initial validation has been performed, and which, subject to further mechanistic and functional studies, may increase the options available for targeting this vital pathway in malignancy. However, in addition to these, several other screens identified interesting lead candidates for future investigation. These include the screen for DUB regulators of PDK1 stability, which identified a number of candidates that have been partly validated, and screens for DUB regulators of p110 isoforms.

Bibliography

1 Hanahan, D. and Weinberg, R. A. (2000) The hallmarks of cancer. Cell. **100**, 57-70

2 Hanahan, D. and Weinberg, R. A. (2011) Hallmarks of cancer: the next generation. Cell. **144**, 646-674

3 Zhang, J., Yang, P. L. and Gray, N. S. (2009) Targeting cancer with small molecule kinase inhibitors. Nat Rev Cancer. **9**, 28-39

4 Fabbro, D., Cowan-Jacob, S. W., Mobitz, H. and Martiny-Baron, G. (2012) Targeting cancer with small-molecular-weight kinase inhibitors. Methods Mol Biol. **795**, 1-34

5 Hopkins, A. L. and Groom, C. R. (2002) The druggable genome. Nat Rev Drug Discov. **1**, 727-730

6 Nazarian, R., Shi, H., Wang, Q., Kong, X., Koya, R. C., Lee, H., Chen, Z., Lee, M. K., Attar, N., Sazegar, H., Chodon, T., Nelson, S. F., McArthur, G., Sosman, J. A., Ribas, A. and Lo, R. S. (2010) Melanomas acquire resistance to B-RAF(V600E) inhibition by RTK or N-RAS upregulation. Nature. **468**, 973-977

7 Suda, K., Mizuuchi, H., Maehara, Y. and Mitsudomi, T. (2012) Acquired resistance mechanisms to tyrosine kinase inhibitors in lung cancer with activating epidermal growth factor receptor mutation-diversity, ductility, and destiny. Cancer Metastasis Rev

8 Komander, D. (2009) The emerging complexity of protein ubiquitination. Biochem Soc Trans. **37**, 937-953

9 Sacco, J. J., Coulson, J. M., Clague, M. J. and Urbé, S. (2010) Emerging roles of deubiquitinases in cancer-associated pathways. IUBMB Life. **62**, 140-157

10 Goldstein, G., Scheid, M., Hammerling, U., Schlesinger, D. H., Niall, H. D. and Boyse, E. A. (1975) Isolation of a polypeptide that has lymphocyte-differentiating properties and is probably represented universally in living cells. Proc Natl Acad Sci U S A. **72**, 11-15

11 K.D., W. (2005) The discovery of ubiquitin-dependent proteolysis. Proceedings of the National Academy of Sciences of the United States of America. **102**, 15280-15282

12 Ciechanover, A., Heller, H., Elias, S., Haas, A. L. and Hershko, A. (1980) ATP-dependent conjugation of reticulocyte proteins with the polypeptide required for protein degradation. Proc Natl Acad Sci U S A. **77**, 1365-1368

13 Hershko, A., Ciechanover, A., Heller, H., Haas, A. L. and Rose, I. A. (1980) Proposed role of ATP in protein breakdown: conjugation of protein with multiple chains of the polypeptide of ATP-dependent proteolysis. Proc Natl Acad Sci U S A. **77**, 1783-1786

14 Wiborg, O., Pedersen, M. S., Wind, A., Berglund, L. E., Marcker, K. A. and Vuust, J. (1985) The human ubiquitin multigene family: some genes contain multiple directly repeated ubiquitin coding sequences. EMBO J. **4**, 755-759

15 Baker, R. T. and Board, P. G. (1991) The human ubiquitin-52 amino acid fusion protein gene shares several structural features with mammalian ribosomal protein genes. Nucleic Acids Res. **19**, 1035-1040

16 Vijay-Kumar, S., Bugg, C. E. and Cook, W. J. (1987) Structure of ubiquitin refined at 1.8 A resolution. J Mol Biol. **194**, 531-544

17 Ramage, R., Green, J., Muir, T. W., Ogunjobi, O. M., Love, S. and Shaw, K. (1994) Synthetic, structural and biological studies of the ubiquitin system: the total chemical synthesis of ubiquitin. Biochem J. **299 (Pt 1)**, 151-158
18 Hirano, T., Serve, O., Yagi-Utsumi, M., Takemoto, E., Hiromoto, T., Satoh, T., Mizushima, T. and Kato, K. (2011) Conformational dynamics of wild-type Lys-48-linked diubiquitin in solution. J Biol Chem. **286**, 37496-37502
19 Komander, D., Reyes-Turcu, F., Licchesi, J. D., Odenwaelder, P., Wilkinson, K. D. and Barford, D. (2009) Molecular discrimination of structurally equivalent Lys 63-linked and linear polyubiquitin chains. EMBO Rep. **10**, 466-473
20 Kim, H. T., Kim, K. P., Lledias, F., Kisselev, A. F., Scaglione, K. M., Skowyra, D., Gygi, S. P. and Goldberg, A. L. (2007) Certain pairs of ubiquitin-conjugating enzymes (E2s) and ubiquitin-protein ligases (E3s) synthesize nondegradable forked ubiquitin chains containing all possible isopeptide linkages. J Biol Chem. **282**, 17375-17386
21 Ikeda, F. and Dikic, I. (2008) Atypical ubiquitin chains: new molecular signals. 'Protein Modifications: Beyond the Usual Suspects' review series. EMBO Rep. **9**, 536-542
22 Kulathu, Y. and Komander, D. (2012) Atypical ubiquitylation - the unexplored world of polyubiquitin beyond Lys48 and Lys63 linkages. Nat Rev Mol Cell Biol. **13**, 508-523
23 Cook, W. J., Jeffrey, L. C., Carson, M., Chen, Z. and Pickart, C. M. (1992) Structure of a diubiquitin conjugate and a model for interaction with ubiquitin conjugating enzyme (E2). J Biol Chem. **267**, 16467-16471
24 Datta, A. B., Hura, G. L. and Wolberger, C. (2009) The structure and conformation of Lys63-linked tetraubiquitin. J Mol Biol. **392**, 1117-1124
25 Virdee, S., Ye, Y., Nguyen, D. P., Komander, D. and Chin, J. W. (2010) Engineered diubiquitin synthesis reveals Lys29-isopeptide specificity of an OTU deubiquitinase. Nat Chem Biol. **6**, 750-757
26 Bremm, A., Freund, S. M. and Komander, D. (2010) Lys11-linked ubiquitin chains adopt compact conformations and are preferentially hydrolyzed by the deubiquitinase Cezanne. Nat Struct Mol Biol. **17**, 939-947
27 Chau, V., Tobias, J. W., Bachmair, A., Marriott, D., Ecker, D. J., Gonda, D. K. and Varshavsky, A. (1989) A multiubiquitin chain is confined to specific lysine in a targeted short-lived protein. Science. **243**, 1576-1583
28 Spence, J., Sadis, S., Haas, A. L. and Finley, D. (1995) A ubiquitin mutant with specific defects in DNA repair and multiubiquitination. Mol Cell Biol. **15**, 1265-1273
29 Xu, P., Duong, D. M., Seyfried, N. T., Cheng, D., Xie, Y., Robert, J., Rush, J., Hochstrasser, M., Finley, D. and Peng, J. (2009) Quantitative proteomics reveals the function of unconventional ubiquitin chains in proteasomal degradation. Cell. **137**, 133-145
30 Kim, W., Bennett, E. J., Huttlin, E. L., Guo, A., Li, J., Possemato, A., Sowa, M. E., Rad, R., Rush, J., Comb, M. J., Harper, J. W. and Gygi, S. P. (2011) Systematic and quantitative assessment of the ubiquitin-modified proteome. Mol Cell. **44**, 325-340
31 Wagner, S. A., Beli, P., Weinert, B. T., Nielsen, M. L., Cox, J., Mann, M. and Choudhary, C. (2011) A proteome-wide, quantitative survey of in vivo ubiquitylation sites reveals widespread regulatory roles. In Mol Cell Proteomics. p. M111 013284, United States

32 Dikic, I., Wakatsuki, S. and Walters, K. J. (2009) Ubiquitin-binding domains - from structures to functions. Nat Rev Mol Cell Biol. **10**, 659-671
33 Young, P., Deveraux, Q., Beal, R. E., Pickart, C. M. and Rechsteiner, M. (1998) Characterization of two polyubiquitin binding sites in the 26 S protease subunit 5a. J Biol Chem. **273**, 5461-5467
34 Sloper-Mould, K. E., Jemc, J. C., Pickart, C. M. and Hicke, L. (2001) Distinct functional surface regions on ubiquitin. J Biol Chem. **276**, 30483-30489
35 Winget, J. M. and Mayor, T. (2010) The diversity of ubiquitin recognition: hot spots and varied specificity. Mol Cell. **38**, 627-635
36 Swanson, K. A., Kang, R. S., Stamenova, S. D., Hicke, L. and Radhakrishnan, I. (2003) Solution structure of Vps27 UIM-ubiquitin complex important for endosomal sorting and receptor downregulation. Embo J. **22**, 4597-4606
37 Wang, Q., Young, P. and Walters, K. J. (2005) Structure of S5a bound to monoubiquitin provides a model for polyubiquitin recognition. J Mol Biol. **348**, 727-739
38 Fisher, R. D., Wang, B., Alam, S. L., Higginson, D. S., Robinson, H., Sundquist, W. I. and Hill, C. P. (2003) Structure and Ubiquitin Binding of the Ubiquitin-interacting Motif. J Biol Chem. **278**, 28976-28984
39 Alam, S. L., Sun, J., Payne, M., Welch, B. D., Blake, B. K., Davis, D. R., Meyer, H. H., Emr, S. D. and Sundquist, W. I. (2004) Ubiquitin interactions of NZF zinc fingers. Embo J. **23**, 1411-1421
40 Kanayama, A., Seth, R. B., Sun, L., Ea, C. K., Hong, M., Shaito, A., Chiu, Y. H., Deng, L. and Chen, Z. J. (2004) TAB2 and TAB3 activate the NF-kappaB pathway through binding to polyubiquitin chains. Mol Cell. **15**, 535-548
41 Meyer, H. H., Wang, Y. and Warren, G. (2002) Direct binding of ubiquitin conjugates by the mammalian p97 adaptor complexes, p47 and Ufd1-Npl4. EMBO J. **21**, 5645-5652
42 Schreiner, P., Chen, X., Husnjak, K., Randles, L., Zhang, N., Elsasser, S., Finley, D., Dikic, I., Walters, K. J. and Groll, M. (2008) Ubiquitin docking at the proteasome through a novel pleckstrin-homology domain interaction. Nature. **453**, 548-552
43 Husnjak, K., Elsasser, S., Zhang, N., Chen, X., Randles, L., Shi, Y., Hofmann, K., Walters, K. J., Finley, D. and Dikic, I. (2008) Proteasome subunit Rpn13 is a novel ubiquitin receptor. Nature. **453**, 481-488
44 Brzovic, P. S., Lissounov, A., Christensen, D. E., Hoyt, D. W. and Klevit, R. E. (2006) A UbcH5/ubiquitin noncovalent complex is required for processive BRCA1-directed ubiquitination. Mol Cell. **21**, 873-880
45 Bellare, P., Small, E. C., Huang, X., Wohlschlegel, J. A., Staley, J. P. and Sontheimer, E. J. (2008) A role for ubiquitin in the spliceosome assembly pathway. Nat Struct Mol Biol. **15**, 444-451
46 Clague, M. J. and Urbe, S. (2010) Ubiquitin: same molecule, different degradation pathways. Cell. **143**, 682-685
47 Thrower, J. S., Hoffman, L., Rechsteiner, M. and Pickart, C. M. (2000) Recognition of the polyubiquitin proteolytic signal. EMBO J. **19**, 94-102
48 Clague, M. J., Liu, H. and Urbe, S. (2012) Governance of endocytic trafficking and signaling by reversible ubiquitylation. Dev Cell. **23**, 457-467
49 Duncan, L. M., Piper, S., Dodd, R. B., Saville, M. K., Sanderson, C. M., Luzio, J. P. and Lehner, P. J. (2006) Lysine-63-linked ubiquitination is required for endolysosomal degradation of class I molecules. Embo J. **25**, 1635-1645

50 Geetha, T., Jiang, J. and Wooten, M. W. (2005) Lysine 63 polyubiquitination of the nerve growth factor receptor TrkA directs internalization and signaling. Mol Cell. **20**, 301-312
51 Lauwers, E., Jacob, C. and Andre, B. (2009) K63-linked ubiquitin chains as a specific signal for protein sorting into the multivesicular body pathway. J Cell Biol. **185**, 493-502
52 Ravikumar, B., Sarkar, S., Davies, J. E., Futter, M., Garcia-Arencibia, M., Green-Thompson, Z. W., Jimenez-Sanchez, M., Korolchuk, V. I., Lichtenberg, M., Luo, S., Massey, D. C., Menzies, F. M., Moreau, K., Narayanan, U., Renna, M., Siddiqi, F. H., Underwood, B. R., Winslow, A. R. and Rubinsztein, D. C. (2010) Regulation of mammalian autophagy in physiology and pathophysiology. Physiol Rev. **90**, 1383-1435
53 Geisler, S., Holmstrom, K. M., Skujat, D., Fiesel, F. C., Rothfuss, O. C., Kahle, P. J. and Springer, W. (2010) PINK1/Parkin-mediated mitophagy is dependent on VDAC1 and p62/SQSTM1. Nat Cell Biol. **12**, 119-131
54 Kim, P. K., Hailey, D. W., Mullen, R. T. and Lippincott-Schwartz, J. (2008) Ubiquitin signals autophagic degradation of cytosolic proteins and peroxisomes. Proc Natl Acad Sci U S A. **105**, 20567-20574
55 Garcia-Higuera, I., Taniguchi, T., Ganesan, S., Meyn, M. S., Timmers, C., Hejna, J., Grompe, M. and D'Andrea, A. D. (2001) Interaction of the Fanconi anemia proteins and BRCA1 in a common pathway. Mol Cell. **7**, 249-262
56 Hoege, C., Pfander, B., Moldovan, G. L., Pyrowolakis, G. and Jentsch, S. (2002) RAD6-dependent DNA repair is linked to modification of PCNA by ubiquitin and SUMO. Nature. **419**, 135-141
57 Trotman, L. C., Wang, X., Alimonti, A., Chen, Z., Teruya-Feldstein, J., Yang, H., Pavletich, N. P., Carver, B. S., Cordon-Cardo, C., Erdjument-Bromage, H., Tempst, P., Chi, S. G., Kim, H. J., Misteli, T., Jiang, X. and Pandolfi, P. P. (2007) Ubiquitination regulates PTEN nuclear import and tumor suppression. Cell. **128**, 141-156
58 Hoeller, D. and Dikic, I. (2009) Targeting the ubiquitin system in cancer therapy. Nature. **458**, 438-444
59 Richardson, P. G., Sonneveld, P., Schuster, M. W., Irwin, D., Stadtmauer, E. A., Facon, T., Harousseau, J. L., Ben-Yehuda, D., Lonial, S., Goldschmidt, H., Reece, D., San-Miguel, J. F., Blade, J., Boccadoro, M., Cavenagh, J., Dalton, W. S., Boral, A. L., Esseltine, D. L., Porter, J. B., Schenkein, D. and Anderson, K. C. (2005) Bortezomib or high-dose dexamethasone for relapsed multiple myeloma. N Engl J Med. **352**, 2487-2498
60 Goy, A., Bernstein, S. H., Kahl, B. S., Djulbegovic, B., Robertson, M. J., de Vos, S., Epner, E., Krishnan, A., Leonard, J. P., Lonial, S., Nasta, S., O'Connor, O. A., Shi, H., Boral, A. L. and Fisher, R. I. (2009) Bortezomib in patients with relapsed or refractory mantle cell lymphoma: updated time-to-event analyses of the multicenter phase 2 PINNACLE study. Ann Oncol. **20**, 520-525
61 Kumar, M. S., Hancock, D. C., Molina-Arcas, M., Steckel, M., East, P., Diefenbacher, M., Armenteros-Monterroso, E., Lassailly, F., Matthews, N., Nye, E., Stamp, G., Behrens, A. and Downward, J. (2012) The GATA2 transcriptional network is requisite for RAS oncogene-driven non-small cell lung cancer. Cell. **149**, 642-655
62 Chauhan, D., Tian, Z., Nicholson, B., Kumar, K. G., Zhou, B., Carrasco, R., McDermott, J. L., Leach, C. A., Fulcinniti, M., Kodrasov, M. P., Weinstock, J.,

Kingsbury, W. D., Hideshima, T., Shah, P. K., Minvielle, S., Altun, M., Kessler, B. M., Orlowski, R., Richardson, P., Munshi, N. and Anderson, K. C. (2012) A small molecule inhibitor of ubiquitin-specific protease-7 induces apoptosis in multiple myeloma cells and overcomes bortezomib resistance. Cancer Cell. **22**, 345-358
63 Kisselev, A. F., van der Linden, W. A. and Overkleeft, H. S. (2012) Proteasome inhibitors: an expanding army attacking a unique target. Chem Biol. **19**, 99-115
64 Lakshmanan, M., Bughani, U., Duraisamy, S., Diwan, M., Dastidar, S. and Ray, A. (2008) Molecular targeting of E3 ligases--a therapeutic approach for cancer. Expert Opin Ther Targets. **12**, 855-870
65 Ray-Coquard, I., Blay, J. Y., Italiano, A., Le Cesne, A., Penel, N., Zhi, J., Heil, F., Rueger, R., Graves, B., Ding, M., Geho, D., Middleton, S. A., Vassilev, L. T., Nichols, G. L. and Bui, B. N. (2012) Effect of the MDM2 antagonist RG7112 on the P53 pathway in patients with MDM2-amplified, well-differentiated or dedifferentiated liposarcoma: an exploratory proof-of-mechanism study. Lancet Oncol. **13**, 1133-1140
66 Hershko, A., Heller, H., Elias, S. and Ciechanover, A. (1983) Components of ubiquitin-protein ligase system. Resolution, affinity purification, and role in protein breakdown. J Biol Chem. **258**, 8206-8214
67 Ye, Y. and Rape, M. (2009) Building ubiquitin chains: E2 enzymes at work. Nat Rev Mol Cell Biol. **10**, 755-764
68 Deshaies, R. J. and Joazeiro, C. A. (2009) RING domain E3 ubiquitin ligases. Annu Rev Biochem. **78**, 399-434
69 Schulman, B. A. and Harper, J. W. (2009) Ubiquitin-like protein activation by E1 enzymes: the apex for downstream signalling pathways. Nat Rev Mol Cell Biol. **10**, 319-331
70 Bernassola, F., Karin, M., Ciechanover, A. and Melino, G. (2008) The HECT family of E3 ubiquitin ligases: multiple players in cancer development. Cancer Cell. **14**, 10-21
71 Ciechanover, A., Heller, H., Katz-Etzion, R. and Hershko, A. (1981) Activation of the heat-stable polypeptide of the ATP-dependent proteolytic system. Proc Natl Acad Sci U S A. **78**, 761-765
72 Ciechanover, A., Elias, S., Heller, H. and Hershko, A. (1982) "Covalent affinity" purification of ubiquitin-activating enzyme. J Biol Chem. **257**, 2537-2542
73 Seol, J. H., Feldman, R. M., Zachariae, W., Shevchenko, A., Correll, C. C., Lyapina, S., Chi, Y., Galova, M., Claypool, J., Sandmeyer, S., Nasmyth, K. and Deshaies, R. J. (1999) Cdc53/cullin and the essential Hrt1 RING-H2 subunit of SCF define a ubiquitin ligase module that activates the E2 enzyme Cdc34. Genes Dev. **13**, 1614-1626
74 Freemont, P. S., Hanson, I. M. and Trowsdale, J. (1991) A novel cysteine-rich sequence motif. Cell. **64**, 483-484
75 Kamura, T., Koepp, D. M., Conrad, M. N., Skowyra, D., Moreland, R. J., Iliopoulos, O., Lane, W. S., Kaelin, W. G., Jr., Elledge, S. J., Conaway, R. C., Harper, J. W. and Conaway, J. W. (1999) Rbx1, a component of the VHL tumor suppressor complex and SCF ubiquitin ligase. Science. **284**, 657-661
76 Ohta, T., Michel, J. J., Schottelius, A. J. and Xiong, Y. (1999) ROC1, a homolog of APC11, represents a family of cullin partners with an associated ubiquitin ligase activity. Mol Cell. **3**, 535-541

77 Ohsumi, Y. (2001) Molecular dissection of autophagy: two ubiquitin-like systems. Nat Rev Mol Cell Biol. **2**, 211-216
78 Mizushima, N., Noda, T., Yoshimori, T., Tanaka, Y., Ishii, T., George, M. D., Klionsky, D. J., Ohsumi, M. and Ohsumi, Y. (1998) A protein conjugation system essential for autophagy. Nature. **395**, 395-398
79 Osaka, F., Saeki, M., Katayama, S., Aida, N., Toh, E. A., Kominami, K., Toda, T., Suzuki, T., Chiba, T., Tanaka, K. and Kato, S. (2000) Covalent modifier NEDD8 is essential for SCF ubiquitin-ligase in fission yeast. EMBO J. **19**, 3475-3484
80 Komander, D., Clague, M. J. and Urbe, S. (2009) Breaking the chains: structure and function of the deubiquitinases. Nat Rev Mol Cell Biol. **10**, 550-563
81 Tamura, K., Peterson, D., Peterson, N., Stecher, G., Nei, M. and Kumar, S. (2011) MEGA5: molecular evolutionary genetics analysis using maximum likelihood, evolutionary distance, and maximum parsimony methods. Mol Biol Evol. **28**, 2731-2739
82 Jones, D. T., Taylor, W. R. and Thornton, J. M. (1992) The rapid generation of mutation data matrices from protein sequences. Comput Appl Biosci. **8**, 275-282
83 Burrows, J. F., Scott, C. J. and Johnston, J. A. (2010) The DUB/USP17 deubiquitinating enzymes: a gene family within a tandemly repeated sequence, is also embedded within the copy number variable beta-defensin cluster. BMC Genomics. **11**, 250
84 Zhu, X., Menard, R. and Sulea, T. (2007) High incidence of ubiquitin-like domains in human ubiquitin-specific proteases. Proteins. **69**, 1-7
85 Komander, D. and Barford, D. (2008) Structure of the A20 OTU domain and mechanistic insights into deubiquitination. Biochem J. **409**, 77-85
86 Nijman, S. M., Luna-Vargas, M. P., Velds, A., Brummelkamp, T. R., Dirac, A. M., Sixma, T. K. and Bernards, R. (2005) A genomic and functional inventory of deubiquitinating enzymes. Cell. **123**, 773-786
87 Sato, Y., Yoshikawa, A., Yamagata, A., Mimura, H., Yamashita, M., Ookata, K., Nureki, O., Iwai, K., Komada, M. and Fukai, S. (2008) Structural basis for specific cleavage of Lys 63-linked polyubiquitin chains. Nature. **455**, 358-362
88 Lee, M. J., Lee, B. H., Hanna, J., King, R. W. and Finley, D. (2011) Trimming of ubiquitin chains by proteasome-associated deubiquitinating enzymes. Mol Cell Proteomics. **10**, R110 003871
89 Curcio-Morelli, C., Zavacki, A. M., Christofollete, M., Gereben, B., de Freitas, B. C., Harney, J. W., Li, Z., Wu, G. and Bianco, A. C. (2003) Deubiquitination of type 2 iodothyronine deiodinase by von Hippel-Lindau protein-interacting deubiquitinating enzymes regulates thyroid hormone activation. J Clin Invest. **112**, 189-196
90 Arrojo E Drigo, R. and Bianco, A. C. (2011) Type 2 deiodinase at the crossroads of thyroid hormone action. Int J Biochem Cell Biol. **43**, 1432-1441
91 Berthouze, M., Venkataramanan, V., Li, Y. and Shenoy, S. K. (2009) The deubiquitinases USP33 and USP20 coordinate beta2 adrenergic receptor recycling and resensitization. Embo J. **28**, 1684-1696
92 Li, Z., Wang, D., Messing, E. M. and Wu, G. (2005) VHL protein-interacting deubiquitinating enzyme 2 deubiquitinates and stabilizes HIF-1alpha. EMBO Rep. **6**, 373-378

93 Yasunaga, J., Lin, F. C., Lu, X. and Jeang, K. T. (2011) Ubiquitin-specific peptidase 20 targets TRAF6 and human T cell leukemia virus type 1 tax to negatively regulate NF-kappaB signaling. J Virol. **85**, 6212-6219
94 Hu, M., Li, P., Song, L., Jeffrey, P. D., Chenova, T. A., Wilkinson, K. D., Cohen, R. E. and Shi, Y. (2005) Structure and mechanisms of the proteasome-associated deubiquitinating enzyme USP14. EMBO J. **24**, 3747-3756
95 Komander, D., Lord, C. J., Scheel, H., Swift, S., Hofmann, K., Ashworth, A. and Barford, D. (2008) The structure of the CYLD USP domain explains its specificity for Lys63-linked polyubiquitin and reveals a B box module. Mol Cell. **29**, 451-464
96 Licchesi, J. D., Mieszczanek, J., Mevissen, T. E., Rutherford, T. J., Akutsu, M., Virdee, S., El Oualid, F., Chin, J. W., Ovaa, H., Bienz, M. and Komander, D. (2012) An ankyrin-repeat ubiquitin-binding domain determines TRABID's specificity for atypical ubiquitin chains. Nat Struct Mol Biol. **19**, 62-71
97 Lin, S. C., Chung, J. Y., Lamothe, B., Rajashankar, K., Lu, M., Lo, Y. C., Lam, A. Y., Darnay, B. G. and Wu, H. (2008) Molecular basis for the unique deubiquitinating activity of the NF-kappaB inhibitor A20. J Mol Biol. **376**, 526-540
98 Johnston, S. C., Riddle, S. M., Cohen, R. E. and Hill, C. P. (1999) Structural basis for the specificity of ubiquitin C-terminal hydrolases. Embo J. **18**, 3877-3887
99 Reyes-Turcu, F. E., Horton, J. R., Mullally, J. E., Heroux, A., Cheng, X. and Wilkinson, K. D. (2006) The ubiquitin binding domain ZnF UBP recognizes the C-terminal diglycine motif of unanchored ubiquitin. Cell. **124**, 1197-1208
100 Reyes-Turcu, F. E., Shanks, J. R., Komander, D. and Wilkinson, K. D. (2008) Recognition of polyubiquitin isoforms by the multiple ubiquitin binding modules of isopeptidase T. J Biol Chem. **283**, 19581-19592
101 Amerik AYu, Swaminathan, S., Krantz, B. A., Wilkinson, K. D. and Hochstrasser, M. (1997) In vivo disassembly of free polyubiquitin chains by yeast Ubp14 modulates rates of protein degradation by the proteasome. EMBO J. **16**, 4826-4838
102 Gong, L., Kamitani, T., Millas, S. and Yeh, E. T. (2000) Identification of a novel isopeptidase with dual specificity for ubiquitin- and NEDD8-conjugated proteins. J Biol Chem. **275**, 14212-14216
103 Ferro, A., Carvalho, A. L., Teixeira-Castro, A., Almeida, C., Tome, R. J., Cortes, L., Rodrigues, A. J., Logarinho, E., Sequeiros, J., Macedo-Ribeiro, S. and Maciel, P. (2007) NEDD8: a new ataxin-3 interactor. Biochim Biophys Acta. **1773**, 1619-1627
104 Hemelaar, J., Borodovsky, A., Kessler, B. M., Reverter, D., Cook, J., Kolli, N., Gan-Erdene, T., Wilkinson, K. D., Gill, G., Lima, C. D., Ploegh, H. L. and Ovaa, H. (2004) Specific and covalent targeting of conjugating and deconjugating enzymes of ubiquitin-like proteins. Mol Cell Biol. **24**, 84-95
105 Wada, H., Kito, K., Caskey, L. S., Yeh, E. T. and Kamitani, T. (1998) Cleavage of the C-terminus of NEDD8 by UCH-L3. Biochem Biophys Res Commun. **251**, 688-692
106 Malakhov, M. P., Malakhova, O. A., Kim, K. I., Ritchie, K. J. and Zhang, D. E. (2002) UBP43 (USP18) specifically removes ISG15 from conjugated proteins. J Biol Chem. **277**, 9976-9981

107 Urbe, S., Liu, H., Hayes, S. D., Heride, C., Rigden, D. J. and Clague, M. J. (2012) Systematic survey of deubiquitinase localization identifies USP21 as a regulator of centrosome- and microtubule-associated functions. Mol Biol Cell. **23**, 1095-1103
108 Baker, R. T., Tobias, J. W. and Varshavsky, A. (1992) Ubiquitin-specific proteases of Saccharomyces cerevisiae. Cloning of UBP2 and UBP3, and functional analysis of the UBP gene family. J Biol Chem. **267**, 23364-23375
109 Mayer, A. N. and Wilkinson, K. D. (1989) Detection, resolution, and nomenclature of multiple ubiquitin carboxyl-terminal esterases from bovine calf thymus. Biochemistry. **28**, 166-172
110 Clague, M. J., Coulson, J. M. and Urbe, S. (2012) Cellular functions of the DUBs. J Cell Sci. **125**, 277-286
111 Fraile, J. M., Quesada, V., Rodriguez, D., Freije, J. M. and Lopez-Otin, C. (2012) Deubiquitinases in cancer: new functions and therapeutic options. Oncogene. **31**, 2373-2388
112 Luise, C., Capra, M., Donzelli, M., Mazzarol, G., Jodice, M. G., Nuciforo, P., Viale, G., Di Fiore, P. P. and Confalonieri, S. (2011) An atlas of altered expression of deubiquitinating enzymes in human cancer. PLoS One. **6**, e15891
113 Bignell, G. R., Warren, W., Seal, S., Takahashi, M., Rapley, E., Barfoot, R., Green, H., Brown, C., Biggs, P. J., Lakhani, S. R., Jones, C., Hansen, J., Blair, E., Hofmann, B., Siebert, R., Turner, G., Evans, D. G., Schrander-Stumpel, C., Beemer, F. A., van Den Ouweland, A., Halley, D., Delpech, B., Cleveland, M. G., Leigh, I., Leisti, J. and Rasmussen, S. (2000) Identification of the familial cylindromatosis tumour-suppressor gene. Nat Genet. **25**, 160-165
114 Biggs, P. J., Wooster, R., Ford, D., Chapman, P., Mangion, J., Quirk, Y., Easton, D. F., Burn, J. and Stratton, M. R. (1995) Familial cylindromatosis (turban tumour syndrome) gene localised to chromosome 16q12-q13: evidence for its role as a tumour suppressor gene. Nat Genet. **11**, 441-443
115 Leonard, N., Chaggar, R., Jones, C., Takahashi, M., Nikitopoulou, A. and Lakhani, S. R. (2001) Loss of heterozygosity at cylindromatosis gene locus, CYLD, in sporadic skin adnexal tumours. J Clin Pathol. **54**, 689-692
116 Biggs, P. J., Chapman, P., Lakhani, S. R., Burn, J. and Stratton, M. R. (1996) The cylindromatosis gene (cyld1) on chromosome 16q may be the only tumour suppressor gene involved in the development of cylindromas. Oncogene. **12**, 1375-1377
117 Masoumi, K. C., Shaw-Hallgren, G. and Massoumi, R. (2011) Tumor Suppressor Function of CYLD in Nonmelanoma Skin Cancer. J Skin Cancer. **2011**, 614097
118 Kuphal, S., Shaw-Hallgren, G., Eberl, M., Karrer, S., Aberger, F., Bosserhoff, A. K. and Massoumi, R. (2011) GLI1-dependent transcriptional repression of CYLD in basal cell carcinoma. Oncogene. **30**, 4523-4530
119 Lam, C. W., Xie, J., To, K. F., Ng, H. K., Lee, K. C., Yuen, N. W., Lim, P. L., Chan, L. Y., Tong, S. F. and McCormick, F. (1999) A frequent activated smoothened mutation in sporadic basal cell carcinomas. Oncogene. **18**, 833-836
120 Xie, J., Murone, M., Luoh, S. M., Ryan, A., Gu, Q., Zhang, C., Bonifas, J. M., Lam, C. W., Hynes, M., Goddard, A., Rosenthal, A., Epstein, E. H., Jr. and de Sauvage, F. J. (1998) Activating Smoothened mutations in sporadic basal-cell carcinoma. Nature. **391**, 90-92

121 Johnson, R. L., Rothman, A. L., Xie, J., Goodrich, L. V., Bare, J. W., Bonifas, J. M., Quinn, A. G., Myers, R. M., Cox, D. R., Epstein, E. H., Jr. and Scott, M. P. (1996) Human homolog of patched, a candidate gene for the basal cell nevus syndrome. Science. **272**, 1668-1671
122 Alameda, J. P., Moreno-Maldonado, R., Navarro, M., Bravo, A., Ramirez, A., Page, A., Jorcano, J. L., Fernandez-Acenero, M. J. and Casanova, M. L. (2010) An inactivating CYLD mutation promotes skin tumor progression by conferring enhanced proliferative, survival and angiogenic properties to epidermal cancer cells. Oncogene. **29**, 6522-6532
123 Massoumi, R. (2011) CYLD: a deubiquitination enzyme with multiple roles in cancer. Future Oncol. **7**, 285-297
124 Zhang, J., Stirling, B., Temmerman, S. T., Ma, C. A., Fuss, I. J., Derry, J. M. and Jain, A. (2006) Impaired regulation of NF-kappaB and increased susceptibility to colitis-associated tumorigenesis in CYLD-deficient mice. J Clin Invest. **116**, 3042-3049
125 Brummelkamp, T. R., Nijman, S. M., Dirac, A. M. and Bernards, R. (2003) Loss of the cylindromatosis tumour suppressor inhibits apoptosis by activating NF-kappaB. Nature. **424**, 797-801
126 Kovalenko, A., Chable-Bessia, C., Cantarella, G., Israel, A., Wallach, D. and Courtois, G. (2003) The tumour suppressor CYLD negatively regulates NF-kappaB signalling by deubiquitination. Nature. **424**, 801-805
127 Trompouki, E., Hatzivassiliou, E., Tsichritzis, T., Farmer, H., Ashworth, A. and Mosialos, G. (2003) CYLD is a deubiquitinating enzyme that negatively regulates NF-kappaB activation by TNFR family members. Nature. **424**, 793-796
128 Reiley, W., Zhang, M. and Sun, S. C. (2004) Negative regulation of JNK signaling by the tumor suppressor CYLD. J Biol Chem. **279**, 55161-55167
129 Reiley, W. W., Zhang, M., Jin, W., Losiewicz, M., Donohue, K. B., Norbury, C. C. and Sun, S. C. (2006) Regulation of T cell development by the deubiquitinating enzyme CYLD. Nat Immunol. **7**, 411-417
130 Reiley, W. W., Jin, W., Lee, A. J., Wright, A., Wu, X., Tewalt, E. F., Leonard, T. O., Norbury, C. C., Fitzpatrick, L., Zhang, M. and Sun, S. C. (2007) Deubiquitinating enzyme CYLD negatively regulates the ubiquitin-dependent kinase Tak1 and prevents abnormal T cell responses. J Exp Med. **204**, 1475-1485
131 Miliani de Marval, P., Lutfeali, S., Jin, J. Y., Leshin, B., Selim, M. A. and Zhang, J. Y. (2011) CYLD inhibits tumorigenesis and metastasis by blocking JNK/AP1 signaling at multiple levels. Cancer Prev Res (Phila). **4**, 851-859
132 Heyninck, K. and Beyaert, R. (2005) A20 inhibits NF-kappaB activation by dual ubiquitin-editing functions. Trends Biochem Sci. **30**, 1-4
133 Honma, K., Tsuzuki, S., Nakagawa, M., Tagawa, H., Nakamura, S., Morishima, Y. and Seto, M. (2009) TNFAIP3/A20 functions as a novel tumor suppressor gene in several subtypes of non-Hodgkin lymphomas. Blood. **114**, 2467-2475
134 Kato, M., Sanada, M., Kato, I., Sato, Y., Takita, J., Takeuchi, K., Niwa, A., Chen, Y., Nakazaki, K., Nomoto, J., Asakura, Y., Muto, S., Tamura, A., Iio, M., Akatsuka, Y., Hayashi, Y., Mori, H., Igarashi, T., Kurokawa, M., Chiba, S., Mori, S., Ishikawa, Y., Okamoto, K., Tobinai, K., Nakagama, H., Nakahata, T., Yoshino, T., Kobayashi, Y. and Ogawa, S. (2009) Frequent inactivation of A20 in B-cell lymphomas. Nature. **459**, 712-716

135 Novak, U., Rinaldi, A., Kwee, I., Nandula, S. V., Rancoita, P. M., Compagno, M., Cerri, M., Rossi, D., Murty, V. V., Zucca, E., Gaidano, G., Dalla-Favera, R., Pasqualucci, L., Bhagat, G. and Bertoni, F. (2009) The NF-{kappa}B negative regulator TNFAIP3 (A20) is inactivated by somatic mutations and genomic deletions in marginal zone lymphomas. Blood. **113**, 4918-4921
136 Schmitz, R., Hansmann, M. L., Bohle, V., Martin-Subero, J. I., Hartmann, S., Mechtersheimer, G., Klapper, W., Vater, I., Giefing, M., Gesk, S., Stanelle, J., Siebert, R. and Kuppers, R. (2009) TNFAIP3 (A20) is a tumor suppressor gene in Hodgkin lymphoma and primary mediastinal B cell lymphoma. J Exp Med. **206**, 981-989
137 Bavi, P., Abubaker, J., Al-Sanea, N., Abduljabbar, A., Ashari, L. H., Alhomoud, S., Al-Dayel, F., Uddin, S., Siraj, A. K. and Al-Kuraya, K. S. (2011) Clinico-pathological significance of TNF alpha-induced protein3 (TNFAIP3) in Middle Eastern colorectal carcinoma. Clin Epigenetics. **2**, 417-418
138 Jensen, D. E., Proctor, M., Marquis, S. T., Gardner, H. P., Ha, S. I., Chodosh, L. A., Ishov, A. M., Tommerup, N., Vissing, H., Sekido, Y., Minna, J., Borodovsky, A., Schultz, D. C., Wilkinson, K. D., Maul, G. G., Barlev, N., Berger, S. L., Prendergast, G. C. and Rauscher, F. J., 3rd. (1998) BAP1: a novel ubiquitin hydrolase which binds to the BRCA1 RING finger and enhances BRCA1-mediated cell growth suppression. Oncogene. **16**, 1097-1112
139 Harbour, J. W., Onken, M. D., Roberson, E. D., Duan, S., Cao, L., Worley, L. A., Council, M. L., Matatall, K. A., Helms, C. and Bowcock, A. M. (2010) Frequent mutation of BAP1 in metastasizing uveal melanomas. Science. **330**, 1410-1413
140 Bott, M., Brevet, M., Taylor, B. S., Shimizu, S., Ito, T., Wang, L., Creaney, J., Lake, R. A., Zakowski, M. F., Reva, B., Sander, C., Delsite, R., Powell, S., Zhou, Q., Shen, R., Olshen, A., Rusch, V. and Ladanyi, M. (2011) The nuclear deubiquitinase BAP1 is commonly inactivated by somatic mutations and 3p21.1 losses in malignant pleural mesothelioma. Nat Genet. **43**, 668-672
141 Yoshikawa, Y., Sato, A., Tsujimura, T., Emi, M., Morinaga, T., Fukuoka, K., Yamada, S., Murakami, A., Kondo, N., Matsumoto, S., Okumura, Y., Tanaka, F., Hasegawa, S., Nakano, T. and Hashimoto-Tamaoki, T. (2012) Frequent inactivation of the BAP1 gene in epithelioid-type malignant mesothelioma. Cancer Sci. **103**, 868-874
142 Pena-Llopis, S., Vega-Rubin-de-Celis, S., Liao, A., Leng, N., Pavia-Jimenez, A., Wang, S., Yamasaki, T., Zhrebker, L., Sivanand, S., Spence, P., Kinch, L., Hambuch, T., Jain, S., Lotan, Y., Margulis, V., Sagalowsky, A. I., Summerour, P. B., Kabbani, W., Wong, S. W., Grishin, N., Laurent, M., Xie, X. J., Haudenschild, C. D., Ross, M. T., Bentley, D. R., Kapur, P. and Brugarolas, J. (2012) BAP1 loss defines a new class of renal cell carcinoma. Nat Genet. **44**, 751-759
143 Fan, L. H., Tang, L. N., Yue, L., Yang, Y., Gao, Z. L. and Shen, Z. (2012) BAP1 is a good prognostic factor in advanced non-small cell lung cancer. Clin Invest Med. **35**, E182
144 Abdel-Rahman, M. H., Pilarski, R., Cebulla, C. M., Massengill, J. B., Christopher, B. N., Boru, G., Hovland, P. and Davidorf, F. H. (2011) Germline BAP1 mutation predisposes to uveal melanoma, lung adenocarcinoma, meningioma, and other cancers. J Med Genet. **48**, 856-859
145 Carbone, M., Korb Ferris, L., Baumann, F., Napolitano, A., Lum, C. A., Flores, E. G., Gaudino, G., Powers, A., Bryant-Greenwood, P., Krausz, T., Hyjek, E., Tate, R., Friedberg, J., Weigel, T., Pass, H. I. and Yang, H. (2012) BAP1 cancer

syndrome: malignant mesothelioma, uveal and cutaneous melanoma, and MBAITs. J Transl Med. **10**, 179
146 Njauw, C. N., Kim, I., Piris, A., Gabree, M., Taylor, M., Lane, A. M., DeAngelis, M. M., Gragoudas, E., Duncan, L. M. and Tsao, H. (2012) Germline BAP1 inactivation is preferentially associated with metastatic ocular melanoma and cutaneous-ocular melanoma families. PLoS One. **7**, e35295
147 Testa, J. R., Cheung, M., Pei, J., Below, J. E., Tan, Y., Sementino, E., Cox, N. J., Dogan, A. U., Pass, H. I., Trusa, S., Hesdorffer, M., Nasu, M., Powers, A., Rivera, Z., Comertpay, S., Tanji, M., Gaudino, G., Yang, H. and Carbone, M. (2011) Germline BAP1 mutations predispose to malignant mesothelioma. Nat Genet. **43**, 1022-1025
148 Wiesner, T., Obenauf, A. C., Murali, R., Fried, I., Griewank, K. G., Ulz, P., Windpassinger, C., Wackernagel, W., Loy, S., Wolf, I., Viale, A., Lash, A. E., Pirun, M., Socci, N. D., Rutten, A., Palmedo, G., Abramson, D., Offit, K., Ott, A., Becker, J. C., Cerroni, L., Kutzner, H., Bastian, B. C. and Speicher, M. R. (2011) Germline mutations in BAP1 predispose to melanocytic tumors. Nat Genet. **43**, 1018-1021
149 Ventii, K. H., Devi, N. S., Friedrich, K. L., Chernova, T. A., Tighiouart, M., Van Meir, E. G. and Wilkinson, K. D. (2008) BRCA1-associated protein-1 is a tumor suppressor that requires deubiquitinating activity and nuclear localization. Cancer Res. **68**, 6953-6962
150 Scheuermann, J. C., de Ayala Alonso, A. G., Oktaba, K., Ly-Hartig, N., McGinty, R. K., Fraterman, S., Wilm, M., Muir, T. W. and Muller, J. (2010) Histone H2A deubiquitinase activity of the Polycomb repressive complex PR-DUB. Nature. **465**, 243-247
151 Yu, H., Mashtalir, N., Daou, S., Hammond-Martel, I., Ross, J., Sui, G., Hart, G. W., Rauscher, F. J., 3rd, Drobetsky, E., Milot, E., Shi, Y. and Affar el, B. (2010) The ubiquitin carboxyl hydrolase BAP1 forms a ternary complex with YY1 and HCF-1 and is a critical regulator of gene expression. Mol Cell Biol. **30**, 5071-5085
152 Oliveira, A. M., Hsi, B. L., Weremowicz, S., Rosenberg, A. E., Dal Cin, P., Joseph, N., Bridge, J. A., Perez-Atayde, A. R. and Fletcher, J. A. (2004) USP6 (Tre2) fusion oncogenes in aneurysmal bone cyst. Cancer Res. **64**, 1920-1923
153 Panoutsakopoulos, G., Pandis, N., Kyriazoglou, I., Gustafson, P., Mertens, F. and Mandahl, N. (1999) Recurrent t(16;17)(q22;p13) in aneurysmal bone cysts. Genes Chromosomes Cancer. **26**, 265-266
154 van de Luijtgaarden, A. C., Veth, R. P., Slootweg, P. J., Wijers-Koster, P. M., Schultze Kool, L. J., Bovee, J. V. and van der Graaf, W. T. (2009) Metastatic potential of an aneurysmal bone cyst. Virchows Arch
155 Oliveira, A. M., Perez-Atayde, A. R., Dal Cin, P., Gebhardt, M. C., Chen, C. J., Neff, J. R., Demetri, G. D., Rosenberg, A. E., Bridge, J. A. and Fletcher, J. A. (2005) Aneurysmal bone cyst variant translocations upregulate USP6 transcription by promoter swapping with the ZNF9, COL1A1, TRAP150, and OMD genes. Oncogene. **24**, 3419-3426
156 Ye, Y., Pringle, L. M., Lau, A. W., Riquelme, D. N., Wang, H., Jiang, T., Lev, D., Welman, A., Blobel, G. A., Oliveira, A. M. and Chou, M. M. (2010) TRE17/USP6 oncogene translocated in aneurysmal bone cyst induces matrix metalloproteinase production via activation of NF-kappaB. Oncogene. **29**, 3619-3629
157 Gupta, K., Chevrette, M. and Gray, D. A. (1994) The Unp proto-oncogene encodes a nuclear protein. Oncogene. **9**, 1729-1731

158 Gray, D. A., Inazawa, J., Gupta, K., Wong, A., Ueda, R. and Takahashi, T. (1995) Elevated expression of Unph, a proto-oncogene at 3p21.3, in human lung tumors. Oncogene. **10**, 2179-2183
159 Zhang, X., Berger, F. G., Yang, J. and Lu, X. (2011) USP4 inhibits p53 through deubiquitinating and stabilizing ARF-BP1. EMBO J. **30**, 2177-2189
160 Zhang, L., Zhou, F., Drabsch, Y., Gao, R., Snaar-Jagalska, B. E., Mickanin, C., Huang, H., Sheppard, K. A., Porter, J. A., Lu, C. X. and ten Dijke, P. (2012) USP4 is regulated by AKT phosphorylation and directly deubiquitylates TGF-beta type I receptor. Nat Cell Biol. **14**, 717-726
161 Xiao, N., Li, H., Luo, J., Wang, R., Chen, H., Chen, J. and Wang, P. (2012) Ubiquitin-specific protease 4 (USP4) targets TRAF2 and TRAF6 for deubiquitination and inhibits TNFalpha-induced cancer cell migration. Biochem J. **441**, 979-986
162 Hibi, K., Liu, Q., Beaudry, G. A., Madden, S. L., Westra, W. H., Wehage, S. L., Yang, S. C., Heitmiller, R. F., Bertelsen, A. H., Sidransky, D. and Jen, J. (1998) Serial analysis of gene expression in non-small cell lung cancer. Cancer Res. **58**, 5690-5694
163 Hibi, K., Westra, W. H., Borges, M., Goodman, S., Sidransky, D. and Jen, J. (1999) PGP9.5 as a candidate tumor marker for non-small-cell lung cancer. Am J Pathol. **155**, 711-715
164 Yamazaki, T., Hibi, K., Takase, T., Tezel, E., Nakayama, H., Kasai, Y., Ito, K., Akiyama, S., Nagasaka, T. and Nakao, A. (2002) PGP9.5 as a marker for invasive colorectal cancer. Clin Cancer Res. **8**, 192-195
165 Tezel, E., Hibi, K., Nagasaka, T. and Nakao, A. (2000) PGP9.5 as a prognostic factor in pancreatic cancer. Clin Cancer Res. **6**, 4764-4767
166 Liu, X., Zeng, B., Ma, J. and Wan, C. (2009) Comparative proteomic analysis of osteosarcoma cell and human primary cultured osteoblastic cell. Cancer Invest. **27**, 345-352
167 Takase, T., Hibi, K., Yamazaki, T., Nakayama, H., Taguchi, M., Kasai, Y., Ito, K., Akiyama, S., Nagasaka, T. and Nakao, A. (2003) PGP9.5 overexpression in esophageal squamous cell carcinoma. Hepatogastroenterology. **50**, 1278-1280
168 Xiang, T., Li, L., Yin, X., Yuan, C., Tan, C., Su, X., Xiong, L., Putti, T. C., Oberst, M., Kelly, K., Ren, G. and Tao, Q. (2012) The ubiquitin peptidase UCHL1 induces G0/G1 cell cycle arrest and apoptosis through stabilizing p53 and is frequently silenced in breast cancer. PLoS One. **7**, e29783
169 Li, L., Tao, Q., Jin, H., van Hasselt, A., Poon, F. F., Wang, X., Zeng, M. S., Jia, W. H., Zeng, Y. X., Chan, A. T. and Cao, Y. (2010) The tumor suppressor UCHL1 forms a complex with p53/MDM2/ARF to promote p53 signaling and is frequently silenced in nasopharyngeal carcinoma. Clin Cancer Res. **16**, 2949-2958
170 Loyo, M., Brait, M., Kim, M. S., Ostrow, K. L., Jie, C. C., Chuang, A. Y., Califano, J. A., Liegeois, N. J., Begum, S., Westra, W. H., Hoque, M. O., Tao, Q. and Sidransky, D. (2011) A survey of methylated candidate tumor suppressor genes in nasopharyngeal carcinoma. Int J Cancer. **128**, 1393-1403
171 Mandelker, D. L., Yamashita, K., Tokumaru, Y., Mimori, K., Howard, D. L., Tanaka, Y., Carvalho, A. L., Jiang, W. W., Park, H. L., Kim, M. S., Osada, M., Mori, M. and Sidransky, D. (2005) PGP9.5 promoter methylation is an independent prognostic factor for esophageal squamous cell carcinoma. Cancer Res. **65**, 4963-4968

172 Yu, J., Tao, Q., Cheung, K. F., Jin, H., Poon, F. F., Wang, X., Li, H., Cheng, Y. Y., Rocken, C., Ebert, M. P., Chan, A. T. and Sung, J. J. (2008) Epigenetic identification of ubiquitin carboxyl-terminal hydrolase L1 as a functional tumor suppressor and biomarker for hepatocellular carcinoma and other digestive tumors. Hepatology. **48**, 508-518
173 Zhong, J., Zhao, M., Ma, Y., Luo, Q., Liu, J., Wang, J., Yuan, X., Sang, J. and Huang, C. (2012) UCHL1 acts as a colorectal cancer oncogene via activation of the beta-catenin/TCF pathway through its deubiquitinating activity. Int J Mol Med. **30**, 430-436
174 Popov, N., Wanzel, M., Madiredjo, M., Zhang, D., Beijersbergen, R., Bernards, R., Moll, R., Elledge, S. J. and Eilers, M. (2007) The ubiquitin-specific protease USP28 is required for MYC stability. Nat Cell Biol. **9**, 765-774
175 Stevenson, L. F., Sparks, A., Allende-Vega, N., Xirodimas, D. P., Lane, D. P. and Saville, M. K. (2007) The deubiquitinating enzyme USP2a regulates the p53 pathway by targeting Mdm2. EMBO J. **26**, 976-986
176 Kim, J., Kim, W. J., Liu, Z., Loda, M. and Freeman, M. R. (2012) The ubiquitin-specific protease USP2a enhances tumor progression by targeting cyclin A1 in bladder cancer. Cell Cycle. **11**, 1123-1130
177 Shi, Y., Solomon, L. R., Pereda-Lopez, A., Giranda, V. L., Luo, Y., Johnson, E. F., Shoemaker, A. R., Leverson, J. and Liu, X. (2011) Ubiquitin-specific cysteine protease 2a (USP2a) regulates the stability of Aurora-A. J Biol Chem. **286**, 38960-38968
178 Graner, E., Tang, D., Rossi, S., Baron, A., Migita, T., Weinstein, L. J., Lechpammer, M., Huesken, D., Zimmermann, J., Signoretti, S. and Loda, M. (2004) The isopeptidase USP2a regulates the stability of fatty acid synthase in prostate cancer. Cancer Cell. **5**, 253-261
179 Priolo, C., Tang, D., Brahamandan, M., Benassi, B., Sicinska, E., Ogino, S., Farsetti, A., Porrello, A., Finn, S., Zimmermann, J., Febbo, P. and Loda, M. (2006) The isopeptidase USP2a protects human prostate cancer from apoptosis. Cancer Res. **66**, 8625-8632
180 Harhaj, E. W. and Dixit, V. M. (2012) Regulation of NF-kappaB by deubiquitinases. Immunol Rev. **246**, 107-124
181 Prasad, S., Ravindran, J. and Aggarwal, B. B. (2009) NF-kappaB and cancer: how intimate is this relationship. Mol Cell Biochem
182 Oeckinghaus, A. and Ghosh, S. (2009) The NF-kappaB family of transcription factors and its regulation. Cold Spring Harb Perspect Biol. **1**, a000034
183 Jono, H., Lim, J. H., Chen, L. F., Xu, H., Trompouki, E., Pan, Z. K., Mosialos, G. and Li, J. D. (2004) NF-kappaB is essential for induction of CYLD, the negative regulator of NF-kappaB: evidence for a novel inducible autoregulatory feedback pathway. J Biol Chem. **279**, 36171-36174
184 Boone, D. L., Turer, E. E., Lee, E. G., Ahmad, R. C., Wheeler, M. T., Tsui, C., Hurley, P., Chien, M., Chai, S., Hitotsumatsu, O., McNally, E., Pickart, C. and Ma, A. (2004) The ubiquitin-modifying enzyme A20 is required for termination of Toll-like receptor responses. Nat Immunol. **5**, 1052-1060
185 Wertz, I. E., O'Rourke, K. M., Zhou, H., Eby, M., Aravind, L., Seshagiri, S., Wu, P., Wiesmann, C., Baker, R., Boone, D. L., Ma, A., Koonin, E. V. and Dixit, V. M. (2004) De-ubiquitination and ubiquitin ligase domains of A20 downregulate NF-kappaB signalling. Nature. **430**, 694-699

186 Enesa, K., Zakkar, M., Chaudhury, H., Luong le, A., Rawlinson, L., Mason, J. C., Haskard, D. O., Dean, J. L. and Evans, P. C. (2008) NF-kappaB suppression by the deubiquitinating enzyme Cezanne: a novel negative feedback loop in pro-inflammatory signaling. J Biol Chem. **283**, 7036-7045
187 Xu, G., Tan, X., Wang, H., Sun, W., Shi, Y., Burlingame, S., Gu, X., Cao, G., Zhang, T., Qin, J. and Yang, J. (2010) Ubiquitin-specific peptidase 21 inhibits tumor necrosis factor alpha-induced nuclear factor kappaB activation via binding to and deubiquitinating receptor-interacting protein 1. J Biol Chem. **285**, 969-978
188 Dupont, S., Mamidi, A., Cordenonsi, M., Montagner, M., Zacchigna, L., Adorno, M., Martello, G., Stinchfield, M. J., Soligo, S., Morsut, L., Inui, M., Moro, S., Modena, N., Argenton, F., Newfeld, S. J. and Piccolo, S. (2009) FAM/USP9x, a deubiquitinating enzyme essential for TGFbeta signaling, controls Smad4 monoubiquitination. Cell. **136**, 123-135
189 Al-Hakim, A. K., Zagorska, A., Chapman, L., Deak, M., Peggie, M. and Alessi, D. R. (2008) Control of AMPK-related kinases by USP9X and atypical Lys(29)/Lys(33)-linked polyubiquitin chains. Biochem J. **411**, 249-260
190 Ibarrola, N., Kratchmarova, I., Nakajima, D., Schiemann, W. P., Moustakas, A., Pandey, A. and Mann, M. (2004) Cloning of a novel signaling molecule, AMSH-2, that potentiates transforming growth factor beta signaling. BMC Cell Biol. **5**, 2
191 Wicks, S. J., Haros, K., Maillard, M., Song, L., Cohen, R. E., Dijke, P. T. and Chantry, A. (2005) The deubiquitinating enzyme UCH37 interacts with Smads and regulates TGF-beta signalling. Oncogene. **24**, 8080-8084
192 Tauriello, D. V., Haegebarth, A., Kuper, I., Edelmann, M. J., Henraat, M., Canninga-van Dijk, M. R., Kessler, B. M., Clevers, H. and Maurice, M. M. Loss of the tumor suppressor CYLD enhances Wnt/beta-catenin signaling through K63-linked ubiquitination of Dvl. Mol Cell. **37**, 607-619
193 Zhao, B., Schlesiger, C., Masucci, M. G. and Lindsten, K. (2009) The Ubiquitin Specific Protease 4 (Usp4) Is a New Player in the Wnt Signalling Pathway. J Cell Mol Med
194 Huang, X., Langelotz, C., Hetfeld-Pechoc, B. K., Schwenk, W. and Dubiel, W. (2009) The COP9 signalosome mediates beta-catenin degradation by deneddylation and blocks adenomatous polyposis coli destruction via USP15. J Mol Biol. **391**, 691-702
195 Lui, T. T., Lacroix, C., Ahmed, S. M., Goldenberg, S. J., Leach, C. A., Daulat, A. M. and Angers, S. (2011) The ubiquitin-specific protease USP34 regulates axin stability and Wnt/β-catenin signaling. Mol Cell Biol. **31**, 2053-2065
196 Tran, H., Hamada, F., Schwarz-Romond, T. and Bienz, M. (2008) Trabid, a new positive regulator of Wnt-induced transcription with preference for binding and cleaving K63-linked ubiquitin chains. Genes Dev. **22**, 528-542
197 Leslie, N. R. and Foti, M. (2011) Non-genomic loss of PTEN function in cancer: not in my genes. Trends Pharmacol Sci. **32**, 131-140
198 Brooks, C. L. and Gu, W. (2011) p53 regulation by ubiquitin. FEBS Lett. **585**, 2803-2809
199 Li, M., Chen, D., Shiloh, A., Luo, J., Nikolaev, A. Y., Qin, J. and Gu, W. (2002) Deubiquitination of p53 by HAUSP is an important pathway for p53 stabilization. Nature. **416**, 648-653

200 Yuan, J., Luo, K., Zhang, L., Cheville, J. C. and Lou, Z. (2010) USP10 regulates p53 localization and stability by deubiquitinating p53. Cell. **140**, 384-396
201 Liu, J., Chung, H. J., Vogt, M., Jin, Y., Malide, D., He, L., Dundr, M. and Levens, D. (2011) JTV1 co-activates FBP to induce USP29 transcription and stabilize p53 in response to oxidative stress. EMBO J. **30**, 846-858
202 Dayal, S., Sparks, A., Jacob, J., Allende-Vega, N., Lane, D. P. and Saville, M. K. (2009) Suppression of the deubiquitinating enzyme USP5 causes the accumulation of unanchored polyubiquitin and the activation of p53. J Biol Chem. **284**, 5030-5041
203 Song, M. S., Salmena, L., Carracedo, A., Egia, A., Lo-Coco, F., Teruya-Feldstein, J. and Pandolfi, P. P. (2008) The deubiquitinylation and localization of PTEN are regulated by a HAUSP-PML network. Nature. **455**, 813-817
204 Hock, A. K., Vigneron, A. M., Carter, S., Ludwig, R. L. and Vousden, K. H. (2011) Regulation of p53 stability and function by the deubiquitinating enzyme USP42. EMBO J. **30**, 4921-4930
205 van der Horst, A., de Vries-Smits, A. M., Brenkman, A. B., van Triest, M. H., van den Broek, N., Colland, F., Maurice, M. M. and Burgering, B. M. (2006) FOXO4 transcriptional activity is regulated by monoubiquitination and USP7/HAUSP. Nat Cell Biol. **8**, 1064-1073
206 Horn, H. F. and Vousden, K. H. (2007) Coping with stress: multiple ways to activate p53. Oncogene. **26**, 1306-1316
207 Bond, G. L., Hu, W. and Levine, A. J. (2005) MDM2 is a central node in the p53 pathway: 12 years and counting. Curr Cancer Drug Targets. **5**, 3-8
208 Cummins, J. M. and Vogelstein, B. (2004) HAUSP is required for p53 destabilization. Cell Cycle. **3**, 689-692
209 Li, M., Brooks, C. L., Kon, N. and Gu, W. (2004) A dynamic role of HAUSP in the p53-Mdm2 pathway. Mol Cell. **13**, 879-886
210 Meulmeester, E., Maurice, M. M., Boutell, C., Teunisse, A. F., Ovaa, H., Abraham, T. E., Dirks, R. W. and Jochemsen, A. G. (2005) Loss of HAUSP-mediated deubiquitination contributes to DNA damage-induced destabilization of Hdmx and Hdm2. Mol Cell. **18**, 565-576
211 Colland, F., Formstecher, E., Jacq, X., Reverdy, C., Planquette, C., Conrath, S., Trouplin, V., Bianchi, J., Aushev, V. N., Camonis, J., Calabrese, A., Borg-Capra, C., Sippl, W., Collura, V., Boissy, G., Rain, J. C., Guedat, P., Delansorne, R. and Daviet, L. (2009) Small-molecule inhibitor of USP7/HAUSP ubiquitin protease stabilizes and activates p53 in cells. Mol Cancer Ther. **8**, 2286-2295
212 Colombo, M., Vallese, S., Peretto, I., Jacq, X., Rain, J. C., Colland, F. and Guedat, P. (2010) Synthesis and biological evaluation of 9-oxo-9H-indeno[1,2-b]pyrazine-2,3-dicarbonitrile analogues as potential inhibitors of deubiquitinating enzymes. ChemMedChem. **5**, 552-558
213 Daviet, L. and Colland, F. (2008) Targeting ubiquitin specific proteases for drug discovery. Biochimie. **90**, 270-283
214 Chen, J., Dexheimer, T. S., Ai, Y., Liang, Q., Villamil, M. A., Inglese, J., Maloney, D. J., Jadhav, A., Simeonov, A. and Zhuang, Z. (2011) Selective and cell-active inhibitors of the USP1/ UAF1 deubiquitinase complex reverse cisplatin resistance in non-small cell lung cancer cells. Chem Biol. **18**, 1390-1400
215 Tian, X., Isamiddinova, N. S., Peroutka, R. J., Goldenberg, S. J., Mattern, M. R., Nicholson, B. and Leach, C. (2011) Characterization of selective ubiquitin and

ubiquitin-like protease inhibitors using a fluorescence-based multiplex assay format. Assay Drug Dev Technol. **9**, 165-173
216 Hirayama, K., Aoki, S., Nishikawa, K., Matsumoto, T. and Wada, K. (2007) Identification of novel chemical inhibitors for ubiquitin C-terminal hydrolase-L3 by virtual screening. Bioorg Med Chem. **15**, 6810-6818
217 Kapuria, V., Peterson, L. F., Fang, D., Bornmann, W. G., Talpaz, M. and Donato, N. J. (2010) Deubiquitinase inhibition by small-molecule WP1130 triggers aggresome formation and tumor cell apoptosis. Cancer Res. **70**, 9265-9276
218 Lee, B. H., Lee, M. J., Park, S., Oh, D. C., Elsasser, S., Chen, P. C., Gartner, C., Dimova, N., Hanna, J., Gygi, S. P., Wilson, S. M., King, R. W. and Finley, D. (2010) Enhancement of proteasome activity by a small-molecule inhibitor of USP14. Nature. **467**, 179-184
219 Orcutt, S. J., Wu, J., Eddins, M. J., Leach, C. A. and Strickler, J. E. (2012) Bioluminescence assay platform for selective and sensitive detection of Ub/Ubl proteases. Biochim Biophys Acta. **1823**, 2079-2086
220 Engelman, J. A., Luo, J. and Cantley, L. C. (2006) The evolution of phosphatidylinositol 3-kinases as regulators of growth and metabolism. Nat Rev Genet. **7**, 606-619
221 Engelman, J. A. (2009) Targeting PI3K signalling in cancer: opportunities, challenges and limitations. Nat Rev Cancer. **9**, 550-562
222 Zagouri, F., Sergentanis, T. N., Chrysikos, D., Filipits, M. and Bartsch, R. (2012) mTOR inhibitors in breast cancer: A systematic review. Gynecol Oncol
223 Coppin, C., Kollmannsberger, C., Le, L., Porzsolt, F. and Wilt, T. J. (2011) Targeted therapy for advanced renal cell cancer (RCC): a Cochrane systematic review of published randomised trials. BJU Int. **108**, 1556-1563
224 McNamara, C. R. and Degterev, A. (2011) Small-molecule inhibitors of the PI3K signaling network. Future Med Chem. **3**, 549-565
225 Whitman, M., Kaplan, D., Roberts, T. and Cantley, L. (1987) Evidence for two distinct phosphatidylinositol kinases in fibroblasts. Implications for cellular regulation. Biochem J. **247**, 165-174
226 Whitman, M., Downes, C. P., Keeler, M., Keller, T. and Cantley, L. (1988) Type I phosphatidylinositol kinase makes a novel inositol phospholipid, phosphatidylinositol-3-phosphate. Nature. **332**, 644-646
227 Vanhaesebroeck, B., Guillermet-Guibert, J., Graupera, M. and Bilanges, B. (2010) The emerging mechanisms of isoform-specific PI3K signalling. Nat Rev Mol Cell Biol. **11**, 329-341
228 Liu, P., Cheng, H., Roberts, T. M. and Zhao, J. J. (2009) Targeting the phosphoinositide 3-kinase pathway in cancer. Nat Rev Drug Discov. **8**, 627-644
229 Falasca, M. and Maffucci, T. (2007) Role of class II phosphoinositide 3-kinase in cell signalling. Biochem Soc Trans. **35**, 211-214
230 Falasca, M. and Maffucci, T. (2009) Rethinking phosphatidylinositol 3-monophosphate. Biochim Biophys Acta. **1793**, 1795-1803
231 MacDougall, L. K., Domin, J. and Waterfield, M. D. (1995) A family of phosphoinositide 3-kinases in Drosophila identifies a new mediator of signal transduction. Curr Biol. **5**, 1404-1415
232 Virbasius, J. V., Guilherme, A. and Czech, M. P. (1996) Mouse p170 is a novel phosphatidylinositol 3-kinase containing a C2 domain. J Biol Chem. **271**, 13304-13307

233 Falasca, M., Hughes, W. E., Dominguez, V., Sala, G., Fostira, F., Fang, M. Q., Cazzolli, R., Shepherd, P. R., James, D. E. and Maffucci, T. (2007) The role of phosphoinositide 3-kinase C2alpha in insulin signaling. J Biol Chem. **282**, 28226-28236
234 Wen, P. J., Osborne, S. L., Morrow, I. C., Parton, R. G., Domin, J. and Meunier, F. A. (2008) Ca2+-regulated pool of phosphatidylinositol-3-phosphate produced by phosphatidylinositol 3-kinase C2alpha on neurosecretory vesicles. Mol Biol Cell. **19**, 5593-5603
235 Schu, P. V., Takegawa, K., Fry, M. J., Stack, J. H., Waterfield, M. D. and Emr, S. D. (1993) Phosphatidylinositol 3-kinase encoded by yeast VPS34 gene essential for protein sorting. Science. **260**, 88-91
236 Volinia, S., Dhand, R., Vanhaesebroeck, B., MacDougall, L. K., Stein, R., Zvelebil, M. J., Domin, J., Panaretou, C. and Waterfield, M. D. (1995) A human phosphatidylinositol 3-kinase complex related to the yeast Vps34p-Vps15p protein sorting system. EMBO J. **14**, 3339-3348
237 Funderburk, S. F., Wang, Q. J. and Yue, Z. (2010) The Beclin 1-VPS34 complex--at the crossroads of autophagy and beyond. Trends Cell Biol. **20**, 355-362
238 Lindmo, K. and Stenmark, H. (2006) Regulation of membrane traffic by phosphoinositide 3-kinases. J Cell Sci. **119**, 605-614
239 Vieira, O. V., Botelho, R. J., Rameh, L., Brachmann, S. M., Matsuo, T., Davidson, H. W., Schreiber, A., Backer, J. M., Cantley, L. C. and Grinstein, S. (2001) Distinct roles of class I and class III phosphatidylinositol 3-kinases in phagosome formation and maturation. J Cell Biol. **155**, 19-25
240 White, M. F. (1998) The IRS-signaling system: a network of docking proteins that mediate insulin and cytokine action. Recent Prog Horm Res. **53**, 119-138
241 Wang, J., Auger, K. R., Jarvis, L., Shi, Y. and Roberts, T. M. (1995) Direct association of Grb2 with the p85 subunit of phosphatidylinositol 3-kinase. J Biol Chem. **270**, 12774-12780
242 Gupta, S., Ramjaun, A. R., Haiko, P., Wang, Y., Warne, P. H., Nicke, B., Nye, E., Stamp, G., Alitalo, K. and Downward, J. (2007) Binding of ras to phosphoinositide 3-kinase p110alpha is required for ras-driven tumorigenesis in mice. Cell. **129**, 957-968
243 Ballou, L. M., Chattopadhyay, M., Li, Y., Scarlata, S. and Lin, R. Z. (2006) Galphaq binds to p110alpha/p85alpha phosphoinositide 3-kinase and displaces Ras. Biochem J. **394**, 557-562
244 Taboubi, S., Garrouste, F., Parat, F., Pommier, G., Faure, E., Monferran, S., Kovacic, H. and Lehmann, M. (2010) Gq-coupled purinergic receptors inhibit insulin-like growth factor-I/phosphoinositide 3-kinase pathway-dependent keratinocyte migration. Mol Biol Cell. **21**, 946-955
245 Maehama, T. and Dixon, J. E. (1998) The tumor suppressor, PTEN/MMAC1, dephosphorylates the lipid second messenger, phosphatidylinositol 3,4,5-trisphosphate. J Biol Chem. **273**, 13375-13378
246 Li, J., Yen, C., Liaw, D., Podsypanina, K., Bose, S., Wang, S. I., Puc, J., Miliaresis, C., Rodgers, L., McCombie, R., Bigner, S. H., Giovanella, B. C., Ittmann, M., Tycko, B., Hibshoosh, H., Wigler, M. H. and Parsons, R. (1997) PTEN, a putative protein tyrosine phosphatase gene mutated in human brain, breast, and prostate cancer. Science. **275**, 1943-1947

247 Steck, P. A., Pershouse, M. A., Jasser, S. A., Yung, W. K., Lin, H., Ligon, A. H., Langford, L. A., Baumgard, M. L., Hattier, T., Davis, T., Frye, C., Hu, R., Swedlund, B., Teng, D. H. and Tavtigian, S. V. (1997) Identification of a candidate tumour suppressor gene, MMAC1, at chromosome 10q23.3 that is mutated in multiple advanced cancers. Nat Genet. **15**, 356-362
248 Di Cristofano, A., Pesce, B., Cordon-Cardo, C. and Pandolfi, P. P. (1998) Pten is essential for embryonic development and tumour suppression. Nat Genet. **19**, 348-355
249 Podsypanina, K., Ellenson, L. H., Nemes, A., Gu, J., Tamura, M., Yamada, K. M., Cordon-Cardo, C., Catoretti, G., Fisher, P. E. and Parsons, R. (1999) Mutation of Pten/Mmac1 in mice causes neoplasia in multiple organ systems. Proc Natl Acad Sci U S A. **96**, 1563-1568
250 Suzuki, A., de la Pompa, J. L., Stambolic, V., Elia, A. J., Sasaki, T., del Barco Barrantes, I., Ho, A., Wakeham, A., Itie, A., Khoo, W., Fukumoto, M. and Mak, T. W. (1998) High cancer susceptibility and embryonic lethality associated with mutation of the PTEN tumor suppressor gene in mice. In Curr Biol. pp. 1169-1178, England
251 Di Cristofano, A., De Acetis, M., Koff, A., Cordon-Cardo, C. and Pandolfi, P. P. (2001) Pten and p27KIP1 cooperate in prostate cancer tumor suppression in the mouse. Nat Genet. **27**, 222-224
252 Di Cristofano, A., Kotsi, P., Peng, Y. F., Cordon-Cardo, C., Elkon, K. B. and Pandolfi, P. P. (1999) Impaired Fas response and autoimmunity in Pten+/- mice. In Science. pp. 2122-2125, United States
253 Alimonti, A., Carracedo, A., Clohessy, J. G., Trotman, L. C., Nardella, C., Egia, A., Salmena, L., Sampieri, K., Haveman, W. J., Brogi, E., Richardson, A. L., Zhang, J. and Pandolfi, P. P. (2010) Subtle variations in Pten dose determine cancer susceptibility. In Nat Genet. pp. 454-458, United States
254 Song, M. S., Salmena, L. and Pandolfi, P. P. (2012) The functions and regulation of the PTEN tumour suppressor. Nat Rev Mol Cell Biol. **13**, 283-296
255 Stambolic, V., Suzuki, A., de la Pompa, J. L., Brothers, G. M., Mirtsos, C., Sasaki, T., Ruland, J., Penninger, J. M., Siderovski, D. P. and Mak, T. W. (1998) Negative regulation of PKB/Akt-dependent cell survival by the tumor suppressor PTEN. Cell. **95**, 29-39
256 Sun, H., Lesche, R., Li, D. M., Liliental, J., Zhang, H., Gao, J., Gavrilova, N., Mueller, B., Liu, X. and Wu, H. (1999) PTEN modulates cell cycle progression and cell survival by regulating phosphatidylinositol 3,4,5,-trisphosphate and Akt/protein kinase B signaling pathway. Proc Natl Acad Sci U S A. **96**, 6199-6204
257 Haslam, R. J., Koide, H. B. and Hemmings, B. A. (1993) Pleckstrin domain homology. Nature. **363**, 309-310
258 Rong, S. B., Hu, Y., Enyedy, I., Powis, G., Meuillet, E. J., Wu, X., Wang, R., Wang, S. and Kozikowski, A. P. (2001) Molecular modeling studies of the Akt PH domain and its interaction with phosphoinositides. J Med Chem. **44**, 898-908
259 Komander, D., Fairservice, A., Deak, M., Kular, G. S., Prescott, A. R., Peter Downes, C., Safrany, S. T., Alessi, D. R. and van Aalten, D. M. (2004) Structural insights into the regulation of PDK1 by phosphoinositides and inositol phosphates. EMBO J. **23**, 3918-3928

260 Mora, A., Komander, D., van Aalten, D. M. and Alessi, D. R. (2004) PDK1, the master regulator of AGC kinase signal transduction. Semin Cell Dev Biol. **15**, 161-170
261 Alessi, D. R., James, S. R., Downes, C. P., Holmes, A. B., Gaffney, P. R., Reese, C. B. and Cohen, P. (1997) Characterization of a 3-phosphoinositide-dependent protein kinase which phosphorylates and activates protein kinase Balpha. Curr Biol. **7**, 261-269
262 Milburn, C. C., Deak, M., Kelly, S. M., Price, N. C., Alessi, D. R. and Van Aalten, D. M. (2003) Binding of phosphatidylinositol 3,4,5-trisphosphate to the pleckstrin homology domain of protein kinase B induces a conformational change. Biochem J. **375**, 531-538
263 Casamayor, A., Morrice, N. A. and Alessi, D. R. (1999) Phosphorylation of Ser-241 is essential for the activity of 3-phosphoinositide-dependent protein kinase-1: identification of five sites of phosphorylation in vivo. Biochem J. **342 (Pt 2)**, 287-292
264 Sarbassov, D. D., Guertin, D. A., Ali, S. M. and Sabatini, D. M. (2005) Phosphorylation and regulation of Akt/PKB by the rictor-mTOR complex. Science. **307**, 1098-1101
265 Kim, D. H., Sarbassov, D. D., Ali, S. M., King, J. E., Latek, R. R., Erdjument-Bromage, H., Tempst, P. and Sabatini, D. M. (2002) mTOR interacts with raptor to form a nutrient-sensitive complex that signals to the cell growth machinery. In Cell. pp. 163-175, United States
266 Hara, K., Maruki, Y., Long, X., Yoshino, K., Oshiro, N., Hidayat, S., Tokunaga, C., Avruch, J. and Yonezawa, K. (2002) Raptor, a binding partner of target of rapamycin (TOR), mediates TOR action. Cell. **110**, 177-189
267 Loewith, R., Jacinto, E., Wullschleger, S., Lorberg, A., Crespo, J. L., Bonenfant, D., Oppliger, W., Jenoe, P. and Hall, M. N. (2002) Two TOR complexes, only one of which is rapamycin sensitive, have distinct roles in cell growth control. Mol Cell. **10**, 457-468
268 Gan, X., Wang, J., Su, B., Wu, D., dan.wu@yale.edu, Gan, X., Wang, J., Su, B. and Wu, D. (2011) Evidence for Direct Activation of mTORC2 Kinase Activity by Phosphatidylinositol 3,4,5-Trisphosphate. Journal of Biological Chemistry. **286**, 10998-11002
269 Tato, I., Bartrons, R., Ventura, F. and Rosa, J. L. (2011) Amino acids activate mammalian target of rapamycin complex 2 (mTORC2) via PI3K/Akt signaling. J Biol Chem. **286**, 6128-6142
270 Staal, S. P., Hartley, J. W. and Rowe, W. P. (1977) Isolation of transforming murine leukemia viruses from mice with a high incidence of spontaneous lymphoma. Proc Natl Acad Sci U S A. **74**, 3065-3067
271 Staal, S. P. (1987) Molecular cloning of the akt oncogene and its human homologues AKT1 and AKT2: amplification of AKT1 in a primary human gastric adenocarcinoma. Proc Natl Acad Sci U S A. **84**, 5034-5037
272 Jones, P. F., Jakubowicz, T., Pitossi, F. J., Maurer, F. and Hemmings, B. A. (1991) Molecular cloning and identification of a serine/threonine protein kinase of the second-messenger subfamily. Proc Natl Acad Sci U S A. **88**, 4171-4175
273 Coffer, P. J. and Woodgett, J. R. (1992) Molecular cloning and characterisation of a novel putative protein-serine kinase related to the cAMP-dependent and protein kinase C families. Eur J Biochem. **205**, 1217

274 Jones, P. F., Jakubowicz, T. and Hemmings, B. A. (1991) Molecular cloning of a second form of rac protein kinase. Cell Regul. **2**, 1001-1009
275 Brodbeck, D., Cron, P. and Hemmings, B. A. (1999) A human protein kinase Bgamma with regulatory phosphorylation sites in the activation loop and in the C-terminal hydrophobic domain. J Biol Chem. **274**, 9133-9136
276 Hornbeck, P. V., Kornhauser, J. M., Tkachev, S., Zhang, B., Skrzypek, E., Murray, B., Latham, V. and Sullivan, M. (2012) PhosphoSitePlus: a comprehensive resource for investigating the structure and function of experimentally determined post-translational modifications in man and mouse. Nucleic Acids Res. **40**, D261-270
277 Dan, H. C., Sun, M., Kaneko, S., Feldman, R. I., Nicosia, S. V., Wang, H. G., Tsang, B. K. and Cheng, J. Q. (2004) Akt phosphorylation and stabilization of X-linked inhibitor of apoptosis protein (XIAP). J Biol Chem. **279**, 5405-5412
278 del Peso, L., Gonzalez-Garcia, M., Page, C., Herrera, R. and Nunez, G. (1997) Interleukin-3-induced phosphorylation of BAD through the protein kinase Akt. Science. **278**, 687-689
279 Wullschleger, S., Loewith, R. and Hall, M. N. (2006) TOR signaling in growth and metabolism. Cell. **124**, 471-484
280 Inoki, K., Li, Y., Zhu, T., Wu, J. and Guan, K. L. (2002) TSC2 is phosphorylated and inhibited by Akt and suppresses mTOR signalling. Nat Cell Biol. **4**, 648-657
281 Manning, B. D., Tee, A. R., Logsdon, M. N., Blenis, J. and Cantley, L. C. (2002) Identification of the tuberous sclerosis complex-2 tumor suppressor gene product tuberin as a target of the phosphoinositide 3-kinase/akt pathway. Mol Cell. **10**, 151-162
282 Garami, A., Zwartkruis, F. J., Nobukuni, T., Joaquin, M., Roccio, M., Stocker, H., Kozma, S. C., Hafen, E., Bos, J. L. and Thomas, G. (2003) Insulin activation of Rheb, a mediator of mTOR/S6K/4E-BP signaling, is inhibited by TSC1 and 2. Mol Cell. **11**, 1457-1466
283 Inoki, K., Li, Y., Xu, T. and Guan, K. L. (2003) Rheb GTPase is a direct target of TSC2 GAP activity and regulates mTOR signaling. Genes Dev. **17**, 1829-1834
284 Sancak, Y., Thoreen, C. C., Peterson, T. R., Lindquist, R. A., Kang, S. A., Spooner, E., Carr, S. A. and Sabatini, D. M. (2007) PRAS40 is an insulin-regulated inhibitor of the mTORC1 protein kinase. Mol Cell. **25**, 903-915
285 Vander Haar, E., Lee, S. I., Bandhakavi, S., Griffin, T. J. and Kim, D. H. (2007) Insulin signalling to mTOR mediated by the Akt/PKB substrate PRAS40. Nat Cell Biol. **9**, 316-323
286 Hahn-Windgassen, A., Nogueira, V., Chen, C. C., Skeen, J. E., Sonenberg, N. and Hay, N. (2005) Akt activates the mammalian target of rapamycin by regulating cellular ATP level and AMPK activity. In J Biol Chem. pp. 32081-32089, United States
287 Ogawara, Y., Kishishita, S., Obata, T., Isazawa, Y., Suzuki, T., Tanaka, K., Masuyama, N. and Gotoh, Y. (2002) Akt enhances Mdm2-mediated ubiquitination and degradation of p53. J Biol Chem. **277**, 21843-21850
288 Zhou, B. P., Liao, Y., Xia, W., Zou, Y., Spohn, B. and Hung, M. C. (2001) HER-2/neu induces p53 ubiquitination via Akt-mediated MDM2 phosphorylation. Nat Cell Biol. **3**, 973-982

289 Shin, I., Yakes, F. M., Rojo, F., Shin, N. Y., Bakin, A. V., Baselga, J. and Arteaga, C. L. (2002) PKB/Akt mediates cell-cycle progression by phosphorylation of p27(Kip1) at threonine 157 and modulation of its cellular localization. Nat Med. **8**, 1145-1152
290 Viglietto, G., Motti, M. L., Bruni, P., Melillo, R. M., D'Alessio, A., Califano, D., Vinci, F., Chiappetta, G., Tsichlis, P., Bellacosa, A., Fusco, A. and Santoro, M. (2002) Cytoplasmic relocalization and inhibition of the cyclin-dependent kinase inhibitor p27(Kip1) by PKB/Akt-mediated phosphorylation in breast cancer. Nat Med. **8**, 1136-1144
291 Liang, J., Zubovitz, J., Petrocelli, T., Kotchetkov, R., Connor, M. K., Han, K., Lee, J. H., Ciarallo, S., Catzavelos, C., Beniston, R., Franssen, E. and Slingerland, J. M. (2002) PKB/Akt phosphorylates p27, impairs nuclear import of p27 and opposes p27-mediated G1 arrest. Nat Med. **8**, 1153-1160
292 Rayasam, G. V., Tulasi, V. K., Sodhi, R., Davis, J. A. and Ray, A. (2009) Glycogen synthase kinase 3: more than a namesake. Br J Pharmacol. **156**, 885-898
293 Dansen, T. B. and Burgering, B. M. (2008) Unravelling the tumor-suppressive functions of FOXO proteins. Trends Cell Biol. **18**, 421-429
294 Paik, J. H., Kollipara, R., Chu, G., Ji, H., Xiao, Y., Ding, Z., Miao, L., Tothova, Z., Horner, J. W., Carrasco, D. R., Jiang, S., Gilliland, D. G., Chin, L., Wong, W. H., Castrillon, D. H. and DePinho, R. A. (2007) FoxOs are lineage-restricted redundant tumor suppressors and regulate endothelial cell homeostasis. Cell. **128**, 309-323
295 Seoane, J., Le, H. V., Shen, L., Anderson, S. A. and Massague, J. (2004) Integration of Smad and forkhead pathways in the control of neuroepithelial and glioblastoma cell proliferation. Cell. **117**, 211-223
296 Medema, R. H., Kops, G. J., Bos, J. L. and Burgering, B. M. (2000) AFX-like Forkhead transcription factors mediate cell-cycle regulation by Ras and PKB through p27kip1. Nature. **404**, 782-787
297 Brunet, A., Bonni, A., Zigmond, M. J., Lin, M. Z., Juo, P., Hu, L. S., Anderson, M. J., Arden, K. C., Blenis, J. and Greenberg, M. E. (1999) Akt promotes cell survival by phosphorylating and inhibiting a Forkhead transcription factor. Cell. **96**, 857-868
298 Tang, T. T., Dowbenko, D., Jackson, A., Toney, L., Lewin, D. A., Dent, A. L. and Lasky, L. A. (2002) The forkhead transcription factor AFX activates apoptosis by induction of the BCL-6 transcriptional repressor. J Biol Chem. **277**, 14255-14265
299 Kops, G. J., de Ruiter, N. D., De Vries-Smits, A. M., Powell, D. R., Bos, J. L. and Burgering, B. M. (1999) Direct control of the Forkhead transcription factor AFX by protein kinase B. Nature. **398**, 630-634
300 Nakae, J., Park, B. C. and Accili, D. (1999) Insulin stimulates phosphorylation of the forkhead transcription factor FKHR on serine 253 through a Wortmannin-sensitive pathway. J Biol Chem. **274**, 15982-15985
301 Rena, G., Guo, S., Cichy, S. C., Unterman, T. G. and Cohen, P. (1999) Phosphorylation of the transcription factor forkhead family member FKHR by protein kinase B. J Biol Chem. **274**, 17179-17183
302 Takaishi, H., Konishi, H., Matsuzaki, H., Ono, Y., Shirai, Y., Saito, N., Kitamura, T., Ogawa, W., Kasuga, M., Kikkawa, U. and Nishizuka, Y. (1999)

Regulation of nuclear translocation of forkhead transcription factor AFX by protein kinase B. Proc Natl Acad Sci U S A. **96**, 11836-11841
303 Tang, E. D., Nuñez, G., Barr, F. G. and Guan, K. L. (1999) Negative regulation of the forkhead transcription factor FKHR by Akt. J Biol Chem. **274**, 16741-16746
304 Samuels, Y., Wang, Z., Bardelli, A., Silliman, N., Ptak, J., Szabo, S., Yan, H., Gazdar, A., Powell, S. M., Riggins, G. J., Willson, J. K., Markowitz, S., Kinzler, K. W., Vogelstein, B. and Velculescu, V. E. (2004) High frequency of mutations of the PIK3CA gene in human cancers. Science. **304**, 554
305 Samuels, Y. and Waldman, T. (2010) Oncogenic mutations of PIK3CA in human cancers. Curr Top Microbiol Immunol. **347**, 21-41
306 Philp, A. J., Campbell, I. G., Leet, C., Vincan, E., Rockman, S. P., Whitehead, R. H., Thomas, R. J. and Phillips, W. A. (2001) The phosphatidylinositol 3'-kinase p85alpha gene is an oncogene in human ovarian and colon tumors. Cancer Res. **61**, 7426-7429
307 Cheung, L. W., Hennessy, B. T., Li, J., Yu, S., Myers, A. P., Djordjevic, B., Lu, Y., Stemke-Hale, K., Dyer, M. D., Zhang, F., Ju, Z., Cantley, L. C., Scherer, S. E., Liang, H., Lu, K. H., Broaddus, R. R. and Mills, G. B. (2011) High frequency of PIK3R1 and PIK3R2 mutations in endometrial cancer elucidates a novel mechanism for regulation of PTEN protein stability. Cancer Discov. **1**, 170-185
308 Carpten, J. D., Faber, A. L., Horn, C., Donoho, G. P., Briggs, S. L., Robbins, C. M., Hostetter, G., Boguslawski, S., Moses, T. Y., Savage, S., Uhlik, M., Lin, A., Du, J., Qian, Y. W., Zeckner, D. J., Tucker-Kellogg, G., Touchman, J., Patel, K., Mousses, S., Bittner, M., Schevitz, R., Lai, M. H., Blanchard, K. L. and Thomas, J. E. (2007) A transforming mutation in the pleckstrin homology domain of AKT1 in cancer. Nature. **448**, 439-444
309 Kim, M. S., Jeong, E. G., Yoo, N. J. and Lee, S. H. (2008) Mutational analysis of oncogenic AKT E17K mutation in common solid cancers and acute leukaemias. Br J Cancer. **98**, 1533-1535
310 Malanga, D., Scrima, M., De Marco, C., Fabiani, F., De Rosa, N., De Gisi, S., Malara, N., Savino, R., Rocco, G., Chiappetta, G., Franco, R., Tirino, V., Pirozzi, G. and Viglietto, G. (2008) Activating E17K mutation in the gene encoding the protein kinase AKT1 in a subset of squamous cell carcinoma of the lung. Cell Cycle. **7**, 665-669
311 Parsons, D. W., Wang, T. L., Samuels, Y., Bardelli, A., Cummins, J. M., DeLong, L., Silliman, N., Ptak, J., Szabo, S., Willson, J. K., Markowitz, S., Kinzler, K. W., Vogelstein, B., Lengauer, C. and Velculescu, V. E. (2005) Colorectal cancer: mutations in a signalling pathway. Nature. **436**, 792
312 Davies, M. A., Stemke-Hale, K., Tellez, C., Calderone, T. L., Deng, W., Prieto, V. G., Lazar, A. J., Gershenwald, J. E. and Mills, G. B. (2008) A novel AKT3 mutation in melanoma tumours and cell lines. Br J Cancer. **99**, 1265-1268
313 Gerlinger, M., Rowan, A. J., Horswell, S., Larkin, J., Endesfelder, D., Gronroos, E., Martinez, P., Matthews, N., Stewart, A., Tarpey, P., Varela, I., Phillimore, B., Begum, S., McDonald, N. Q., Butler, A., Jones, D., Raine, K., Latimer, C., Santos, C. R., Nohadani, M., Eklund, A. C., Spencer-Dene, B., Clark, G., Pickering, L., Stamp, G., Gore, M., Szallasi, Z., Downward, J., Futreal, P. A. and Swanton, C. (2012) Intratumor heterogeneity and branched evolution revealed by multiregion sequencing. N Engl J Med. **366**, 883-892

314 Pedrero, J. M., Carracedo, D. G., Pinto, C. M., Zapatero, A. H., Rodrigo, J. P., Nieto, C. S. and Gonzalez, M. V. (2005) Frequent genetic and biochemical alterations of the PI 3-K/AKT/PTEN pathway in head and neck squamous cell carcinoma. Int J Cancer. **114**, 242-248
315 Woenckhaus, J., Steger, K., Werner, E., Fenic, I., Gamerdinger, U., Dreyer, T. and Stahl, U. (2002) Genomic gain of PIK3CA and increased expression of p110alpha are associated with progression of dysplasia into invasive squamous cell carcinoma. J Pathol. **198**, 335-342
316 Massion, P. P., Kuo, W. L., Stokoe, D., Olshen, A. B., Treseler, P. A., Chin, K., Chen, C., Polikoff, D., Jain, A. N., Pinkel, D., Albertson, D. G., Jablons, D. M. and Gray, J. W. (2002) Genomic copy number analysis of non-small cell lung cancer using array comparative genomic hybridization: implications of the phosphatidylinositol 3-kinase pathway. Cancer Res. **62**, 3636-3640
317 Bjorkqvist, A. M., Husgafvel-Pursiainen, K., Anttila, S., Karjalainen, A., Tammilehto, L., Mattson, K., Vainio, H. and Knuutila, S. (1998) DNA gains in 3q occur frequently in squamous cell carcinoma of the lung, but not in adenocarcinoma. Genes Chromosomes Cancer. **22**, 79-82
318 Ma, Y. Y., Wei, S. J., Lin, Y. C., Lung, J. C., Chang, T. C., Whang-Peng, J., Liu, J. M., Yang, D. M., Yang, W. K. and Shen, C. Y. (2000) PIK3CA as an oncogene in cervical cancer. Oncogene. **19**, 2739-2744
319 Byun, D. S., Cho, K., Ryu, B. K., Lee, M. G., Park, J. I., Chae, K. S., Kim, H. J. and Chi, S. G. (2003) Frequent monoallelic deletion of PTEN and its reciprocal associatioin with PIK3CA amplification in gastric carcinoma. Int J Cancer. **104**, 318-327
320 Miller, C. T., Moy, J. R., Lin, L., Schipper, M., Normolle, D., Brenner, D. E., Iannettoni, M. D., Orringer, M. B. and Beer, D. G. (2003) Gene amplification in esophageal adenocarcinomas and Barrett's with high-grade dysplasia. Clin Cancer Res. **9**, 4819-4825
321 Brugge, J., Hung, M. C. and Mills, G. B. (2007) A new mutational AKTivation in the PI3K pathway. Cancer Cell. **12**, 104-107
322 Crowder, R. J., Phommaly, C., Tao, Y., Hoog, J., Luo, J., Perou, C. M., Parker, J. S., Miller, M. A., Huntsman, D. G., Lin, L., Snider, J., Davies, S. R., Olson, J. A., Jr., Watson, M. A., Saporita, A., Weber, J. D. and Ellis, M. J. (2009) PIK3CA and PIK3CB inhibition produce synthetic lethality when combined with estrogen deprivation in estrogen receptor-positive breast cancer. Cancer Res. **69**, 3955-3962
323 Cheng, J. Q., Ruggeri, B., Klein, W. M., Sonoda, G., Altomare, D. A., Watson, D. K. and Testa, J. R. (1996) Amplification of AKT2 in human pancreatic cells and inhibition of AKT2 expression and tumorigenicity by antisense RNA. Proc Natl Acad Sci U S A. **93**, 3636-3641
324 Ruggeri, B. A., Huang, L., Wood, M., Cheng, J. Q. and Testa, J. R. (1998) Amplification and overexpression of the AKT2 oncogene in a subset of human pancreatic ductal adenocarcinomas. Mol Carcinog. **21**, 81-86
325 Bellacosa, A., de Feo, D., Godwin, A. K., Bell, D. W., Cheng, J. Q., Altomare, D. A., Wan, M., Dubeau, L., Scambia, G., Masciullo, V., Ferrandina, G., Benedetti Panici, P., Mancuso, S., Neri, G. and Testa, J. R. (1995) Molecular alterations of the AKT2 oncogene in ovarian and breast carcinomas. Int J Cancer. **64**, 280-285
326 Maurer, M., Su, T., Saal, L. H., Koujak, S., Hopkins, B. D., Barkley, C. R., Wu, J., Nandula, S., Dutta, B., Xie, Y., Chin, Y. R., Kim, D. I., Ferris, J. S., Gruvberger-Saal,

S. K., Laakso, M., Wang, X., Memeo, L., Rojtman, A., Matos, T., Yu, J. S., Cordon-Cardo, C., Isola, J., Terry, M. B., Toker, A., Mills, G. B., Zhao, J. J., Murty, V. V., Hibshoosh, H. and Parsons, R. (2009) 3-Phosphoinositide-dependent kinase 1 potentiates upstream lesions on the phosphatidylinositol 3-kinase pathway in breast carcinoma. Cancer Res. **69**, 6299-6306
327 Frederick, L., Wang, X. Y., Eley, G. and James, C. D. (2000) Diversity and frequency of epidermal growth factor receptor mutations in human glioblastomas. Cancer Res. **60**, 1383-1387
328 Paez, J. G., Janne, P. A., Lee, J. C., Tracy, S., Greulich, H., Gabriel, S., Herman, P., Kaye, F. J., Lindeman, N., Boggon, T. J., Naoki, K., Sasaki, H., Fujii, Y., Eck, M. J., Sellers, W. R., Johnson, B. E. and Meyerson, M. (2004) EGFR mutations in lung cancer: correlation with clinical response to gefitinib therapy. Science. **304**, 1497-1500
329 Lynch, T. J., Bell, D. W., Sordella, R., Gurubhagavatula, S., Okimoto, R. A., Brannigan, B. W., Harris, P. L., Haserlat, S. M., Supko, J. G., Haluska, F. G., Louis, D. N., Christiani, D. C., Settleman, J. and Haber, D. A. (2004) Activating mutations in the epidermal growth factor receptor underlying responsiveness of non-small-cell lung cancer to gefitinib. N Engl J Med. **350**, 2129-2139
330 Slamon, D. J., Clark, G. M., Wong, S. G., Levin, W. J., Ullrich, A. and McGuire, W. L. (1987) Human breast cancer: correlation of relapse and survival with amplification of the HER-2/neu oncogene. Science. **235**, 177-182
331 Toikkanen, S., Helin, H., Isola, J. and Joensuu, H. (1992) Prognostic significance of HER-2 oncoprotein expression in breast cancer: a 30-year follow-up. J Clin Oncol. **10**, 1044-1048
332 Park, D. I., Yun, J. W., Park, J. H., Oh, S. J., Kim, H. J., Cho, Y. K., Sohn, C. I., Jeon, W. K., Kim, B. I., Yoo, C. H., Son, B. H., Cho, E. Y., Chae, S. W., Kim, E. J., Sohn, J. H., Ryu, S. H. and Sepulveda, A. R. (2006) HER-2/neu amplification is an independent prognostic factor in gastric cancer. Dig Dis Sci. **51**, 1371-1379
333 Garcia, J. M., Silva, J., Pena, C., Garcia, V., Rodriguez, R., Cruz, M. A., Cantos, B., Provencio, M., Espana, P. and Bonilla, F. (2004) Promoter methylation of the PTEN gene is a common molecular change in breast cancer. Genes Chromosomes Cancer. **41**, 117-124
334 Goel, A., Arnold, C. N., Niedzwiecki, D., Carethers, J. M., Dowell, J. M., Wasserman, L., Compton, C., Mayer, R. J., Bertagnolli, M. M. and Boland, C. R. (2004) Frequent inactivation of PTEN by promoter hypermethylation in microsatellite instability-high sporadic colorectal cancers. Cancer Res. **64**, 3014-3021
335 Wang, X., Trotman, L. C., Koppie, T., Alimonti, A., Chen, Z., Gao, Z., Wang, J., Erdjument-Bromage, H., Tempst, P., Cordon-Cardo, C., Pandolfi, P. P. and Jiang, X. (2007) NEDD4-1 is a proto-oncogenic ubiquitin ligase for PTEN. Cell. **128**, 129-139
336 Amodio, N., Scrima, M., Palaia, L., Salman, A. N., Quintiero, A., Franco, R., Botti, G., Pirozzi, P., Rocco, G., De Rosa, N. and Viglietto, G. (2010) Oncogenic role of the E3 ubiquitin ligase NEDD4-1, a PTEN negative regulator, in non-small-cell lung carcinomas. Am J Pathol. **177**, 2622-2634
337 Berns, K., Horlings, H. M., Hennessy, B. T., Madiredjo, M., Hijmans, E. M., Beelen, K., Linn, S. C., Gonzalez-Angulo, A. M., Stemke-Hale, K., Hauptmann, M., Beijersbergen, R. L., Mills, G. B., van de Vijver, M. J. and Bernards, R. (2007) A

functional genetic approach identifies the PI3K pathway as a major determinant of trastuzumab resistance in breast cancer. Cancer Cell. **12**, 395-402
338 Fujita, T., Doihara, H., Kawasaki, K., Takabatake, D., Takahashi, H., Washio, K., Tsukuda, K., Ogasawara, Y. and Shimizu, N. (2006) PTEN activity could be a predictive marker of trastuzumab efficacy in the treatment of ErbB2-overexpressing breast cancer. Br J Cancer. **94**, 247-252
339 Nagata, Y., Lan, K. H., Zhou, X., Tan, M., Esteva, F. J., Sahin, A. A., Klos, K. S., Li, P., Monia, B. P., Nguyen, N. T., Hortobagyi, G. N., Hung, M. C. and Yu, D. (2004) PTEN activation contributes to tumor inhibition by trastuzumab, and loss of PTEN predicts trastuzumab resistance in patients. Cancer Cell. **6**, 117-127
340 Perren, A., Weng, L. P., Boag, A. H., Ziebold, U., Thakore, K., Dahia, P. L., Komminoth, P., Lees, J. A., Mulligan, L. M., Mutter, G. L. and Eng, C. (1999) Immunohistochemical evidence of loss of PTEN expression in primary ductal adenocarcinomas of the breast. Am J Pathol. **155**, 1253-1260
341 Courtney, K. D., Corcoran, R. B. and Engelman, J. A. (2010) The PI3K pathway as drug target in human cancer. J Clin Oncol. **28**, 1075-1083
342 Hudes, G., Carducci, M., Tomczak, P., Dutcher, J., Figlin, R., Kapoor, A., Staroslawska, E., Sosman, J., McDermott, D., Bodrogi, I., Kovacevic, Z., Lesovoy, V., Schmidt-Wolf, I. G., Barbarash, O., Gokmen, E., O'Toole, T., Lustgarten, S., Moore, L. and Motzer, R. J. (2007) Temsirolimus, interferon alfa, or both for advanced renal-cell carcinoma. N Engl J Med. **356**, 2271-2281
343 Yao, J. C., Shah, M. H., Ito, T., Bohas, C. L., Wolin, E. M., Van Cutsem, E., Hobday, T. J., Okusaka, T., Capdevila, J., de Vries, E. G., Tomassetti, P., Pavel, M. E., Hoosen, S., Haas, T., Lincy, J., Lebwohl, D. and Oberg, K. (2011) Everolimus for advanced pancreatic neuroendocrine tumors. N Engl J Med. **364**, 514-523
344 Baselga, J., Campone, M., Piccart, M., Burris, H. A., 3rd, Rugo, H. S., Sahmoud, T., Noguchi, S., Gnant, M., Pritchard, K. I., Lebrun, F., Beck, J. T., Ito, Y., Yardley, D., Deleu, I., Perez, A., Bachelot, T., Vittori, L., Xu, Z., Mukhopadhyay, P., Lebwohl, D. and Hortobagyi, G. N. (2012) Everolimus in postmenopausal hormone-receptor-positive advanced breast cancer. N Engl J Med. **366**, 520-529
345 Fruman, D. A. and Rommel, C. (2011) PI3Kdelta inhibitors in cancer: rationale and serendipity merge in the clinic. Cancer Discov. **1**, 562-572
346 Schimmer, A. D., Dalili, S., Batey, R. A. and Riedl, S. J. (2006) Targeting XIAP for the treatment of malignancy. Cell Death Differ. **13**, 179-188
347 Su, L., Cheng, H., Sampaio, A. V., Nielsen, T. O. and Underhill, T. M. (2010) EGR1 reactivation by histone deacetylase inhibitors promotes synovial sarcoma cell death through the PTEN tumor suppressor. Oncogene. **29**, 4352-4361
348 Noro, R., Gemma, A., Miyanaga, A., Kosaihira, S., Minegishi, Y., Nara, M., Kokubo, Y., Seike, M., Kataoka, K., Matsuda, K., Okano, T., Yoshimura, A. and Kudoh, S. (2007) PTEN inactivation in lung cancer cells and the effect of its recovery on treatment with epidermal growth factor receptor tyrosine kinase inhibitors. Int J Oncol. **31**, 1157-1163
349 Sun, G., Yu, R. T., Evans, R. M. and Shi, Y. (2007) Orphan nuclear receptor TLX recruits histone deacetylases to repress transcription and regulate neural stem cell proliferation. Proc Natl Acad Sci U S A. **104**, 15282-15287
350 Suizu, F., Hiramuki, Y., Okumura, F., Matsuda, M., Okumura, A. J., Hirata, N., Narita, M., Kohno, T., Yokota, J., Bohgaki, M., Obuse, C., Hatakeyama, S., Obata, T. and Noguchi, M. (2009) The E3 ligase TTC3 facilitates ubiquitination and degradation of phosphorylated Akt. Dev Cell. **17**, 800-810

351 Yang, W. L., Wang, J., Chan, C. H., Lee, S. W., Campos, A. D., Lamothe, B., Hur, L., Grabiner, B. C., Lin, X., Darnay, B. G. and Lin, H. K. (2009) The E3 ligase TRAF6 regulates Akt ubiquitination and activation. Science. **325**, 1134-1138
352 Chan, C. H., Li, C. F., Yang, W. L., Gao, Y., Lee, S. W., Feng, Z., Huang, H. Y., Tsai, K. K., Flores, L. G., Shao, Y., Hazle, J. D., Yu, D., Wei, W., Sarbassov, D., Hung, M. C., Nakayama, K. I. and Lin, H. K. (2012) The Skp2-SCF E3 ligase regulates Akt ubiquitination, glycolysis, herceptin sensitivity, and tumorigenesis. Cell. **149**, 1098-1111
353 Mitra, S., Sammani, S., Wang, T., Boone, D. L., Meyer, N. J., Dudek, S. M., Moreno-Vinasco, L., Garcia, J. G. and Jacobson, J. R. (2011) Role of GADD45a in Akt Phosphorylation and Ubiquitination Following Mechanical Stress-Induced Vascular Injury. Am J Respir Crit Care Med
354 Hussain, S., Foreman, O., Perkins, S. L., Witzig, T. E., Miles, R. R., van Deursen, J. and Galardy, P. J. (2010) The de-ubiquitinase UCH-L1 is an oncogene that drives the development of lymphoma in vivo by deregulating PHLPP1 and Akt signaling. Leukemia. **24**, 1641-1655
355 Li, X., Liu, J. and Gao, T. (2009) beta-TrCP-mediated ubiquitination and degradation of PHLPP1 are negatively regulated by Akt. Mol Cell Biol. **29**, 6192-6205
356 Li, X., Stevens, P. D., Yang, H., Gulhati, P., Wang, W., Evers, B. M. and Gao, T. (2012) The deubiquitination enzyme USP46 functions as a tumor suppressor by controlling PHLPP-dependent attenuation of Akt signaling in colon cancer. Oncogene
357 Zhiqiang, Z., Qinghui, Y., Yongqiang, Z., Jian, Z., Xin, Z., Haiying, M. and Yuepeng, G. (2012) USP1 regulates AKT phosphorylation by modulating the stability of PHLPP1 in lung cancer cells. J Cancer Res Clin Oncol. **138**, 1231-1238
358 Uras, I. Z., List, T. and Nijman, S. M. (2012) Ubiquitin-specific protease 4 inhibits mono-ubiquitination of the master growth factor signaling kinase PDK1. PLoS One. **7**, e31003
359 Van Themsche, C., Leblanc, V., Parent, S. and Asselin, E. (2009) X-linked inhibitor of apoptosis protein (XIAP) regulates PTEN ubiquitination, content, and compartmentalization. J Biol Chem. **284**, 20462-20466
360 Maddika, S., Kavela, S., Rani, N., Palicharla, V. R., Pokorny, J. L., Sarkaria, J. N. and Chen, J. (2011) WWP2 is an E3 ubiquitin ligase for PTEN. Nat Cell Biol. **13**, 728-733
361 Maccario, H., Perera, N. M., Gray, A., Downes, C. P. and Leslie, N. R. (2010) Ubiquitination of PTEN (phosphatase and tensin homolog) inhibits phosphatase activity and is enhanced by membrane targeting and hyperosmotic stress. J Biol Chem. **285**, 12620-12628
362 Tolkacheva, T., Boddapati, M., Sanfiz, A., Tsuchida, K., Kimmelman, A. C. and Chan, A. M. (2001) Regulation of PTEN binding to MAGI-2 by two putative phosphorylation sites at threonine 382 and 383. Cancer Res. **61**, 4985-4989
363 Torres, J. and Pulido, R. (2001) The tumor suppressor PTEN is phosphorylated by the protein kinase CK2 at its C terminus. Implications for PTEN stability to proteasome-mediated degradation. J Biol Chem. **276**, 993-998
364 Vazquez, F., Ramaswamy, S., Nakamura, N. and Sellers, W. R. (2000) Phosphorylation of the PTEN tail regulates protein stability and function. Mol Cell Biol. **20**, 5010-5018

365 Yang, J. Y., Zong, C. S., Xia, W., Yamaguchi, H., Ding, Q., Xie, X., Lang, J. Y., Lai, C. C., Chang, C. J., Huang, W. C., Huang, H., Kuo, H. P., Lee, D. F., Li, L. Y., Lien, H. C., Cheng, X., Chang, K. J., Hsiao, C. D., Tsai, F. J., Tsai, C. H., Sahin, A. A., Muller, W. J., Mills, G. B., Yu, D., Hortobagyi, G. N. and Hung, M. C. (2008) ERK promotes tumorigenesis by inhibiting FOXO3a via MDM2-mediated degradation. Nat Cell Biol. **10**, 138-148
366 Huang, H., Regan, K. M., Wang, F., Wang, D., Smith, D. I., van Deursen, J. M. and Tindall, D. J. (2005) Skp2 inhibits FOXO1 in tumor suppression through ubiquitin-mediated degradation. Proc Natl Acad Sci U S A. **102**, 1649-1654
367 Li, F., Xie, P., Fan, Y., Zhang, H., Zheng, L., Gu, D., Patterson, C. and Li, H. (2009) C terminus of Hsc70-interacting protein promotes smooth muscle cell proliferation and survival through ubiquitin-mediated degradation of FoxO1. J Biol Chem. **284**, 20090-20098
368 Kato, S., Ding, J., Pisck, E., Jhala, U. S. and Du, K. (2008) COP1 functions as a FoxO1 ubiquitin E3 ligase to regulate FoxO1-mediated gene expression. J Biol Chem. **283**, 35464-35473
369 Brenkman, A. B., de Keizer, P. L., van den Broek, N. J., Jochemsen, A. G. and Burgering, B. M. (2008) Mdm2 induces mono-ubiquitination of FOXO4. PLoS One. **3**, e2819
370 Burrows, J. F., McGrattan, M. J. and Johnston, J. A. (2005) The DUB/USP17 deubiquitinating enzymes, a multigene family within a tandemly repeated sequence. Genomics. **85**, 524-529
371 Chojnowska-Monga, M. (2011) Involvement of deubiquitinating enzymes in TGF-beta receptor trafficking and signalling. ed.)^eds.), University of liverpool
372 Kittler, R., Heninger, A. K., Franke, K., Habermann, B. and Buchholz, F. (2005) Production of endoribonuclease-prepared short interfering RNAs for gene silencing in mammalian cells. Nat Methods. **2**, 779-784
373 Moss, A. C., Jacobson, G. M., Walker, L. E., Blake, N. W., Marshall, E. and Coulson, J. M. (2009) SCG3 transcript in peripheral blood is a prognostic biomarker for REST-deficient small cell lung cancer. Clin Cancer Res. **15**, 274-283
374 Dignam, J. D., Lebovitz, R. M. and Roeder, R. G. (1983) Accurate transcription initiation by RNA polymerase II in a soluble extract from isolated mammalian nuclei. Nucleic Acids Res. **11**, 1475-1489
375 Poliseno, L., Salmena, L., Zhang, J., Carver, B., Haveman, W. J. and Pandolfi, P. P. (2010) A coding-independent function of gene and pseudogene mRNAs regulates tumour biology. Nature. **465**, 1033-1038
376 Livak, K. J. and Schmittgen, T. D. (2001) Analysis of relative gene expression data using real-time quantitative PCR and the 2(-Delta Delta C(T)) Method. Methods. **25**, 402-408
377 Komander, D. (2009) The emerging complexity of protein ubiquitination. Biochem Soc Trans. **37**, 937-953
378 Evert, B. O., Araujo, J., Vieira-Saecker, A. M., de Vos, R. A., Harendza, S., Klockgether, T. and Wüllner, U. (2006) Ataxin-3 represses transcription via chromatin binding, interaction with histone deacetylase 3, and histone deacetylation. J Neurosci. **26**, 11474-11486
379 Song, E. J., Werner, S. L., Neubauer, J., Stegmeier, F., Aspden, J., Rio, D., Harper, J. W., Elledge, S. J., Kirschner, M. W. and Rape, M. (2010) The Prp19

complex and the Usp4Sart3 deubiquitinating enzyme control reversible ubiquitination at the spliceosome. Genes Dev. **24**, 1434-1447
380 Duex, J. E. and Sorkin, A. (2009) RNA interference screen identifies Usp18 as a regulator of epidermal growth factor receptor synthesis. Mol Biol Cell. **20**, 1833-1844
381 Yao, T. and Cohen, R. E. (2002) A cryptic protease couples deubiquitination and degradation by the proteasome. Nature. **419**, 403-407
382 Clague, M. J. and Urbe, S. (2006) Endocytosis: the DUB version. Trends Cell Biol. **16**, 551-559
383 Liu, J., Xia, H., Kim, M., Xu, L., Li, Y., Zhang, L., Cai, Y., Norberg, H. V., Zhang, T., Furuya, T., Jin, M., Zhu, Z., Wang, H., Yu, J., Hao, Y., Choi, A., Ke, H., Ma, D. and Yuan, J. (2011) Beclin1 controls the levels of p53 by regulating the deubiquitination activity of USP10 and USP13. Cell. **147**, 223-234
384 Nijman, S. M., Huang, T. T., Dirac, A. M., Brummelkamp, T. R., Kerkhoven, R. M., D'Andrea, A. D. and Bernards, R. (2005) The deubiquitinating enzyme USP1 regulates the Fanconi anemia pathway. Mol Cell. **17**, 331-339
385 Buus, R., Faronato, M., Hammond, D. E., Urbe, S. and Clague, M. J. (2009) Deubiquitinase Activities Required for Hepatocyte Growth Factor-Induced Scattering of Epithelial Cells. Curr Biol. **19**, 1463-1466
386 Liu, H., Buus, R., Clague, M. J. and Urbe, S. (2009) Regulation of ErbB2 receptor status by the proteasomal DUB POH1. PLoS One. **4**, e5544
387 Echeverri, C. J. and Perrimon, N. (2006) High-throughput RNAi screening in cultured cells: a user's guide. Nat Rev Genet. **7**, 373-384
388 Echeverri, C. J., Beachy, P. A., Baum, B., Boutros, M., Buchholz, F., Chanda, S. K., Downward, J., Ellenberg, J., Fraser, A. G., Hacohen, N., Hahn, W. C., Jackson, A. L., Kiger, A., Linsley, P. S., Lum, L., Ma, Y., Mathey-Prevot, B., Root, D. E., Sabatini, D. M., Taipale, J., Perrimon, N. and Bernards, R. (2006) Minimizing the risk of reporting false positives in large-scale RNAi screens. Nat Methods. **3**, 777-779
389 Kittler, R., Surendranath, V., Heninger, A. K., Slabicki, M., Theis, M., Putz, G., Franke, K., Caldarelli, A., Grabner, H., Kozak, K., Wagner, J., Rees, E., Korn, B., Frenzel, C., Sachse, C., Sönnichsen, B., Guo, J., Schelter, J., Burchard, J., Linsley, P. S., Jackson, A. L., Habermann, B. and Buchholz, F. (2007) Genome-wide resources of endoribonuclease-prepared short interfering RNAs for specific loss-of-function studies. Nat Methods. **4**, 337-344
390 Thorne, C., Eccles, R. L., Coulson, J. M., Urbé, S. and Clague, M. J. (2011) Isoform-specific localization of the deubiquitinase USP33 to the Golgi apparatus. Traffic. **12**, 1563-1574
391 Shen, W. H., Balajee, A. S., Wang, J., Wu, H., Eng, C., Pandolfi, P. P. and Yin, Y. (2007) Essential role for nuclear PTEN in maintaining chromosomal integrity. Cell. **128**, 157-170
392 Edling, C. E., Selvaggi, F., Buus, R., Maffucci, T., Di Sebastiano, P., Friess, H., Innocenti, P., Kocher, H. M. and Falasca, M. (2010) Key role of phosphoinositide 3-kinase class IB in pancreatic cancer. Clin Cancer Res. **16**, 4928-4937
393 Ng, S. K., Neo, S. Y., Yap, Y. W., Karuturi, R. K., Loh, E. S., Liau, K. H. and Ren, E. C. (2009) Ablation of phosphoinositide-3-kinase class II alpha suppresses hepatoma cell proliferation. Biochem Biophys Res Commun. **387**, 310-315

394 Dubiel, W., Ferrell, K., Dumdey, R., Standera, S., Prehn, S. and Rechsteiner, M. (1995) Molecular cloning and expression of subunit 12: a non-MCP and non-ATPase subunit of the 26 S protease. FEBS Lett. **363**, 97-100
395 Verma, R., Aravind, L., Oania, R., McDonald, W. H., Yates, J. R., 3rd, Koonin, E. V. and Deshaies, R. J. (2002) Role of Rpn11 metalloprotease in deubiquitination and degradation by the 26S proteasome. Science. **298**, 611-615
396 Guenou, H., Kaabeche, K., Dufour, C., Miraoui, H. and Marie, P. J. (2006) Down-regulation of ubiquitin ligase Cbl induced by twist haploinsufficiency in Saethre-Chotzen syndrome results in increased PI3K/Akt signaling and osteoblast proliferation. Am J Pathol. **169**, 1303-1311
397 Paulding, C. A., Ruvolo, M. and Haber, D. A. (2003) The Tre2 (USP6) oncogene is a hominoid-specific gene. Proc Natl Acad Sci U S A. **100**, 2507-2511
398 Gonzalez, E. and McGraw, T. E. (2009) The Akt kinases: isoform specificity in metabolism and cancer. Cell Cycle. **8**, 2502-2508
399 Inoki, K., Li, Y., Zhu, T., Wu, J. and Guan, K. L. (2002) TSC2 is phosphorylated and inhibited by Akt and suppresses mTOR signalling. Nat Cell Biol. **4**, 648-657
400 Carracedo, A., Ma, L., Teruya-Feldstein, J., Rojo, F., Salmena, L., Alimonti, A., Egia, A., Sasaki, A. T., Thomas, G., Kozma, S. C., Papa, A., Nardella, C., Cantley, L. C., Baselga, J. and Pandolfi, P. P. (2008) Inhibition of mTORC1 leads to MAPK pathway activation through a PI3K-dependent feedback loop in human cancer. J Clin Invest. **118**, 3065-3074
401 O'Reilly, K. E., Rojo, F., She, Q. B., Solit, D., Mills, G. B., Smith, D., Lane, H., Hofmann, F., Hicklin, D. J., Ludwig, D. L., Baselga, J. and Rosen, N. (2006) mTOR inhibition induces upstream receptor tyrosine kinase signaling and activates Akt. Cancer Res. **66**, 1500-1508
402 Mao, J. H., Kim, I. J., Wu, D., Climent, J., Kang, H. C., DelRosario, R. and Balmain, A. (2008) FBXW7 targets mTOR for degradation and cooperates with PTEN in tumor suppression. Science. **321**, 1499-1502
403 Konig, R., Chiang, C. Y., Tu, B. P., Yan, S. F., DeJesus, P. D., Romero, A., Bergauer, T., Orth, A., Krueger, U., Zhou, Y. and Chanda, S. K. (2007) A probability-based approach for the analysis of large-scale RNAi screens. Nat Methods. **4**, 847-849
404 Vaux, D. L., Fidler, F. and Cumming, G. (2012) Replicates and repeats--what is the difference and is it significant? A brief discussion of statistics and experimental design. EMBO Rep. **13**, 291-296
405 Koller, A. and Wätzig, H. (2005) Precision and variance components in quantitative gel electrophoresis. Electrophoresis. **26**, 2470-2475
406 Kiyatkin, A. and Aksamitiene, E. (2009) Multistrip western blotting to increase quantitative data output. Methods Mol Biol. **536**, 149-161
407 Zhong, X. and Pittman, R. N. (2006) Ataxin-3 binds VCP/p97 and regulates retrotranslocation of ERAD substrates. Hum Mol Genet. **15**, 2409-2420
408 Kuhlbrodt, K., Janiesch, P. C., Kevei, É., Segref, A., Barikbin, R. and Hoppe, T. (2011) The Machado-Joseph disease deubiquitylase ATX-3 couples longevity and proteostasis. Nat Cell Biol. **13**, 273-281

409 Argenzio, E., Bange, T., Oldrini, B., Bianchi, F., Peesari, R., Mari, S., Di Fiore, P. P., Mann, M. and Polo, S. (2011) Proteomic snapshot of the EGF-induced ubiquitin network. Mol Syst Biol. **7**, 462
410 Pena, V., Liu, S., Bujnicki, J. M., Lührmann, R. and Wahl, M. C. (2007) Structure of a multipartite protein-protein interaction domain in splicing factor prp8 and its link to retinitis pigmentosa. Mol Cell. **25**, 615-624
411 Achsel, T., Ahrens, K., Brahms, H., Teigelkamp, S. and Lührmann, R. (1998) The human U5-220kD protein (hPrp8) forms a stable RNA-free complex with several U5-specific proteins, including an RNA unwindase, a homologue of ribosomal elongation factor EF-2, and a novel WD-40 protein. Mol Cell Biol. **18**, 6756-6766
412 Han, S. S., Yun, H., Son, D. J., Tompkins, V. S., Peng, L., Chung, S. T., Kim, J. S., Park, E. S. and Janz, S. (2010) NF-kappaB/STAT3/PI3K signaling crosstalk in iMyc E mu B lymphoma. Mol Cancer. **9**, 97
413 Kloo, B., Nagel, D., Pfeifer, M., Grau, M., Düwel, M., Vincendeau, M., Dörken, B., Lenz, P., Lenz, G. and Krappmann, D. (2011) Critical role of PI3K signaling for NF-kappaB-dependent survival in a subset of activated B-cell-like diffuse large B-cell lymphoma cells. Proc Natl Acad Sci U S A. **108**, 272-277
414 Park, S., Zhao, D., Hatanpaa, K. J., Mickey, B. E., Saha, D., Boothman, D. A., Story, M. D., Wong, E. T., Burma, S., Georgescu, M. M., Rangnekar, V. M., Chauncey, S. S. and Habib, A. A. (2009) RIP1 activates PI3K-Akt via a dual mechanism involving NF-kappaB-mediated inhibition of the mTOR-S6K-IRS1 negative feedback loop and down-regulation of PTEN. Cancer Res. **69**, 4107-4111
415 Sowa, M. E., Bennett, E. J., Gygi, S. P. and Harper, J. W. (2009) Defining the human deubiquitinating enzyme interaction landscape. Cell. **138**, 389-403
416 Sun, W., Tan, X., Shi, Y., Xu, G., Mao, R., Gu, X., Fan, Y., Yu, Y., Burlingame, S., Zhang, H., Rednam, S. P., Lu, X., Zhang, T., Fu, S., Cao, G., Qin, J. and Yang, J. (2010) USP11 negatively regulates TNFalpha-induced NF-kappaB activation by targeting on IkappaBalpha. Cell Signal. **22**, 386-394
417 Akhavantabasi, S., Akman, H. B., Sapmaz, A., Keller, J., Petty, E. M. and Erson, A. E. (2010) USP32 is an active, membrane-bound ubiquitin protease overexpressed in breast cancers. Mamm Genome. **21**, 388-397
418 Suzuki, M., Setsuie, R. and Wada, K. (2009) Ubiquitin carboxyl-terminal hydrolase l3 promotes insulin signaling and adipogenesis. Endocrinology. **150**, 5230-5239
419 Burgering, B. M. (2008) A brief introduction to FOXOlogy. Oncogene. **27**, 2258-2262
420 Nakae, J., Barr, V. and Accili, D. (2000) Differential regulation of gene expression by insulin and IGF-1 receptors correlates with phosphorylation of a single amino acid residue in the forkhead transcription factor FKHR. EMBO J. **19**, 989-996
421 Zanella, F., Rosado, A., Garcia, B., Carnero, A. and Link, W. (2008) Chemical genetic analysis of FOXO nuclear-cytoplasmic shuttling by using image-based cell screening. Chembiochem. **9**, 2229-2237
422 Kau, T. R., Schroeder, F., Ramaswamy, S., Wojciechowski, C. L., Zhao, J. J., Roberts, T. M., Clardy, J., Sellers, W. R. and Silver, P. A. (2003) A chemical genetic screen identifies inhibitors of regulated nuclear export of a Forkhead transcription factor in PTEN-deficient tumor cells. Cancer Cell. **4**, 463-476

423 Jackson, S. P., Schoenwaelder, S. M., Goncalves, I., Nesbitt, W. S., Yap, C. L., Wright, C. E., Kenche, V., Anderson, K. E., Dopheide, S. M., Yuan, Y., Sturgeon, S. A., Prabaharan, H., Thompson, P. E., Smith, G. D., Shepherd, P. R., Daniele, N., Kulkarni, S., Abbott, B., Saylik, D., Jones, C., Lu, L., Giuliano, S., Hughan, S. C., Angus, J. A., Robertson, A. D. and Salem, H. H. (2005) PI 3-kinase p110beta: a new target for antithrombotic therapy. Nat Med. **11**, 507-514
424 Hirai, H., Sootome, H., Nakatsuru, Y., Miyama, K., Taguchi, S., Tsujioka, K., Ueno, Y., Hatch, H., Majumder, P. K., Pan, B. S. and Kotani, H. (2010) MK-2206, an allosteric Akt inhibitor, enhances antitumor efficacy by standard chemotherapeutic agents or molecular targeted drugs in vitro and in vivo. Mol Cancer Ther. **9**, 1956-1967
425 Brunet, A., Sweeney, L. B., Sturgill, J. F., Chua, K. F., Greer, P. L., Lin, Y., Tran, H., Ross, S. E., Mostoslavsky, R., Cohen, H. Y., Hu, L. S., Cheng, H. L., Jedrychowski, M. P., Gygi, S. P., Sinclair, D. A., Alt, F. W. and Greenberg, M. E. (2004) Stress-dependent regulation of FOXO transcription factors by the SIRT1 deacetylase. Science. **303**, 2011-2015
426 Zanella, F., Rosado, A., Blanco, F., Henderson, B. R., Carnero, A. and Link, W. (2007) An HTS approach to screen for antagonists of the nuclear export machinery using high content cell-based assays. Assay Drug Dev Technol. **5**, 333-341
427 Blake, D. C., Mikse, O. R., Freeman, W. M. and Herzog, C. R. (2010) FOXO3a elicits a pro-apoptotic transcription program and cellular response to human lung carcinogen nicotine-derived nitrosaminoketone (NNK). Lung Cancer. **67**, 37-47
428 Kozaczkiewicz, L. (2009) **USPL1, a novel SUMO isopeptidase**. ed.)^eds.). p. 108, Georg August University GЂttingen
429 Geiss-Friedlander, R. and Melchior, F. (2007) Concepts in sumoylation: a decade on. Nat Rev Mol Cell Biol. **8**, 947-956
430 Behrends, C., Sowa, M. E., Gygi, S. P. and Harper, J. W. (2010) Network organization of the human autophagy system. Nature. **466**, 68-76
431 Huang, T. T., Nijman, S. M., Mirchandani, K. D., Galardy, P. J., Cohn, M. A., Haas, W., Gygi, S. P., Ploegh, H. L., Bernards, R. and D'Andrea, A. D. (2006) Regulation of monoubiquitinated PCNA by DUB autocleavage. Nat Cell Biol. **8**, 339-347
432 Zhiqiang, Z., Qinghui, Y., Yongqiang, Z., Jian, Z., Xin, Z., Haiying, M. and Yuepeng, G. (2012) USP1 regulates AKT phosphorylation by modulating the stability of PHLPP1 in lung cancer cells. J Cancer Res Clin Oncol. **138**, 1231-1238
433 Dobzhansky, T. (1946) Genetics of Natural Populations. Xiii. Recombination and Variability in Populations of Drosophila Pseudoobscura. Genetics. **31**, 269-290
434 Lucchesi, J. C. (1968) Synthetic lethality and semi-lethality among functionally related mutants of Drosophila melanfgaster. Genetics. **59**, 37-44
435 Ooi, S. L., Pan, X., Peyser, B. D., Ye, P., Meluh, P. B., Yuan, D. S., Irizarry, R. A., Bader, J. S., Spencer, F. A. and Boeke, J. D. (2006) Global synthetic-lethality analysis and yeast functional profiling. Trends Genet. **22**, 56-63
436 Farmer, H., McCabe, N., Lord, C. J., Tutt, A. N., Johnson, D. A., Richardson, T. B., Santarosa, M., Dillon, K. J., Hickson, I., Knights, C., Martin, N. M., Jackson, S. P., Smith, G. C. and Ashworth, A. (2005) Targeting the DNA repair defect in BRCA mutant cells as a therapeutic strategy. Nature. **434**, 917-921

437 Nijman, S. M. (2011) Synthetic lethality: general principles, utility and detection using genetic screens in human cells. FEBS Lett. **585**, 1-6
438 Edward, R. (2012) Red/far-red fluorescing DNA-specific anthraquinones for nucl:cyto segmentation and viability reporting in cell-based assays. Methods Enzymol. **505**, 23-45
439 Vossenkämper, A., Marchès, O., Fairclough, P. D., Warnes, G., Stagg, A. J., Lindsay, J. O., Evans, P. C., Luong, l. A., Croft, N. M., Naik, S., Frankel, G. and MacDonald, T. T. (2010) Inhibition of NF-κB signaling in human dendritic cells by the enteropathogenic Escherichia coli effector protein NleE. J Immunol. **185**, 4118-4127
440 Colombo, M., Vallese, S., Peretto, I., Jacq, X., Rain, J. C., Colland, F. and Guedat, P. Synthesis and biological evaluation of 9-oxo-9H-indeno[1,2-b]pyrazine-2,3-dicarbonitrile analogues as potential inhibitors of deubiquitinating enzymes. ChemMedChem. **5**, 552-558
441 Cao, Z., Wu, X., Yen, L., Sweeney, C. and Carraway, K. L., 3rd. (2007) Neuregulin-induced ErbB3 downregulation is mediated by a protein stability cascade involving the E3 ubiquitin ligase Nrdp1. Mol Cell Biol. **27**, 2180-2188
442 Panner, A., Crane, C. A., Weng, C., Feletti, A., Fang, S., Parsa, A. T. and Pieper, R. O. (2010) Ubiquitin-specific protease 8 links the PTEN-Akt-AIP4 pathway to the control of FLIPS stability and TRAIL sensitivity in glioblastoma multiforme. Cancer Res. **70**, 5046-5053
443 Row, P. E., Prior, I. A., McCullough, J., Clague, M. J. and Urbe, S. (2006) The ubiquitin isopeptidase UBPY regulates endosomal ubiquitin dynamics and is essential for receptor down-regulation. J Biol Chem. **281**, 12618-12624
444 Meijer, I. M. and van Leeuwen, J. E. (2011) ERBB2 is a target for USP8-mediated deubiquitination. Cell Signal. **23**, 458-467
445 Guedat, P. and Colland, F. (2007) Patented small molecule inhibitors in the ubiquitin proteasome system. BMC Biochem. **8 Suppl 1**, S14
446 Ho, K. K., Myatt, S. S. and Lam, E. W. (2008) Many forks in the path: cycling with FoxO. Oncogene. **27**, 2300-2311
447 Dimri, G. P., Lee, X., Basile, G., Acosta, M., Scott, G., Roskelley, C., Medrano, E. E., Linskens, M., Rubelj, I. and Pereira-Smith, O. (1995) A biomarker that identifies senescent human cells in culture and in aging skin in vivo. Proc Natl Acad Sci U S A. **92**, 9363-9367
448 Tenbaum, S. P., Ordóñez-Morán, P., Puig, I., Chicote, I., Arqués, O., Landolfi, S., Fernández, Y., Herance, J. R., Gispert, J. D., Mendizabal, L., Aguilar, S., Ramón y Cajal, S., Schwartz, S., Vivancos, A., Espín, E., Rojas, S., Baselga, J., Tabernero, J., Muñoz, A. and Palmer, H. G. (2012) β-catenin confers resistance to PI3K and AKT inhibitors and subverts FOXO3a to promote metastasis in colon cancer. Nat Med. **18**, 892-901
449 Wike-Hooley, J. L., Haveman, J. and Reinhold, H. S. (1984) The relevance of tumour pH to the treatment of malignant disease. Radiother Oncol. **2**, 343-366
450 Burrows, J. F., Kelvin, A. A., McFarlane, C., Burden, R. E., McGrattan, M. J., De la Vega, M., Govender, U., Quinn, D. J., Dib, K., Gadina, M., Scott, C. J. and Johnston, J. A. (2009) USP17 regulates Ras activation and cell proliferation by blocking RCE1 activity. J Biol Chem. **284**, 9587-9595
451 de la Vega, M., Burrows, J. F., McFarlane, C., Govender, U., Scott, C. J. and Johnston, J. A. (2010) The deubiquitinating enzyme USP17 blocks N-Ras

membrane trafficking and activation but leaves K-Ras unaffected. J Biol Chem. **285**, 12028-12036
452 Ramakrishna, S., Suresh, B., Lee, E. J., Lee, H. J., Ahn, W. S. and Baek, K. H. (2011) Lys-63-specific deubiquitination of SDS3 by USP17 regulates HDAC activity. J Biol Chem. **286**, 10505-10514
453 Pereg, Y., Liu, B. Y., O'Rourke, K. M., Sagolla, M., Dey, A., Komuves, L., French, D. M. and Dixit, V. M. (2010) Ubiquitin hydrolase Dub3 promotes oncogenic transformation by stabilizing Cdc25A. Nat Cell Biol. **12**, 400-406
454 Tse, W. K., Eisenhaber, B., Ho, S. H., Ng, Q., Eisenhaber, F. and Jiang, Y. J. (2009) Genome-wide loss-of-function analysis of deubiquitylating enzymes for zebrafish development. BMC Genomics. **10**, 637
455 Ewing, R. M., Chu, P., Elisma, F., Li, H., Taylor, P., Climie, S., McBroom-Cerajewski, L., Robinson, M. D., O'Connor, L., Li, M., Taylor, R., Dharsee, M., Ho, Y., Heilbut, A., Moore, L., Zhang, S., Ornatsky, O., Bukhman, Y. V., Ethier, M., Sheng, Y., Vasilescu, J., Abu-Farha, M., Lambert, J. P., Duewel, H. S., Stewart, I. I., Kuehl, B., Hogue, K., Colwill, K., Gladwish, K., Muskat, B., Kinach, R., Adams, S. L., Moran, M. F., Morin, G. B., Topaloglou, T. and Figeys, D. (2007) Large-scale mapping of human protein-protein interactions by mass spectrometry. Mol Syst Biol. **3**, 89
456 Ahmed, S. F., Deb, S., Paul, I., Chatterjee, A., Mandal, T., Chatterjee, U. and Ghosh, M. K. (2012) The chaperone assisted E3 ligase CHIP targets PTEN for proteasomal degradation. J Biol Chem
457 Weeks, S. D., Grasty, K. C., Hernandez-Cuebas, L. and Loll, P. J. (2011) Crystal structure of a Josephin-ubiquitin complex: evolutionary restraints on ataxin-3 deubiquitinating activity. J Biol Chem. **286**, 4555-4565
458 Song, M. S., Carracedo, A., Salmena, L., Song, S. J., Egia, A., Malumbres, M. and Pandolfi, P. P. (2011) Nuclear PTEN regulates the APC-CDH1 tumor-suppressive complex in a phosphatase-independent manner. Cell. **144**, 187-199
459 Wu, X., Hepner, K., Castelino-Prabhu, S., Do, D., Kaye, M. B., Yuan, X. J., Wood, J., Ross, C., Sawyers, C. L. and Whang, Y. E. (2000) Evidence for regulation of the PTEN tumor suppressor by a membrane-localized multi-PDZ domain containing scaffold protein MAGI-2. Proc Natl Acad Sci U S A. **97**, 4233-4238
460 Yang, Y., Zhou, F., Fang, Z., Wang, L., Li, Z., Sun, L., Wang, C., Yao, W., Cai, X., Jin, J. and Zha, X. (2009) Post-transcriptional and post-translational regulation of PTEN by transforming growth factor-beta1. J Cell Biochem. **106**, 1102-1112
461 Li, F., Macfarlan, T., Pittman, R. N. and Chakravarti, D. (2002) Ataxin-3 is a histone-binding protein with two independent transcriptional corepressor activities. J Biol Chem. **277**, 45004-45012
462 Gorski, J. J., Pathak, S., Panov, K., Kasciukovic, T., Panova, T., Russell, J. and Zomerdijk, J. C. (2007) A novel TBP-associated factor of SL1 functions in RNA polymerase I transcription. EMBO J. **26**, 1560-1568
463 Booker, M., Samsonova, A. A., Kwon, Y., Flockhart, I., Mohr, S. E. and Perrimon, N. (2011) False negative rates in Drosophila cell-based RNAi screens: a case study. BMC Genomics. **12**, 50
464 Mahoney, C. L., Choudhury, B., Davies, H., Edkins, S., Greenman, C., Haaften, G., Mironenko, T., Santarius, T., Stevens, C., Stratton, M. R. and Futreal, P. A. (2009) LKB1/KRAS mutant lung cancers constitute a genetic subset of NSCLC with increased sensitivity to MAPK and mTOR signalling inhibition. Br J Cancer. **100**, 370-375

465 Omerovic, J., Clague, M. J. and Prior, I. A. (2010) Phosphatome profiling reveals PTPN2, PTPRJ and PTEN as potent negative regulators of PKB/Akt activation in Ras-mutated cancer cells. Biochem J. **426**, 65-72
466 Kwabi-Addo, B., Giri, D., Schmidt, K., Podsypanina, K., Parsons, R., Greenberg, N. and Ittmann, M. (2001) Haploinsufficiency of the Pten tumor suppressor gene promotes prostate cancer progression. In Proc Natl Acad Sci U S A. pp. 11563-11568, United States
467 Trotman, L. C., Niki, M., Dotan, Z. A., Koutcher, J. A., Di Cristofano, A., Xiao, A., Khoo, A. S., Roy-Burman, P., Greenberg, N. M., Van Dyke, T., Cordon-Cardo, C. and Pandolfi, P. P. (2003) Pten dose dictates cancer progression in the prostate. PLoS Biol. **1**, E59
468 Zhang, Y., Gan, B., Liu, D. and Paik, J. H. (2011) FoxO family members in cancer. Cancer Biol Ther. **12**, 253-259
469 Katoh, M., Igarashi, M., Fukuda, H. and Nakagama, H. (2012) Cancer genetics and genomics of human FOX family genes. Cancer Lett
470 Dong, X. Y., Chen, C., Sun, X., Guo, P., Vessella, R. L., Wang, R. X., Chung, L. W., Zhou, W. and Dong, J. T. (2006) FOXO1A is a candidate for the 13q14 tumor suppressor gene inhibiting androgen receptor signaling in prostate cancer. Cancer Res. **66**, 6998-7006
471 Myatt, S. S., Wang, J., Monteiro, L. J., Christian, M., Ho, K. K., Fusi, L., Dina, R. E., Brosens, J. J., Ghaem-Maghami, S. and Lam, E. W. (2010) Definition of microRNAs that repress expression of the tumor suppressor gene FOXO1 in endometrial cancer. Cancer Res. **70**, 367-377
472 Xie, L., Ushmorov, A., Leithauser, F., Guan, H., Steidl, C., Farbinger, J., Pelzer, C., Vogel, M. J., Maier, H. J., Gascoyne, R. D., Moller, P. and Wirth, T. (2012) FOXO1 is a tumor suppressor in classical Hodgkin lymphoma. Blood. **119**, 3503-3511
473 Huang, H. and Tindall, D. J. (2011) Regulation of FOXO protein stability via ubiquitination and proteasome degradation. Biochim Biophys Acta. **1813**, 1961-1964

Appendix A: DUB library siRNA sequences

The DUB library used in my project was obtained from Qiagen (Crawley, UK) and contains four siRNA oligonucleotides against each of 92 DUB targets. These had been arrayed on storage plates and lyophilised prior to being shipped to us. The oligonucleotides were arrayed in two different ways. In the first, the four oligonucleotides against each DUB were pooled prior to being arrayed; these plates were used for the initial screening phase. In the second, the library was arrayed on four storage plates, such that each plate contained an individual oligonucleotide targeting each of 92 DUBs. These plates were used for the deconvolution phase. The siRNA sequences for all of the oligonucleotides included in the library are shown in table A1 below.

Entrez Gene Id	NCBI gene symbol	First siRNA Sequence (C)		Second siRNA sequence (A)		Third siRNA sequence (D)		Fourth siRNA sequence (B)	
7345	UCHL1	Hs_UCHL1_1	CACGCAGTGGCCAATAATCAA	Hs_UCHL1_2	CTCCGCGAAGATGCAGCTCAA	Hs_UCHL1_4	CAGCCACACCCAGGCACTTAA	Hs_UCHL1_5	AACGTGGATGGCCACCTCTAT
7347	UCHL3	Hs_UCHL3_2	CAGGGACAAGATGTTACATCA	Hs_UCHL3_3	TAGAAGTTTGCAAGAAGTTTA	Hs_UCHL3_4	CTGGCAATTCGTTGATGTATA	Hs_UCHL3_5	CCCGAGGTCACCAACCAGTTT
51377	UCHL5	Hs_UCHL5_2	TCGATTTAATTTAATGGCCAT	Hs_UCHL5_5	ATGGATACAGATCAAGGTAAT	Hs_UCHL5_6	CAGCAGTTAATACCACTAGTA	Hs_UCHL5_7	TCAGATGTGATTCGACAAGTA
8314	BAP1	Hs_BAP1_1	CAGCAGCTGATAAGAGTAACA	Hs_BAP1_2	CTCAATTCCTCTGTCCATCAA	Hs_BAP1_3	CCCGCTGGTGCTGGAAGCAAA	Hs_BAP1_5	AAGGTGAACCGTCAGACAGTA
7398	USP1	Hs_USP1_6	ATGTGGCAGAATTACCTACTA	Hs_USP1_9	CTGGGACCCATGAATCTGATA	Hs_USP1_10	ACAGGCATTAATATTAGTGGA	Hs_USP1_11	AACCCTATGTATGAAGGATAT
9099	USP2	Hs_USP2_5	CAGATTGTGGTTACTGTTCTA	Hs_USP2_6	CAGGAGAATGGCACACTTTCA	Hs_USP2_4	CCGCGCTTTGTTGGCTATAAT	Hs_USP2_7	CCCTAAGAGACCTGGACTTAA
9960	USP3	Hs_USP3_2	AGCGCTCTAAGAATCAAGAAA	Hs_USP3_3	CTGGATCGGATAAACTTTAAT	Hs_USP3_4	CAGAAGTAAGCGCTCTAAGAA	Hs_USP3_5	CAGGGCGGTTTCAACGGTGTT
7375	USP4	Hs_USP4_1	ACCGAGGCGTGGAATAAACTA	Hs_USP4_3	TAGATGAATTAAGACGGTTAA	Hs_USP4_6	CAGGCAGACCTTGCAGTCAAA	Hs_USP4_7	CACCTACGAGCAGTTGAGCAA
8078	USP5	Hs_USP5_1	ACCGACGATCCGGGTCCCTAA	Hs_USP5_2	TACGTCTGCCACATCAAGAAA	Hs_USP5_3	AGCGAGGAGAAGTTTGAATTA	Hs_USP5_5	CCCAGCGAGTTGACTACATCA
9098	USP6	Hs_USP6_2	CCCAGGATCGTGATAACTGTA	Hs_USP6_3	TGCGGAGAGGTTCACAACAAA	Hs_USP6_5	GCGGAAGGACATACTTATGAA	Hs_USP6_6	AAGCACAGTAGCAAACTCATA
7874	USP7	Hs_USP7_1	CGGGCCGACACCAGTACATAA	Hs_USP7_2	ATGGAGTTGCGTGGGATTCAA	Hs_USP7_3	CCCAAATTATTCCGCGGCAAA	Hs_USP7_5	AAGCGTCCCTTTAGCATTACA
9101	USP8	Hs_USP8_1	CAGGGTCAATTCAAATCTACA	Hs_USP8_2	AAGGCTCGTATTCATGCAGAA	Hs_USP8_3	CAGGTTCAGGCAAGCCATTTA	Hs_USP8_5	GAGGATACAGACGATACCGAA
8239	USP9X	Hs_USP9X_1	CCGCCAGATAGCACAACGATA	Hs_USP9X_3	CAGCTAGTATTTAGCCCAAAT	Hs_USP9X_4	CCGCCTGCAGTGGAAAGTGTA	Hs_USP9X_5	GACGATGTATTCTCAATCGTA
8287	USP9Y	Hs_USP9Y_1	ATGACTGGTCCTAATCTGTAA	Hs_USP9Y_2	AACCGATTGCAATATAGTTTA	Hs_USP9Y_3	CACTAAGGTCTTATAGTCCAA	Hs_USP9Y_5	CAGCGTTGGATGCACTTAGTA
9100	USP10	Hs_USP10_5	AACACAGCTTCTGTTGACTCT	Hs_USP10_1	TCGCTTTGGATGGAAGTTCTA	Hs_USP10_3	AAGGGAACTGGTGCTACATTA	Hs_USP10_4	CAGCTTTGTTCGGCTAATGAA
8237	USP11	Hs_USP11_6	ACCGATTCTATTGGCCTAGTA	Hs_USP11_5	CTGCGTCGGGTACGTGATGAA	Hs_USP11_3	AAGGTCGAAGTGTACCCAGTA	Hs_USP11_4	CCCATTGAACGCAAGGTCATA
219333	USP12	Hs_USP12_5	CCGATCATGGTAGTTGATTTA	Hs_USP12_1	AAGAAGTTCATCACAAGATTA	Hs_USP12_3	ATGGATCAACTTCATCGATAT	Hs_USP12_4	TCACAAGATTACGGAAAGAAA
8975	USP13	Hs_USP13_1	TCGCTTATGAACTAACGAGAA	Hs_USP13_2	AGCGACGATTATGAATATGAA	Hs_USP13_5	CACTACGAGCAACGAATAATA	Hs_USP13_6	CCACCCGGAATTCTCCTCTAA
9097	USP14	Hs_USP14_1	CAGAGTTGAAATGCCTTTCAA	Hs_USP14_2	CCCATCCTTTGCCTTATCTAA	Hs_USP14_3	CCGCTCTACTCCGTTACTGTA	Hs_USP14_4	TGGCTTCAGCGCAGTATATTA

Entrez Gene Id	NCBI gene symbol	First siRNA Sequence (C)		Second siRNA sequence (A)		Third siRNA sequence (D)		Fourth siRNA sequence (B)	
9958	USP15	Hs_USP15_1	ATGAATAATGTTGTAACTCGA	Hs_USP15_2	TATGTCGGAATTCTTAATTAA	Hs_USP15_3	AAGATGATACCAGGCATATAA	Hs_USP15_5	CAGTCGATACATGAGAGACAA
10600	USP16	Hs_USP16_7	ACCCGTAATGAGAAACTTCGA	Hs_USP16_8	CCAGTGCTTAGAGAACTACTA	Hs_USP16_9	CAAGGGTACTCTATTCCTTAT	Hs_USP16_10	TTGGGTCAAGTGGTTGATTAT
391627	USP17	Hs_USP17_1	TGGAAATTCCTTCAAGAGCAA	Hs_USP17_2	CCCGACGTACTTGTGATTCAT	Hs_USP17_3	ATGAAGAACCATCATCCTGAA	Hs_USP17_4	CACAGGCAACAAGATTGCCAA
391622	DUB4	Hs_DUB4_1	GCCCTTGGCTCTGAAGACTAA	Hs_DUB4_2	AGCAGGTAGATCATCACTCTA	Hs_DUB4_3	TGGGAAATACCTGCTACGTGA	Hs_DUB4_4	CGCCGGCCTCCAAGACGTTAA
377630	DUB3	Hs_DUB3_4	GACGTACTTGTGATTCATCAA	Hs_DUB3_5	AAGCCTGAGTTCAACGTCAGA	Hs_DUB3_9	CGCCGGCCTCCAAGACGTTAA	Hs_DUB3_10	AGCAGGTAGATCATCACTCTA
11274	USP18	Hs_USP18_1	TAAGCGCTTCCTGGAAGTGAA	Hs_USP18_2	AAGATGGAGTGCTAATGGAAA	Hs_USP18_6	TTCGCTTTCCATTCAGTGGAA	Hs_USP18_7	CTGGATCTACGGAGTCTTCTA
10869	USP19	Hs_USP19_1	TTCAGTGGTGGTGCACGTGTA	Hs_USP19_2	AACGTGTTCTATCCTCTGGTA	Hs_USP19_3	CACGAGGACCTGAATCGCATT	Hs_USP19_4	CTGGCGTGACAAGATCAATGA
10868	USP20	Hs_USP20_1	CCGGATGATGAAACAGGGATA	Hs_USP20_2	CAGGCTTGTTGAAACGACCAA	Hs_USP20_3	ACCGTCGTACGTGCTCAAGAA	Hs_USP20_4	TCGAGTGACACGGATGAGAAA
27005	USP21	Hs_USP21_2	CAACCTAATGTGGAAACGTTA	Hs_USP21_3	GCGGCTACACCTTGAAATCAA	Hs_USP21_5	CAGTACAAAGATTCCCTCGAA	Hs_USP21_6	CCGAGCTGTCTTCCAGAAATA
23326	USP22	Hs_USP22_8	CTGAGTTTATACAGAAATTTA	Hs_USP22_7	AAGGTGAATTTCATAAATGTA	Hs_USP22_1	AAGAAGCATATTCACGAGCAT	Hs_USP22_2	CAGGACTACATCTATGACAAA
23358	USP24	Hs_USP24_5	AAGAGCAATCAGGAAGCAGTA	Hs_USP24_6	ACCACAGAGTAATGTCTCTAA	Hs_USP24_7	CACCGTGTATATTATACGCTT	Hs_USP24_8	CTAATGAAACATCAACTGGAA
29761	USP25	Hs_USP25_5	CAAGAGGAGTTTAATAAAGAA	Hs_USP25_6	CTGGCAATGATAGATACATCA	Hs_USP25_7	ACCTCACGGTATTACAACAAA	Hs_USP25_8	TTCATCGAGATCAGTAATACA
83844	USP26	Hs_USP26_5	TACGATGATATGCGGGTGTTA	Hs_USP26_6	CAGCTTAATAGCAAGGAGGTA	Hs_USP26_7	AAGATTATCAATAATCGGAGA	Hs_USP26_8	AACCGTTAGCTCACTTAATGA
389856	USP27X	Hs_LOC389856_1	ACGGAGGTATATACTGCTTTA	Hs_LOC389856_2	GCCGTTTATGGCCTCAAGTAA	Hs_LOC389856_3	CAGAATGAATGGACAATTGCA	Hs_LOC389856_4	CAGTCTGATGTCACCTGTCAA
57646	USP28	Hs_USP28_5	AAGGATTAGGTGGGCACATAA	Hs_USP28_6	CTACAAGAGATTAGAAATATA	Hs_USP28_7	ATGAAGGTGGCTCAAGCGAAA	Hs_USP28_8	CCGTGATTGCTTTATACCGAA
57663	USP29	Hs_USP29_5	AAGAATAACGAGCAAGTTTAT	Hs_USP29_6	CAGCTAGGGACTGATTAGAAA	Hs_USP29_7	CTCAAGGTAGAACCTAATAAT	Hs_USP29_8	GGAGATGATTTCTGAGATCAA
84749	USP30	Hs_USP30_2	CACACCAGTATTTATCCTTAA	Hs_USP30_5	AACAAATTACCTGCCGCACAA	Hs_USP30_6	CTCCGATGACACTGTCCGCAA	Hs_USP30_7	CTCACGAATTATTCCATGTCA
57478	USP31	Hs_USP31_1	CCCGAAATATTTAGGCCTGAA	Hs_USP31_2	CCGAGTTCATGAAGACCTCAA	Hs_USP31_3	GAGCGTCATCATCAGCCTCAA	Hs_USP31_5	CACCGAGCTCTTCGCCGAGTA
84669	USP32	Hs_USP32_5	TTCACGAATATCTATCTCAAA	Hs_USP32_6	TTGAAGTTCGCAACAAAGATA	Hs_USP32_7	AGGCTGCGCATTAAAGAGGAA	Hs_USP32_8	CAGGATGAACAACACCTGGTA
23032	USP33	Hs_USP33_2	CTGCAAGTAGTGGACACTATA	Hs_USP33_3	AAGAATTCCTTCGATGTTTAA	Hs_USP33_4	AAGAAGATCCGCAAACCATAA	Hs_USP33_5	TTCGAGTATGGTGTTATGCTT
9736	USP34	Hs_USP34_2	CTGGATTGAGTCAGATAACAA	Hs_USP34_4	AAGCCTAGATCTTGCATTTAA	Hs_USP34_5	AGCAGTGATAATAGCGATACA	Hs_USP34_6	GTGGATTGAACTGTTGACGAA
57558	USP35	Hs_USP35_2	CCCTTCTAACTTCTAACCGAA	Hs_USP35_5	TTCCTTCGAATCTGTCAGCAA	Hs_USP35_6	CAAGGACTTGATGGAAGCCAT	Hs_USP35_7	CTGCTCGGAGTATCTGAAGTA
57602	USP36	Hs_USP36_1	TCCGTATATGTCCCAGAATAA	Hs_USP36_2	CCCGAGTGTGATTCCAGATCA	Hs_USP36_3	CAAGAGCGTCTCGGACACCTA	Hs_USP36_4	CCGCATCGAGATGCCATGCAT
57695	USP37	Hs_USP37_5	AAGGATTTACTCAAGAAGGTT	Hs_USP37_6	ATGGTCCTATCAGAATTCGAA	Hs_USP37_7	CTCGGACGATTCCTTCTTTGA	Hs_USP37_8	ATCCGGGTAGAGGATCGATTA
84640	USP38	Hs_USP38_1	CAGCATAGTACTAATGGTTTA	Hs_USP38_2	CAGGAAGTAGCTAGTAAAGCA	Hs_USP38_3	ATGGGTAATTGCACTCCTGAA	Hs_USP38_4	CTGGTCTTATTAACCTAGGAA
10713	USP39	Hs_USP39_5	ACCAAGTTGCCTCCATATCTA	Hs_USP39_6	CCCGTACCTGGACACCATTAA	Hs_USP39_7	CAGGCTCTATCTAATGTTCCT	Hs_USP39_8	CTGGAACCCTCGAAATTTCAA
55230	USP40	Hs_USP40_5	AAGGTTCGAATCATCCCTTTA	Hs_USP40_6	ATGGTGTTTGATATTCGAATT	Hs_USP40_7	AAAGTCGGCCAAATTACGTAA	Hs_USP40_8	CTGAAGCTCGAGCTAATCCAA
373856	USP41	Hs_USP41_5	CAAACTCTGGAACCTGATTAA	Hs_USP41_7	CTGCCTTAACTCCTTGATTCA	Hs_USP41_8	TCGCCAGGATATTGAAGAGGA	Hs_USP41_6	CCGGATGAAGGACTCCTTGAT
84132	USP42	Hs_USP42_2	TTGGAGGATACCTAAGATCTA	Hs_USP42_5	ATCTTGATATTCGGCCATATA	Hs_USP42_6	CACTATCCATAGATCCTCTAA	Hs_USP42_7	CAGCTTCAAAGAGGTTCACTA

Entrez Gene Id	NCBI gene symbol	First siRNA Sequence (C)		Second siRNA sequence (A)		Third siRNA sequence (D)		Fourth siRNA sequence (B)	
124739	USP43	Hs_USP43_2	CACCTTTCAGAGAGTCAAATA	Hs_USP43_5	ACGGTGGAACCGCTTCGAGAA	Hs_USP43_6	CCCGCTGGACTTCCTGTACGA	Hs_USP43_7	CTCCGTCGAGTTGGTGGAGTA
84101	USP44	Hs_USP44_2	TTGCATGTGACAACAAATCAA	Hs_USP44_3	ACGGCAGGAATTGGAGTATCA	Hs_USP44_5	CTCGCTCAGTCGACCATAATA	Hs_USP44_6	TACGACGTACATTAAGTGCCA
85015	USP45	Hs_USP45_5	CAGGAAATTATCGGAACATAA	Hs_USP45_6	CGGGTGAAAGATCCAACTAAA	Hs_USP45_9	CACATGGATTATATGGTGTTA	Hs_USP45_10	CAGCTAGTACTTACTTCTGAT
64854	USP46	Hs_USP46_5	TAGGGAAATGTTTGTACTATA	Hs_USP46_4	CAGCACGGCATTGTTCCTTAT	Hs_USP46_7	CAGGGAACGCTTACCAATGAA	Hs_USP46_10	CAGGTTGTCAATTACACGGAT
55031	USP47	Hs_USP47_4	CAGGATGCTCATAGCTTAATA	Hs_USP47_5	AGGATTAAACTGAATGATCGA	Hs_USP47_6	TGGCGTCAAGTCAACATATAT	Hs_USP47_7	TGGATCGGCATGCAAATACAA
84196	USP48	Hs_USP48_5	ACCAGATGCGTTGGTCCATAA	Hs_USP48_1	ATGGCTGAGATGCGTAAGCAA	Hs_USP48_2	CACAGTCTGGTGAATGGTATA	Hs_USP48_6	AGGCGATACATTGATCCATCA
25862	USP49	Hs_MGC20741_4	TCCAGTCAATATCCCACTTAA	Hs_USP49_7	CTGGAATTCCCTGAACGCTAT	Hs_USP49_8	CCGAGTCATGTGGTCCGGGAA	Hs_USP49_9	TACGTGCTCAATGATAACCCA
373509	USP50	Hs_USP50_1	CAGCTCAATTATAGCATCGTA	Hs_USP50_2	CCCGGAGAAGATCATATGAGA	Hs_USP50_5	CAGGAAGTGGATTACCACTGA	Hs_USP50_6	TGCAGATGACTTCGATATCTA
158880	USP51	Hs_USP51_2	GAGGACTTACTCTACAGTGAA	Hs_USP51_3	CCAGAGACTAGGAAACGTAAA	Hs_USP51_4	AGGCCTGAGAGGGCTAATCAA	Hs_USP51_5	CTCAAGCGGTTTGAGCATGTA
9924	PAN2	Hs_USP52_5	AAGGTGCTCAAGGGTCTTTAT	Hs_USP52_6	AGCCGATATCTTTCATGTGAA	Hs_USP52_7	CATCGTCATCATGAACTTTGA	Hs_USP52_8	CAGCCCTTCAGCTGTACCGAA
54532	USP53	Hs_USP53_5	TTGTACTATGCTGGTAAACTA	Hs_USP53_6	CAGATTACGACAAGCAACCTA	Hs_USP53_7	ACCGAGGTTGGAAACCTATGA	Hs_USP53_8	CTTCGTCCTGTTAAAGATAAA
159195	USP54	Hs_USP54_2	CAGGGTGCAATCCTCAACTAA	Hs_USP54_6	CAGCAGAGCCCTAGTCGATAA	Hs_USP54_7	AAGGGATGTTTGCACCTCGAA	Hs_USP54_8	AAGGAGTTAGAGGCAGCGAAA
1540	CYLD	Hs_CYLD_2	AAGGGTAGAACCTTTGCTAAA	Hs_CYLD_3	AAAGAACGATGTAGAATATTA	Hs_CYLD_4	AAGGTTCATCCAGTCATAATA	Hs_CYLD_5	CACCAAGATGCCCAATACCAA
10208	USPL1	Hs_USPL1_1	CAAGACCAATTTGTGGACATA	Hs_USPL1_2	CCAGGGACTGATATAGGGATA	Hs_USPL1_3	AAGGTATAAACCAGAAGGCCA	Hs_USPL1_4	ATGCCTGCGTTAGAACATTAA
55611	OTUB1	Hs_OTUB1_1	CAGCAGGACCGAATTCAGCAA	Hs_OTUB1_3	CACTACGATATCCTCTACAAA	Hs_OTUB1_4	CTGCCAGGCGCTAGACATGTA	Hs_OTUB1_5	CTCCGACTACCTTGTGGTCTA
78990	OTUB2	Hs_OTUB2_6	CAGGGAGATCTTCAAGTTCAA	Hs_OTUB2_2	CAGCCGATAAACATTGATTAA	Hs_OTUB2_7	AAGGTTCACCGCCATCCGCAA	Hs_OTUB2_8	TTCCGTTTACCTGCTCTATAA
56957	OTUD7B	Hs_ZA20D1_2	CAGGATGACATCGTTCAAGAA	Hs_OTUD7B_1	AACCCATCCCTTGGAACGTAA	Hs_OTUD7B_2	ATCCGTTTGTTTAGATGGGAA	Hs_OTUD7B_3	ACCGAGTGGCTGATTCCTATA
161725	OTUD7A	Hs_OTUD7A_1	CACGCCGTCGCCCACAGACAA	Hs_OTUD7A_2	CCACGTGGCAAGTGAATGCAA	Hs_OTUD7A_3	CGGGACCTGGTGTTACGGAAA	Hs_OTUD7A_4	CCGCGATTCGGTGTGCAGCAA
54726	OTUD4	Hs_OTUD4_1	AAAGATAAGAATATTCTTCGA	Hs_OTUD4_2	CAGAGAGAAATTTGAAGCGTT	Hs_OTUD4_3	CAGGCGGAGAATGGATACAGA	Hs_OTUD4_4	CACGTTGGAAGTAGCTGATGA
57097	PARP11	Hs_PARP11_3	ATGGATCGCAACCGAATTAAA	Hs_PARP11_6	TTGATTGGAGAATAAATGGTA	Hs_PARP11_7	CTCAACTAATGTGGTCATTGA	Hs_PARP11_8	CAGCGGCATCTGTTTAGAACA
54764	ZRANB1	Hs_ZRANB1_1	CAGATCTGTAATGACCCTAAA	Hs_ZRANB1_2	CAAGGGTGAAATCTTCGTATA	Hs_ZRANB1_3	CACATATTCTTAGACGACCAA	Hs_ZRANB1_4	TAGGATAATTCAATGTCGAAA
80124	VCPIP1	Hs_VCIP135_3	CCCGATGATTATACTCCTGTA	Hs_VCPIP1_1	TACCAGAAGCTTTCCCTATTA	Hs_VCPIP1_2	CAGGGACAGACTTTAGTAATA	Hs_VCPIP1_3	CAGCTCCGGTAGAAACCATTA
55432	YOD1	Hs_YOD1_2	ATAAGCTATGGTAACCCTAAA	Hs_YOD1_4	GACCGTCAAATTAGAGCTTTA	Hs_YOD1_5	CAGCGTAACTTCCCTGATCCA	Hs_YOD1_6	AAACTGGTATAGGCTATGTAA
7128	TNFAIP3	Hs_TNFAIP3_1	CCGAGCTGTTCCACTTGTTAA	Hs_TNFAIP3_3	CAGATGTATGGCTAACCGGAA	Hs_TNFAIP3_4	CTCGGCTATGACAGCCATCAT	Hs_TNFAIP3_5	CAGCCTTTACTCATACTATTA
51633	OTUD6B	Hs_CGI-77_3	AGGGTCATTGATAGCAAGTAA	Hs_OTUD6B_2	TTCGGTTACACGGTTGGTAAA	Hs_OTUD6B_3	AAGGAGCGAGAAGAACGGATA	Hs_OTUD6B_4	CAGACCGCTGAGTATATGCAA
139562	OTUD6A	Hs_HSHIN6_1	CAAGACGACAGTAGCATTGAA	Hs_OTUD6A_1	CTACGACGACTTCATGATCTA	Hs_OTUD6A_2	AGGCCCAGATCCGGAGCTTAA	Hs_OTUD6A_3	AAGAGTGAACAGCAGCGCATA
55593	OTUD5	Hs_DKFZp761A052_1	CAGGCCGGCTTGGACAATGAA	Hs_OTUD5_1	TACCACCTACATTAACAGGAA	Hs_OTUD5_2	TGCCGACTACTTCTCCAACTA	Hs_OTUD5_3	CCCATTCGTGTTAGCTACCAT
220213	OTUD1	Hs_OTUD1_1	CTGAATGTGAATATCCATTTA	Hs_OTUD1_2	CACGGTGTCTACCATGATTCA	Hs_OTUD1_3	AACGGACACTATGATGCTGTA	Hs_OTUD1_4	ACGAAGAACTTGCCAAATCTA
79184	BRCC3	Hs_CXorf53_1	TACGATGTTGATTATAACATT	Hs_CXorf53_2	CAGATTGAGATGAATTTGCAA	Hs_CXorf53_3	CAGCATTTGCAGGAATTACAA	Hs_BRCC3_1	TACGACGTTCTGATAAGAGGA

Entrez Gene Id	NCBI gene symbol	First siRNA Sequence (C)		Second siRNA sequence (A)		Third siRNA sequence (D)		Fourth siRNA sequence (B)	
10987	COPS5	Hs_COPS5_3	TAGGACATACCCAAAGGGCTA	Hs_COPS5_5	AAGAACAATATCCGCAGGGAA	Hs_COPS5_6	ATGCAATCGGGTGGTATCATA	Hs_COPS5_7	CTGGACTAAGGATCACCATTA
10980	COPS6	Hs_COPS6_1	CCCAACCTTATAAACATGATA	Hs_COPS6_4	CCCGGTGCTCAGCACAGACAA	Hs_COPS6_5	CCGCGTCAAGCTCATCTTGGA	Hs_COPS6_6	CTCGGACATCCACGTCCATAA
8667	EIF3H	Hs_EIF3S3_1	GCGGAGCCTTCGCCATGTAAA	Hs_EIF3S3_5	CCCAAGGATCTCTCTCACTAA	Hs_EIF3S3_8	CAGATAGATGGCCTTGTGGTA	Hs_EIF3S3_9	CTCGGGAGATTCAGCCGTGAA
8665	EIF3F	Hs_EIF3S5_1	TACGCGTACTACGACACTGAA	Hs_EIF3S5_3	CACAATGAGTCAGAAGATGAA	Hs_EIF3S5_5	AACGGCCGCATGAGCATCAAA	Hs_EIF3S5_6	CGCCTCCTTCTTTCTCGACAA
5713	PSMD7	Hs_PSMD7_5	AAGAATAGTTGGCTGGTACCA	Hs_PSMD7_1	CCGAATCGGCAAGGTTGGAAA	Hs_PSMD7_3	TTCCGTATTGGTCATCATTGA	Hs_PSMD7_6	CACGTGACCAGTGAAATTGGA
10213	PSMD14	Hs_PSMD14_1	CAGGCATTAATTCATGGACTA	Hs_PSMD14_3	TTGGATACTGTCGTATTTAAA	Hs_PSMD14_4	ACAGACATTATTACTCCATTA	Hs_PSMD14_5	CTGGGTCACTTAAACAAGCCA
10594	PRPF8	Hs_PRPF8_2	ACGGGCATGTATCGATACAAA	Hs_PRPF8_3	ATGGCTTGTCATCCTGAATAA	Hs_PRPF8_4	CAACGTCGTCATCAACTATAA	Hs_PRPF8_5	CTCATCGTGGACCACAACATA
10617	STAMBP	Hs_STAMBP_5	AAGGAGATTGCATTTCCCAAA	Hs_STAMBP_6	ACAGAGGGTAGCACAACAGAA	Hs_STAMBP_7	ATCACGCTCTTTATTGAGAAA	Hs_STAMBP_8	CCGCTCTGGAGTTGAGATTAT
84954	MPND	Hs_FLJ14981_5	TCAGGTAATAAAGAAACGGAA	Hs_FLJ14981_6	CCGGATGGGCTCAGGTAATAA	Hs_FLJ14981_2	ACGGAGTGAGGTCGTGGGTTA	Hs_FLJ14981_3	CACCTACCTCGACAAGCTTAA
57559	STAMBPL1	Hs_AMSH-LP_1	CAGGCTGTTCAGTATATGCAA	Hs_AMSH-LP_2	CCCAAATACTATGGCCAGATA	Hs_AMSH-LP_3	AACCATCGAGATTACCAGCAA	Hs_AMSH-LP_4	ACCGTCAACATCAGACACCTA
114803	MYSM1	Hs_MYSM1_3	TATAATCGAAATAATCCCTTA	Hs_MYSM1_4	AAGACCGGCCATAATCTTCAA	Hs_MYSM1_5	TGGGATGATTGTTAGTCCCTA	Hs_MYSM1_6	GAGGCGGATGTGGATATCGAA
4287	ATXN3	Hs_ATXN3_1	TACGATGGGATCATTATTTCA	Hs_ATXN3_3	TCGGAAGAGACGAGAAGCCTA	Hs_ATXN3_4	TGCGTCGGTTGTAGGACTAAA	Hs_ATXN3_5	CAGGGCTATTCAGCTAAGTAT
92552	ATXN3L	Hs_ATXN3L_5	AACAAGTTCGAGAGCAATTGA	Hs_ATXN3L_6	CAACACTGGTTTACTATTAGA	Hs_ATXN3L_7	CACAGTTCATACCTACACGAA	Hs_ATXN3L_8	CTCGGCATTGATCCTATAAAT
9929	JOSD1	Hs_KIAA0063_2	CAACCTCGACTCCAAACTCAA	Hs_KIAA0063_3	CACAATTCAGTAGACACTCTA	Hs_KIAA0063_4	TAGCCATCTCTGGAACCTAAA	Hs_JOSD1_1	CTGGTGGTACCAGAAGAGGTA
126119	JOSD2	Hs_SBBI54_1	CTGCCGCTGCTGCCTCAATAA	Hs_SBBI54_2	CTGGGAAAGGCCAGCACTTCA	Hs_SBBI54_3	ACCGGCAACTATGATGTCAAT	Hs_JOSD2_1	CCAGGTGGACGGTGTCTACTA

Table A1. DUB siRNA library. The siRNA sequences for all of the oligonucleotides included in the Qiagen DUB si RNA library are shown. For three of the DUBs, highlighted in red, siRNAs were re-purchased separately to replenish depleted oligonucleotides in the library (USP8, USP20 and ATXN3). DUB screens were performed with pools of oligonucleotides that were made up of all four oligonucleotides against each target which were arrayed on a single 96-well plate. Columns 3 to 7 each contain a set of siRNA oligonucleotides targeting all the DUBs in the library, and these were also arrayed on separate plates for the purposes of deconvolution experiments. However, as discussed below, these were mislabelled, and the designation of each set of siRNA oligonucleotides (C, A, D and B) in columns 3-7 is explained below.

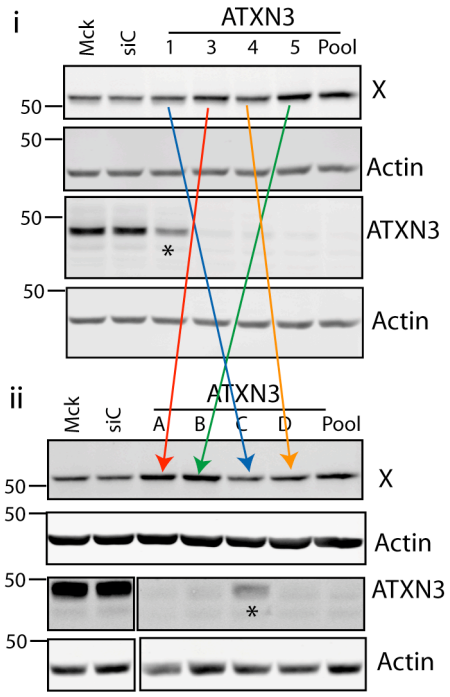

Fig A1. Correlation between re-purchased siRNA oligonucleotides and the original DUB library. A 72 hour depletion of ATXN3 was performed in A549 cells with either a set of oligonucleotides purchased individually from Qiagen (1, 2, 3 and 5), or the same oligonucleotides, which had previously been arrayed on four individual 96 well plates (A, B, C, and D). Immunoblotting was performed for PTEN (X), ATXN3 and actin. The phenotypic effects observed were reproducible in at least 3 experiments in each case. The arrows indicate the probable identity of the oligonucleotides on the plates based on their phenotypic effects, and results from similar experiments contrasting the re-purchased oligonucleotides with the library oligonucleotides (data not shown). (mck: mock transfected, siC: non-targeting siRNA control).

Three siRNA oligonucleotides from the library (USP8, USP102 and ATXN3) were used extensively and were therefore repurchased. Experiments performed using these oligonucleotides showed the same range of phenotypic effects as seen using the original library oligonucleotides, however the results indicated that the original plates had been correctly arrayed but systematically mislabelled. A comparison of depletion of ATXN3 using the library and replacement siRNA is given in fig A1 as an example; similar findings were obtained with USP20, USP8 and by colleagues using other oligonucleotides from the library. Based on these experiments, the most likely designation of each plate is given in the table A1 above. Confirmation of this will involve mass spectroscopy but is yet to be carried out.

Appendix C: USP20 and USP33 sequence alignments

Reference sequences for USP20 and USP33 were obtained from Uniprot (www.uniprot.org/), while alignments were performed using Clustal W (www.ebi.ac.uk/Tools/msa/clustalw2/).

The positions of the Bethyl (A301-189A) and Aviva (ARP59314) antigens are depicted in green and red respectively.

```
sp|Q9Y2K6|UBP20_HUMAN      ------------------------------MGDSRDLCPHLDSIGEVTK 19
sp|Q8TEY7|UBP33_HUMAN      MTGSNSHITILTLKVLPHFESLGKQEKIPNKMSAFRNHCPHLDSVGEITK 50
                                                  *.  *: ******:**:**

sp|Q9Y2K6|UBP20_HUMAN      EDLLLKSKGTCQSCGVTGPNLWACLQVACPYVGCGESFADHSTIHAQAKK 69
sp|Q8TEY7|UBP33_HUMAN      EDLIQKSLGTCQDCKVQGPNLWACLENRCSYVGCGESQVDHSTIHSQETK 100
                           ***: ** ****.* * ********:  *.******* .******:* .*

sp|Q9Y2K6|UBP20_HUMAN      HNLTVNLTTFRLWCYACEKEVFLEQRL----AAPLLGSSSKFSE---QDS 112
sp|Q8TEY7|UBP33_HUMAN      HYLTVNLTTLRVWCYACSKEVFLDRKLGTQPSLPHVRQPHQIQENSVQDF 150
                           * *******:*:*****.*****:::*    : * : .. ::.*   **

sp|Q9Y2K6|UBP20_HUMAN      PPPS-HPLKAVPIAVADEGESES-EDDDLKPRGLTGMKNLGNSCYMNAAL 160
sp|Q8TEY7|UBP33_HUMAN      KIPSNTTLKTPLVAVFDDLDIEADEEDELRARGLTGLKNIGNTCYMNAAL 200
                             **  .**:  :** *: : *: *:*:*:.*****:**:**:*******

sp|Q9Y2K6|UBP20_HUMAN      QALSNCPPLTQFFLECGGLVRTDKKPALCKSYQKLVSEVWHKKRPSYVVP 210
sp|Q8TEY7|UBP33_HUMAN      QALSNCPPLTQFFLDCGGLARTDKKPAICKSYLKLMTELWHKSRPGSVVP 250
                           **************:****.*******:**** **::*:***.**. ***


sp|Q9Y2K6|UBP20_HUMAN      TSLSHGIKLVNPMFRGYAQQDTQEFLRCLMDQLHEELKEPVVATVALTEA 260
```

```
sp|Q8TEY7|UBP33_HUMAN      TTLFQGIKTVNPTFRGYSQQDAQEFLRCLMDLLHEELKEQVMEVE----- 295
                           *:* :*** *** ****:***:********* ******* *: .

sp|Q9Y2K6|UBP20_HUMAN      RDSDSSDTDEKREGDRSPSEDEFLSCD--SSSDRGEGDGQGRGGGSSQAE 308
sp|Q8TEY7|UBP33_HUMAN      EDPQTITTEETMEEDKSQSDVDFQSCESCSNSDRAENENGSRCFSEDNNE 345
                           .*.::  *:*. * *:* *: :* **:  *.***.*.:. .*  ...: *

sp|Q9Y2K6|UBP20_HUMAN      TELLIPDEAGRAISEKERMKDRKFSWGQQRTNSE-QVDEDADVDTAMAAL 357
sp|Q8TEY7|UBP33_HUMAN      TTMLIQDDENNSEMSKDWQKE-KMCNKINKVNSEGEFDKDRDSISETVDL 394
                           * :** *: ..:  .*:  *: *:.   ::.*** :.*:* *  :  . *

sp|Q9Y2K6|UBP20_HUMAN      DDQPAEAQPPSPRSSSPCRTPEPDNDAHLRSSSRPCSPVHHHEGHAKLSS 407
sp|Q8TEY7|UBP33_HUMAN      NNQETVKVQIHSRAS------EYITDVHSNDLSTPQILPSNEGVNPRLSA 438
                           ::* :      .*:*      *  .*.* .. * *     :.  :.:**:
                                      Sequence identity 24%

sp|Q9Y2K6|UBP20_HUMAN      SPPRASPVRMAPSYVLKKAQVLSAGSRRRKEQRYRSVISDIFDGSILSLV 457
sp|Q8TEY7|UBP33_HUMAN      SPPKSGNLWPGLAPPHKKAQSASP-KRKKQHKKYRSVISDIFDGTIISSV 487
                           ***::. :  . :   ****  *. .*:::.::************:*:* *

sp|Q9Y2K6|UBP20_HUMAN      QCLTCDRVSTTVETFQDLSLPIPGKEDLAKLHSAIYQNVPAKPGACGDSY 507
sp|Q8TEY7|UBP33_HUMAN      QCLTCDRVSVTLETFQDLSLPIPGKEDLAKLHSSSHPTSIVKAGSCGEAY 537
                           *********.*:********************: : .  .*.*:**::*

sp|Q9Y2K6|UBP20_HUMAN      AAQGWLAFIVEYIRRFVVSCTPSWFWGPVVTLEDCLAAFFAADELKGDNM 557
sp|Q8TEY7|UBP33_HUMAN      APQGWIAFFMEYVKRFVVSCVPSWFWGPVVTLQDCLAAFFARDELKGDNM 587
                           *.***:**::**::******.***********:******** ********

sp|Q9Y2K6|UBP20_HUMAN      YSCERCKKLRNGVKYCKVLRLPEILCIHLKRFRHEVMYSFKINSHVSFPL 607
sp|Q8TEY7|UBP33_HUMAN      YSCEKCKKLRNGVKFCKVQNFPEILCIHLKRFRHELMFSTKISTHVSFPL 637
                           ****:*********:*** .:***************:*:* **.:******
```

```
sp|Q9Y2K6|UBP20_HUMAN      EGLDLRPFLAKECTSQITTYDLLSVICHHGTAGSGHYIAYCQNVINGQWY 657
sp|Q8TEY7|UBP33_HUMAN      EGLDLQPFLAKDSPAQIVTYDLLSVICHHGTASSGHYIAYCRNNLNNLWY 687
                           *****:*****:..:**.*************.*********:* :*. **

sp|Q9Y2K6|UBP20_HUMAN      EFDDQYVTEVHETVVQNAEGYVLFYRKSSEEAMRERQQVVSLAAMREPSL 707
sp|Q8TEY7|UBP33_HUMAN      EFDDQSVTEVSESTVQNAEAYVLFYRKSSEEAQKERRRISNLLNIMEPSL 737
                           ***** **** *:.*****.************ :**::: .*  : ****

sp|Q9Y2K6|UBP20_HUMAN      LRFYVSREWLNKFNTFAEPGPITNQTFLCSHGGIPPHKYHYIDDLVVILP 757
sp|Q8TEY7|UBP33_HUMAN      LQFYISRQWLNKFKTFAEPGPISNNDFLCIHGGVPPRKAGYIEDLVLMLP 787
                           *:**:**:*****:*********:*: *** ***:**:*  **:***::**

sp|Q9Y2K6|UBP20_HUMAN      QNVWEHLYNRFGGGPAVNHLYVCSICQVEIEALAKRRRIEIDTFIKLNKA 807
sp|Q8TEY7|UBP33_HUMAN      QNIWDNLYSRYGGGPAVNHLYICHTCQIEAEKIEKRRKTELEIFIRLNRA 837
                           **:*::**.*:**********:*  **:* * : ***: *:: **:**:*

sp|Q9Y2K6|UBP20_HUMAN      FQAEESPGVIYCISMQWFREWEAFVKGKDNEPPGPIDNSRIAQVKGSGHV 857
sp|Q8TEY7|UBP33_HUMAN      FQKEDSPATFYCISMQWFREWESFVKGKDGDPPGPIDNTKIAVTK-CGNV 886
                           ** *:**..:************:******.:********:** .* .*:*

sp|Q9Y2K6|UBP20_HUMAN      QLKQGADYGQISEETWTYLNSLYGGGPEIAIRQSVAQPLGPENLHGEQKI 907
sp|Q8TEY7|UBP33_HUMAN      MLRQGADSGQISEETWNFLQSIYGGGPEVILRPPVVH-VDPDILQAEEKI 935
                            *:**** ********.:*:*:******: :* .*.: :.*: *:.*:**
```

Sequence identity 57%

```
sp|Q9Y2K6|UBP20_HUMAN      EAETRAV 914
sp|Q8TEY7|UBP33_HUMAN      EVETRSL 942
                           *.***::
```